12 March 2010 | $10

Science

AAAS


SIGMA
Life Science
Where bio begins™

INTERNATIONAL SCIENCE & ENGINEERING
VISUALIZATION CHALLENGE

CALL FOR ENTRIES

ENTRY DEADLINE: SEPTEMBER 15, 2010

SCIENCE AND ENGINEERING'S MOST POWERFUL STATEMENTS
ARE NOT MADE FROM WORDS ALONE

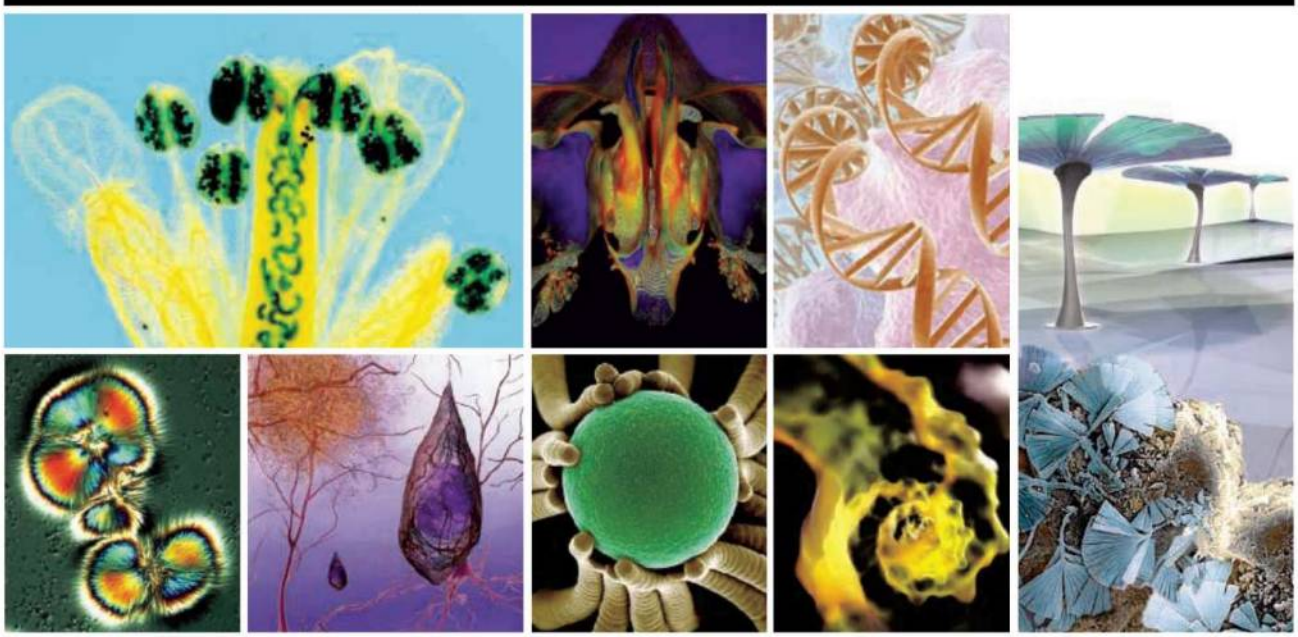

Visualization in all its forms has the power to illuminate and educate. It explains and makes clear all aspects of the world around us. It feeds insight and provokes curiosity.

The National Science Foundation (NSF) and the journal *Science*, published by the American Association for the Advancement of Science, invite you to participate in this year's Challenge. The competition recognizes scientists, engineers, visualization specialists, and artists who produce innovative work in visual communication.

Winning entries will be published in *Science* and *Science* Online, and will be displayed on the NSF web site.

Award Categories

- Photographs/Pictures
- Illustrations/Drawings
- Informational Posters and Graphics
- Interactive Games
- Non-Interactive Media

COMPLETE ENTRY INFORMATION:
WWW.NSF.GOV/NEWS/SCIVIS

NSF

Science
AAAS

GE Healthcare
Life Sciences

GE02-10. First published January 2010.

Drop. Measure. Done.

NanoVue™ Plus: intelligent performance across all spectrophotometer applications

It's all the convenience you want in a spectrophotometer, packaged in a portable, ergonomic device. NanoVue Plus features a new hydrophobic, gold-colored sample plate coating that delivers outstanding results for sub-microliter amounts of proteins and nucleic acids. It operates without a PC and does not require time-consuming third-party path length recalibration.

NanoVue Plus enables easy protocol selection using advanced software that includes intuitive drop-down lists for the full range of CyDye™ fluorescent dyes, as well as lists for common fluors. Results can exported using a USB cable or Bluetooth™ connections for print via computer (PVC) or stored using the new SD card option. An integrated printer is also available.

- Swift, accurate analysis of 0.5 µl samples of nucleic acids and proteins
- Practical drop and measure mechanism
- Outstanding sample recovery
- Reliable and reproducible measurements
- Automatic self-calibration on start up
- Path length recalibration kit available as accessory

Experience the NanoVue Plus first hand.
Register for a trial at:

www.gelifesciences.com/tryNanoVuePlus

I ÄKTA I Amersham I Biacore I IN Cell Analysis I Whatman I GE Service I

imagination at work

EDITORIAL

NEWS OF THE WEEK

NEWS FOCUS

LETTERS

BOOKS *ET AL.*

POLICY FORUM

PERSPECTIVES

CONTENTS continued >>

page 1318

page 1331

COVER

Substances deposited by a mother bird into her eggs influence how intensely her offspring beg for food after hatching. In canaries, these substances are effectively a prenatal signal of parental generosity. In contrast to the common assumption, they function primarily to serve the evolutionary interests of the offspring rather than the mother. See page 1373.

Photo: Fernando Trabanco

DEPARTMENTS

Enjoy first-time success

Gene expression and function analysis sample and assay technologies by QIAGEN

Rely on QIAGEN's manual and automated workflow solutions for:

- **Sample collection and disruption, and RNA purification**
- **Real-time PCR and RT-PCR, and gene expression assays**
- **RNAi and gene silencing**
- **miRNA purification and assays**
- **Methylation analysis in epigenetics research**
- **Protein sample preparation and assays**

Making improvements in life possible — www.qiagen.com

GEPor01106WW

QIAGEN®

Sample & Assay Technologies

REVIEW

RESEARCH ARTICLE

REPORTS

CONTENTS continued >>

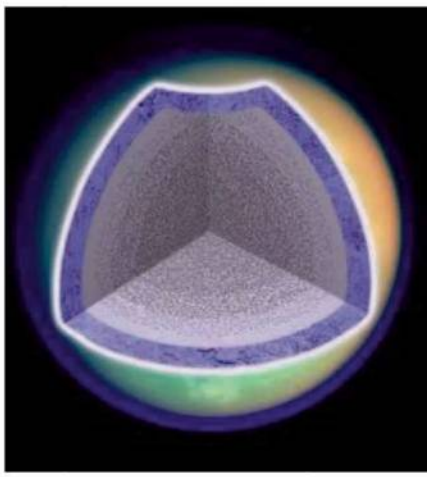

pages 1338 & 1367

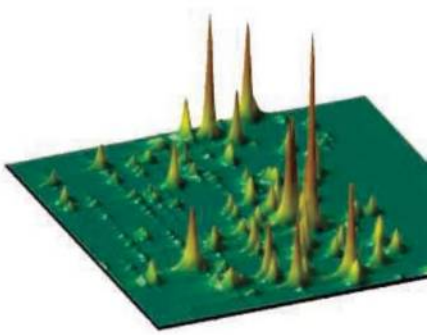

pages 1333 & 1352

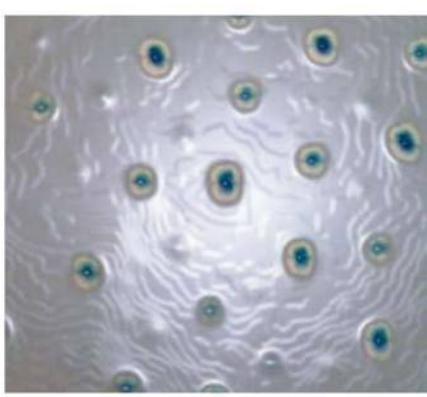

page 1385

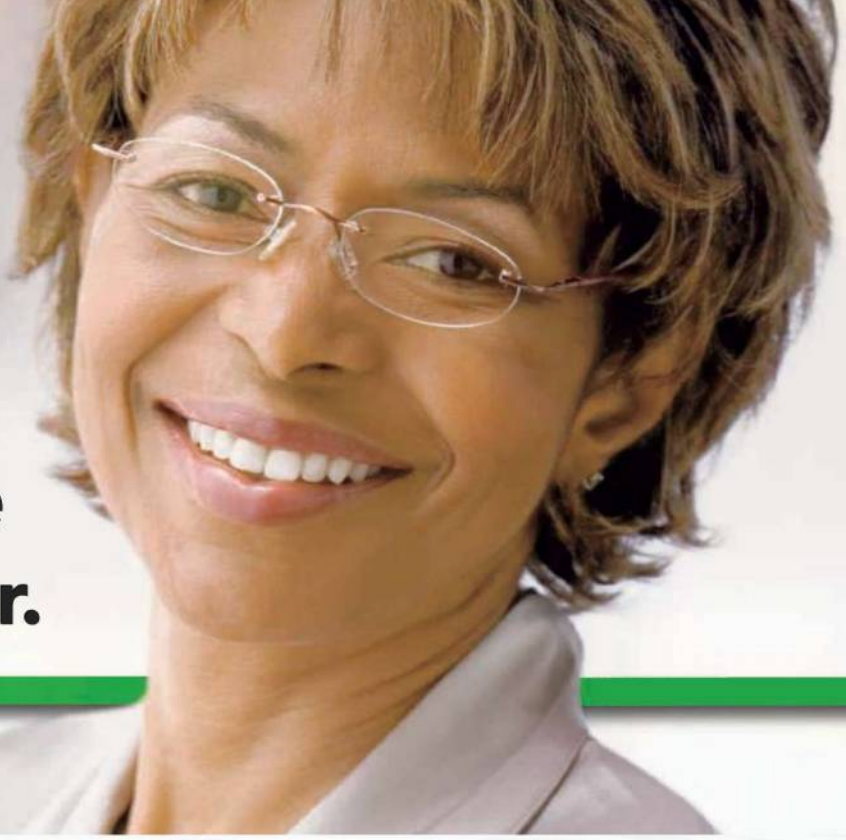

You've built your life around helping others.

It's time someone returned the favor.

We'll give you the guidance that can help bring your total financial picture into focus.

As someone who helps others for a living, your own financial well-being is often the last thing on your mind. That's why Fidelity is here to help you develop a real, relevant plan for your investments. And we can do it on your terms.

How Fidelity can help you:

- **A complimentary consultation to review both your personal and workplace investments**
- **Experience to help you build a comprehensive financial plan**
- **Guidance to help you with your needs, from charitable giving to estate planning**

Schedule a complimentary one-on-one consultation with a Fidelity Representative today.

800.328.6608
Fidelity.com/reserve

Turn here℠

Fidelity INVESTMENTS

Investing involves risk, including the risk of loss.

Products or services mentioned above may not be applicable depending on your particular financial situation. Restrictions may apply. Please contact Fidelity for additional information.

Guidance provided by Fidelity is educational in nature, is not individualized, and is not intended to serve as the primary or sole basis for your investment or tax-planning decisions.

SCIENCEONLINE

SCIENCEXPRESS
www.sciencexpress.org

Caspase-Dependent Conversion of Dicer Ribonuclease into a Death-Promoting Deoxyribonuclease
A. Nakagawa et al.
An enzyme that chops up RNA can be switched to DNA fragmentation and can trigger programmed cell death in worms.
10.1126/science.1182374

Analysis of Genetic Inheritance in a Family Quartet by Whole-Genome Sequencing
J. C. Roach et al.
Genomic sequencing of an entire family reveals the rate of spontaneous mutations in humans and identifies disease genes.
10.1126/science.1186802

A Peroxidase/Dual Oxidase System Modulates Midgut Epithelial Immunity in *Anopheles gambiae*
S. Kumar et al.
Bonding between cell-surface proteins forms a physical barrier in mosquito guts to prevent microbe invasion.
10.1126/science.1184008

Detection of a Large-Scale Structure of Intracluster Globular Clusters in the Virgo Cluster
M. G. Lee et al.
Extensive regions of mass have been located between the galaxies of the Virgo cluster.
10.1126/science.1186496

A Fast Soluble Carbon-Free Molecular Water Oxidation Catalyst Based on Abundant Metals
Q. Yin et al.
Bulky polytungstate ligands stabilize a cobalt-based catalyst highly active for splitting water.
10.1126/science.1185372

SCIENCENOW
www.sciencenow.org
Highlights From Our Daily News Coverage

For Pregnant Mice, Eating Matters More for Their Sons
Expectant moms' bad eating habits may hurt boys more than girls.

And the Winners of Our Blogging Contest Are …
Science picks its favorites from our supplementary coverage of the 2010 AAAS annual meeting.

Pain's in the Genes
A subtle genetic variant seems to dictate how much pain people feel.

SCIENCESIGNALING
www.sciencesignaling.org
The Signal Transduction Knowledge Environment

RESEARCH ARTICLE: Pin1 and PKMζ Sequentially Control Dendritic Protein Synthesis
P. R. Westmark et al.

PERSPECTIVE: PINing for Things Past
T. C. Sacktor
Memory storage requires the inhibition of a peptidyl-prolyl isomerase to enable synthesis of the kinase PKMζ.

REVIEW: Stress-Activated Cap'n'Collar Transcription Factors in Aging and Human Disease
G. P. Sykiotis and D. Bohmann
The oxidative stress response is an attractive target for treating human diseases and extending the healthy life span.

NETWATCH: PhosphoSitePlus
Explore a database of posttranslational protein modifications; in Protein Databases.

NETWATCH: The CAspase Substrate dataBAse Homepage (CASBAH)
Search and browse a collection of caspase substrates; in Protein Databases.

SCIENCECAREERS
www.sciencecareers.org/career_magazine
Free Career Resources for Scientists

Audacity, Part 4: Taking Liberties With Research Grants?
A. Sasso
Should you propose safe research and then use the money for riskier work?

New Opportunities and Jobs Coming in Comparative Effectiveness Research
K. Hede
Recovery Act funding will boost a field focused on health care costs and quality.

SCIENCETRANSLATIONAL MEDICINE
www.sciencetranslationalmedicine.org
Integrating Medicine and Science

COMMENTARY: The Road We Must Take—Multidisciplinary Team Science
M. L. Disis and J. T. Slattery
Solutions to today's complex health problems will require multidisciplinary innovative thinking and collaboration.

PERSPECTIVE: Bladder Cancer—Optimal Application of Preclinical Models to Suitable Translational Questions
D. Raghavan
New reagents tested in bladder cancer xenografts allow for better economy and focus in clinical cancer trials.

SCIENCETRANSLATIONAL MEDICINE
Monkeys reveal genetics advantage against HIV.

RESEARCH ARTICLE: MHC Heterozygote Advantage in Simian Immunodeficiency Virus-Infected Mauritian Cynomolgus Macaques
S. L. O'Connor et al.
Heterozygote advantage in macaque monkeys reveals that HIV vaccine should elicit broad $CD8^+$ T cell responses.

SCIENCEPODCAST
www.sciencemag.org/multimedia/podcast
Free Weekly Show
Download the 12 March *Science* Podcast to hear about parent-offspring conflict among birds, peace through vaccine diplomacy, ocean versus land biodiversity, and more.

SCIENCEINSIDER
blogs.sciencemag.org/scienceinsider
Science Policy News and Analysis

SCIENCE (ISSN 0036-8075) is published weekly on Friday, except the last week in December, by the American Association for the Advancement of Science, 1200 New York Avenue, NW, Washington, DC 20005. Periodicals Mail postage (publication No. 484460) paid at Washington, DC, and additional mailing offices. Domestic individual membership and subscription (51 issues): $146 ($74 allocated to subscription). Domestic institutional subscription (51 issues): $910; Foreign postage extra: Mexico, Caribbean (surface mail) $55; other countries (air assist delivery) $85. First class, airmail, student, and emeritus rates on request. Canadian rates with GST available upon request, GST #1254 88122. Publications Mail Agreement Number 1069624. **Printed in the U.S.A.**

Change of address: Allow 4 weeks, giving old and new addresses and 8-digit account number. **Postmaster:** Send change of address to AAAS, P.O. Box 96178, Washington, DC 20090–6178. **Single-copy sales:** $10.00 current issue, $15.00 back issue prepaid includes surface postage; bulk rates on request. **Authorization to photocopy** material for internal or personal use under circumstances not falling within the fair use provisions of the Copyright Act is granted by AAAS to libraries and other users registered with the Copyright Clearance Center (CCC) Transactional Reporting Service, provided that $20.00 per article is paid directly to CCC, 222 Rosewood Drive, Danvers, MA 01923. The identification code for *Science* is 0036-8075. *Science* is indexed in the *Reader's Guide to Periodical Literature* and in several specialized indexes.

AAAS
ADVANCING SCIENCE, SERVING SOCIETY

CREDIT: CHRIS BICKEL/AAAS

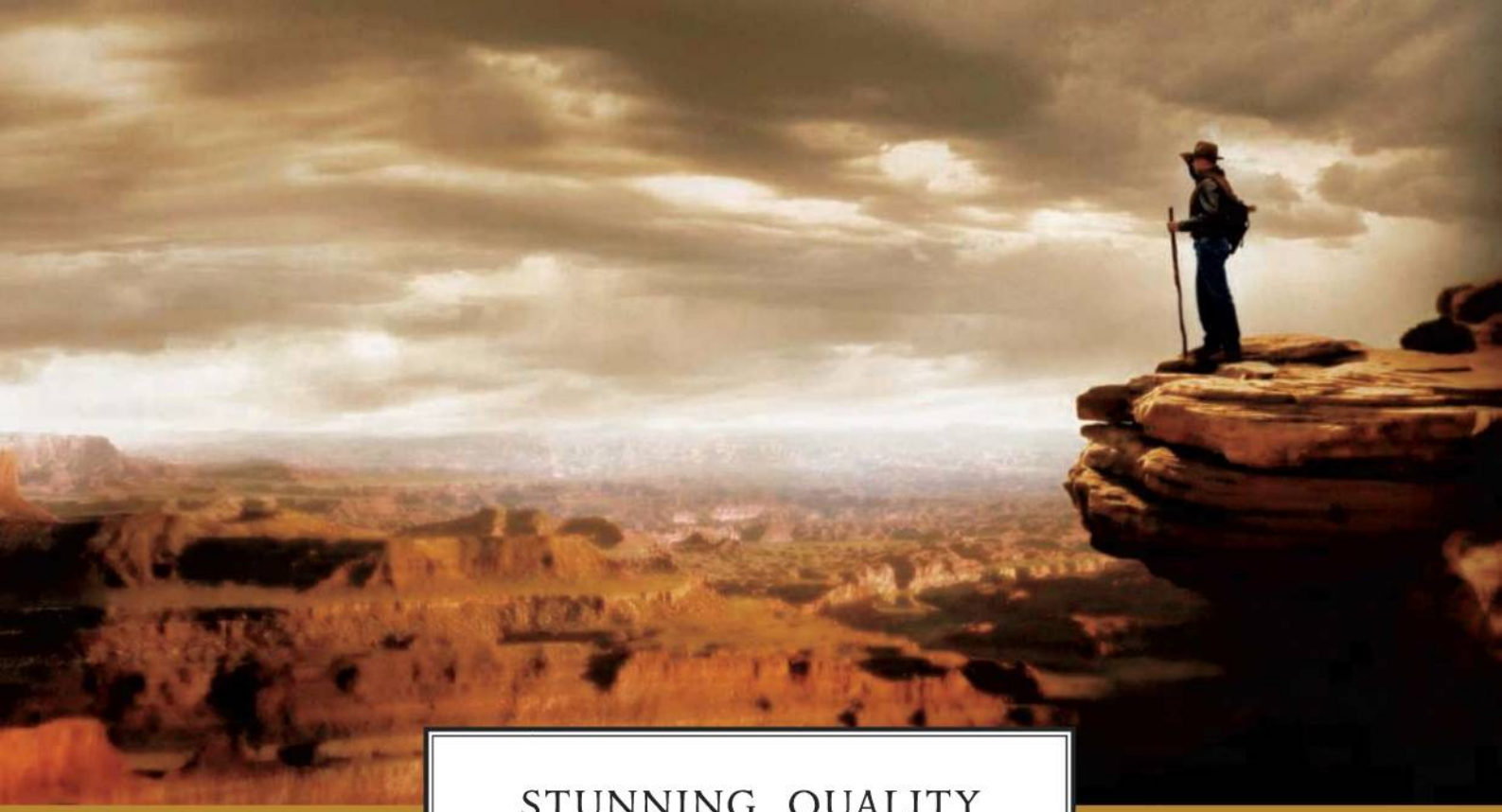

STUNNING QUALITY

Reagents for Sample Preparation from New England Biolabs

Introducing NEBNext™, a series of highly pure reagents that facilitate sample preparation for downstream applications such as next generation sequencing and expression library construction. Available in sets, master mixes and modules, these robust reagents undergo stringent quality controls and functional validation, ensuring maximum yield, convenience and value.

Sequencing coverage map of the *E. coli* genome after using NEBNext™ DNA Sample Prep Reagent Set 1 for Sample Preparation

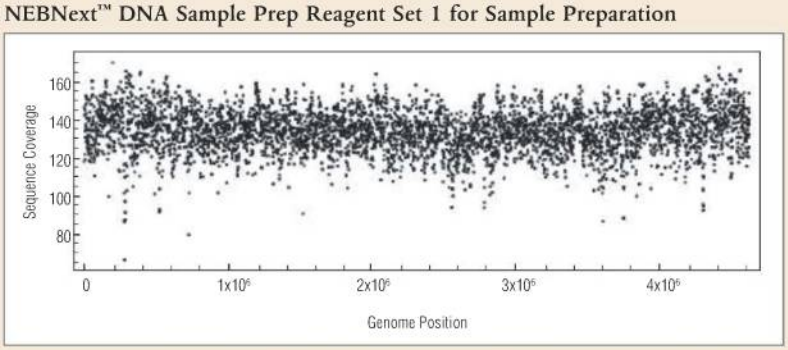

E. coli strain MG1655 gDNA was prepared with NEBNext DNA Sample Prep Reagent Set I and sequenced on an Illumina Genome Analyzer II.

For more information about NEBNext, including customized solutions, please contact NEBNext@neb.com.

Now available:
NEBNext™ dsDNA Fragmentase™
an enzyme-based solution for the fragmentation of DNA

CELEBRATING 35 YEARS
NEW ENGLAND BioLabs® Inc.
enabling technologies in the life sciences

CLONING & MAPPING	**DNA AMPLIFICATION & PCR**	RNA ANALYSIS	PROTEIN EXPRESSION & ANALYSIS	GENE EXPRESSION & CELLULAR ANALYSIS

www.neb.com

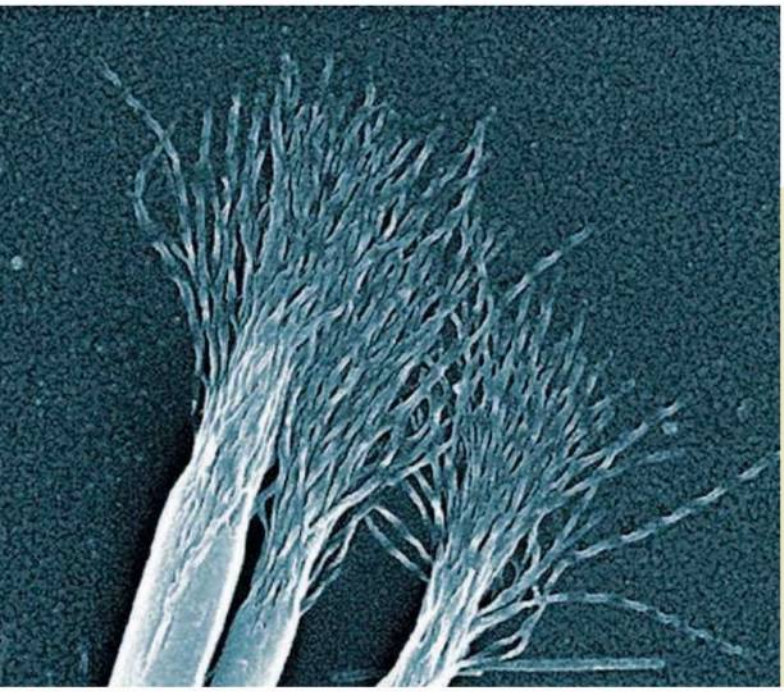

<< Nanoparticles, Lightly Twisted

The helical structures that are widespread in natural macromolecules result from well-coordinated bonding interactions and affect their physical properties in striking ways. To obtain helical nanoparticles, **Srivastava *et al.*** (p. 1355, published online 11 February) slowly oxidized cadmium-tellurium under visible light and assembled ribbons of nanostructure. The ribbons were persuaded to twist into helices because they were doped with cadmium sulfide nanoparticles, which underwent surface oxidation and caused localized stresses that could only be relieved by a conformational change. The pitch of the twisted ribbons that were produced could be controlled by the intensity of illumination applied. This behavior offers promise for application in the development of materials with interesting optical properties.

Thalidomide Teratogenicity Target

In the late 1950s and early 1960s, thalidomide was prescribed to pregnant women as a cure for morning sickness, but it was then found to have developmental defects, most obviously, stunted limbs in thousands of babies. Although its use was banned worldwide, thalidomide has since been found to be a valuable treatment for a range of cancers, inflammatory disorders, and leprosy. Several hypotheses have been proposed, but the mechanism of action of thalidomide is unknown. Using zebrafish and chicken as animal models, **Ito *et al.*** (p. 1345) show that the protein cereblon is a primary target of thalidomide. Thalidomide exerts teratogenic effects by binding to cereblon and inhibiting associated enzymatic activity important for limb development. Knowing the mechanism of action of thalidomide should encourage the search for thalidomide derivatives without teratogenic activity.

Scattered and Coupled

Cavity electrodynamics explores the coupling of light with matter—ideally, that of a single photon with a single atom. Typically, this requires that the photon and the atom be confined to increase the likelihood of interaction, but scattering of light is an unavoidable product of an engineered device and is usually considered to be detrimental because it leads to loss of the photons from the cavity. **Sapienza *et al.*** (p. 1352; see the Perspective by **Wiersma**) saw extreme light scattering as an opportunity for the spontaneous generation of localized modes of light that can be exploited to induce light-matter coupling. Thus, working with a process where scattering is considered a resource rather than a nuisance, as in this case, may prove useful for realizing robust quantum information devices.

Slightly Cracked

While there are detailed theories to explain the propagation of a crack in the bulk of a material, our understanding of cracking breaks down near the tip of the crack. Experimentally, it is very hard to observe the propagation of a crack at the tip region because it tends to move very quickly. **Livne *et al.*** (p. 1359) approached this problem by working with a polyacrylamide gel in which cracks progress slowly enough to monitor them. A hierarchy of linear and nonlinear regions was observed through which energy is transported before being dissipated by the growing crack. How stresses are distributed during cracking will determine whether the resulting failure will be brittle or ductile.

Speak to Me, Mama

Maternal effects are effects of the mother (for example, hormones) on her offspring that are independent of genetic inheritance, but related to the mother's phenotype and her environment. Despite their universal occurrence, little is known about the evolutionary influence of maternal effects. **Hinde *et al.*** (p. 1373; see the cover) modeled maternal effects in birds and showed that nestling begging, as well as provoking feeding, also provides parents with information about offspring vigor. Conversely, maternal effects provide information to the unborn offspring about parental quality. Experimental studies with canaries provided support for the theoretical predictions, and together these studies show that parent-offspring conflict (that is, the conflict between the offspring for its immediate needs and the need of the parent to conserve resources for any future offspring) is resolved by the reciprocal exchange of information before and after birth. Hormonal signaling ensures a match between parental capacity for resource provisioning and offspring behavior and development after hatching that meet the mother's capacity to provide resources.

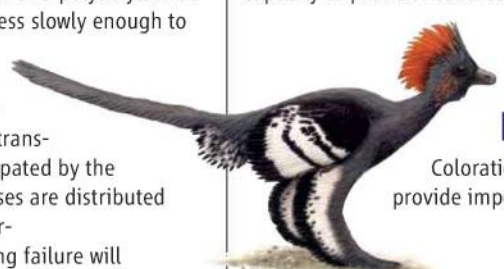

Dinosaur Plumage

Coloration and appearance provide important behavioral and evolutionary information in animals. However, for the most part, we do not know the coloration of fossil terrestrial animals. **Li *et al.*** (p. 1369, published online 4 February) have reconstructed the appearance of a theropod dinosaur by mapping features of its well-preserved feathers and comparing them with modern samples from birds. Feather color is partly determined by melanosome density and shape, and this information is preserved in a recently discovered fossil from China. The dinosaur was gray with white limbs and had a reddish crest and a speckled face.

Continued on page 1299

CREDITS (TOP TO BOTTOM): S. SRIVASTAVA, N. KOTOV/UNIVERSITY OF MICHIGAN; LI *ET AL.*

Call for Papers

Science Translational Medicine

Integrating Medicine and Science

Science Translational Medicine, from AAAS, the publisher of *Science*, focuses on the conversion of basic biomedical research into practical applications, thus bridging the research-to-application gap, linking basic scientists and researchers.

Submit your manuscripts for review in the following areas of translational medicine:

- Cardiovascular Disease
- Neuroscience/Neurology/ Psychiatry
- Infectious Diseases
- Cancer
- Health Policy
- Bioengineering
- Chemical Genomics/ Drug Discovery
- Applied Physical Sciences
- Drug Delivery
- Gene Therapy/ Regenerative Medicine
- Cell Culture, Animal, and Human Studies
- Other Interdisciplinary Approaches to Medicine

Submit your research at www.submit2scitranslmed.org

Subscribing to ***Science Translational Medicine*** ensures that you and your lab have the latest translational medicine resources. For more information, visit **ScienceTranslationalMedicine.org**

For more information see ScienceTranslationalMedicine.org or contact scitranslmededitors@aaas.org

Science Translational Medicine
AAAS

ScienceTranslationalMedicine.org

Continued from page 1297

Titan Through to the Core

Gravity measurements acquired from orbiting spacecraft can provide useful information about the interior of planets and their moons. **Iess *et al.*** (p. 1367; see the Perspective by **Sohl**) used gravity data from four flybys of the Cassini spacecraft past Saturn's moon, Titan, to model the moon's gravity field and probe its deep interior structure. Their analysis implies that Titan is a partially differentiated body with a core consisting of a mix of ice and rock or hydrated silicates.

Moving Signals

Many types of human breast cancers overexpress a cell-surface receptor—EphA2—a tyrosine kinase activated by the ligand ephrin-A1 present on adjoining cells. **Salaita *et al.*** (p. 1380; see the Perspective by **Paszek and Weaver**) studied the regulation of mechanically stimulated EphA2 signaling by inducing intermembrane signaling between living EphA2-expressing human breast cancer cells and supported membranes displaying laterally mobile ephrin-A1. When the receptors engaged their ligands, they formed clusters that moved radially to the junction between the cells and the membranes. Physically impeding this movement altered the cellular response to ephrin-A1. Different breast cancer cell lines showed differences in receptor movement that correlated with their invasion potential, and might indicate their capacity for metastasis formation.

Diheme Conversion

A dehydrogenase enzyme found in methylotrophic and autotrophic bacteria, which converts methylamine to ammonia and formaldehyde, must be posttranslationally modified to create a covalently bound cofactor. Synthesis of the cofactor is completed by a diheme enzyme, MauG, which oxidatively links two tryptophan residues to form tryptophan tryptophylquinone. **Jensen *et al.*** (p. 1392; see the Perspective by **Bollinger and Matthews**) describe the crystal structure of a catalytically competent complex of MauG bound to the methylamine dehydrogenase precursor. The reactive tryptophans are buried and well-separated from both heme irons. The heme closest to the nascent tryptophylquinone site is a 6-coordinate with an unusual His-Tyr axial link. The axial Tyr likely stabilizes a *bis*-Fe(IV) state involved in catalysis. Two other tyrosine residues are positioned to participate in long-range interprotein electron and radical transfer.

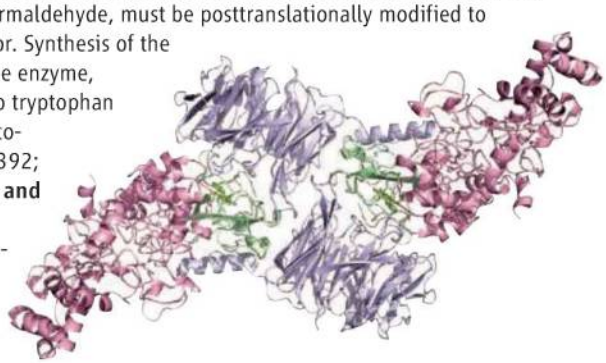

CREDIT: JENSEN *ET AL.*

Hair Today, Skin Tomorrow

The epidermis of mammals contains hair follicles, sebaceous glands, and interfollicular epidermis, but it has not been clear how the development and repair of these structures is regulated. **Snippert *et al.*** (p. 1385) show that a stem-cell cluster in the hair follicle, characterized by the expression of Lgr6, a close homolog of the Lgr5 marker for stem cells in the small intestine and colon, resides directly above the hair bulge and gives rise to all cell lineages of the skin. Skin wounds in adult mice are repaired by Lgr6 stem cells in the hair follicles that flank the damage. After hair morphogenesis, Lgr6 stem cells give rise to epidermal and sebaceous gland lineages to generate fully differentiated new skin.

Steady As She Blows

A fundamental characteristic of many biological control networks is the capacity to maintain the concentration of a particular component at steady state within a narrow range, in spite of variations in the amounts of other network components that might change as a result of environmental variables in the state of a cell. In a mathematical analysis, **Shinar and Feinberg** (p. 1389) reveal the essential requirements of a network robust to perturbation. Using this method, the sources of robustness in two bacterial systems—one that functions in osmoregulation and another that controls carbon flux in metabolism—were explained.

What is your taste?

BGI'S GENOMICS BAR

华大基因 BGI

tech@genomics.cn
www.genomics.cn
86-755-25273395

Would 128 Illumina HiSeq 2000 Sequencing Systems, 500 bioinformaticians and the use of cutting-edge software programs developed by BGI satisfy your taste?

One of the world's biggest genome centers is looking for collaborators!

Peter J. Hotez is Distinguished Research Professor at the George Washington University and president of the Sabin Vaccine Institute in Washington, DC. E-mail: photez@gwu.edu

Peace Through Vaccine Diplomacy

CAN VACCINATIONS HELP TO RESOLVE CONFLICTS AND NURTURE DIPLOMACY? LATER THIS MONTH, Indonesia, the world's most populous Islamic country, will host U.S. President Obama, a visit that could establish important scientific ties between the United States and Indonesia and implement a potentially powerful piece of vaccine diplomacy.

The oral polio vaccine is a substantive example of how vaccination diplomacy has driven cooperation in times of crisis, allowing groups and states to put aside ideological differences to eradicate disease. Even today, the Taliban leader in Afghanistan is cooperating with the Afghan government and United Nations agencies to eradicate polio in Afghanistan.* There is now an unprecedented opportunity to lock the United States and Islamic nations into a meaningful program of vaccine R&D and potentially improve foreign relations and promote peace.

When the United States and Soviet Union entered a deep Cold War chill after the 1957 Sputnik launch, they also entered into a little-known scientific collaboration that led to one of the most important medical advances of the 20th century. With both countries suffering horrific epidemics of childhood poliomyelitis, Soviet and U.S. scientists, led by Albert Sabin, worked together to develop an oral polio vaccine that was deployed worldwide and ultimately eliminated the disease in most of the world by 2008 (the disease still persists in Afghanistan, India, Pakistan, and Nigeria). Similar international cooperative efforts with the Soviet Union led to an improved vaccine that eradicated naturally occurring smallpox by 1977.

Today, up to one-half of the world's neglected tropical diseases occur in Islamic countries, mainly Indonesia, Pakistan, Nigeria, Bangladesh, Sudan, and to some extent Afghanistan, Iran, and Iraq. The most common of these diseases, including hookworm infection, schistosomiasis, and leishmaniasis are notorious for more than their long-term disabling health effects. Impaired healthy development adversely affects rural worker productivity and can lead to agricultural insecurity, a condition that increases the likelihood of conflict among groups and states.

Although more than one billion people suffer from neglected tropical diseases, the corresponding vaccines have essentially no commercial market, relegating their development to nonprofit product development partnerships funded by sources such as the Bill & Melinda Gates Foundation, the Wellcome Trust, and the U.S. National Institutes of Health. Recently, the pharmaceutical giants Novartis and Merck also initiated global health vaccine development partnerships. But more needs to be done. Joint scientific cooperation between the United States and technologically advanced member countries of the Organisation of the Islamic Conference (OIC)—especially the Asian OIC nations of Indonesia, Pakistan, and Malaysia, and selected Middle Eastern countries—could advance vaccine development for treating neglected tropical diseases in Islamic countries. Indeed, leishmaniasis vaccines are under development in Iran, but these efforts would benefit from greater cooperation with scientific institutions in the West.

Last year, the Obama Administration launched a new Science Envoy program to Islamic nations to foster scientific collaboration in ways that address economic, social, and ecological challenges.** In that connection, a vigorous new program of vaccine R&D diplomacy could create opportunities for the United States to address the world's most terrible disease scourges while simultaneously creating a new foreign policy venue. The globally beneficial legacy of the oral polio vaccine should spur the United States and its international product development partnerships to connect with scientists in the Islamic world and produce a new generation of life-saving products. The incentive and opportunity to improve international public health, reduce poverty, and promote global security have never been so clear. **– Peter J. Hotez**

10.1126/science.1189028

*Y. Trofimov, *Wall Street Journal*, 15 January 2010, p. A14. **R. Koenig, *Science* **326**, 920 (2009).

It's more than genetic analysis.
It's the unstoppable drive to know more.
To find answers. To be the first.

The power of sequencing. The speed of arrays.
Limitless applications harnessed with intensity
and implemented with imagination.

The intangible force that fuels the
dynamic Illumina Community.

That's

genetic energy™

www.illumina.com/geneticenergy

illumina®

ECOLOGY

Collecting Coral

The global decline in reef-building corals and the many threats to coral reefs are well documented, but proven practical solutions that prevent coral loss and increase reef resilience are lacking. Marine protected areas are a potential tool to enable local and regional managers to conserve corals. Selig and Bruno have now confirmed that marine protected areas can delay the loss of coral cover from tropical reef systems relative to unprotected areas undergoing reductions in coral cover. Differences were observed among regions in the effectiveness of marine protected areas, probably due to the differences in the locations of establishment as well as regional enforcement, but, on the whole, the protected areas tended to show a reduced decline in coral. Marine protected areas needed time to stabilize and become effective—most did not prevent coral loss until they were at least 5 to 15 years old. Thus, long-term benefits can be obtained by the establishment of protected areas. — LMZ

PLoS ONE 10.1371/journal.pone.0009278 (2010).

GEOCHEMISTRY

Split When the Going Gets Hot

When magma within Earth cools, minerals precipitate according to their crystallization temperatures. Because the isotopic distribution of elements within the resultant mineral grains is assumed to be relatively stable at high temperatures, this information has been used to estimate the composition of the parent melt and also to deduce the region in Earth's interior where the grains formed. However, Huang *et al.* observed mass-dependent calcium isotope fractionation between two different silicate mineral phases (orthopyroxene and clinopyroxene) in peridotite rocks from the upper mantle. This fractionation, which was previously observed only at low temperatures between seawater and calcite, probably depends on Ca-O bond strengths and not kinetic processes related to isotopic diffusion. These measurements provide a robust estimate for Ca isotope composition of the upper mantle, which can be used to make comparisons of isotopic abundances between other former melts in the solar system, such as the Moon and meteorites. — NW

Earth Planet. Sci. Lett. 10.1016/j.epsl.2010.01.042 (2010).

ASTRONOMY

Bursting Expectations

The gamma-ray burst GRB 090423 is the most distant astronomical object known. Chandra *et al.* detected its radio afterglow using the Very Large Array radio astronomy observatory. In combination with previous x-ray and infrared measurements, the data imply that the amount of energy released by GRB 090423 and the properties of its afterglow are not sufficiently different from those of less distant gamma-ray bursts to implicate a different type of progenitor star. Thus, even though GRB 090423 occurred only 630 million years after the Big Bang, there is no reason to believe its progenitor star belonged to the initial generation of metal-free stars, which are thought to have been brighter, hotter, and more massive than stars today. Regardless of distance, there is evidence that long-duration gamma-ray bursts occur preferentially in low-metallicity environments, as expected from stellar evolution theory. Using the Keck telescope, Levesque *et al.* acquired spectra of the host galaxy and explosion site of GRB 020819—an unusual long-duration gamma-ray burst originally detected in 2002, with no optical afterglow—and their data imply that the burst did occur in a high-metallicity environment. — MJC

Astrophys. J. **712**, L31; L26 (2010).

CELL BIOLOGY

p75 Goes Nuclear

The p75 neurotrophin receptor binds to all members of the neurotrophin family, which promote differentiation, growth, and survival of diverse cell types in the nervous system. On its own, p75 can also produce signals, which appear to require its proteolysis by a presenilin-dependent γ-secretase. In the case of the receptor Notch, such cleavage produces an intracellular domain (ICD) fragment that moves to the nucleus to regulate gene expression. Parkhurst *et al.* present evidence that the p75 ICD may similarly regulate gene expression. A fusion protein was produced with p75 linked to a transcriptional activator that would cause expression of green fluorescent protein (GFP) if the cleaved fragment of the receptor reached the nucleus. Production of GFP was indeed detected in human cells transfected with the receptor construct, which was prevented by inhibition of γ-secretase. In PC12 cells (a cell line with neuronal characteristics), the endogenous p75 protein ICD fragment was detected in the nucleus.

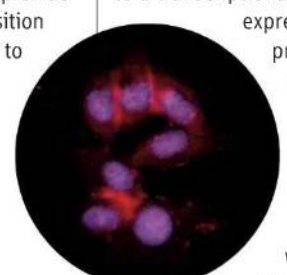

Continued on page 1305

CREDITS (TOP TO BOTTOM): WILLIAM CROSSE/CONSERVATION INTERNATIONAL; PARKHURST *ET AL.*, *J. BIOL. CHEM.* **285**, 5361 (2010)

Forget DNA purification

Choose Direct PCR

Take the direct route from sample to results

Finnzymes' Direct PCR approach saves you time and cost by allowing amplification of DNA directly from the source material. No DNA purification is needed. Direct PCR is suitable for various kinds of sample materials such as plant and animal tissues, blood, and FFPE tissue samples.

Direct PCR is based on Finnzymes' unique PCR enzymes, Phusion® High-Fidelity and Phire® Hot Start DNA Polymerases. These polymerases are exceptionally tolerant of many PCR inhibitors. To achieve the shortest possible protocols, combine the Direct PCR approach with Finnzymes' Piko® Thermal Cyclers and UTW® reaction vessels.

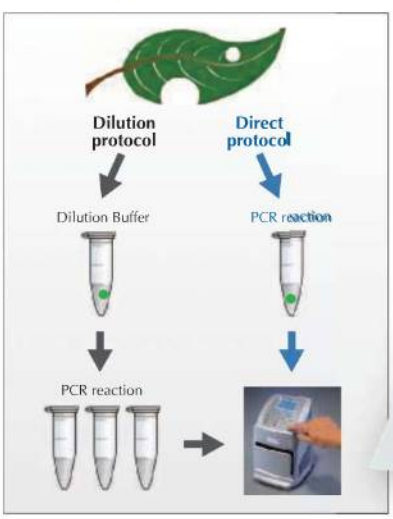

NEW!

Optimized kits available:

Phire® Plant Direct PCR Kit
for plant material

Phire® Animal Tissue Direct PCR Kit
for various animal tissues

Phusion® Blood Direct PCR Kit
for blood

See the latest results, application notes and product updates at www.finnzymes.com/directpcr

NEW ENGLAND BioLabs inc.
enabling technologies in the life sciences

Reagents distributed in US and Canada by New England Biolabs.
For other products and countries visit www.finnzymes.com

FINNZYMES
TOOLS FOR MOLECULAR BIOLOGY

Continued from page 1303

Furthermore, the p75 ICD associated with the promoter of the cyclin E1 gene when PC12 cells were treated with nerve growth factor for 3 hours. The ICD can interact with multiple intracellular proteins and may thus influence numerous signaling events. Thus, a primary action of the p75 ICD (and possibly fragments of the related receptors) may be direct regulation of transcription in the nucleus. — LBR

J. Biol. Chem. **285**, 5361 (2010).

PHYSICS

A Coherent Sonic Boom Box

This year marks the 50th anniversary of the invention of the laser, which now has an extraordinarily diverse and growing range of applications, from consumer electronics to the highest-precision metrology. Two independent studies using quite different approaches now report successful coherent sound wave amplification, in which mechanical vibrations are produced by processes that mimic stimulated light emission in laser operation. Grudinin *et al.* use a coupled optomechanical resonator system in which excitation by an optical laser induces mechanical oscillations. Above a critical threshold power of the pump laser, amplification and gain of the mechanical oscillations are observed, producing coherent sound from radio to microwave frequencies. Beardsley *et al.* use a superlattice semiconductor system to which an electric field is applied. Precise tuning of the superlattice structure produces coherent sound at several hundred GHz, in range of the clothes-penetrating THz scanners being rolled out at airports. The ability to produce intense and coherent beams of sound in these frequency ranges should find immediate application in the imaging technology sector. — ISO

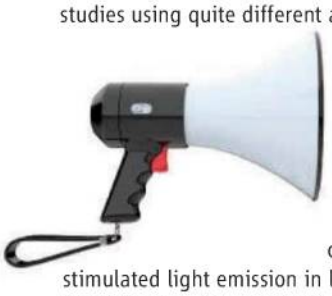

CREDIT: PHOTOS.COM

Phys. Rev. Lett. **104**, 83901; 85501 (2010).

CANCER

Enzymes Adopt New M.O. in Cancer

Identification of genes that are recurrently mutated in human tumors can potentially lead to new cancer treatments, but first we need to understand how the mutations alter the biochemical activity of the encoded protein and contribute to tumor development and progression. The recent discovery that a subset of human brain tumors harbor mutations in the gene encoding isocitrate dehydrogenase 1 (IDH1) has focused interest on this cytosolic metabolic enzyme and its mitochondrial homolog IDH2. Mutations in these genes have been detected in acute myeloid leukemia that always alter the same amino acid in the enzymes' catalytic sites and are always present in heterozygous form, suggesting that tumor cells contain "normal," as well as mutant, versions of the enzymes. Ward *et al.* and Dang *et al.* now show how the tumor-associated mutations alter the biochemical activity of IDH1 and IDH2. The mutant enzymes not only lose their normal activity (the conversion of isocitrate to α-ketoglutarate) but also acquire a new activity: the reduction of α-ketoglutarate to 2-hydroxyglutarate. Indeed, elevated levels of 2-hydroxyglutarate were detected in human tumor samples that contained either IDH1 or IGH2 mutations. Determining how 2-hydroxyglutarate, a so-called "oncometabolite," contributes to the biology of brain tumors and leukemia will be an important next step in moving from mutant gene to therapy. — PAK

Cancer Cell **17**, 1 (2010); *Nature* **462**, 739 (2009).

DEVELOPMENT

Methylation Map

Epigenetic modification, such as DNA methylation at CpG sequences, functions in normal cell differentiation and development. Dysregulation of DNA methylation is associated with altered gene expression and disease. Now Laurent *et al.* have used bisulfite sequencing technology and bioinformatices to identify whole-genome DNA methylation maps with single–base pair resolution for three cell types at various stages of differentiation: human embryonic stem cells (hESs), neonatal fibroblasts, and a fibroblast derivative from hESs. These maps were compared to those of mature peripheral blood mononuclear cells. Methylation of CpGs, and to a lesser degree CpAs, was higher in the gene body and lower in promoter regions. At areas of higher DNA methylation, there was depressed binding of histone H3 trimethylation. Furthermore, the pattern of methylation around exons and introns suggests a possible role in regulation of mRNA splicing. Overall, methylation decreased with differentiation progression; however, many differentially methylated regions, some of which are key pluripotency and differentiation-associated genes, increased methylation during differentiation. — BAP

Genome Res. 10.1101/gr.101907.109 (2010).

www.sciencemag.org

Science

1200 New York Avenue, NW
Washington, DC 20005
Editorial: 202-326-6550, FAX 202-289-7562
News: 202-326-6581, FAX 202-371-9227
Bateman House, 82-88 Hills Road
Cambridge, UK CB2 1LQ
+44 (0) 1223 326500, FAX +44 (0) 1223 326501

Subscription Services For change of address, missing issues, new orders and renewals, and payment questions: 866-434-AAAS (2227) or 202-326-6417, FAX 202-842-1065. Mailing addresses: AAAS, P.O. Box 96178, Washington, DC 20090-6178 or AAAS Member Services, 1200 New York Avenue, NW, Washington, DC 20005

Institutional Site Licenses please call 202-326-6755 for any questions or information

Reprints: Author Inquiries 800-635-7181
Commercial Inquiries 803-359-4578

Permissions 202-326-7074, FAX 202-682-0816

Member Benefits AAAS/Barnes&Noble.com bookstore www.aaas.org/bn; AAAS Online Store www.apisource.com/aaas/ code MKB6; AAAS Travels: Betchart Expeditions 800-252-4910; Apple Store www.apple.com/eppstore/aaas; Bank of America MasterCard 1-800-833-6262 priority code FAA3YU; Cold Spring Harbor Laboratory Press Publications www.cshlpress.com/affiliates/aaas.htm; GEICO Auto Insurance www.geico.com/landingpage/go51.htm?logo=17624; Hertz 800-654-2200 CDP#343457; Office Depot https://bsd.officedepot.com/portalLogin.do; Seabury & Smith Life Insurance 800-424-9883; Subaru VIP Program 202-326-6417; VIP Moving Services www.vipmayflower.com/domestic/index.html; Other Benefits: AAAS Member Services 202-326-6417 or www.aaasmember.org.

science_editors@aaas.org	(for general editorial queries)
science_letters@aaas.org	(for queries about letters)
science_reviews@aaas.org	(for returning manuscript reviews)
science_bookrevs@aaas.org	(for book review queries)

Published by the American Association for the Advancement of Science (AAAS), *Science* serves its readers as a forum for the presentation and discussion of important issues related to the advancement of science, including the presentation of minority or conflicting points of view, rather than by publishing only material on which a consensus has been reached. Accordingly, all articles published in *Science*—including editorials, news and comment, and book reviews—are signed and reflect the individual views of the authors and not official points of view adopted by AAAS or the institutions with which the authors are affiliated.

AAAS was founded in 1848 and incorporated in 1874. Its mission is to advance science, engineering, and innovation throughout the world for the benefit of all people. The goals of the association are to: enhance communication among scientists, engineers, and the public; promote and defend the integrity of science and its use; strengthen support for the science and technology enterprise; provide a voice for science on societal issues; promote the responsible use of science in public policy; strengthen and diversify the science and technology workforce; foster education in science and technology for everyone; increase public engagement with science and technology; and advance international cooperation in science.

Information for Authors
See pages 352 and 353 of the 15 January 2010 issue or access www.sciencemag.org/about/authors

EDITOR-IN-CHIEF **Bruce Alberts**
EXECUTIVE EDITOR **Monica M. Bradford** NEWS EDITOR **Colin Norman**
MANAGING EDITOR, RESEARCH JOURNALS **Katrina L. Kelner**
DEPUTY EDITORS **R. Brooks Hanson, Barbara R. Jasny, Andrew M. Sugden**

Editorial senior editors/commentary Lisa D. Chong, Brad Wible; **senior editors** Gilbert J. Chin, Pamela J. Hines, Paula A. Kiberstis (Boston), Marc S. Lavine (Toronto), Beverly A. Purnell, L. Bryan Ray, Guy Riddihough, H. Jesse Smith, Phillip D. Szuromi (Tennessee), Valda Vinson, Jake S. Yeston; **associate editors** Kristen L. Mueller, Jelena Stajic, Nicholas S. Wigginton, Laura M. Zahn; **research associate** Alexis Wynne Mogul; **online editor** Stewart Wills; **associate online editors** Robert Frederick, Tara S. Marathe; **web content developers** Martyn Green, Andrew Whitesell; **book review editor** Sherman J. Suter; **associate letters editor** Jennifer Sills; **editorial manager** Cara Tate; **senior copy editors** Jeffrey E. Cook, Cynthia Howe, Harry Jach, Barbara P. Ordway, Trista Wagoner; **copy editors** Chris Filiatreau, Lauren Kmec; **editorial coordinators** Carolyn Kyle, Beverly Shields; **publications assistants** Ramatoulaye Diop, Joi S. Granger, Jeffrey Hearn, Lisa Johnson, Scott Miller, Jerry Richardson, Jennifer A. Seibert, Brian White, Anita Wynn; **editorial assistants** Emily Guise, Michael Hicks, Patricia M. Moore, Miriam Weinberg; **executive assistants** Alison Crawford, Sylvia S. Kihara; **administrative support** Maryrose Madrid; **editorial fellow** Melissa R. McCartney

News deputy news editors Robert Coontz, Eliot Marshall, Jeffrey Mervis, Leslie Roberts; **contributing editors** Elizabeth Culotta, Polly Shulman; **news writers** Yudhijit Bhattacharjee, Adrian Cho, Jennifer Couzin, David Grimm, Constance Holden, Jocelyn Kaiser, Richard A. Kerr, Eli Kintisch, Greg Miller, Elizabeth Pennisi, Robert F. Service (Pacific NW), Erik Stokstad, Jue Wang; **intern** Lauren Schenkman; **contributing correspondents** Jon Cohen (San Diego, CA), Daniel Ferber, Ann Gibbons, Sam Kean, Robert Koenig, Andrew Lawler, Mitch Leslie, Charles C. Mann, Virginia Morell, Gary Taubes; **copy editors** Linda B. Felaco, Melvin Gatling, Melissa Raimondi; **administrative support** Scherraine Mack; **bureaus** San Diego, CA: 760-942-3252, FAX 760-942-4979; Pacific Northwest: 503-963-1940

Production director James Landry; **senior manager** Wendy K. Shank; **assistant manager** Rebecca Doshi; **senior specialists** Steve Forrester, Chris Redwood; **specialist** Anthony Rosen; **Preflight director** David M. Tompkins; **manager** Marcus Spiegler; **specialist** Jason Hillman

Art director Yael Kats; **associate art director** Laura Creveling; **senior illustrators** Chris Bickel, Katharine Sutliff; **illustrator** Yana Greenman; **senior art associates** Holly Bishop, Preston Huey, Nayomi Kevitiyagala; **art associates** Kay Engman, Matthew Twombly; **photo editor** Leslie Blizard

***Science* International**

Europe (science@science-int.co.uk) **editorial: international managing editor** Andrew M. Sugden; **senior editor/commentary** Julia Fahrenkamp-Uppenbrink; **senior editors** Caroline Ash, Stella M. Hurtley, Ian S. Osborne, Peter Stern; **associate editor** Maria Cruz; **locum editor** Helen Pickersgill; **editorial support** Deborah Dennison, Rachel Roberts, Alice Whaley; **administrative support** John Cannell, Janet Clements, Louise Hartwell; **news: europe news editor** John Travis; **deputy news editor** Daniel Clery; **contributing correspondents** Michael Balter (Paris), John Bohannon (Vienna), Martin Enserink (Amsterdam and Paris), Gretchen Vogel (Berlin); **intern** Tim Wogan

Latin America contributing correspondent Antonio Regalado

Asia Japan Office: Asca Corporation, Tomoko Furusawa, Rustic Bldg. 7F, 77 Tenjin-cho, Shinjuku-ku, Tokyo 162-0808, Japan; +81 3 6802 4616, FAX +81 3 6802 4615, inquiry@sciencemag.jp; **asia news editor** Richard Stone (Beijing: rstone@aaas.org); **contributing correspondents** Dennis Normile [Japan: +81 (0) 3 3391 0630, FAX +81 (0) 3 5936 3531; dnormile@gol.com]; Hao Xin [China: +86 (0) 10 6307 4439 or 6307 3676, FAX +86 (0) 10 6307 4358; cindyhao@gmail.com]; Pallava Bagla [South Asia: +91 (0) 11 2271 2896; pbagla@vsnl.com]

EXECUTIVE PUBLISHER **Alan I. Leshner**
PUBLISHER **Beth Rosner**

Fulfillment Systems and Operations (membership@aaas.org); **director** Waylon Butler; **customer service supervisor** Pat Butler; **specialists** Latoya Casteel, LaVonda Crawford, Vicki Linton, April Marshall; **data entry supervisor** Cynthia Johnson; **specialists** Shirlene Hall, Tarrika Hill, William Jones

Business Operations and Administration director Deborah Rivera-Wienhold; **business systems and financial analysis director** Randy Yi; **manager, business analysis** Eric Knott; **manager, business operations** Jessica Tierney; **financial analysts** Priti Pamnani, Celeste Troxler; **rights and permissions: administrator** Emilie David; **associate** Elizabeth Sandler; **marketing director** Ian King; **marketing managers** Allison Pritchard, Alison Chandler, Julianne Wielga; **marketing associates** Aimee Aponte, Mary Ellen Crowley, Wendy Wise; **senior marketing executive** Jennifer Reeves; **director, site licensing** Tom Ryan; **director, corporate relations** Eileen Bernadette Moran; **publisher relations, eresources specialist** Kiki Forsythe; **senior publisher relations specialist** Catherine Holland; **publisher relations, east coast** Phillip Smith; **publisher relations, west coast** Philip Tsolakidis; **fulfillment supervisor** Iquo Edim; **fulfillment coordinator** Carrie MacDonald; **marketing manager** Christina Schlecht; **electronic media: manager** Lizabeth Harman; **project manager** Trista Snyder; **assistant manager** Lisa Stanford; **senior production specialists** Ryan Atkins, Christopher Coleman, **computer specialist** Walter Jones; **production specialists** Nichele Johnston, Kimberly Oster; **director, web and new media** Will Collins

advertising director, worldwide ad sales Bill Moran
commercial editor Sean Sanders: 202-326-6430
project director, outreach Brianna Blaser

Product (science_advertising@aaas.org); **midwest** Rick Bongiovanni: 330-405-7080, FAX 330-405-7081; **east coast/e. canada** Laurie Faraday: 508-747-9395, FAX 617-507-8189; **west coast/w. canada** Lynne Stickrod: 415-931-9782, FAX 415-520-6940; **uk/europe/asia** Roger Goncalves: TEL/FAX +41 43 243 1358; **japan** ASCA Corporation, Nanako Ide +81 (0) 3 6802 4616, FAX +81 (0) 3 6802 4615; ads@sciencemag.jp; **senior traffic associate** Deiandra Simms

worldwide associate director of *Science* Careers Tracy Holmes: +44 (0) 1223 326525, FAX +44 (0) 1223 326532

Classified (advertise@sciencecareers.org); **u.s.: sales manager** Daryl Anderson: 202-326-6543; **midwest** Tina Burks: 202-326-6577; **east coast** 202-326-6543; **west/south central** Nicholas Hintibidze: 202-326-6533; **sales coordinators** Rohan Edmonson, Shirley Young; **sales** Susanne Kharraz, Dan Pennington, Alex Palmer; **sales assistant** Lisa Patterson; **japan** ASCA Corporation, Jie Chin +81 (0) 3 6802 4616, FAX +81 (0) 3 6802 4615; careerads@sciencemag.jp; **advertising support manager** Karen Foote: 202-326-6740; **advertising production operations manager** Deborah Tompkins; **senior production specialist/graphic designer** Amy Hardcastle; **senior production specialist** Robert Buck; **senior traffic associate** Christine Hall

AAAS Board of Directors retiring president, chair Peter C. Agre; **president** Alice Huang; **president-elect** Nina Fedoroff; **treasurer** David E. Shaw; **chief executive officer** Alan I. Leshner; **board** Linda P. B. Katehi, Nancy Knowlton, Stephen Mayo, Cherry A. Murray, Julia M. Phillips, David D. Sabatini, Thomas A. Woolsey

AAAS
ADVANCING SCIENCE, SERVING SOCIETY

People's Choice Mini-Grants

Casting around for cash to pay for those extra chemicals or some DNA sequencing? Look no farther than Facebook, where BenchFly, in the name of "restoring science as a viable career path," is staging a "microgrant" competition. Applications are limited to 100 words. "We're definitely a short-attention-span generation these days," says Alan Marnett, a chemist who founded BenchFly.com, a Web site for lab researchers, last year after finishing his postdoc at the Massachusetts Institute of Technology.

The 8-week competition will end on 7 May. Those who log on to Facebook can vote for the winners, who will be announced on 12 May. Scientists won't be named on Facebook but must allow BenchFly to verify their identities. BenchFly will dole out grants of at least $500.

Marnett can't predict the number of winners or how much money they'll get: That depends on how many people have downloaded from BenchFly a "Search for Research" toolbar developed by a company named FreeCause. An undisclosed amount trickles in from FreeCause every time it's used for Internet searching; the money is matched by the life sciences company Sigma-Aldrich.

SONG OF THE SHELF

Shortly before he had planned to leave work on 11 February, Lars Kindermann heard a surprising crash. Kindermann, a biophysicist at the Alfred Wegener Institute for Polar and Marine Research in Bremerhaven, Germany, was listening to a live feed from underwater microphones beneath the Antarctic ice shelf. "I always have it on in the office," he says. Usually he hears the calls of whales and seals. This time, the mics were feeding acoustic data from a rare event: an iceberg the size of a small city smashing into the shelf ice near the German research station Neumayer III.

Kindermann's colleague Christine Wesche says those data, combined with seismic measurements and satellite photos, will offer scientists the most detailed look ever at such a collision and will provide new insights into the behavior of the shelf ice. Scientists monitoring global warming need to get the right physics of iceberg behavior plugged into their models so they'll know what it takes to break up the ice shelves that hold glaciers in place.

Kindermann says he also plans to study marine mammals' reactions to the event, to get a baseline for measuring animals' responses to humanmade noise sources.

Inheriting Mental Illness

What are the odds of being mentally ill if both of your parents have bipolar illness or schizophrenia? The answer, from a long-term study of psychiatric admissions in Denmark: extremely high.

Psychologist Irving Gottesman of the University of Minnesota, Twin Cities, and colleagues analyzed all Danish psychiatric admissions from 1970 to 2007. They found 196 pairs of parents in which both had been diagnosed with schizophrenia. Of the 270 offspring, 27% had been diagnosed with schizophrenia by the age of 52—and for all psychiatric admissions it was a whopping 67.5%. Among 8000 pairs with one schizophrenic member, only 7% of the offspring were schizophrenic. The rate in the general population is about 1%.

Similar results held for 83 couples with bipolar disorder—36% of their offspring had major depression, and two-thirds of those were also bipolar. The authors report the findings in the March issue of *Archives of General Psychiatry*.

David Goldman, chief of the lab of neurogenetics at the National Institute on Alcohol Abuse and Alcoholism in Bethesda, Maryland, calls the study "a major advance." The excess risk from two afflicted parents is "pretty remarkable," he says. Ordinary "additive" gene effects can't explain it, Goldman says. "The most likely explanation [is] epistasis," in which different genes interact nonadditively with one another.

The authors say a better evaluation of the risks of transmitting mental illness should be helpful to genetic counselors advising people on family decisions.

CREDITS (TOP TO BOTTOM): HINNERK HEUCK/ALFRED WEGENER INSTITUTE; ROYAL MAIL

Great Brains of Science

The United Kingdom's Royal Society this year celebrates its anniversary—"350 years of scientific brilliance and fearless doubt"—with the help of the Royal Mail, which has issued 10 stamps featuring the achievements of some of the society's members.

Behind North Korea's new TB lab
1312

ARPA-E's coming-out party
1317

LATIN AMERICA

Chile's Earthquake May Set Back Research for Years

Scientists in Chile have lost years of research from last month's massive earthquake, which overturned microscopes, destroyed research labs, and took the life of a young marine biologist. Researchers in fields from developmental biology to oceanography are trying to regroup.

The worst structural damage was to the two research universities in Concepción and Talca, both close to the epicenter of the magnitude-8.8 quake that struck on 27 February. At the University of Concepción, a fire ravaged the building that houses one of Chile's leading chemistry centers, including an advanced polymers lab. The building, although "still standing, burned completely," says Jaime Baeza, the university's vice-rector for research.

Because of aftershocks and structural damage, faculty members returned to the university only this week to rescue what might be left of research projects, Baeza says. Given losses of equipment and lab space, Baeza says, "the quake may have set us back 3 or 4 years, even 10 years." The university plans to reopen in April.

At the University of Talca 260 kilometers north of Concepción, damage to a modern agricultural biotechnology center and other buildings has surpassed $10 million, officials say. Bioinformatics researcher Danilo González says that high-performance computers were also destroyed and, as a result, several undergraduate and Ph.D. students' theses may be lost.

Some Chilean scientists worry about the long-term impact of the quake. The scientific community in Chile "has grown exponentially in the last 20 years," but it's still small and vulnerable, says Roberto Mayor, a Chilean developmental biologist at University College London. "The effect will be amplified," predicts Mayor, who is trying to raise funds to help. María Elena Boisier Pons, president of CONICYT, Chile's science funding agency, says, "We'll need as a country to reconstruct our labs and our science."

Aftermath. The massive earthquake that struck Chile last month battered the biotechnology building at the University of Talca (*top*). The quake also left a biology lab at the University of Chile in Santiago in disarray.

A tsunami that followed the quake also wreaked havoc, killing a researcher involved in an ecology expedition to Robinson Crusoe Island off Chile's coast. Ecologist Álvaro Palma of Pontifical Catholic University of Chile in Santiago, who had dispatched the team of five to the island, says the group scrambled uphill from their house near shore to escape the wall of water. But Paula Ayerdi, a 28-year-old research assistant in marine biology, became separated. Her body was found along the shore the next day.

The wave also gutted a marine research station operated by the University of Concepción in Dichato, a fishing town about 50 kilometers from the city, and left its research vessel, the *Kay-Kay*, stranded half a mile from shore, according to Carola Espinoza, a marine biologist at the university.

"Our laboratory was totally destroyed by the tsunami. It's turned upside down and full of sediment and algae," Espinoza says. Washed away were marine samples dating from the 1960s, aquariums used in breeding experiments, the station's library, and microscopes and other valuable equipment.

The university's oceanography program at Dichato and on the main campus in Concepción is "very strong" and attracted many collaborators from the United States and Europe to study a region of upwelling and high productivity off the Chilean coast, says Daniel Repeta, a marine chemist at Woods Hole Oceanographic Institution in Massachusetts. "I'm sure it's a big setback," says Repeta, who visited Dichato several years ago.

Farther north at the University of Chile in Santiago, the earthquake severely shook the modern four-story Millennium building that houses biology labs, toppling glassware, microscopes, incubators, PCR machines, and refrigerators. A flood from a broken water pipe on the top floor

CREDITS (TOP TO BOTTOM): CLAUDIO C. RAMIREZ/UNIVERSIDAD DE TALCA; MIGUEL ALLENDE/UNIVERSITY OF CHILE SANTIAGO

The land/sea diversity disparity
1318

Mining NASA's "lost" data
1322

and an electricity shutoff added to the damage, says Miguel Allende, who heads a cell genomics center in the building.

Researchers rushed to their labs the morning after the quake to slosh through chemical-laced water and salvage cell cultures and other frozen samples and reagents. But many materials were lost, Allende says.

About half of the biology department's 40 or so research groups suffered losses from the quake, says department chair Ana Preller. "The big problem is equipment," Preller says. Her preliminary estimate is $600,000 in losses. The quake also shifted and may have damaged a cyclotron in the physics department.

Allende and other faculty members have sent some students to colleagues' labs for now. Colleagues abroad have also offered to take in students from Concepción and Santiago. "It's taken 11 years to get where I am now. Doing science here is very hard. It's discouraging. But maybe it will be an opportunity to do some new things," Allende says.

–JOCELYN KAISER AND ANTONIO REGALADO

PHARMACOLOGY

The Puzzling Rise and Fall of a Dark-Horse Alzheimer's Drug

The announcement last week that a closely watched phase III clinical trial for Alzheimer's disease had failed to show a significant effect deals yet another demoralizing blow to patients, families, and caregivers. It may also mark the beginning of the end to one of the most unusual stories in Alzheimer's drug development.

The trial involved a drug called Dimebon, which catapulted into the limelight with a spectacularly successful trial published in *The Lancet* in 2008. "It looked better than anything we'd ever seen before," says Samuel Gandy, an Alzheimer's researcher at Mount Sinai School of Medicine in New York City.

Dimebon was an unlikely Alzheimer's drug. An antihistamine introduced in Russia in 1983, it turned up in a screen for potential Alzheimer's drugs led by scientists at the Institute of Physiologically Active Compounds in Chernogolovka, Russia. In follow-up experiments, the drug improved the performance of memory-impaired rats, and a pilot study with 14 Russian Alzheimer's patients showed encouraging results, published in a 2001 paper in the *Annals of the New York Academy of Sciences*.

Based on those findings, one of the Russian scientists, Sergey Bachurin, came to the United States to seek investors and partners in developing the drug. Bachurin persuaded San Francisco–based biotech entrepreneur David Hung to establish a company, called Medivation, and reportedly exchanged the rights to the drug for equity in the company. With initial support from private investors, Medivation recruited several top experts to design a larger clinical trial. The experts included Paul Aisen, a neurologist at the University of California, San Diego, who oversees government-sponsored clinical trials as director of the Alzheimer's Disease Cooperative Study; Rachelle Doody of Baylor College of Medicine in Houston, Texas; and Mary Sano of Mount Sinai.

The results were remarkable: The 2008 *Lancet* study, a double-blind, placebo-controlled trial, reported that 89 people with mild to moderate Alzheimer's disease who took Dimebon showed significant improvements in memory and cognition, as well as the ability to carry out the activities of daily life. The effects far surpassed those of any Alzheimer's drug on the market or in development, and Hung says several pharmaceutical companies bid to purchase the rights to Dimebon. Pfizer won, paying $225 million.

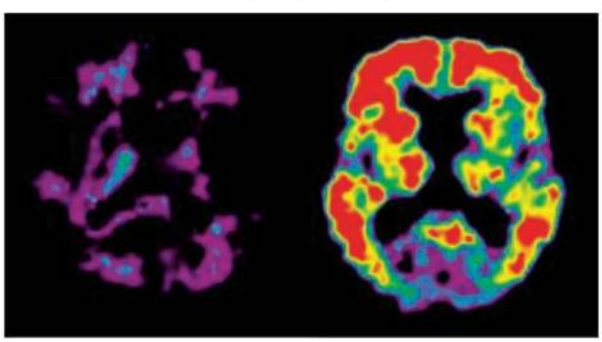

Bad news. A recent trial dims hopes that Dimebon will be an effective treatment for Alzheimer's disease, which loads the brain with amyloid plaques (*right*).

CREDIT: W. E. KLUNK AND C. A. MATHIS, UNIVERSITY OF PITTSBURGH

The *Lancet* findings struck many researchers as too good to be true, says Rudolph Tanzi, an Alzheimer's researcher at Harvard University. "Nobody could figure out what an antihistamine does" to fight Alzheimer's disease, says Sam Sisodia of the University of Chicago in Illinois. Several ideas have been floated, Sisodia says, but supporting evidence is scant. Still, he and others say they were willing to suspend their disbelief, largely because of the involvement of Aisen, Doody, and Sano. "If you had to pick the five best trialists in the world, they would be three of them," Gandy says.

But the new trial, despite a design almost identical to that of the *Lancet* study, yielded dramatically different results. It enrolled 598 patients with mild to moderate Alzheimer's. This time, however, there were no significant differences between the Dimebon and placebo groups. "It's hugely disappointing," says Aisen. He says he's at a loss to explain the discrepancy, although he notes that it's not unheard of for a drug to have both positive and negative trials before winning approval. Gandy, however, says, "I'm not sure that there has ever been such a night-and-day difference in replicate trials that turned out to be biological variation." Medivation and Pfizer are poring over the data in search of an explanation, says Hung, who declined to discuss their leading hypotheses. For now, the companies will continue with three other Dimebon trials already under way for Alzheimer's disease, in addition to one for Huntington's disease.

But to some, Dimebon is starting to look like a dark horse whose race is run. "I don't think that the drug is dead and buried today, but we need to get some clarity or good news soon," Gandy says.

–GREG MILLER

Eppendorf & *Science* Prize for Neurobiology

Get recognized!

US$ 25,000 Prize

2009 Winner
Richard Benton, Ph.D.
Assistant Professor
University of Lausanne
Switzerland

Kurstin Roe Photography

eppendorf & Science PRIZE FOR NEUROBIOLOGY

Deadline for entries
June 15, 2010

It's easy to apply! Learn more at
www.eppendorf.com/prize

Congratulations to Dr. Richard Benton on winning the 2009 Eppendorf & *Science* Prize for his studies on odor detection in the fruit fly, *Drosophila*. His findings have revealed unexpected evolutionary parallels between insect chemosensation, immune recognition and synaptic transmission.

The annual international Eppendorf & *Science* Prize for Neurobiology honors young scientists for their outstanding contributions to neurobiology research based on methods of molecular and cell biology. The winner and finalists are selected by a committee of independent scientists, chaired by *Science*'s Senior Editor, Dr. Peter Stern.

To be eligible, you must be 35 years of age or younger. If you're selected as this year's winner, you will receive US$ 25,000, have your work published in the prestigious journal *Science* and be invited to visit Eppendorf in Hamburg, Germany.

eppendorf
In touch with life

Science
AAAS

ECOLOGY

Severe Drought Puts Spotlight on Chinese Dams

XISHUANGBANNA, CHINA—Smoky haze hangs over the hills in this subtropical corner of China bordering Laos and Myanmar. The smoke is familiar: During the dry season, farmers across Yunnan Province burn fallen leaves, banana fronds, and more to make ash-based fertilizer. More unusual here, and more troubling, are the sickly yellow bamboo stands and the exposed bed of the Lancang River. "It's the worst drought in that region since 1949," the founding of the People's Republic of China, says Lu Juan, vice director of the Institute of Water Resources and Hydropower Research in Beijing.

Southwest China's monsoon-driven climate doesn't bring much precipitation in autumn and winter. But this year's dry season—coupled with a late start and early end to last year's rainy season—has left the region parched. Yunnan officials estimate that some 6 million people are short of drinking water and that the dry spell has ravaged winter wheat and other crops, inflicting $1.5 billion in losses.

The drought's effects have spilled across China's borders, stoking tensions with neighbors and prompting scientific debate. Rice yields in Thailand are expected to take a big hit, and the Mekong River—the name for the Lancang south of China—is in many stretches less than a meter deep, its lowest level in decades, making it impassable to tour boats and cargo ships. Researchers worry about how the low water level may affect fisheries and critically endangered species such as the Mekong giant catfish, which in the coming weeks would normally spawn in the upper Mekong.

Environmental groups in Thailand and elsewhere lay at least part of the blame on China's doorstep. They claim that China's management of a series of dams on the Lancang has aggravated the unfolding crisis. The Thai media has helped stir up emotions; one editorial in the *Bangkok Post* last month was headlined "China's dams killing Mekong." Yet Chinese engineers and some other scientists say the criticism is unfounded.

Rising tensions in Asia could usher in a protracted regional conflict over resources, especially as many key rivers cross several borders. In Asia, "competition for transboundary water utilization will be fierce," says He Daming, director of the Asian International River Centre of Yunnan University in Kunming. China will be at the center of many squabbles. With some 110 rivers and lakes straddling its borders with 19 countries, says He, "China is the most important upstream riparian country in Asia, even in the world."

A major feature in this vast waterworks is the 800,000-square-kilometer Lancang-Mekong basin, home to some 60 million people. From glacier-fed headwaters on the Qinghai-Tibetan plateau, the Lancang wends 2160 kilometers through southwestern China before entering the Golden Triangle region of Burma, Laos, and Thailand. The river finally spills into the South China Sea off Cambodia. In the late 1980s, China began work on eight cascades, or hydroelectric dams, on the Lancang's lower reaches, aiming to supply 15.6 gigawatts a year. Four have been completed, including Xiaowan, the tallest at 292 meters.

Parched. Fan Ze-xin examines seedlings in southern Yunnan; a prolonged drought is draining the lifeblood from forest life and (*above*) the upper Mekong.

Some environmental groups contend that the Mekong flow regime has been altered by dredging and dam construction, suppressing fish catches. Living River Siam, a nonprofit based in Chiang Mai, Thailand, has called on governments to "immediately stop all works on hydropower and river development on the Lancang-Mekong."

Yet the dams on the lower Lancang reduce runoff only during the rainy season, when reservoirs are filling, according to Chen Guanfu of Hydrochina Corp. Dry season water releases should increase river volume by 35%. "There are a lot of accusations that the dams in China are exacerbating the current low water levels, but the Chinese have informed [downstream nations] that they will not fill any reservoir during the dry season," says Roger Mollot, a fisheries expert with the World Wide Fund for Nature in Vientiane, Laos. The dams would also help rein in flooding, says Zhou Shichun of the General Institute of Hydropower and Water Resource Planning and Design in Beijing.

The biggest ecological impact could be less sediment swept downstream as silt accumulates in the reservoirs. But that would be a good thing, Zhou insists: It would "facilitate irrigation and navigation" on the Mekong. Others, however, point out that decreased sediment loads will likely lead to erosion of downstream riverbanks and the Mekong Delta.

Hydropower authorities have taken ecological effects into consideration, Zhou says. Work on one dam—the Mengsong Cascade, which would be sited nearest the border—has been postponed indefinitely, he says, to protect four species of migratory fish, including the giant pangasius (*Pangasius sanitwongsei*), whose conservation status is uncertain (*Science*, 22 June 2007, p. 1684). The freshwater goliath has not been reported above the Mengsong dam site, so the other dams would not affect it, Zhou says.

The first victim of an ecological crisis could be the Mekong giant catfish, which has been on the ropes for years. "It is not clear if the current drought conditions will impact successful spawning of the wild population of giant catfish, but low water levels may make them more vulnerable to fishing pressure," says Mollot.

Things may get worse due to climate change. After examining weather and tree ring data, Fan Ze-xin, a tree physiologist at Xishuangbanna Tropical Botanical Garden, has found that in the past 40 years Yunnan has grown warmer and drier—a trend that started long before the dams were built. In a nature reserve near the botanical garden, he grabs leaves from a seedling; dry as parchment, they disintegrate. "Some of these leaves are fresh," Fan says. "I haven't seen it as bad as this." **–RICHARD STONE**

ScienceNOW.org

From *Science*'s Online Daily News Site

And the Winners of Our Blogging Contest Are ...
Last month, *Science* reporters traveled to San Diego, California, to cover the annual meeting of the American Association for the Advancement of Science (which publishes *Science*NOW). To help us out, we recruited meeting attendees to share their insights and experiences on our guest blog, *Science*Bloggers. We were impressed with many of the entries, but in the end we could only choose three winners. http://bit.ly/cM5Sv0

New HIV Hiding Spot Revealed
Powerful anti-HIV drugs have come tantalizingly close to eradicating the virus from people, driving the blood level of HIV so low that standard tests cannot detect it. But no one has been cured: The virus comes roaring back in everyone who stops taking the drugs. A new study has identified one of HIV's main hideaways, raising intriguing possibilities about how to remove it. http://bit.ly/aIapaY

Pain's in the Genes

The difference between a child who laughs off skinned knees and one who cries at the smallest pinch could be in their DNA. Subtle changes to a certain gene seem to determine how sensitive people are to pain, according to new research. http://bit.ly/cw26KN

Solving the Rangeland Paradox
There's a saying in Texas: We don't have a water problem, we have a brush problem. The idea is that when shrubs and trees invade former grazing lands, they soak up so much groundwater that streams slow down and water supplies to cities and towns decrease. But a new study suggests that the opposite is true: Trees and shrubs on the prairies may actually help recharge the groundwater. The findings should force a rethink of land-management techniques for much of the United States's former rangelands. http://bit.ly/9Bt4jf

Read the full postings, comments, and more on **sciencenow.sciencemag.org**.

NORTH KOREA

New Tuberculosis Lab Hailed as Breakthrough in Health Diplomacy

Last fall, Sharon Perry pulled her first shift on a North Korean labor brigade. The Stanford University epidemiologist spent 10 days in November in Pyongyang, working side by side with Ministry of Public Health colleagues—from student nurses on up to senior physicians—to help set up the isolated nation's first laboratory capable of growing the mycobacterium that causes tuberculosis (TB) and detecting drug-resistant strains. The weather was unseasonably cold, so for 12 hours a day the unlikely comrades toiled in their parkas on tasks that included smashing old floor tiles with sledgehammers, testing microscopes, and installing ultramodern cabinets in which pathogens can be handled. "We all pitched in," says Perry, director of the Stanford-led Bay Area TB Consortium.

Perry and her colleagues have defied the odds in getting the project off the ground. U.S. scientists have long had fitful relations with counterparts in North Korea: No matter how noble the intentions, science cooperation efforts have, with few exceptions, ended up stillborn or abandoned. In recent months, some U.S. nonprofits engaged with North Korea "have found their counterparts to be reeling from the effects of intensive reeducation, dispersed overseas or to the provinces, or moved behind intermediaries," says one seasoned observer. Yet the budding TB lab has proceeded at a fevered clip. "We've kept our heads down and stayed out of politics," explains Heidi Linton, executive director of Christian Friends of Korea (CFK) in Black Mountain, North Carolina, a humanitarian organization and project partner along with the Bay Area TB Consortium and the Nuclear Threat Initiative (NTI). A team plans to return to Pyongyang next month to get the lab up and running.

That can't happen a moment too soon. Following years of economic decline and the severe famines of the mid-1990s, TB and other infectious diseases have surged in North Korea. Due to increased surveillance and an expanding epidemic, Perry says, between 2006 and 2008 the number of TB cases doubled to 344 per 100,000 people. "That's similar to rates seen in sub-Saharan Africa," says Gary Schoolnik, an infectious disease researcher and physician at Stanford University School of Medicine in California.

Until now, North Korean clinicians have relied on the age-old diagnostic technique of staining sputum for acid-fast bacilli, which catches about half of TB cases. But this approach can't reveal whether patients are infected with drug-resistant strains. "The prevalence of drug resistance could be very high," says Schoolnik.

A looming drug shortage threatens to make matters far worse. More than 90% of North Korea's TB drug stocks have been supplied by the Global Drug Facility, a nonprofit housed at the World Health Organization (WHO), under a grant that will run out this year. An agreement with the Global Fund to Fight AIDS, Tuberculosis and Malaria would continue supplying the drugs, but the earliest that could happen, sources say, is next year—leaving a minimum 6-month gap in coverage. "It's a nightmare scenario," says Linton. "You can't just leave TB patients without medi-

CREDITS (TOP TO BOTTOM): COURTESY OF HEIDI LINTON/CHRISTIAN FRIENDS OF KOREA; STOCKBYTE/GETTY IMAGES

Team spirit. Sharing the grunt work, TB project members roll a water tank into position.

CREDIT: COURTESY OF SHARON PERRY

cine." Based on discussions with WHO officials, Perry estimates that at least $1 million must be raised by July to purchase drugs. She and others are courting potential donors.

An unchecked TB epidemic would pose "a direct threat to China and other neighbors," says epidemiologist Louise Gresham, director of NTI's Global Health Security and Epidemiology initiative. NTI, a nonprofit in Washington, D.C., hopes the project might strengthen ties between two countries that are still technically at war. Experts not affiliated with the effort agree. "Collaboration and data sharing between North Korean and U.S. experts in the area of health security can, one hopes, help build the trust so necessary to resolving other urgent security issues," says Stuart Thorson, a political scientist at Syracuse University's Maxwell School in New York state who leads a U.S.–North Korea informatics exchange.

It was a veteran North Korea analyst, Stanford political scientist John Lewis, who got the ball rolling on the TB lab. In 2007, when North Korea–U.S. relations were particularly fraught, Lewis cast around for ideas for an overture that could ease tensions. Lewis consulted David Heymann, then the director of communicable diseases at WHO, who highlighted the unfolding TB emergency. Lewis next contacted Stanford's resident TB experts, Perry and Schoolnik.

To lay the groundwork, the Bay Area TB Consortium hosted a five-person delegation from the North Korean health ministry in January 2008. "We identified their most pressing needs," says Schoolnik. These were the TB lab and an uninterrupted supply of drugs. Perry, who Schoolnik calls "the driving force" of the project, rang up Gail Cassell, a vice-president at the pharmaceutical giant Eli Lilly who has worked on TB in the former Soviet Union. Cassell approached NTI, which in short order invited Stanford to submit a proposal. NTI awarded them $230,000 to purchase a WHO-recommended inventory of lab equipment—biosafety cabinets, incubators, centrifuges, freezers, and culture plates—and power conditioners, generators, and other devices to cope with an unreliable power grid. "The stuff is state-of-the-art," says Schoolnik. "It made us envious."

Getting the goods to Pyongyang was the next challenge. In stepped CFK, which for 15 years has been providing humanitarian assistance to North Korea. "For years, we'd been hearing from North Korean doctors and health officials about the need for a TB lab," says Linton. In mid-2008, she got wind of the nascent Stanford effort and called Perry. "We had expertise they needed," Linton says. For starters, CFK had experience rehabilitating hospitals in North Korea and knew how to navigate the procedures for obtaining export licenses from the U.S. Department of Commerce.

CFK has proved to be the project's linchpin. The North Koreans trusted it. "We experienced extraordinary cooperation," says Perry. By December 2008, the Koreans were on board for the TB lab. The following May, CFK, which has also spent about $230,000 on the project, arranged for Perry, Linton, and others to visit the health ministry's National Tuberculosis Institute in Pyongyang to hash out a plan. As with past projects, says Linton, "we realized we would have to bring every nut, bolt, and light bulb."

Trial run. California-based microbiologist Grace Lin puts the new lab through its paces.

The lab equipment arrived in Pyongyang on a rainy day last October. "When we opened the containers, the Korean researchers' eyes lit up," Linton says. "You could feel the energy—they realized this was finally going to happen." A CFK team will return next month to complete the wiring and plumbing and check on other renovations that the North Koreans were due to complete. The Stanford team hopes to hold training workshops when the lab is operational, and NTI intends to make periodic visits to verify that the equipment is being used as agreed.

Down the road, the U.S. side hopes that the bonds formed in bringing the lab into being will blossom into a full-fledged collaboration. "As trust grows, we may be able to build on this relationship and start scientist-to-scientist and lab-to-lab cooperation," says Gresham. In the annals of U.S.–North Korea relations, they are already off to a remarkable start.

–RICHARD STONE

ScienceInsider

From the *Science* Policy Blog

The H1N1 virus may have had less impact this winter than expected, but a new report from Hong Kong suggests that the virus in pigs has picked up genes from the human version. http://bit.ly/blj67G

China will increase its science and technology budget by 8%, to $24 billion, in 2010. "We need to emancipate our minds and boldly make breakthroughs and innovations," Premier Wen Jiabao told the legislators meeting at the National People's Congress. http://bit.ly/bc1VTZ

Meanwhile, **Canada's pending budget is light on new funds for science.** Finance Minister James Flaherty moved to partially offset scheduled cuts in funding for the nation's three granting science councils, though they'll still take a blow, and there will be tighter competition for research operating grants. http://bit.ly/am3kOk

A new study of 30 unnamed federal workers found **no difference in their experiences regarding research integrity** in the Obama and Bush Administrations. The George Washington University study looked at accessing data, reviewing potential research, clearing papers for publication, and communicating with the public. http://bit.ly/bP6IDZ

The National Research Council has recommended that U.S. funding agencies support **an interdisciplinary research program on how past climate influenced human evolution.** It would include drilling ancient lakebeds, studying new fossil sites, modeling paleoclimate, and educating the public. http://bit.ly/d6723P

A panel has recommended that the European Southern Observatory (ESO) build the record-setting **European Extremely Large Telescope** at Cerro Armazones in northern Chile. But Spain may continue its fight for a site on its La Palma island. None of ESO's current scopes in Chile was harmed in the recent earthquake. http://bit.ly/dBRExg

For the full postings and more, go to **blogs.sciencemag.org/scienceinsider.**

PSYCHIATRY

APA Seeks to Overhaul Personality Disorder Diagnoses

Personality disorders are hard to pin down. They don't have a common defining mood or behavior, people don't get hospitalized for having one, and a drug won't cure one. But they can cause all kinds of havoc. People with antisocial personalities, regularly encountered in crime news, are well-known. But other types of these disorders feed into high rates of alcoholism, drug addiction, suicide, and the dysfunction found in many offices, families, or soap operas.

A personality disorder "at the core" involves "failure to develop healthy functioning in self and interpersonal domains," according to psychologist Lee Anna Clark of the University of Iowa in Iowa City, a member of the American Psychiatric Association's (APA's) work group that is proposing revisions for personality disorders in the forthcoming fifth version of the *Diagnostic and Statistical Manual of Mental Disorders* (*DSM-V*), often referred to as psychiatry's bible (*Science*, 12 February, p. 770). These disorders are in for a "major overhaul," says APA psychiatrist Darrell Regier, co-chair of the broader effort. The goal is to create a more flexible and precise system, but some critics say the changes are too complicated for the busy clinician.

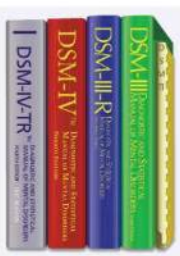

DSM-V
Fifth in a series

The current edition, *DSM-IV*, identifies 10 personality disorders, with a list of criteria for each. But these have been criticized for having arbitrary diagnostic thresholds and for clumping together people with quite different symptoms. Work group chair Andrew Skodol, a psychologist at the University of New Mexico, Albuquerque, says, for example, that with nine criteria (five required for a diagnosis), there are 256 ways that a person can be diagnosed with "borderline" personality disorder. Furthermore, "more than half of people diagnosed with one personality disorder are diagnosed with a second or third or even fourth," says Clark. And despite all the choices, many end up in the "not otherwise specified" (NOS) category. The work group is proposing a system members feel will better capture the range of pathology.

Take borderline personality disorder. "Borderline" used to be a way of referring to a state somewhere between neurotic and psychotic. But since the 1970s, it has become one of the more extensively researched personality types—often found in young women who tend to be self-centered, hysterical, emotionally dependent, and often suicidal. Marilyn Monroe is often cited as an example; another is Glenn Close's character in *Fatal Attraction*.

Under *DSM-IV*, a clinician would make a diagnosis of borderline personality disorder if a patient displayed at least five from a list of nine symptoms such as impulsiveness, self-mutilating behavior, and "chronic feelings of emptiness." Under the new regime, the clinician would first determine whether the person's functioning is so impaired that she qualifies for a general diagnosis of personality disorder. The heart of the assessment would be a "trait profile" compiled from a list of six major domains of personality covering areas such as "introversion," "antagonism," and "schizotypy" (odd or eccentric behavior).

The clinician could also refer to five suggested "types" of personality disorders—including "borderline type"—pared down from the current 10 (see box). The four others would be antisocial/psychopathic, avoidant (anxious and fearful of rejection), obsessive-compulsive, and schizotypal. The latter two contain elements of more serious diagnoses in the categories of anxiety and psychosis but do not meet all the criteria.

One venerable type did not make the cut: narcissistic personality disorder. That's controversial, says psychologist Drew Westen of Emory University in Atlanta. The diagnosis is "widely used—and nobody has suggested it doesn't exist." Skodol says narcissism is a trait seen in more than one type of disorder and is covered under the domain of "antagonism."

Clark and Skodol say that in practice, many people with personality disorders will fall outside those five types. But they'll get better diagnoses because, instead of being designated "NOS," they will be profiled based on the six traits.

Some experts question how useful the new system will be. Westen lauds the group for trying to make diagnosis "more sophisticated clinically." But, he says, by trying to combine the list of five personality types with six crosscutting traits, "what they've come up with is a camel—a horse made by committee."

Psychologist Thomas Widiger of the University of Kentucky in Lexington thinks the proposed overhaul is "terrible," leaves too much to the clinician's subjective judgment, and will create new headaches for insurance companies. It is "so complicated, it will not be used," he says. "Clinicians will match to one of those five [types]. Then they'll be done." Skodol is more optimistic, saying that clinicians can choose how deeply detailed their diagnosis is based on "available time, information, and expertise."

Skodol's group also wants to put personality disorders on the same footing as other mental disorders. *DSM* lists disorders in two different categories, or "axes." Most are on Axis I; personality disorders are on Axis II (along with intellectual disabilities) because they are seen as stable, chronic conditions rather than episodic illnesses. Moving them to Axis I, says Clark, "makes the statement that personality disorder is just as critical to assess as any other diagnosis."

–CONSTANCE HOLDEN

Personality Disorders

OUT	RETAINED
~~Paranoid~~	Schizotypal
~~Schizoid~~	Obsessive-compulsive
~~Histrionic~~	Borderline
~~Narcissistic~~	Antisocial/psychopathic
~~Dependent~~	Avoidant

Slimmed down. Proposed changes would reduce the number of personality "types."

On the edge. Alex Forrest, played by Glenn Close in *Fatal Attraction*, fits the diagnosis of a borderline personality.

CREDIT: (TOP) PARAMOUNT PICTURES/NEWSCOM

NEWSMAKER INTERVIEW

A Civil Conversation About Animals in Research

In 2006, neuroscientist Dario Ringach of the University of California, Los Angeles (UCLA), sent an e-mail to several animal-rights groups announcing that he would give up his primate research if they would leave him and his family alone. After years of threats and harassment, including masked protesters banging on his windows at night, Ringach shifted his research on the visual system to studies with human volunteers and theoretical work.

After keeping a low profile for a few years, Ringach has recently begun speaking out about the benefits of animal research and against a spate of attacks on researchers at UCLA and elsewhere (*Science*, 21 December 2007, p. 1856; 8 August 2008, p. 755). Along with UCLA neuroscientist David Jentsch, whose car was torched by animal-rights activists in March 2009, Ringach co-founded a pro-research group called UCLA Pro-Test (*Science*, 1 May 2009, p. 574). In February, Pro-Test teamed up with Bruins for Animals, an animal-rights group on campus, to organize a panel discussion among experts with differing views on animal research that was open to UCLA students and staff. Last week, Ringach spoke with *Science* about the event and the renewed attention he's gotten from animal-rights extremists. For a video of the UCLA event and links to related blog coverage, see http://news.sciencemag.org/2010/03/ringach.html. **–GREG MILLER**

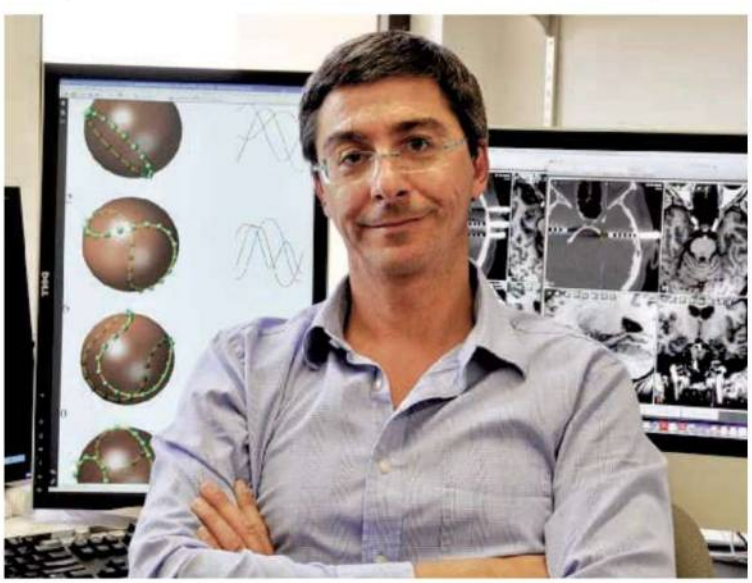

CREDIT: COURTESY OF DARIO RINGACH

Q: What made you decide to start speaking publicly in favor of animal research?

D.R.: After my decision [in 2006], I was left alone [by activists] for a while, but it was hard to watch my colleagues here at UCLA still being targeted with such violence and hate. I was really inspired by David Jentsch. After his car was blown up, he walked into my office and asked if I thought a good response would be to hold a pro-research rally on campus. I decided to join him. It was almost an immediate reaction.

Q: What did you hope to accomplish with the recent panel discussion?

D.R.: We never discussed in detail what the goal was. On the personal side, it was really modest. I wanted to show that we could hold a civilized discussion on this topic.

Q: Who was on the panel?

D.R.: We had six speakers. It was me, Colin Blakemore [a neuroscientist at the University of Oxford in the United Kingdom], Janet Stemwedel [a philosopher at San Jose State University in California] on the side in favor of animal research. And on the other side was Ray Greek [president of Americans for Medical Advancement, a group that opposes animal research], Niall Shanks [a professor of history and philosophy of science at Wichita State University in Kansas], and Robert Jones [a philosopher at California State University, Chico].

Our goal was to bring to the panel individuals with a range of positions. One of the misperceptions is that people segregate into these binary positions, that we either support all types of animal research or we condemn everything, and it's not true. People hold a continuum of views on this issue.

Q: What was the tone of the discussion?

D.R.: The tone was civil. Everyone got to speak their mind. At the end of it all, I had more animal-rights activists coming up to thank me for my participation than my own colleagues, which was kind of refreshing.

Q: Did this accomplish anything?

D.R.: I think we got to know each other a little better. I understand their concerns about animals. And I think they understand that scientists are not the monsters some people are trying to convince the public we are. Our work is not driven by the pleasure of harming an animal, nor by greed, but by our honest belief that we're trying to advance medical knowledge and medicine.

Q: Restricting entrance to current UCLA students and staff may have kept out some of the more extreme activists. How have they reacted?

D.R.: To begin with, we started to get these protests at our homes in the weeks leading up to this event. They were trying to prevent this from happening. Then, after the event, one of these groups decided to justify the targeting of my children by [saying activists should begin] protesting at their school. I'm not even doing any animal research at the moment, I've been targeted just for speaking my mind.

Q: Has there been a counter-response?

D.R.: After they made these threats public, some of the science bloggers expressed outrage to this notion that my children were fair game. And that's when Bruins for Animals joined us in a joint statement denouncing the harassment and intimidation tactics. We're hoping other animal-rights groups will join us. It would be a tremendous step forward. Most of the time when asked, many animal-rights activists will reply that they're not really for violence, but they understand the frustration of some activists. At least the local organizations we're trying to engage have been very positive in saying that we should give dialogue a chance.

Q: Do you really think this type of event can end the threats and intimidation?

D.R.: There is a small group of individuals who are set on using threats and intimidation to convince others of their views, and I don't think there's anything we can do about that. But I think they will become increasingly marginalized, both by the public and by their colleagues in the animal-rights movement. I am hopeful that more open dialogue will force them to decide exactly what they want to do, whether they want to continue with their threats or join us at the table.

SCIENTIFIC PUBLISHING

Elsevier to Editor: Change Controversial Journal or Resign

Withdrawn. Two *Medical Hypotheses* papers—including one by Peter Duesberg—were retracted after five reviewers unanimously panned them.

The editor of the journal *Medical Hypotheses*—an oddity in the world of scientific publishing because it does not practice peer review—will apparently lose his job over the publication last summer of a paper that says HIV does not cause AIDS. Publishing powerhouse Elsevier this week told Editor-in-Chief Bruce Charlton that it won't renew his contract, which expires at the end of 2010, and it asked that Charlton resign immediately or implement a series of changes in his editorial policy, including putting a system of peer review in place. Charlton, who teaches evolutionary psychology at Newcastle University in the United Kingdom, says he will do neither, and some on the editorial advisory board say they may resign in protest if he is fired.

Elsevier's move is the latest in an 8-month battle over the journal; it comes after a panel convened by Elsevier recommended drastic changes to the journal's course, and five scientists reviewed the controversial paper and unanimously panned it.

Medical Hypotheses, which says it "will consider radical, speculative and non-mainstream scientific ideas" is the only Elsevier journal not to practice peer review. Scientist, entrepreneur, and author David Horrobin, who founded the journal in 1975, believed reviewers tend to dislike what lies outside the scientific mainstream. Charlton, who succeeded Horrobin in 2003, decides what gets published on his own—although he occasionally will consult another scientist—and manuscripts are edited only very lightly.

Peerless. Editor-in-Chief Bruce Charlton refuses to introduce peer review.

It's a policy that leads to occasional wild and wacky papers—a 2009 article for which the author studied his own navel lint became an instant classic—but the journal is also a "unique and excellent" venue for airing new ideas, says neuroscientist Vilayanur Ramachandran of the University of California (UC), San Diego, who published in the journal 15 times himself and sits on its editorial advisory board. "There are ideas that may seem implausible but which are very important if true," Ramachandran says. "This is the only place you can get them published."

But the journal got in hot water in July after Charlton accepted a paper, previously rejected by the *Journal of Acquired Immune Deficiency Syndromes*, in which molecular virologist Peter Duesberg of UC Berkeley and colleagues assert that HIV does not cause AIDS and that medical statistics and demographical data do not support the existence of a massive AIDS epidemic in South Africa. Duesberg, a so-called AIDS denialist, has disputed the link between HIV and AIDS since the 1980s.

Charlton says he is "agnostic" on the question of whether HIV causes AIDS but adds that even papers that are wrong can make interesting points that make the reader think. "If he believes that, he should have a great big health warning on every page saying, 'This may be rubbish,' " says Nicoli Nattrass, an economist at the University of Cape Town who has studied the effects of AIDS denialism in her country. "This is not just some stupid academic debate. Many people in South Africa still don't believe HIV causes AIDS because there are scientists who say so. And they are dying because of it."

After the paper's publication, prominent HIV scientists John Moore of Weill Cornell Medical College in New York City and Nobelist Françoise Barré-Sinoussi of the Pasteur Institute in Paris wrote Elsevier to ask that the paper be withdrawn. Others asked the National Library of Medicine to delist *Medical Hypotheses* from the MEDLINE database of biomedical literature, and called on scientists to urge their librarians to cancel the journal. (They also took aim at a second AIDS paper by molecular biologist Marco Ruggiero of the University of Florence, which they say was denialist in nature as well.)

Following the advice of a private external panel, Elsevier told Charlton on 22 January that *Medical Hypotheses* would have to become a peer-reviewed journal. Potentially controversial papers should receive careful scrutiny, the publisher said, and some topics—including "hypotheses that could be interpreted as supporting racism"—should be off limits.

Elsevier also had its flagship medical journal, *The Lancet*, organize a review of the two papers by five anonymous experts. The reviews, which have been obtained by *Science*, were unanimously negative; they said that the Duesberg paper was riddled with errors and misinterpretations. "It does not belong in a scientific journal," one reviewer wrote. On 24 February, Elsevier wrote Duesberg that his paper—which had not yet been printed and which the publisher had pulled from the journal's Web site in August—would be "permanently withdrawn." Ruggiero received a similar letter.

Charlton calls the review a "show trial" and says the publisher had no right to override his editorial decision. On his Web site, he has published a selection of more than 150 letters from *Medical Hypotheses* authors who support him. And on 12 February, 13 of the 19 board members wrote Elsevier to demand that the papers be returned to the journal's Web site and to reject the proposed changes to its editorial policies. Not having peer review "is an integral part of our identity, indeed our very raison d'être," the group wrote. But board member Antonio Damasio, head of the University of Southern California's Brain and Creativity Institute in Los Angeles, didn't know of the letter and now says that the paper should never have been published. The signatories don't all love the paper either, says board member David Healy of Cardiff University School of Medicine in the United Kingdom. "It's a defense of Bruce, not of the Duesberg paper," he says.

Duesberg says Elsevier's measures are an example of "censorship" imposed by the "AIDS establishment." But *Medical Hypotheses*' critics applaud the publisher's latest step. "It seems clear that Elsevier has come to realize that there is a problem with *Medical Hypotheses* and that they are doing what they can to rectify it," says Moore. **–MARTIN ENSERINK**

CREDIT: (BOTTOM) COURTESY OF B. G. CHARLTON

ENERGY RESEARCH

Matchmaking Is Part of the Party As ARPA-E Marks Its First Birthday

A little more than a year after the U.S. Congress bestowed $400 million in stimulus funding on an agency that at the time consisted of little more than file cabinets, the Advanced Research Projects Agency–Energy (ARPA-E) is firing on all cylinders. Last week, it marked its first anniversary with a coming-out party. But the 1700 politicians, scientists, industrialists, and investors who attended the 3-day summit in a suburb of Washington, D.C., did more than celebrate a good start. The meeting heralded the agency's fresh approach to doing business, including giving researchers—both funded and rejected by ARPA-E—a chance to interest prospective backers in their scientific wares.

"The signing of a contract with ARPA-E provides validation to potential investors," says Riccardo Signorelli of FastCAP SYSTEMS, a Boston-based startup that received $5.4 million from ARPA-E in December to develop supercapacitors. After the award was announced, ARPA-E program manager David Danielson helped the company find potential business collaborators and sped up the process of securing its next round of funding—$2 million for the 12-person company to pay salaries and market its technology.

Director Arun Majumdar says that speed is essential for ARPA-E to meet its mission of catalyzing "game changing" energy technologies. And participants say that so far the agency is living up to that promise. Its lean profile—fewer than a dozen program managers, with broad authority to make decisions—has allowed it to move paperwork "like a bullet," said Ammi Amarnath of the Electric Power Research Institute (EPRI) in Palo Alto, California, which is part of a collaboration that has received $5 million from ARPA-E for smart windows research.

FastCAP and EPRI were two of 37 winners in ARPA-E's first solicitation, an open $150 million competition that attracted 3700 applicants. A second, more focused call for $100 million issued in December has yielded 500 concept papers, with winners to be announced in the spring. And last week, Majumdar announced a third, $100 million solicitation, for improvements in energy converters and storage and more efficient buildings.

Notwithstanding the importance of federal support—President Barack Obama has requested $300 million in the 2011 fiscal year so that the agency can sustain its momentum—Majumdar emphasizes that part of ARPA-E's success will be measured in how much private money its grantees are able to attract. So far, so good: Companies have invested an additional $32 million in FastCAP and other first-round winners.

ARPA-E's sudden arrival on the federal research scene has naturally prompted many questions from the energy community. So Majumdar began the summit with a 1-day, closed-door workshop for attendees to meet face to face with ARPA-E staffers. Later, in public sessions that featured energy rock stars such as investor Vinod Khosla and *New York Times* columnist Thomas Friedman, officials fleshed out some of ARPA-E's inner workings.

CREDIT: ALGAE VENTURE SYSTEMS

Greener pastures. Algaeventure Systems in Marysville, Ohio, received a $6 million award to develop an algae-processing system for biofuel.

One facet that has attracted a lot of attention has been its review process. Whereas the first solicitation had required hundreds of volunteers to sift through the deluge of applications, the next rounds will rely more on input from its own program managers, drawing upon their expertise in particular fields. It's a balancing act, says chemical engineer Mark Hartney, who says he took a "fairly significant pay cut" to join ARPA-E after working at the Massachusetts Institute of Technology's Lincoln Laboratory, at DARPA, and in the semiconductor industry. Unlike in basic research, which relies on a proposal's scientific merit, or applied programs, which hinge on meeting strict technical goals, ARPA-E managers look at a mixture of fundamental science, the commercial track record of applicants, and their potential to partner with other scientists. When technical reviewers say "it's possible but very challenging," says Hartney, "that may be an ARPA-E program."

To some, however, that process—whose first step is an eight-page concept paper—can look overly subjective. "Absolutely no reasons are given [for the rejection]. … There is no transparency." says David Doty of Doty Energy in Columbia, South Carolina, who had proposed research into what are called wind fuels.

A key goal of the summit was to connect ARPA-E's inaugural grantees—and 64 finalists who didn't get funded—with hundreds of private investors. Chemist Ilan Gur of the Berkeley, California–based SEEO, which fell just short of getting funding last year, said his status as a finalist helped expose him to influential policymakers, investors, and technologists. But physicist Dileep Agnihotri of startup Graphene Energy in Austin, Texas, said he "hadn't seen much advantage" to being a finalist.

Although ARPA-E sits outside the Department of Energy's existing research infrastructure, with its director reporting directly to Energy Secretary Steven Chu, DOE officials emphasized at the meeting that their units are well connected to ARPA-E. Top DOE officials spent "hundreds of hours" helping set up the agency last year, said an aide. And ARPA-E has given back, too, says Henry Kelly of DOE's Energy Efficiency and Renewable Energy branch in Washington, D.C. At a recent meeting on power systems, Kelly recounts, ARPA-E's program managers "brought in a guy who built the energy systems for the 787 Dreamliner."

But will such collaborations, even in the service of impressive research, impress lawmakers looking to trim federal spending? Majumdar said he was "optimistic" that Congress would support the president's $300 million request for 2011. But in a keynote address, Chu was realistic about the audacity of his effort. "When you start a program and you ask for hundreds of millions of dollars," he says, lawmakers tend to see it "just like this big piñata." **–ELI KINTISCH**

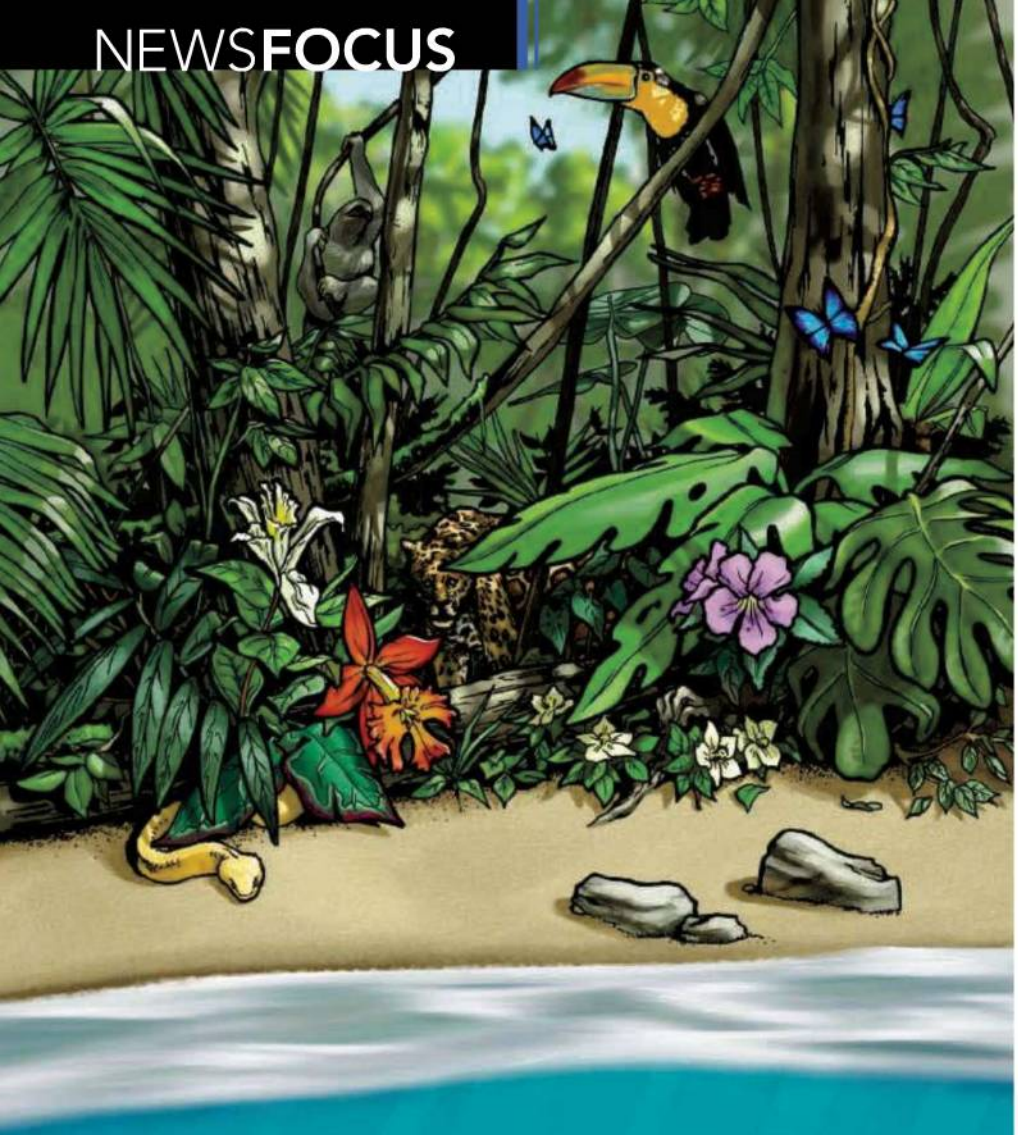

On Rarity And Richness

Two researchers take a stab at explaining why oceans have far fewer species than terrestrial habitats

IF BIODIVERSITY WERE AN OLYMPIC SPORT, life on land would take home the gold and the sea might not even enter a team. Given the vastness of the oceans and the length of time life has thrived there, you might expect marine species to outnumber terrestrial ones. Yet, microbes aside, upward of nine in 10 species crowd into the 30% of Earth's surface that's dry.

It wasn't always that way, say Richard Grosberg and Geerat Vermeij. These researchers from the University of California (UC), Davis, have been studying land and ocean features to understand how evolution proceeds in these two realms. At a recent meeting,* they argued that the difference in diversity is a recent phenomenon.

Back in the Devonian period, 400 million years ago, the seas were home to an abundance of species, perhaps even more than on land. But about 110 million years ago, land plants went through a burst of speciation; so did the pollinators, fungi, and herbivores associated with them. These relationships made "rare" species possible, as plants acquired help in dispersing their pollen and seeds, resulting in relatively low population densities for individual species. Quickly, their numbers left marine biodiversity behind. The trigger for this terrestrial explosion, Grosberg and Vermeij say, was the evolution of a more efficient way in which land plants use water.

"This is an excellent and thoughtful paper addressing an issue in biodiversity that has rarely been tackled," says Michael Benton, a paleontologist at the University of Bristol in the United Kingdom. Jeremy Jackson, a marine ecologist at the Scripps Institution of Oceanography in San Diego, California, calls it "a very big-picture paper. … It's the kind of paper that you think about forever."

A physical phenomenon?

Grosberg started thinking about these issues when he was preparing a series of talks for the 200th anniversary of Charles Darwin's birth. "To me, the interesting question is why are there so many fewer species in the sea than on the land," says Grosberg.

The difference is striking. In 1994, Robert May of the University of Oxford in the United Kingdom concluded that 85% of the world's macroscopic species lived on land, based on the existing record of species across the globe. A 2009 study by Benton found landlubbers to be even more common, accounting for 95% to 98% of the world's multicelled species. "Both recognized that the estimates were ballparks, simply because we don't actually know how

*The Society for Integrative and Comparative Biology meeting was held 3 to 7 January in Seattle, Washington.

CREDIT: M. TWOMBLY/SCIENCE

many species there really are," says Grosberg.

The land-sea disparity occurs even in diversity hot spots. A single hectare in a tropical rainforest may contain some 475 tree species and more than 25,000 insect species. But a hectare of coral reef, often called the sea's "rainforest," might be home to at most 300 coral, 600 fish, and about 200 algal species.

Grosberg wasn't the first to wonder what lies behind these numbers. In 1990, Richard Strathmann, a marine biologist at the University of Washington, Seattle, wrote an influential paper pointing to physical characteristics of water that could slow down speciation in the seas. Denser and much more viscous than air, water makes travel more challenging. Gases diffuse more slowly. The much higher specific heat of water means aquatic organisms must work harder to stay functional. Organisms can usually detect food, mates, or enemies by sight or smell over longer distances in air than in water. Strathmann; Mark Denny of Hopkins Marine Station of Stanford University in Pacific Grove, California; and Grosberg have all noted that these differences help make terrestrial environments more hospitable and, most likely, more conducive to the evolution of new species.

Grosberg recognized, however, that physical differences couldn't be the whole explanation. Some polar terrestrial ecosystems are less diverse than nearby marine environments, and freshwater habitats tend to be species-poor compared with similar marine habitats. But he was stumped as to what else might be a factor.

Then Vermeij heard Grosberg give his talk at UC Davis. "He said to me, 'You've missed the point,' " says Grosberg.

Rarity a boon to biodiversity

A paleontologist, Vermeij tends to see events in a long perspective. "It struck me that this enormous difference can't be very old," Vermeij recalls.

Vermeij pointed out that the degree of diversity in the two realms was pretty much equal until about 110 million years ago. About that time, flowering plants took off, as did insects that pollinated them, with species tending to become ever more specialized. Plants came to prefer certain microclimate and soil regimes. Insects pollinated only particular plants; parasites became quite picky about their hosts, and so on. Many kinds of fungi became associated with a favorite host plant. The rise in potential biotic interactions, coupled with more complex habitats than available in the sea, created many more opportunities for new species to form, particularly in the tropics.

Leaf power. Grosberg (*left*) and Vermeij think the evolution of denser leaf veins (*above*) helped boost terrestrial biodiversity.

Along with increased specialization, terrestrial evolution led to dispersed communities. "The medium of air permits … extensive and rapid locomotion," Vermeij notes. Mobile organisms can locate mates over long distances and easily travel to them. And many stationary plants have gotten animals to do the work of finding mates, transferring pollen, and spreading seeds. The strategy works well: Today, more than 200,000 species are pollinators. In such a system, Vermeij points out, mobile pollinators and dispersers can maintain populations of rare individuals.

With few exceptions, animal-mediated transfer of gametes, fertilized eggs or larvae, or seeds occurs only on land. Grosberg and Vermeij note that arrying such loads is too challenging under water because of water's viscosity. Instead, marine organisms tend to live in higher-density communities and sometimes employ extraordinary measures for fertilization. Consider barnacles, which have penises that are 10 times the diameter of the barnacle in order to reach a potential mate.

The development of dispersed communities "is the key to the current extraordinary diversity of species on land," Grosberg says: High-density populations are at increased risk of being eaten or wiped out by disease, while dispersed communities face reduced competition and predation.

The missing trigger

Yet even with this scenario worked out, Grosberg and Vermeij still lacked an explanation for why the gap in diversity between land and sea began to widen when it did. Then, they heard about a February 2009 paper on the evolution of leaf-vein density in flowering plants. C. Kevin Boyce of the University of Chicago in Illinois and his colleagues had measured the densities of leaf veins in many kinds of plants. They also gathered fossil leaf-vein measurements from the published literature. They found that ferns, conifers, and early flowering plants had relatively low leaf-vein densities. But flowering plants that evolved later sometimes squeezed in three to 10 times as many veins per millimeter. Those extra veins correlated with increased photosynthetic capacity, Boyce and his colleagues reported online on 25 February 2009 in the *Proceedings of the Royal Society B.*

"That paper was the bridge that Vermeij and I crossed in understanding why the disparity gap happened when it did," Grosberg recalls. About 110 million years ago, higher leaf-vein densities—and increases in the number of leaves—resulted in greater biomass production. All this added energy set in motion a positive feedback loop that encouraged more specialization. Speciation took off, particularly in the tropics.

"The idea of key innovations in plant and animal evolution [such as denser leaf veins] is a very old one," says Michael Hart of Simon Fraser University in Burnaby, Canada, "but connecting it to the land-sea difference in species diversity is important and new."

However, the explanation Vermeij and Grosberg propose has some critics. Evolutionary biologist A. Richard Palmer of the University of Alberta in Edmonton, Canada, says so much terrestrial diversity is due to insects and flowering plants that they may overwhelm the real biodiversity picture. And while he calls Grosberg and Vermeij's case for extreme rarity being more feasible on land "a novel contribution," he points out that some deep-ocean species are also quite rare. "Rarity doesn't seem unique to land," he says. And Strathmann points out that the difference in the number of species on land versus the number in the sea may be exaggerated because many marine species have gone unrecognized.

Nevertheless, Grosberg and Vermeij's ideas are attracting attention. "Every step of the way [in their argument] is to some degree conjectural," says Jackson. "But every step of the way makes sense." **–ELIZABETH PENNISI**

Online
sciencemag.org
Podcast interview with author Elizabeth Pennisi.

CREDITS (TOP TO BOTTOM): KEVIN BOYCE/UNIVERSITY OF CHICAGO; KARIN HIGGINS/UC DAVIS; (ILLUSTRATION) M. TWOMBLY/*SCIENCE*

PHYSICS

Ironing Out Consensus on the Iron-Based Superconductors

The emerging understanding of the 2-year-old materials could change physicists' views on the decades-old mystery of high-temperature superconductivity

The first superconductors—materials that carry electricity without any resistance—were discovered in 1911. Half a century passed before physicists figured out how metals such as niobium perform that mind-bending feat at a few degrees above absolute zero. In 1986, researchers discovered complex compounds containing copper and oxygen that become superconductors at much higher "critical temperatures"—now as high as 138 kelvin. Twenty-four years later, such "high-temperature superconductivity" remains the biggest puzzle in condensed-matter physics.

Given those struggles, it's no wonder that Paul Canfield, a physicist at Ames Laboratory in Iowa and Iowa State University, bristles when asked if scientists have deciphered the newest superconducting marvels, iron-based materials that emerged 2 years ago and have critical temperatures as high as 56 kelvin (*Science*, 25 April 2008, p. 432). "Here we are at 2 years and you're asking, 'Are we there yet, Daddy?' Come on!"

Yet progress on the materials has been phenomenal, say Canfield and others. In February 2008, Hideo Hosono, a materials scientist at the Tokyo Institute of Technology, and colleagues reported that a compound of lanthanum, iron, arsenic, oxygen, and fluorine ($LaFeAsO_{1-x}F_x$) becomes a superconductor at 26 kelvin. Researchers have since discovered four families of iron-based superconductors with distinct crystal structures. Using tools honed on the copper-and-oxygen superconductors, or "cuprates," they have made measurements that took decades to achieve in the older materials.

Most important, although physicists cannot say exactly how the iron-based superconductors work, they have developed a scheme that many say captures the essence of what's going on. "There is a kind of general consensus of where the superconductivity is coming from," says Patrick Lee, a theorist at the Massachusetts Institute of Technology in Cambridge. "We don't have a full solution yet, but the situation is better than in the cuprates."

In fact, the emerging portrait of the iron-based superconductors jibes with some theories of the cuprates and seems to undermine more-exotic alternatives. So if physicists are on the right track with the iron-based superconductors, then the cuprates may not be so inscrutable after all.

Grab your partner!

For electrons in a metal, moving is usually a drag, as they ricochet off the jiggling ions in the crystalline material and lose energy. In a superconductor, electrons avoid such energy-sapping collisions. In 1957, the American theoretical physicists John Bardeen, Leon Cooper, and John Robert Schrieffer explained how that happens in ordinary superconductors such as niobium chilled to 9.3 kelvin.

The electrons form pairs, the theorists explained. Deflecting an electron then requires breaking the pair, and at low temperatures there isn't enough energy around to do that. So the pairs glide freely. The negatively charged electrons are glued together by vibrations of the positively charged ions called "phonons," the theorists showed; the motion of one electron sets off a phonon that attracts another electron.

The details of this "BCS theory" are hairier. In a metal, the electron clouds of individual atoms meld into riverlike "bands." The electrons flow through the bands in quantum waves in which their momenta are precisely defined but—thanks to quantum uncertainty—their positions are undetermined. In an abstract "momentum space," the momenta of the most energetic electrons trace the so-called Fermi surface—typically a three-dimensional blob. Phonons bind electrons on opposite sides of the surface.

Most physicists agree that the BCS theory cannot explain the cuprates, however, as phonons do not pull hard enough to produce their sky-high critical temperatures. For 24 years, researchers have debated what else makes the cuprates' electrons pair.

The answer lies in waves of magnetism, some say. A cuprate, such as yttrium barium copper oxide, consists of planes of copper and oxygen ions arranged in a square pattern with the other elements sandwiched between the planes. To turn the compound into a superconductor, researchers must season, or "dope," it with a little extra oxygen, which soaks up some of the electrons in the copper-and-oxygen planes. (See figure, p. 1321.)

The undoped "parent compound" also displays an internal patterning called antiferromagnetism in which neighboring copper ions are magnetized in opposite directions. This pattern fades as doping increases and superconductivity sets in. However, fleeting ripples of it remain, and such fluctuations draw the electrons together, more or less replacing the phonons as the "glue," many researchers argue.

Others say that this scenario ignores the most important fact of the cuprates. "Band theory" calculations predict that the materials should be metals. In fact, they're insulators, as the electrons in the copper-and-oxygen planes repel one another so fiercely that they get stuck, one electron to one copper ion, in a "Mott insulator" state.

As doping increases and the impasse eases, pairing emerges without any glue at all, some physicists say. In their "strong correlations" theories, pairing arises solely from quantum-mechanical symmetries and the interactions

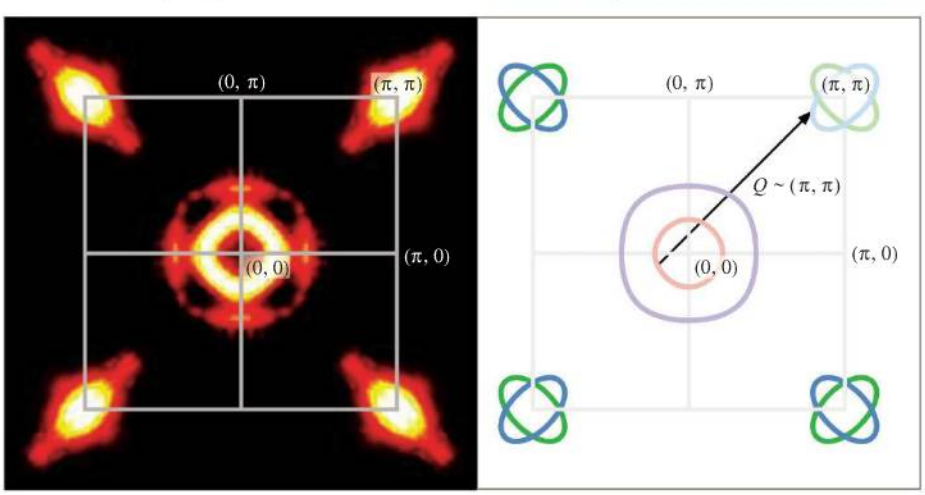

Lay it on me. The Fermi surfaces of potassium-doped barium iron arsenide (*left*) map the momenta of its electrons. Superconductivity may arise because one surface can be shifted to cover another.

CREDIT: H. DING/INSTITUTE OF PHYSICS, CHINESE ACADEMY OF SCIENCES, T. SATO AND K. NAKAYAMA/TOHOKU UNIVERSITY, JAPAN

among electrons shuffling past one another like commuters on a crowded bus—even though the electrons only repel one another.

A shifty solution

As soon as the iron-based superconductors were discovered, physicists noted some uncanny similarities between them and the cuprates. The iron-based compounds are also layer-cake materials with planes of iron ions in squares. In them, superconductivity emerges as a parent material is doped with various elements. And, as in the cuprates, that parent material is antiferromagnetic, with neighboring rows of iron ions magnetized in opposite ways.

The iron-based superconductors differ from the cuprates in an obvious way, however: The parent compounds are metals, not insulators. That fact and other data show that the electrons within them interact less strongly than those in the cuprates, making the materials easier to analyze, says Andrey Chubukov, a theorist at the University of Wisconsin, Madison. "The problem has a chance to be solved, and it's a matter of refining existing theoretical tools," he says.

Drawing on a torrent of data, theorists have sketched a scheme that seems to apply to materials as diverse as samarium iron arsenic oxide, calcium iron arsenide, and iron selenide. At its heart lies the superconductors' Fermi surface—the map of the momenta, or wavelengths, of the waves of electrons within them—which experimenters have traced using photons to blast electrons out of the materials in a technique called angle-resolved photoemission spectroscopy (ARPES). The results show that an iron-based superconductor actually has several ringlike Fermi surfaces. Crucially, one specific ring can be shifted as a whole to overlap another, an arrangement called "nesting." (See diagram, p. 1320.) In fact, the ring must be shifted by a wavelength and in a direction that exactly match the spacing and orientation of the antiferromagnetic striping in the parent compound.

That's no coincidence, Chubukov says. In the undoped compound, the nesting actually causes waves of electrons to interfere to make the antiferromagnetic pattern, much as ripples on a pond can interfere to make striking patterns. Then, in the doped compound, lingering ripples of antiferromagnetism zip between electrons to produce pairing. "The interaction that gives you the antiferromagnetism and the superconductivity is the same," Chubukov says.

Strong circumstantial evidence supports this scheme, physicists say. Using ARPES, researchers have shown that if they dope a material so much that one of the nested Fermi surfaces disappears, then so does the superconductivity. And scientists using neutrons to probe the materials have detected antiferromagnetic fluctuations of just the right character in the superconducting state.

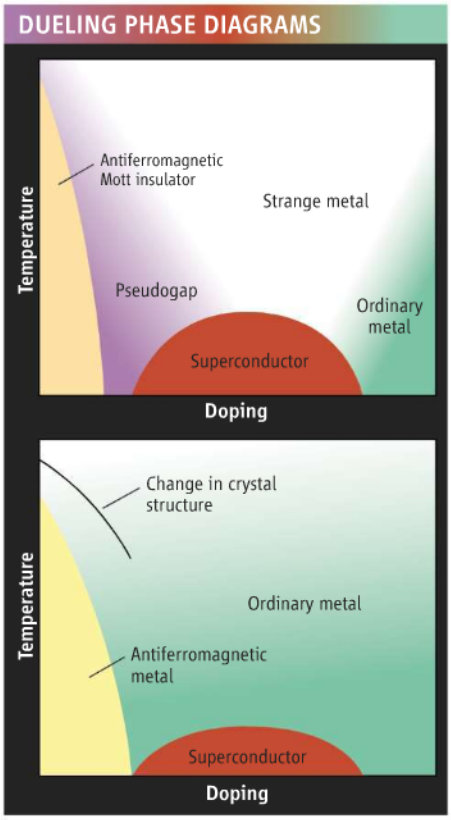

Lookalikes. Cuprate superconductors (*top*) and newer ion-based ones (*bottom*) display some striking similarities as temperature and composition vary.

A key detail remains to be confirmed, however. When pairs form on a Fermi surface, then they gather into a quantum wave of their own called an "order parameter." The order parameters on the nested Fermi surfaces must have opposite signs, says Igor Mazin of the Naval Research Laboratory in Washington, D.C.

That's because, discounting phonons, the electrons should only repel each other. But through some complicated quantum mechanics, that push can turn into a pull if exchanging a magnetic ripple also bounces a pair from one Fermi surface to another with an order parameter of the opposite sign. "If your interaction has the wrong sign, you can reverse it by making your order parameters have opposite signs," Mazin says. "It's a bit mathematical; it's not so physical."

No one has proved experimentally that the order parameters on the two Fermi surfaces have opposite signs, says Michael Norman, a theorist at Argonne National Laboratory in Illinois. "My impression is that sometime this year, this will be cleared up," he says, although he cautions that surprising results are emerging all the time.

Strong dissent

Some researchers doubt that this scheme gets to the crux of the physics in the iron-based superconductors. Several pieces of data show that the electrons in the materials interact as strongly as those in the cuprates do, says Steven Kivelson, a theorist at Stanford University in Palo Alto, California. For example, in the metallic state, their conductivities are as low as 1% of those in typical metals, suggesting that the electrons impede one another enough to spoil quantum waves of definite momentum.

But if that's the case, the "nesting" model of antiferromagnetism goes out the window, says Qimiao Si, a theorist at Rice University in Houston, Texas. Si thinks the antiferromagnetism originates in the tangled physics of the jammed-up Mott insulator state, even though the iron-based compounds are never in that condition. "The system could be on the verge of the Mott [insulator] transition," he argues.

At any rate, the iron-based materials offer little insight into their cuprate cousins, says Philip Anderson, a theorist at Princeton University and a champion of the strong-correlations approach. "To take [them] as giving you information about the cuprates is to try to reconstruct the human figure from a cubist painting," he says. The essence of the cuprates remains their evolution from the Mott insulator state, Anderson says.

But others argue that if the emerging portrait of the iron-based superconductors holds up, then similar physics may explain the cuprates, which also have nested Fermi surfaces. The Mott state in the cuprates would then be irrelevant, says Dung-Hai Lee, a theorist at the University of California, Berkeley. "The iron-based superconductors liberate us from the belief that the Mott physics is essential for high-temperature superconductivity, which is what has kept us stuck for such a long time," he says.

Even if the current conception of the iron-based superconductors is correct, physicists will still have to fill in a huge amount of detail before they have a theory as precise and powerful as the BCS theory—and many doubt they'll ever have one. So it's far too early to write the book on the iron-based superconductors. But given what physicists have learned about the iron-based materials so far, some say it's not too early to start revising the saga of the cuprates.

–ADRIAN CHO

CREDIT: KAY ENGMAN/SCIENCE

SPACE SCIENCE

NASA Dives Into Its Past to Retrieve Vintage Satellite Data

Once forgotten or erased, 1960s-era satellite images are being salvaged from old equipment and proving valuable in climate and space science

On 23 September 1966, NASA's Nimbus II satellite soared over Earth in a polar orbit every 108 minutes, taking pictures of cloud cover and measuring heat radiated from the planet's surface. The data documented the extent of polar ice shelves and the paths of two typhoons, but like thousands of other Nimbus II records, the information was originally stored on analog tapes and later forgotten for decades.

Then last month, researchers working out of an abandoned McDonald's restaurant on the grounds of NASA Ames Research Center in Mountain View, California, recovered the Nimbus data from that day in 1966, creating a photo mosaic of the globe 43 years ago. The resulting image is the oldest and most detailed from NASA's Earth-observing satellites. It's also the latest success story in what researchers call techno-archaeology: pulling data from archaic storage systems. Once forgotten and largely unreadable with modern equipment, old data tapes are providing researchers with new information on changes in the surfaces of Earth and the moon.

The recovered Nimbus II image, georectified and overlaid on Google Earth, significantly pushes back key climate data sets. Until now, researchers had little satellite data prior to 1979. But Nimbus II captured some 2457 records—including visible light and infrared information—over a 9-month period, beginning in May 1966. Moreover, researchers at the Lunar Orbiter Image Recovery Project (LOIRP) in Mountain View who have been methodically tracking down tapes from early spacecraft are opening an even larger window on the past. They have now located tapes from Nimbus I, III, and IV, launched in 1964, 1969, and 1970, respectively. "The period from the 1940s to the 1960s was a cooling interlude," says Dennis Wingo, co-team leader of LOIRP, "so to have heat balance and thermal maps of the Earth from this period, and to be able to compare these to today, should yield a lot of insights."

Already, the rediscovered Nimbus data are creating a stir among climate scientists. Walt Meier, a research scientist at the National Snow and Ice Data Center in Boulder, Colorado, says the finds promise to shed new light on the problem of declining sea ice. "A lot of Nimbus data was collected in the months of August and September, which is when you have the minimum sea ice in the Arctic and the maximum in Antarctica," Meier notes. "So the hope is that once [LOIRP] gets all this data processed, we could take a look at the ice edge during this period and work out sheet-ice extent on a monthly average basis back to the mid-1960s."

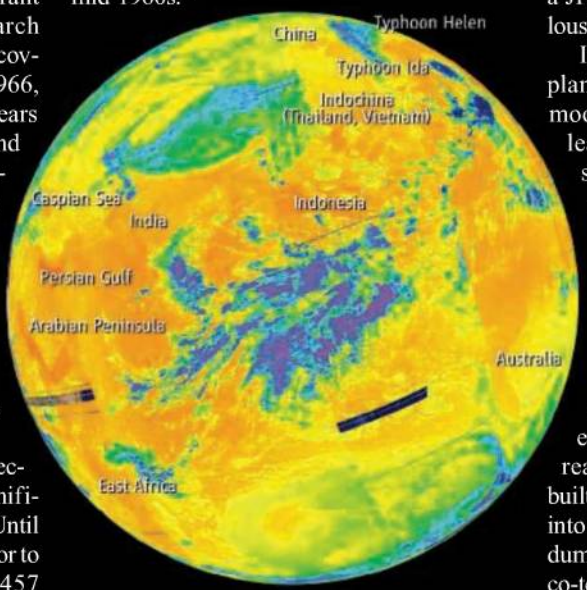

Sixties icon. Satellite data from 23 September 1966 were used to create a thermal map of Asia and show very high, cold clouds over the Indian Ocean in blue and purple and warmer areas such as the Arabian peninsula in orange.

Such scientific interest shows the importance of NASA's early mission records. But during the 1980s, the agency lost much of its old high-quality data. Its early tracking stations recorded satellite data on high-resolution master tapes that used whale oil to bind iron particles to the acetate. The whale oil made the tapes far more durable, but when commercial whaling was phased out in the mid-1980s, NASA couldn't get such long-lasting tapes. So it reused old ones. NASA engineers taped over some 200,000 previously recorded master tapes, including high-resolution records from spacecraft as diverse as early Landsat satellites and Apollo 11, and preserved only low-resolution copies. "A huge amount of data was lost," says Wingo.

NASA also gave away as government surplus the Ampex tape drives—sophisticated versions of old videotape recorders—needed to play back surviving master tapes. Nancy Evans, an engineer and scientist at the Jet Propulsion Laboratory (JPL) in Pasadena, California, obtained four of the aging drives on her own and eventually stored them in her garage in Sun Valley, California, hoping to raise funds one day to rebuild them. "These were the last four in existence," says Evans. "I later found out that most of these FR-900 drives were dumped into the ocean to make coral reefs."

Evans also saved some 1500 master tapes from five Lunar Orbiter missions launched between 1966 and 1967. The tapes were slated to be recycled, but Evans stowed them away at a JPL warehouse. "I thought it was a fabulously worthwhile data set," she says.

In 2007, as NASA drew up now-scuttled plans to send a new crewed mission to the moon, Wingo and colleague Keith Cowing learned of the existence of both the preserved tapes and the tape drives. They contacted Evans, who had since retired, and retrieved the 454-kilogram tape drives from her garage. Each drive is the size of a large refrigerator and was furry with dust and grime.

The LOIRP team obtained $750,000 from NASA and private enterprise and enlisted the assistance of a retired Ampex engineer. They cleaned, rebuilt, and reassembled one drive, then designed and built equipment to convert the analog signals into an exact 16-bit digital copy. "It was like dumpster diving for science," says Cowing, co-team leader at LOIRP.

In November 2008, the team recovered their first image: a famous picture of an earthrise taken by Lunar Orbiter 1 on 23 August 1966. The team's new high-resolution version was so crisp and clear that it revealed many previously obscured details, such as a fog bank lying along the coast of Chile. "We thought if the Earth's surface looks that good a quarter of a million miles away, what does the moon's surface look like 100 miles beneath it?" says Cowing.

So they recovered additional images of the moon itself. With a resolution of 1 meter per pixel, these old images compare well with current Lunar Reconnaissance Orbiter photos, which have an average resolution of 1.21 meters per pixel. Most of the old images were taken under optimum illumina-

CREDIT: NSIDC/LOIRP

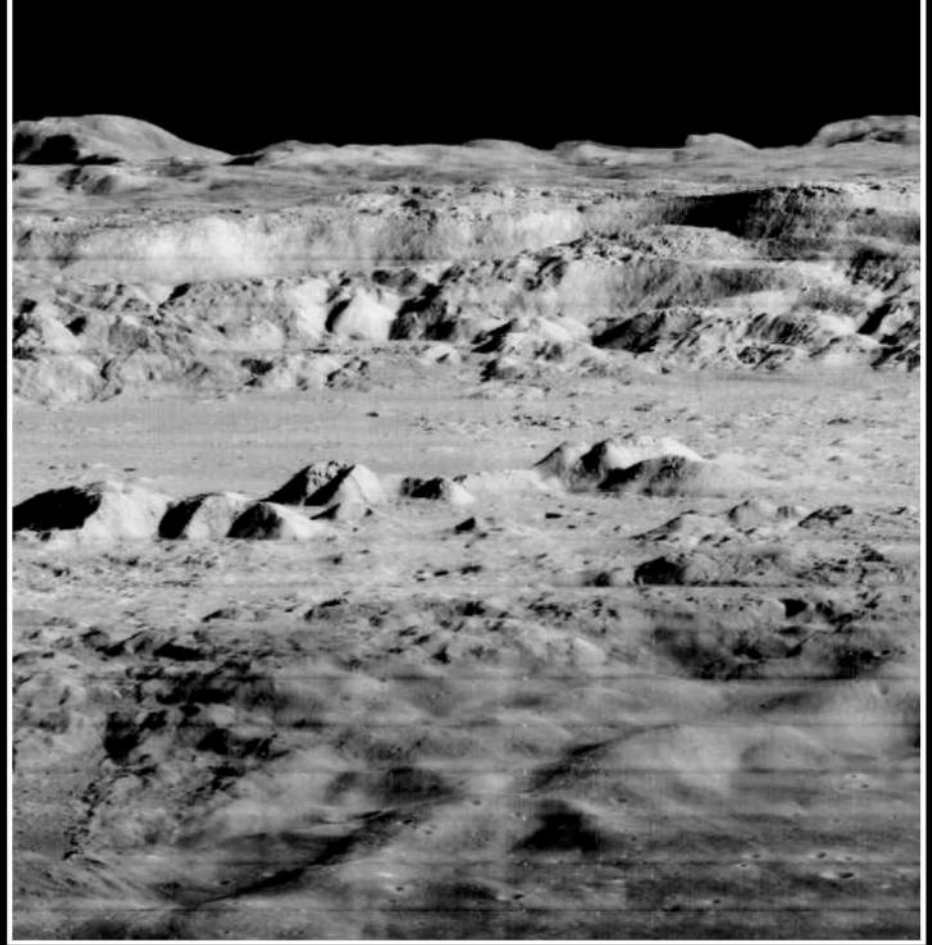

McMoon project. Working from old tapes in an abandoned McDonald's restaurant, researchers recovered images from the 1960s Lunar Orbiter, including a close-up of Copernicus Crater on the moon (*upper right*) and an earthrise (*below*).

tion conditions, says Paul Spudis, a senior scientist at the Lunar and Planetary Institute in Houston, Texas, and "are invaluable both as a scientific and historical resource" for detecting changes on the moon. For example, by comparing the number of small impact craters per unit area in 1966 with the number seen now, analysts will be able to estimate how often asteroids fall in specific areas of the moon, establishing the risk that a future human crew working there would face.

Some of this analysis could even take place in high school or college classrooms, says John Olson, a director in NASA's Exploration Systems Mission Directorate in Washington, D.C., who dreams of "giving students a modern snapshot of a location on the moon and the corresponding LOIRP image" for them to compare.

Certainly, the value of the old mission tapes is no longer in doubt. "By using modern image processing, the LOIRP effort is giving us a window on the moon we have never had before," says S. Alan Stern of the Southwest Research Institute in Boulder, a former NASA associate administrator in charge of all science missions. The larger message to the scientific community is clear, says Meier. "Don't throw away data unless you are absolutely, positively sure you don't need it anymore. Being a pack rat can be a good thing."

–HEATHER PRINGLE

Heather Pringle is a contributing editor at *Archaeology* magazine.

CREDITS: LOIRP/MOONVIEWS.COM

LETTERS

edited by Jennifer Sills

Rebuilding Haiti Smarter

R. KERR'S RECENT NEWS OF THE WEEK STORY "FORESHADOWING Haiti's catastrophe" (22 January, p. 398) nicely summarized the geological and seismological knowledge behind the earthquake that struck Port-au-Prince on 12 January this year. However, he failed to draw an obvious conclusion. Why not take this opportunity to move the capital's critical infrastructure to safer ground? A large part of central Haiti is roughly equidistant from the two major plate boundary faults (Enriquillo in the south, Septentrional in the north), far enough from each to be much safer than the current location. Even relocating 10 to 20 km north of the current airport would be a big improvement because it would be outside of the region of thickest sedimentary fill in Port-au-Prince's alluvial valley.

We can't predict the timing of the next big earthquake, but most Earth scientists agree that another major event in Haiti is inevitable. Comparison of satellite imagery and aftershock patterns to historical descriptions of past ruptures (*1*–*3*) suggests that the recent 12 January event ruptured only part of the segment that last ruptured in 1751; if so, the likelihood of another major event close to Port-au-Prince in the next few decades is quite high. It is usually not feasible to relocate urban infrastructure, but one exception is immediately after a major disaster, when damaged infrastructure has to be rebuilt anyway, and there is heightened awareness among the public and government officials.

One way to begin such a migration is to rebuild some of the most important infrastructure, such as schools, hospitals, and key government buildings—many of them already heavily damaged or destroyed—in a new, safer location. Private-sector construction would follow naturally. Earth scientists did an excellent job of forecasting the seismic risk for Haiti, in some cases decades in advance (*1*–*5*), but unfortunately it had little practical effect. Now Earth scientists have a chance to make a real difference, by speaking with a unified voice about the obvious need and unique opportunity for a safer location for Haiti's capital.

TIM DIXON,* FALK AMELUNG, CHRIS HARRISON, SHIMON WDOWINKSI, GUOQING LIN

Rosenstiel School of Marine and Atmospheric Science, University of Miami, Miami, FL 33149, USA.

*To whom correspondence should be addressed. E-mail: tdixon@rsmas.miami.edu

References

1. J. Kelleher *et al.*, *J. Geophys. Res.* **78**, 2547 (1973).
2. W. R. McCann *et al.*, *Pure Appl. Geophys.* **117**, 1082 (1979).
3. L. R. Sykes *et al.*, *J. Geophys. Res.* **87**, 10,656 (1982).
4. T. H. Dixon *et al.*, *J. Geophys. Res.* **103**, 15157 (1998).
5. D. M. Manaker *et al.*, *Geophys. J. Int.* **174**, 889 (2008).

The Hidden Face of Haiti's Tragedy

WE READ WITH GREAT INTEREST YOUR RECENT News of the Week story "Haiti's quake shifts clinic's focus from AIDS to aid" (J. Cohen, 29 January, p. 509). In addition to the destruction of major civil services, including hospitals and medical centers, there is a less-attended but equally important effect of this disaster. This earthquake will probably lead to an extreme rise in mental disorders—especially stress-related illnesses such as acute stress disorder and posttraumatic stress disorder (PTSD)—in victims who have lost family support systems and face economic instability and an uncertain future. The impact of stress disorders is especially devastating in developing countries, where already underdeveloped health services cannot cope with the flood of traumatized people seeking refuge and help (*1*).

Handling mental disorders is understandably second to treating the physical injuries of survivors. However, the increased prevalence of stress disorders will impede Haiti's recovery; these types of disorders are associated with other psychiatric illnesses (*2*) and have debilitating effects that will burden the health services. It is our hope that along with the recovery and aid to Haiti, there will be international programs put in place to assist refugees suffering from stress disorders and aid them in recuperating and rebuilding their lives.

MENACHEM BEN-EZRA,[1]* AMIT SHRIRA,[2] YUVAL PALGI[2]

[1]Department of Social Work, Ariel University Center of Samaria, Ariel, 40700, Israel. [2]Department of Psychology, Tel Aviv University, Tel Aviv, 69978, Israel.

*To whom correspondence should be addressed. E-mail: menbe@ariel.ac.il

References

1. M. Ben-Ezra, *Nature* **430**, 611 (2004).
2. P. P. Schnurr *et al.*, *Science* **303**, 168 (2004).

The Fate of Atlantic Bluefin Tuna

FOR SEVERAL YEARS, NONGOVERNMENTAL organizations (NGOs) have made Atlantic bluefin tuna (BFT) the archetype of overfishing and general mismanagement of the world fisheries. There are good reasons for this, as BFT crystallizes most of the problems of many fisheries: severe overcapacity, open access in international waters, high market value, and deficient governance at both the international and national levels.

Because of this situation, Monaco has proposed that BFT be listed under Appendix 1 (the "most endangered" category) of the Convention of International Trade in Endangered Species of Wild Fauna and Flora (CITES). However, it is unclear whether current BFT stock status really meets the biological listing criteria for CITES; the media has sometimes exaggerated the threat to BFT, and BFT management has changed for the better during the past two years.

From a strict scientific standpoint, current scientific knowledge does not unequivocally support BFT listing under Appendix 1 (which bans international trade), but it fully supports Appendix 2 (which does not ban fishing in international waters or trade, but mandates monitoring by CITES and the International Commission for the Conservation of Atlantic Tunas).

If Monaco's proposal is adopted at the March CITES meeting in Doha, Qatar, BFT will become the first commercially exploited marine species to be listed under Appendix 1. This could generate a revolution in fisheries management, as more than 100 exploited marine species are currently equally or more overfished than BFT—these include many species of sharks, rays, billfishes, sturgeons, salmons, eels, groupers, snappers, flat fish, deep-sea fish, gadoids, shrimps, and clams. This could finally lead to the implicit substitution of current management fisheries organizations by CITES. Is CITES ready to manage the world fisheries in near future, and is it the right multilateral organization to do it?

JEAN-MARC FROMENTIN

IFREMER, Centre de Recherche Halieutique Méditerranéenne et Tropicale, avenue Jean Monnet, BP 171, 34203 Sète cedex, France. E-mail: jean.marc.fromentin@ifremer.fr

Letters to the Editor

Letters (~300 words) discuss material published in *Science* in the previous 3 months or issues of general interest. They can be submitted through the Web (www.submit2science.org) or by regular mail (1200 New York Ave., NW, Washington, DC 20005, USA). Letters are not acknowledged upon receipt, nor are authors generally consulted before publication. Whether published in full or in part, letters are subject to editing for clarity and space.

Applying Privacy Guidelines

IN HIS PERSPECTIVE "MINING OUR REALITY" (18 December 2009, p. 1644), T. M. Mitchell states that the potential of online data cannot be fully realized unless rules for data sharing and use are put in place to address privacy issues. Several sets of international or regional guidelines that address personal digital information and privacy already exist. These include the United Nations Guidelines Concerning Computerized Personal Data Files, adopted by the General Assembly on 14 December 1990 (*1*); the Organisation for Economic Co-operation and Development Guidelines on the Protection of Privacy and Transborder Flows of Personal Data, adopted on 23 September 1980 (*2*); and the Asia-Pacific Economic Cooperation Privacy Framework, endorsed by APEC Ministers in November 2004 (*3*).

These guidelines can be applied to diverse organizations to regulate data collection, sharing, retention, and use. However, because they are voluntary choices rather than legally

binding instruments, implementation is difficult to enforce, and unauthorized access to or misuse of personal data is difficult to prosecute.

To protect privacy and foster Internet advances, online businesses and anyone else collecting personal data must provide policy-makers with clear and up-to-date information about how that personal data is collected and how and where the data flows. Using this information, policy-makers can supplement, refine, complete, and legalize these guidelines.

SHESEN GUO,* GANZHOU ZHANG, RUN ZHAI

Qianjiang College, Hangzhou Normal University, Zhejiang 310012, China.

*To whom correspondence should be addressed. E-mail: guoshesen@126.com

References

1. World LII, Privacy Law Resources, "United Nations guidelines concerning computerized personal data files" (www.worldlii.org/int/other/PrivLRes/1990/1.html).
2. Organisation for Economic Co-operation and Development, Directorate for Science, Technology and Industry, "OECD guidelines on the protection of privacy and transborder flows of personal data"(www.oecd.org/document/18/0,3343,en_2649_34255_1815186_1_1_1_1,00.html).
3. Australian Government, Department of the Prime Minister and Cabinet, APEC Privacy (www.dpmc.gov.au/privacy/apec/index.cfm).

Response

I AGREE WITH GUO, ZHANG, AND ZHAI THAT multiple guidelines already exist that suggest principles for protecting privacy and use of personal data, and that guidelines lacking teeth are not particularly effective.

I would add one important point: Many of these guidelines and many discussions of data privacy issues are based on outdated assumptions about privacy-enhancing technologies. For example, many assume that the only way to extract useful information from data that is distributed across different organizations is to first collect this data together into a central repository, exacerbating the impact on privacy. This assumption is incorrect. New technologies for privacy-enhancing data mining can in many cases analyze data sets that remain distributed across multiple organizations, producing the same results as if the data were centralized, but with a much-reduced impact on privacy. Guidelines and debates about how to balance the potential benefits and privacy impacts of mining personal data must take such technologies into account if we as a society are to achieve the best tradeoffs. Technologists must play their role in helping to author these guidelines and in helping to assure an informed debate.

TOM MITCHELL

Machine Learning Department, Carnegie Mellon University, Pittsburgh, PA 15213, USA. E-mail: tom.mitchell@cs.cmu.edu

CORRECTIONS AND CLARIFICATIONS

Reports: "100-million-year dynasty of giant planktivorous bony fishes in the Mesozoic seas" by M. Friedman *et al.* (19 February, p. 990). Matt Friedman's affiliation should have been "Committee on Evolutionary Biology, University of Chicago, 1025 East 57th Street, Chicago, IL 60637, USA." The affiliation that was listed is his present address.

News of the Week: "*DSM-V* at a glance" by G. Miller and C. Holden (12 February, p. 770). In the sidebar, it was reported that the term "gender identity disorder" has been retained. In fact, a different term—"gender incongruence"—has been proposed.

News Focus: "The tangled roots of agriculture" by M. Balter (22 January, p. 404). The first paragraph refers to "hunter-gatherers in what is now Israel, Jordan, Syria, and Lebanon." This list, although not comprehensive, also could have included the Palestinian territories, as a few sites are within those borders.

News Focus: "Sex and social structure" by E. Pennisi (23 October 2009, p. 518). Mary Jane West-Eberhard should have been listed as affiliated with the Smithsonian Tropical Research Institute in Panama.

Because of this situation, Monaco has proposed that BFT be listed under Appendix 1 (the "most endangered" category) of the Convention of International Trade in Endangered Species of Wild Fauna and Flora (CITES). However, it is unclear whether current BFT stock status really meets the biological listing criteria for CITES; the media has sometimes exaggerated the threat to BFT, and BFT management has changed for the better during the past two years.

From a strict scientific standpoint, current scientific knowledge does not unequivocally support BFT listing under Appendix 1 (which bans international trade), but it fully supports Appendix 2 (which does not ban fishing in international waters or trade, but mandates monitoring by CITES and the International Commission for the Conservation of Atlantic Tunas).

If Monaco's proposal is adopted at the March CITES meeting in Doha, Qatar, BFT will become the first commercially exploited marine species to be listed under Appendix 1. This could generate a revolution in fisheries management, as more than 100 exploited marine species are currently equally or more overfished than BFT—these include many species of sharks, rays, billfishes, sturgeons, salmons, eels, groupers, snappers, flat fish, deep-sea fish, gadoids, shrimps, and clams. This could finally lead to the implicit substitution of current management fisheries organizations by CITES. Is CITES ready to manage the world fisheries in near future, and is it the right multilateral organization to do it?

JEAN-MARC FROMENTIN

IFREMER, Centre de Recherche Halieutique Méditerranéenne et Tropicale, avenue Jean Monnet, BP 171, 34203 Sète cedex, France. E-mail: jean.marc.fromentin@ifremer.fr

Letters to the Editor

Letters (~300 words) discuss material published in *Science* in the previous 3 months or issues of general interest. They can be submitted through the Web (www.submit2science.org) or by regular mail (1200 New York Ave., NW, Washington, DC 20005, USA). Letters are not acknowledged upon receipt, nor are authors generally consulted before publication. Whether published in full or in part, letters are subject to editing for clarity and space.

Applying Privacy Guidelines

IN HIS PERSPECTIVE "MINING OUR REALITY" (18 December 2009, p. 1644), T. M. Mitchell states that the potential of online data cannot be fully realized unless rules for data sharing and use are put in place to address privacy issues. Several sets of international or regional guidelines that address personal digital information and privacy already exist. These include the United Nations Guidelines Concerning Computerized Personal Data Files, adopted by the General Assembly on 14 December 1990 (*1*); the Organisation for Economic Co-operation and Development Guidelines on the Protection of Privacy and Transborder Flows of Personal Data, adopted on 23 September 1980 (*2*); and the Asia-Pacific Economic Cooperation Privacy Framework, endorsed by APEC Ministers in November 2004 (*3*).

These guidelines can be applied to diverse organizations to regulate data collection, sharing, retention, and use. However, because they are voluntary choices rather than legally

binding instruments, implementation is difficult to enforce, and unauthorized access to or misuse of personal data is difficult to prosecute.

To protect privacy and foster Internet advances, online businesses and anyone else collecting personal data must provide policy-makers with clear and up-to-date information about how that personal data is collected and how and where the data flows. Using this information, policy-makers can supplement, refine, complete, and legalize these guidelines.

SHESEN GUO,* GANZHOU ZHANG, RUN ZHAI

Qianjiang College, Hangzhou Normal University, Zhejiang 310012, China.

*To whom correspondence should be addressed. E-mail: guoshesen@126.com

References

1. World LII, Privacy Law Resources, "United Nations guidelines concerning computerized personal data files" (www.worldlii.org/int/other/PrivLRes/1990/1.html).
2. Organisation for Economic Co-operation and Development, Directorate for Science, Technology and Industry, "OECD guidelines on the protection of privacy and transborder flows of personal data"(www.oecd.org/document/18/0,3343,en_2649_34255_1815186_1_1_1_1,00.html).
3. Australian Government, Department of the Prime Minister and Cabinet, APEC Privacy (www.dpmc.gov.au/privacy/apec/index.cfm).

Response

I AGREE WITH GUO, ZHANG, AND ZHAI THAT multiple guidelines already exist that suggest principles for protecting privacy and use of personal data, and that guidelines lacking teeth are not particularly effective.

I would add one important point: Many of these guidelines and many discussions of data privacy issues are based on outdated assumptions about privacy-enhancing technologies. For example, many assume that the only way to extract useful information from data that is distributed across different organizations is to first collect this data together into a central repository, exacerbating the impact on privacy. This assumption is incorrect. New technologies for privacy-enhancing data mining can in many cases analyze data sets that remain distributed across multiple organizations, producing the same results as if the data were centralized, but with a much-reduced impact on privacy. Guidelines and debates about how to balance the potential benefits and privacy impacts of mining personal data must take such technologies into account if we as a society are to achieve the best tradeoffs. Technologists must play their role in helping to author these guidelines and in helping to assure an informed debate.

TOM MITCHELL

Machine Learning Department, Carnegie Mellon University, Pittsburgh, PA 15213, USA. E-mail: tom.mitchell@cs.cmu.edu

CORRECTIONS AND CLARIFICATIONS

Reports: "100-million-year dynasty of giant planktivorous bony fishes in the Mesozoic seas" by M. Friedman *et al.* (19 February, p. 990). Matt Friedman's affiliation should have been "Committee on Evolutionary Biology, University of Chicago, 1025 East 57th Street, Chicago, IL 60637, USA." The affiliation that was listed is his present address.

News of the Week: "*DSM-V* at a glance" by G. Miller and C. Holden (12 February, p. 770). In the sidebar, it was reported that the term "gender identity disorder" has been retained. In fact, a different term—"gender incongruence"—has been proposed.

News Focus: "The tangled roots of agriculture" by M. Balter (22 January, p. 404). The first paragraph refers to "hunter-gatherers in what is now Israel, Jordan, Syria, and Lebanon." This list, although not comprehensive, also could have included the Palestinian territories, as a few sites are within those borders.

News Focus: "Sex and social structure" by E. Pennisi (23 October 2009, p. 518). Mary Jane West-Eberhard should have been listed as affiliated with the Smithsonian Tropical Research Institute in Panama.

briefly touches on the point: No matter how strongly a theory has been embedded in the cultural zeitgeist (as the trauma model certainly has), we should always be prepared to discard it on the basis of persuasive evidence. Such behavior is a hallmark of good science, which will shed ideas that are contradicted by evidence. Clancy says the trauma model has to go. We would not completely do away with it, but we do agree the model must be discarded in the cases of many victims to whom it does not apply. Clancy approaches child abuse with sensitivity, empathy, and thoughtfulness. Is anybody out there listening?

10.1126/science.1187716

SOCIOLOGY

Putting Law into Practice in Personnel

Anna-Maria Marshall

Anyone who has been employed in the United States has, at one time or another, filled out an equal opportunity form, sat through a sexual harassment prevention program, or followed an affirmative action protocol to hire a new employee. Designed to make the workplace a more fair and equitable place, these policies were vaguely mandated by law, but corporate human resources offices directed their shape and their breadth. Frank Dobbin's impressive *Inventing Equal Opportunity* documents the crucial role played by the personnel profession in translating equal employment law into practice.

Inventing Equal Opportunity
by Frank Dobbin
Princeton University Press, Princeton, NJ, 2009. 320 pp. $35, £24.95. ISBN 9780691137438.

The book provides a corrective for existing explanations for the structure of the American workplace. Some scholars credit social movements whose agendas included the effort to ensure equality in the workplace. The civil rights movement, the women's movement, the disability rights movement, among others, made political demands that led to legal changes. However, Dobbin (a sociologist at Harvard) notes that there is little evidence demonstrating a causal link from social movement activism to corporate policy. Others cite the law as the agent for change: new statutes and judicial opinions recognized new rights for workers; employers responded to those new laws through fear of litigation.

What previous models have in common is that they omit many intervening variables that explain the proliferation of policies—an expansion that has occurred even in a legal climate that has been increasingly hostile to workers' rights. They assume a direct causal arrow between the passage of a law, for example, and the adoption of a corporate policy. According to Dobbin, however, this explanation ignores the ambiguity in the laws and their silence about what compliance looks like. With its separation of powers, government in the United States is considered weak by many political sociologists. Responsibility for creating and enforcing the law is dispersed among many different authorities, thus making it almost impossible to dictate the shape of compliance. Dobbin argues that into this vacuum created by the weak state marched "an army of equal opportunity experts" who defined the meaning of compliance and gave it the force of law.

Dobbin's analysis explores the long-overlooked role of the private sector in defining compliance and in designing many of the policies and procedures that shape the existing American workplace. Specifically, he documents the efforts by generations of human resources professionals to counter discrimination. Dobbin writes: "By institutionalizing equal opportunity as a specialty within personnel, the profession created a place for an internal constituency to champion new rounds of [corporate] equal opportunity and diversity measures."

The author illustrates this model through discussions of several developments in personnel policies, including diversity management, work-family programs, and sexual harassment grievance procedures. For example, in the United States sexual harassment is a form of employment discrimination, although the laws prohibiting discrimination never describe such conduct. The law expanded to embrace sexual harassment through the steady accretion of bureaucratic definitions (regulations issued by the Equal Employment Opportunity Commission) and judicial opinions. But the regulations remained vague, and the judicial opinions offered only piecemeal guidance on how to avoid lawsuits. Thus, simply defining sexual harassment as a form of employment discrimination was not enough to tell employers how to handle it.

In this ambiguous legal environment, employers struggled to find appropriate means to comply with the law's vague prescriptions. Personnel managers stepped into this void. Relying on well-established traditions, they encouraged corporate executives to adopt training programs and grievance procedures. With scant legal evidence, they argued that such policies would inoculate employers from dreaded lawsuits. This prediction became a self-fulfilling prophecy: As more and more employers adopted similar programs, courts took notice, and the U.S. Supreme Court eventually ruled that an employer could successfully defend against a sexual harassment claim by demonstrating that it had a grievance procedure.

Dobbin makes a powerful argument about the importance of long-overlooked personnel managers in creating the legal environment that governs so much of an American's working life. In doing so, he also makes a compelling argument that legal rules do not directly affect behavior. Rather, organizations exert a powerful influence on the meaning of law in particular contexts. It is perhaps understandable that in staking out this new territory, he trivializes the role of law, which after all provided the symbolic raw material that personnel professionals were using to expand their influence. By emphasizing the importance of human resources officials, Dobbin also ignores the role of employees, whose grievances and complaints were the engine of the many changes in the personnel field. Their complaints reflected changed expectations for how they deserved to be treated in the workplace; the demands they placed on their employers prompted personnel professionals to get creative. Although Dobbin skirts these topics, *Inventing Equal Opportunity* lays a strong foundation for further research on them.

10.1126/science.1185959

CREDIT: PHOTOS.COM

The reviewer is at the Department of Sociology, University of Illinois, Urbana-Champaign, 326 Lincoln Hall, 702 South Wright Street, Urbana, IL 61801, USA. E-mail: amarshll@illinois.edu

CONSERVATION

Elephants, Ivory, and Trade

Trade decisions made by the Convention on International Trade in Endangered Species must place science over politics.

Samuel Wasser,[1]† Joyce Poole,[2,3] Phyllis Lee,[3,4] Keith Lindsay,[3] Andrew Dobson,[5] John Hart,[6] Iain Douglas-Hamilton,[7] George Wittemyer,[7,8] Petter Granli,[2] Bethan Morgan,[4,9] Jody Gunn,[10] Susan Alberts,[11] Rene Beyers,[12] Patrick Chiyo,[11] Harvey Croze,[3] Richard Estes,[13] Kathleen Gobush,[1] Ponjoli Joram,[14] Alfred Kikoti,[15] Jonathan Kingdon,[16] Lucy King,[7] David Macdonald,[16] Cynthia Moss,[3] Benezeth Mutayoba,[17] Steve Njumbi,[18]* Patrick Omondi,[19] Katarzyna Nowak[5,16]†

Tanzania and Zambia are petitioning the Convention on International Trade in Endangered Species (CITES) to "downlist" the conservation status of their elephants to allow sale of stockpiled ivory. But just 2 years after CITES placed a 9-year moratorium on future ivory sales (*1*), elephant poaching is on the rise. The petitioning countries are major sources and conduits of Africa's illegal ivory (*2*–*4*). The petitions highlight the controversy surrounding ivory trade (*5*) and broader issues underlying CITES trade decisions.

With illegal wildlife trade in all species worth tens of billions of dollars annually (*4*), CITES must link decisions on legal trade in vulnerable species to (i) the species' role in its ecosystem, (ii) adequate controls on exploitation that can be verified by independent and effective monitoring programs, and (iii) the petitioning country's record in combating illegal trade.

An adult female and a juvenile examine the broken tusk of a fallen elephant. Elephants often spend long periods inspecting bones of their dead.

CREDIT: KARL AMMANN/HTTP://KARLAMMANN.COM/

Ecological Impacts

Loss of keystone species like elephants impacts the integrity of ecosystems and their services (*6*). Repercussions are likely to be marked in Central Africa, coinciding with major reductions in elephant populations (*7*–*9*). Local extirpation of the primary seed disperser of large trees in Central African forests may substantially affect long-term viability of the second most important carbon capture forests in the world (*9*, *10*).

In Zambia, elephants maintain the transition zone separating the habitats of genetically distinct savannah and forest elephants. In Tanzania, they play a major role in shaping woodland structure of extensive areas like the Selous Game Reserve (SGR)—the second largest World Heritage site on Earth.

Lack of Adequate, Verifiable Controls

Recent work strongly suggests that poaching is reducing Africa's continent-wide elephant population (*3*). Elephant population declines were under way at many locations (*7*–*9*) in 2007 when CITES gave its final approval to petitions allowing South Africa, Botswana, Namibia, and Zimbabwe to sell 110 tons of stockpiled ivory to China and Japan, despite heated debate. This debate focused on one key question: Does legal sale influence levels of poaching across Africa (*11*)? That question could not be resolved, partly because MIKE (Monitoring Illegal Killing of Elephants), created by CITES in 1997 to assess poaching rates on a continental scale, is unable to deliver data relevant to the causality mandate (*12*–*14*). With no reliable verification in place, the European Union brokered a compromise, making the 2008 sale contingent on a 9-year moratorium on future stockpile sales. The moratorium would provide time to enhance enforcement and to monitor the impact of the sales in the absence of further legal trade. CITES, however, restricted the moratorium to the four countries involved in the initial sale (*1*) and never addressed whether poaching levels were so serious that any further trade could ultimately jeopardize elephant survival throughout most of Africa.

Ivory Trade from Tanzania and Zambia

Tanzania and Zambia (*15*, *16*) are exploiting this restricted moratorium in their petitions. Approval requires demonstration that their elephant populations are secure, law enforcement is effective, and sales will not be detrimental to elephants. Yet, Zambia

[1]University of Washington, Seattle, WA 98195, USA. [2]ElephantVoices, 3236 Sandefjord, Norway. [3]Amboseli Trust for Elephants, Langata, Nairobi 00509, Kenya. [4]University of Stirling, Stirling FK9 4LA, UK. [5]Department of Ecology and Evolutionary Biology, Princeton University, Princeton, NJ 08540, USA. [6]Tshuapa-Lomami-Lualaba Project, Kinshasa, Democratic Republic of Congo. [7]Save the Elephants, Nairobi 00200, Kenya. [8]Colorado State University, Fort Collins, CO 80523, USA. [9]Zoological Society of San Diego, Central Africa Program, Yaoundé, Cameroon. [10]Anglia Ruskin University, Cambridge CB1 1PT, UK. [11]Duke University, Durham, NC 27708, USA. [12]University of British Columbia, Vancouver, BC, V6T 1Z4, Canada. [13]5 Granite Street, Peterborough, NH 03458, USA. [14]Udzungwa Mountains National Park, Sanje, Tanzania. [15]University of Massachusetts, Amherst, MA 01003, USA. [16]WildCRU, Zoology, University of Oxford, Oxford OX13 5QL, UK. [17]Sokoine University of Agriculture, Morogoro, Tanzania. [18]International Fund for Animal Welfare, Nairobi 00603, Kenya. [19]Kenya Wildlife Service, Nairobi 00100, Kenya.

*The views expressed in this paper are his own and not necessarily those of IFAW.

†Authors for correspondence. E-mail: wassers@u.washington.edu (S.W.); knowak@princeton.edu (K.N.).

and Tanzania are among the largest sources of, and transit countries for, Africa's illegal ivory (*3*, *4*). China and Japan, the only two approved importing countries, are also among the three largest consumers of illegal ivory (*2*, *4*). They too are failing to control illegal trade, risking legal sales becoming cover for black-market ivory.

Ivory seizures are one of the most rigorous metrics of illegal ivory markets, illustrating the scale of involvement by country. Since the ivory ban, seizures of illegal ivory peaked in 2002, 2006, and 2009 (*2*). Zambia and Tanzania were among the most heavily involved in this trade during each peak; they also petitioned CITES to downlist their elephants in those same years. The largest single ivory seizure since the ivory trade ban (6.5 tons in Singapore) in 2002 was shown by DNA analyses to have originated almost entirely from Zambia (*3*). Zambia unsuccessfully petitioned CITES to downlist their elephants that year, and other similarly sized seizures followed (*17*).

Tanzania shipped 41% of the seizures in the 2006 peak (11 of 27 tons) (*2*, *4*). DNA testing on 2600 kg from Hong Kong and 5200 kg from Taiwan confirmed origins from the Selous (southern Tanzania) and Niassa (northern Mozambique) Game Reserves complex (*4*). Tanzania also submitted, but then withdrew, a petition to downlist their elephants in 2006, only to resubmit in 2009—when more than 14 tons of ivory shipped from Tanzania were seized (*18*, *19*). Tanzania has the greatest average seizure size of any country in the Elephant Trade Information System (ETIS)—established by CITES to monitor trends in the illegal ivory trade. These large seizures are indicative of organized crime and suggest that Tanzania and Zambia's abilities to address these challenges are considerably compromised (*2*). But this was not always the case.

In 1989, Tanzania launched Operation Uhai, a highly successful antipoaching offensive by the wildlife department, police, and military. That year, Tanzania submitted one of six proposals to CITES that led to the 1989 ivory trade ban.

In recent years, Tanzania and Zambia have become less transparent about population sizes and poaching-related mortalities. Three weeks before the CITES decision, information on Tanzanian elephant population trends and mortalities was still unavailable, impeding scientific assessment. Carcass counts, often an important metric of population trends (*20*), were either not collected or inaccurate in many recent aerial surveys. This year, SGR's carcass count was reportedly less than 2%, low even for populations with minimal mortality (*20*). Transparent, scientific peer review of census methods and results is needed for verification.

The proportion of elephant mortality attributed to illegal killing (PIKE)—an index of poaching threat (*12*, *21*)—in Tanzania's SGR rose from 22% in 2003 to 63% in 2009 (*2*, *12*). Recent PIKE values are unavailable for western Tanzania, where illegal killing of elephants when reported was as high as or higher than in the Selous (*12*), and reputedly remains so. In Zambia, PIKE is rising, with record levels of 88% in 2008 (*12*). Monitoring data for Zambia are deficient, with small sample sizes limiting interpretation.

CITES decisions should be based not only on national trends in population size and illegal killing but also on trends for subpopulations within ecological aggregations (some of which span national boundaries) (*5*, *22*, *23*). Tanzania shares elephant populations with Kenya (Tsavo-Mkomazi, Amboseli-Kilimanjaro, and Mara-Serengeti) and Mozambique (via the Selous-Niassa Corridor), but neither country was consulted by Tanzania on its downlisting and trade proposal.

Review of petitions is undertaken only by bodies selected by the CITES secretariat, with no engagement of the wider scientific community. The report of the Panel of (four) Experts evaluating the current petitions is a case in point. A system of peer review should be adopted, with greater reliance on knowledgeable independent experts.

Conclusion

Proceeds of a sale of Tanzania's 90 tons and Zambia's 22 tons of ivory are likely to be on the order of $14 million and $3.5 million, respectively, depending on ivory price at auction [~$150/kg at average values achieved in 2008 sales (*24*)]. This represents less than 1% of annual tourism revenues for Tanzania (*25*). Ivory sales could jeopardize those revenues, either from tourist sanctions or by triggering widespread poaching.

The scale of illegal ivory trade demonstrates that most of Africa lacks adequate controls for protection of elephants. The petitioning countries are not succeeding in responsibly controlling their illegal trade, nor are the countries likely to act as buyers of the ivory. Furthermore, MIKE, the system of verification, is currently unable to meet its full mandate, and an analysis integrating data from both MIKE and ETIS is lacking (*12*). In the absence of data, precautionary principles should be applied.

We contend that no "one-off" ivory sales should be approved, regardless of who is the seller or buyer. Such sales split the appendix listing of a single species (which CITES itself recommends against); introduce uncertainty of supply into the marketplace, encouraging poaching; and stimulate conflict among people working for effective elephant conservation. Ultimately, CITES will only meet its mandate to protect wildlife if criteria that place science above politics are applied to all CITES trade decisions. The implications reach far beyond trade species, potentially affecting ecosystem health (*6*), climate (*10*), and even the spread of zoonotic disease (*26*).

References and Notes

1. CITES, "Amendments to Appendices I and II of the Convention" (CoP14, No. 2007/022, CITES, Geneva, 2007); www.cites.org/eng/notif/2007/E022.pdf.
2. T. Milliken, R. W. Burn, L. Sangalakula, *The Elephant Trade Information System (ETIS) and the Illicit Trade in Ivory* (CoP15, Doc. 44.1, TRAFFIC, Cambridge, MA, 2009); www.cites.org/eng/cop/15/doc/E15-44-01A.pdf.
3. S. K. Wasser *et al.*, *Conserv. Biol.* **22**, 1065 (2008).
4. S. K. Wasser, B. Clark, C. Laurie, *Sci. Am.* **301**, 68, 76 (2009).
5. E. Stokstad, *Science* **327**, 632 (2010).
6. P. Coppollilo, H. Gomez, F. Maisels, R. Wallace, *Biol. Conserv.* **115**, 419 (2004).
7. R. Beyers, thesis, University of British Columbia, Vancouver (2008); https://circle.ubc.ca/handle/2429/960.
8. J. J. Blanc *et al.*, *African Elephant Status Report 2007* (IUCN, Gland, 2007).
9. S. Blake, S. L. Deem, E. Mossimbo, F. Maisels, P. Walsh, *Biotropica* **41**, 459 (2009).
10. S. L. Lewis *et al.*, *Nature* **457**, 1003 (2009).
11. E. Bulte, R. Damania, L. Gillson, K. Lindsay, *Science* **306**, 420 (2004).
12. CITES, "Monitoring of illegal hunting in elephant range states" (CoP15, Doc. 44.2, 2009); www.cites.org/eng/cop/15/doc/E15-44-02.pdf.
13. CITES, "Monitoring of illegal hunting in elephant range states" (CoP13, Doc 29.3, 2004); www.cites.org/eng/cop/13/doc/E13-29-3.pdf.
14. CITES, "Monitoring of illegal hunting in elephant range states" (CoP14, Doc 53.3, 2007); www.cites.org/eng/cop/14/doc/E14-53-3.pdf.
15. CITES, "Consideration of proposals for amendment of Appendices I and II" (CoP15, Prop. 4, Rev. 1, 2009); www.cites.org/eng/cop/15/prop/E-15-Prop-04.pdf.
16. CITES, "Consideration of proposals for amendment of Appendices I and II" (CoP15, Prop. 5, 2009); www.cites.org/eng/cop/15/prop/E-15-Prop-05.pdf.
17. J. Nielsen, "Poachers target African elephant for ivory tusks," *NPR*, 2 January 2007; www.npr.org/templates/story/story.php?storyId=6677444.
18. "Consignee, broker of elephant tusk shipments to be sanctioned," *GMA News.TV*, 20 May 2009; www.gmanews.tv/story/162084/Consignee-broker-of-elephant-tusk-shipments-to-be-sanctioned.
19. "Selous: The killing fields," *ThisDay*, 29 October 2009; www.savetheelephants.org/news-reader/items/selous-the-killing-fields-40tanzania41.html.
20. I. Douglas-Hamilton, A. Burrill, in *African Wildlife: Research and Management* (International Council of Scientific Unions, Paris, France, 1991), pp. 98–105.
21. O. Kahindi *et al.*, *Afr. J. Ecol.*, published online 15 December 2009; www3.interscience.wiley.com/journal/123215025/abstract.
22. R. J. Van Aarde, S. M. Ferreira, *Environ. Conserv.* **36**, 8 (2009).
23. B. Frank, P. B. Maurseth, *Ecol. Econ.* **60**, 320 (2006).
24. CITES, "Report on the one-off ivory sale in Southern African countries" (SC58 Doc. 36.3, 2009); www.cites.org/eng/com/SC/58/E58-36-3.pdf.
25. World Travel and Tourism Council (2009); www.wttc.org/bin/pdf/original_pdf_file/tanzania.pdf.
26. K. F. Smith *et al.*, *Science* **324**, 594 (2009).

27. We thank A. Estes, D. Stiles, S. Waterland, W. Travers, and M. Rice for comments.

10.1126/science.1187811

PHYSICS

Random Quantum Networks

Diederik S. Wiersma

The optical modes of disordered materials can couple with atomic emission and could create states that would be useful in quantum information processing.

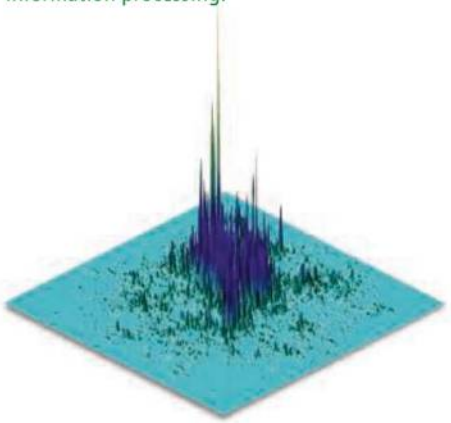

Optical modes spring from disorder. A disordered array of scattering elements can still set up well-defined optical modes, called Anderson-localized modes. Here, a model study shows a localized optical mode created in a two-dimensional planar waveguide containing a random array of holes (*12*).

The interaction between light and matter at the quantum level offers intriguing ways to process and transport information [see, for example, (*1*)]. Experimental realizations of quantum computers are, however, still in their infancy. A major challenge is the realization of a qubit—the quantum version of a bit that entangles quantum states—that can be manipulated and coupled to other qubits. For example, one strategy for coupling light and matter places an atom or quantum dot in a tiny cavity, where it couples resonantly with the cavity's optical modes (*2*). Practical difficulties of this approach arise because a highly efficient cavity is needed, and it must also be exactly tuned to the emission frequency of the source. On page 1352 of this issue, Sapienza *et al.* report an approach that simplifies this problem enormously (*3*). They have created a photonic structure that intentionally is very disordered, in which efficient random cavities are formed at many frequencies.

Humans, especially when engineering a mechanism or structure, often favor neat and perfect structures, and often miss the opportunities offered by irregular and disordered systems (*4*, *5*). Biological systems optimize functionality but not necessarily symmetry—the patterns of trees in a forest or cells in our brain are not periodic lattices. Even the highly refined silicon crystals used in electronic devices need the addition of impurities, called dopants, to become useful materials for transistors. In this regard, physicists have tried for years to create clean, periodic photonic crystals (*6*, *7*)—materials that block light over narrow frequency bands. These materials could be used to create high–quality-factor microcavities that can trap light for long periods of time. However, manufacturing problems continue to be encountered that arise from residual disorder in the structure (*8*).

A very different approach to create photonic materials exploits the fascinating optical properties offered by disorder itself. We might expect that light becomes incoherent in random structures and would not be able to exhibit interference effects, but this does not occur. The optical response just becomes more complex as the light undergoes multiple scattering events. An example of interference from a disordered photonic material can be observed when coherent laser light is scattered from a translucent material, such as white paper or milk glass. "Speckle," a grainy pattern of randomly distributed dots, results from the interference of a number of randomly scattered light waves.

Another powerful example of interference in multiple scattering is Anderson localization of light, which occurs when counterpropagating waves in a random structure interfere constructively to form standing wave patterns (*9*). These localized modes have a random, irregular spatial profile, but their behavior is similar to that of regular optical cavity modes (see the first figure). It is this principle that Sapienza *et al.* used to create a system in which quantized light sources (in their case, quantum dots) are coupled to optical cavities that are engineered to deviate from a perfect lattice.

To obtain a useful building block for quantum information processing, the atoms or quantum dots must be strongly coupled to a cavity mode (*10*)—so strongly that the presence of a single photon in the cavity saturates the excited state of the atom. An excited atom can then repeatedly emit and reabsorb a photon before it has time to escape from the cavity. This process creates an entangled state between the atom and the photon—the photon state is directly connected to the state of the atom. The beauty of this approach is that such an entangled photon can travel to distances far away from the particle, still carrying its quantum information, and couple to other atoms to form a quantum network (*11*).

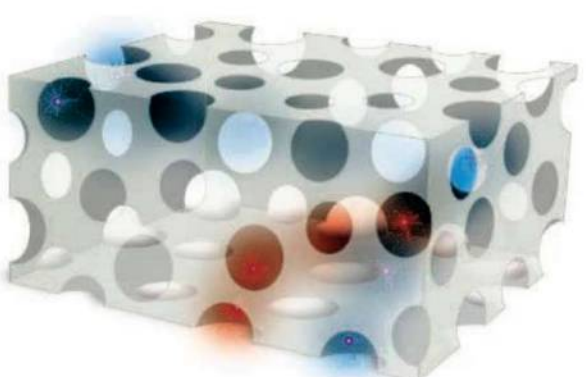

Random yet robust coupling. Sapienza *et al.* created disordered 1D waveguides to create such modes, but it should be possible to create these modes in a 3D random network of holes. Atoms within this material can couple to these modes, and if the coupling is sufficiently strong, act as single-photon emitters and form quantum networks. Here, two sets of coupled atoms are shown that emit strongly at different frequencies (depicted in red and blue). The localized modes can exchange photons (shown as blue or red light moving between the atoms) and thereby share quantum information.

In the disordered materials used by Sapienza *et al.*, Anderson-localized modes are formed at random locations and the wave patterns have random central frequencies. Such modes are not formed around a specific defect of the structure, but rather build up over a volume that contains a certain number of scattering elements. The matching of emitters (in this case, quantum dots) and cavities occurs through a statistical process: In certain positions, the emission frequency of a dot matches exactly that of a localized mode, and efficient coupling is obtained.

The dimensionality of the structure plays a crucial role in Anderson localization. The waveguides in the disordered structures used by Sapienza *et al.* create effectively one-dimensional (1D) localized modes. This is the easiest route for obtaining localization, because any nonzero disorder can generate localized modes in the 1D case,

European Laboratory for Non-linear Spectroscopy, CNR-INO, via Nello Carrara, 1 Sesto Fiorentino, Florence 50019, Italy. E-mail: wiersma@lens.unifi.it

and the amount of scattering determines only the spatial extent of the modes (and thereby the cavity volume). For 3D structures, like powders or porous networks, light can also be localized, but the amount of scattering has to exceed a certain critical value. Although Sapienza *et al.* did not reach the strong coupling regime, they did see a large effect on the emission of the dots, in the form of a strong emission enhancement. This so-called Purcell effect is a precursor to strong coupling and shows that the strategy is very promising.

The benefits of using disordered materials can be realized both in fabrication and device operation. Disordered structures are much easier and cheaper to make than extremely precise nanoscale cavities. It sounds almost trivial, but disordered structures are robust against disorder. We cannot predict in advance which source will couple to which mode, but the end result will be a broad set of sources in a range of frequencies that are all coupled to cavity modes. For example, it may be possible to build a single-photon source that is also broadband, meaning that it emits not at just one frequency but over a range of frequencies. The emitters could then be controlled by secondary light beams at frequencies outside the localization band.

The approach of Sapienza *et al.* also raises interesting possibilities in quantum information processing. When Anderson-localized modes occur at the same or nearby frequencies, they can couple to each other to form so-called necklace states. A series of localized modes can exchange photons and thereby share the quantum information of the atoms or dots located in each mode. It might be much simpler to construct a large-size quantum memory or information processor this way than with perfect, periodic coupled nanocavities (see the second figure). The information contained in such a random structure can be written, read, and erased by external light beams that are also multiply scattered, but not localized, and carry within their speckle pattern the information stored in the quantum network. This is but one of many possibilities that may arise from the use of disordered photonic structures.

References and Notes

1. M. A. Nielsen, I. L. Chuang, *Quantum Computation and Quantum Information* (Cambridge Univ. Press, Cambridge, UK, 2000).
2. T. Wilk, S. C. Webster, A. Kuhn, G. Rempe, *Science* **317**, 488 (2007).
3. L. Sapienza *et al.*, *Science* **327**, 1352 (2010).
4. For an inspiring alternative view on beauty, see (*5*).
5. T. Itoh, *Wabi Sabi Suki: The Essence of Japanese Beauty* (Mazda Motor Corporation, Hiroshima, 1993).
6. J. D. Joannopoulos, R. D. Meade, J. N. Winn, *Photonic Crystals: Molding the Flow of Light* (Princeton Univ. Press, Princeton, NJ, 1995).
7. K. Sakoda, *Optical Properties of Photonic Crystals* (Springer-Verlag, Berlin, 2001).
8. A. F. Koenderink *et al.*, *Phys. Rev. B* **72**, 153102 (2005).
9. A. Lagendijk, B. van Tiggelen, D. S. Wiersma, *Phys. Today* **62**, 24 (2009).
10. D. P. DiVincenzo, *Fortschr. Phys.* **48**, 771 (2000).
11. H. J. Kimble, *Nature* **453**, 1023 (2008).
12. D. S. Wiersma, *Nat. Phys.* **4**, 359 (2008).

10.1126/science.1187084

EVOLUTION

Trees, Fast and Accurate

A scalable and fast method for building very large evolutionary trees achieves greater accuracy than previously thought.

Elizabeth S. Allman and John A. Rhodes

Inferring evolutionary relationships from DNA or protein sequence data is now routine in biological investigations. Although techniques have improved for using such information to generate phylogenetic trees that represent these histories (*1*), challenges remain. In particular, the computational demands of preferred statistical approaches make them infeasible for finding large phylogenies. However, on page 1376 of this issue (*2*), Roch theorizes that a less comprehensive analysis might be surprisingly reliable.

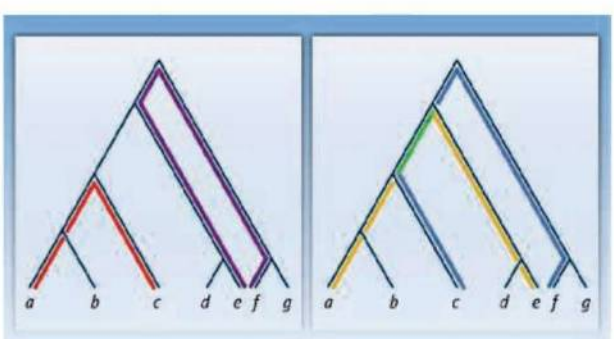

Distance estimates. Shown is an example of a "true" phylogenetic tree representing the evolutionary history of seven taxa (*a*, *b*, *c*, *d*, *e*, *f*, and *g*). Pairwise distances between taxa are computed from orthologous gene sequences. Distances are random variables reflecting path lengths in the tree. (**Left**) The paths between *a* and *c* (red) and between *e* and *f* (purple) do not share a common history, so the random variables [distances $d(a, c)$ and $d(e, f)$] are independent of each other. (**Right**) The paths between *a* and *e* and between *c* and *f* share a common history (green), so independence is lost; $d(a, e)$ (yellow and green) and $d(c, f)$ (blue and green) are correlated.

For a moderate number of taxa, the now-dominant methods adopt a probabilistic model of sequence evolution and then, using either maximum likelihood (ML) or Bayesian frameworks, determine the trees that best fit the sequence data. Such analyses are well grounded in statistical tradition and, if the model approximates reality, can be expected to perform well. However, they are computationally intensive: ML leads to a complex optimization problem not only over many numerical parameters, but also over all trees that might relate the taxa. Bayesian approaches involve a random walk over these trees. For n taxa there are $1 \cdot 3 \cdot 5 \cdot \ldots \cdot (2n - 5)$ trees to be considered, so that when n is large, the size of tree space is a fundamental impediment. This explosion in the number of trees results in unacceptably long run times of computer analyses, so searches for optimal trees may be incomplete.

An alternative faster approach is to algorithmically construct a single tree by successively grouping closely related taxa. The sequences for each pair of taxa a, b are compared, and a single number $d(a, b)$ is computed to express their distance (relationship) along the unknown tree. The sequences are then discarded, as all decisions on joining taxa are based solely on these distances. Two well-known examples of such agglomerative algorithms are the unweighted pair group method with arithmetic mean and the more reliable neighbor-joining (NJ) method.

The apparent drawback of distance-based techniques lies in only comparing sequences pairwise—the full information that could be extracted from n-way comparisons is not used. Thus, distance methods do not perform as well as more complete statistical

Department of Mathematics and Statistics, University of Alaska, P.O. Box 756660, Fairbanks, AK 99775, USA. E-mail: e.allman@alaska.edu; j.rhodes@alaska.edu

approaches. However, for large trees, only distance methods are practical.

Roch shows, through a theoretical examination, that agglomerative construction of trees from distances can perform better than one might expect. The basic insight is to take advantage of correlations among the distances that result from a shared evolutionary history (see the figure). Agglomeration joins groups of taxa iteratively, so that at any stage, partial knowledge of the tree allows an algorithm to make use of such correlations. Using additional ideas—in particular, a "blindfolded cherry-picking" algorithm that allows mistaken groupings to be dissolved (*3*)—Roch provides an agglomerative algorithm that effectively exploits this extra information in the distances.

This new method is surprisingly efficient, as measured by the length of sequences required to return the correct tree with high probability. Roch determined that the required sequence length had the same dependence on key tree features—the number of taxa, the depth of the tree, and the shortest edge length—as that conjectured for ML, up to an undetermined constant factor. Although the sequence length requirement for a different, nonagglomerative distance method (*4*) matches Roch's if some tree branches are long, it is notable that agglomeration need not weaken performance.

Another surprise of the analysis by Roch is that when all tree branches are short, the sequence length requirement is independent of the depth of the tree. It has long been known that deep divergences in trees can be difficult to infer, as more recent mutations obscure the signal of older ones. However, short branches imply that more bifurcations occur in the tree, giving additional sources of information. A "phase transition" occurs at a critical value of branch length, below which depth is irrelevant to the required sequence length. This sort of behavior holds for a more elaborate statistical method of phylogenetic reconstruction (*3*), but now we learn that even distance methods can achieve it.

Unfortunately, theoretical results on sequence length requirements for ML are lacking, as are precise values of the constants in Roch's result, preventing a full comparison of the methods. Moreover, although ML simultaneously fits numerical model parameters and trees, Roch's method assumes that the mutation rate parameters are known, so in practice they would have to be inferred by some other procedure. Additionally, the models Roch considers lack mutation rate variation among sites along the sequence. Still, all models are likely to be deficient under some circumstances, and the potential shown for both speed and accuracy, even under restrictive assumptions, is tantalizing.

Most current practical agglomerative algorithms, including NJ, were not designed to account for distance correlations. A notable exception is the BIONJ algorithm (*5*), which does consider distance covariances to some extent, and through simulation appears to offer improved performance. Roch's algorithm, while ingenious, is complex and designed for the theoretical analysis of what is possible. The next challenge is to translate the understanding that Roch provides into fast, practical algorithms that more fully exploit the distance correlations. New software must strike a balance between extracting more information from distances and possible speed reductions over simpler agglomerative methods. Although Roch provides a roadmap for one approach, practical trade-offs remain to be seen.

References and Notes

1. J. Felsenstein, *Inferring Phylogenies* (Sinauer, Sunderland, MA, 2004).
2. S. Roch, *Science* **327**, 1376 (2010).
3. C. Daskalakis, E. Mossel, S. Roch, *Probab. Theory Relat. Fields* 10.1007/s00440-009-0246-2 (2009).
4. P. L. Erdős, M. A. Steel, L. A. Székely, T. J. Warnow, *Random Struct. Alg.* **14**, 153 (1999).
5. O. Gascuel, *Mol. Biol. Evol.* **14**, 685 (1997).

6. Supported by NSF grant DMS 0714830.

10.1126/science.1187797

BIOPHYSICS

Enforcing Order on Signaling

Mechanical forces constrain the spatial organization of a cell surface receptor, thereby altering its signaling function and cell behavior.

Matthew Paszek[1] and Valerie Weaver[1,2,3,4]

Mechanical forces provide important regulatory information that directs development. Even throughout adulthood, tissue homeostasis remains tightly linked to tensional homeostasis, the perturbation of which often leads to chronic conditions such as cardiovascular disease, arthritis, and cancer (*1*, *2*). Environmental cues affect cell behavior by triggering signal transduction networks, but how cells actually integrate mechanical cues with these biochemical networks remains largely unresolved. On page 1380 in this issue, Salaita *et al*. describe how mechanical force, spatial organization of large clusters of cell surface receptors, and receptor-mediated signal transduction are coupled (*3*). Disruption of this mechanical-coupling mechanism in tumor cells may explain the invasive characteristics of aggressive, metastatic cancers.

Most models of cellular "mechanotransduction" incorporate the idea that proteins subjected to force undergo conformational changes that alter their function. One example is illustrated by the force-dependent assembly of integrin adhesion structures called focal adhesions. An integrin is a cell surface transmembrane receptor that interacts with the extracellular matrix outside the cell and with cytoskeletal and signaling molecules through its intracellular domain. In a "protein-centric" model of mechanotransduction, cytoskeletal tension on integrins and associated focal adhesion proteins drives the unfolding of key adaptor proteins that are linked to the "tensed" integrin. These conformational changes reveal binding sites that permit association with a network of proteins essential for signal transduction (*4*).

In contrast to this classic protein-based mechanotransduction model, Salaita *et al*. postulate that mechanical cues can impose spatial patterning on cell surface receptors that alter their signaling function. Many transmembrane receptors at the cell surface assemble into dimers, trimers, or higher-order oligomers to initiate intracellular signaling. In a "membrane-centric" mechanotransduction mechanism (*5*), Salaita *et al*. propose that either applied force or cellular tension can affect lateral receptor movement within the membrane to change the size (degree of oligomerization) of receptor clusters, or alter their spatial organization throughout the

[1]Center for Bioengineering and Tissue Regeneration, Department of Surgery, University of California, San Francisco (UCSF), San Francisco, CA 94143, USA. [2]Department of Anatomy, UCSF, San Francisco, CA 94143, USA. [3]Department of Bioengineering and Therapeutic Sciences, Eli and Edythe Broad Center of Regeneration Medicine and Stem Cell Research, and Helen Diller Comprehensive Cancer Center, UCSF, San Francisco, CA 94143, USA. [4]Department of Bioengineering, University of Pennsylvania, Philadelphia, PA 19104, USA. E-mail: valerie.weaver@ucsfmedctr.org

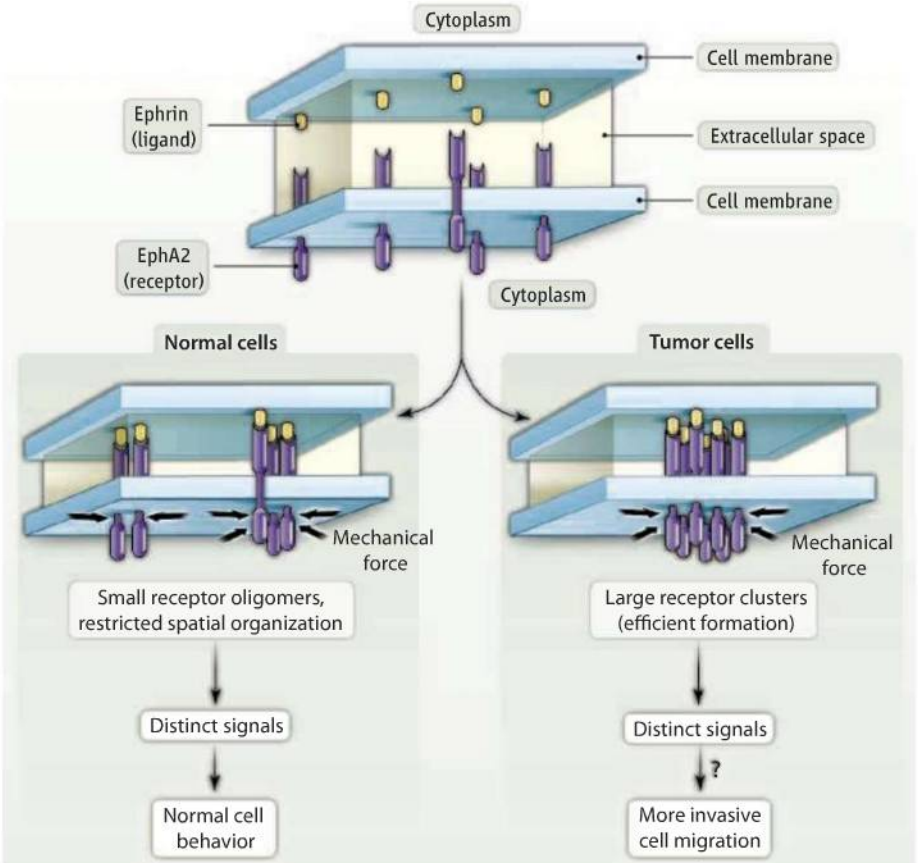

Opposing forces. EphA2 receptors on one cell membrane bind to ephrin ligands on an apposing membrane. In normal cells, receptors oligomerize and activate signaling pathways that control cell growth, survival, and movement. Contractile forces of the cytoskeleton drive oligomer assembly, whereas mechanical impediments (whose source is unclear) on receptor or ligand movement restrict assembly and dictate the organization of oligomers in the membrane. In tumor cells, receptor movement is more efficient, resulting in larger clusters that trigger distinct responses including cytoskeletal changes and more robust activation of signaling molecules. Normal mechanical constraints may be lost in tumor cells.

membrane. Consequently, different cellular responses emerge depending on the spatial configuration of receptors.

To test their predictions, Salaita *et al.* evaluated signaling between the transmembrane receptor tyrosine kinase EphA2 and its ligand, ephrin-A1, which is normally presented on an apposed cell membrane. After binding to their ligands, Eph receptors assemble into dimers or small oligomers, become active, and trigger signaling cascades (*6*). Salaita *et al.* show that over time, ligand-bound EphA2 receptors expressed in a human breast cancer cell line condensed into very large macroscopic clusters exceeding several micrometers in diameter and presumably containing thousands of receptors (see the figure). Two opposing forces controlled this process: Myosin motors, which act on the cytoskeleton, transported associated receptors into the clusters, whereas mechanical restriction of ligand (or receptor) movement in the membrane impaired clustering. These results suggest that EphA2 receptor organization is coupled to the local mechanical environment.

Salaita *et al.* further developed a model membrane system to mechanically control the spatial organization of receptor clusters. A fluid lipid bilayer containing ephrin ligand was supported on a glass substrate and then presented to live cells expressing EphA2. With advanced lithography techniques, grid-like barriers were introduced into the model membrane to physically restrict ligand within corrals of defined size. These "spatial mutations" of ligand perturbed the mobility of ligand-bound EphA2 receptors and consequently modified receptor cluster size and distribution throughout the cell membrane. Although EphA2 was locally activated regardless of spatial constraint, cellular response such as actin organization depended on receptor organization.

Cell signaling networks are compromised in cancer, and deregulation of mechanical coupling to these networks may represent a major yet underappreciated underlying disease mechanism (*1*, *7*, *8*). Salaita *et al.* found that the extent of active EphA2 receptor movement into clusters correlated positively with cell invasiveness and metastatic potential. They also identified the association of Src and CD44, molecules involved in tumorigenesis and metastasis, with increased radial movement of EphA2 into clusters. Thus, tumor cells may deregulate the normal mechanical constraints on EphA2 movement in the membrane to acquire an aggressive phenotype, possibly by collaborating with molecules already implicated in cancer.

Eph receptors guide cell migration and tissue patterning during specific stages of embryogenesis and tissue development (*6*). Given the exquisite mechanical movements that underlie these fundamental processes (*9*), every push, twist, and turn made by cells could relay contextual information essential for proper coordinated development. Subtle changes in spatial organization of these and other transmembrane receptors could lead to developmental abnormalities and functional aberrations. Receptors that regulate programmed cell death (apoptosis) also form lower-order clusters (trimers) upon ligand binding and assemble into higher-order structures after association with the actin cytoskeleton (*10*, *11*). These larger clusters are commonly formed in tumor cells after exposure to their cognate ligand (TRAIL) (*11*). The notion that normal mechanical constraints on these receptors may be lost in tumors could explain the enhanced sensitivity of transformed cells to TRAIL.

Further studies should clarify the resistance of Eph receptors to clustering in normal cells, and whether ephrin ligands are naturally constrained in cell membranes. For instance, it is not clear whether local lipid organization in the membrane could influence these dynamics. Nor is it clear why large EphA2 clusters efficiently elicit distinct cellular signals, whereas smaller but more numerous complexes do not. Physical perturbations unique to tumors could be targeted with the goal of overcoming resistance to treatments that so frequently plague current antitumor therapies.

References

1. D. T. Butcher, T. Alliston, V. M. Weaver, *Nat. Rev. Cancer* **9**, 108 (2009).
2. D. E. Ingber, *Ann. Med.* **35**, 564 (2003).
3. K. Salaita *et al.*, *Science* **327**, 1380 (2010).
4. A. del Rio *et al.*, *Science* **323**, 638 (2009).
5. P. A. Janmey, D. A. Weitz, *Trends Biochem. Sci.* **29**, 364 (2004).
6. E. B. Pasquale, *Cell* **133**, 38 (2008).
7. M. J. Paszek *et al.*, *Cancer Cell* **8**, 241 (2005).
8. K. R. Levental *et al.*, *Cell* **139**, 891 (2009).
9. P. J. Keller, A. D. Schmidt, J. Wittbrodt, E. H. Stelzer, *Science* **322**, 1065 (2008).
10. F. L. Scott *et al.*, *Nature* **457**, 1019 (2009).
11. B. Pennarun *et al.*, *Biochim. Biophys. Acta* 10.1016/j.bbcan.2009.11.004 (2009).

10.1126/science.1187865

BIOCHEMISTRY

Remote Enzyme Microsurgery

Protein structures reveal a surprising mechanism for construction of a complex enzyme cofactor from standard amino acids.

J. Martin Bollinger Jr. and Megan L. Matthews

Enzymes achieve astounding rate enhancements of even difficult reactions. They often covalently modify their substrates by their own functional groups, a tactic that enables them to access mechanistic pathways that would not be feasible in solution. The standard amino acid building blocks of enzymes are replete with nucleophiles to use in this "covalent catalysis," but they are essentially devoid of useful electrophiles. An enzyme can bind an exogenous cofactor such as pyridoxal 5′-phosphate in its active site to correct this deficiency. An elegant alternative is the in situ construction of an electrophile, subsequent to protein synthesis, from amino acids in the active site (*1*). On page 1392 of this issue, Jensen *et al*. reveal how a particularly intricate example of this enzyme microsurgery is accomplished (see the figure) (*2*).

In a surprising number of these active-site surgeries, the enzyme is both patient and doctor, directing the construction of its own cofactor. Less commonly, the patient relies on a surgical specialist: an accessory enzyme that catalyzes cofactor construction. The extensive surgery needed to activate methylamine dehydrogenase (MADH) is one such case. Prior to Jensen *et al*.'s study, genetic and biochemical studies had shown that the two-heme protein MauG (*3*) operates on the inactive preMADH to install an unusual tryptophan tryptophyl quinone (TTQ) cofactor in the enzyme's β subunit (see the figure) (*4*, *5*). The surgery involves three steps: cross-linking of tryptophan (Trp) and 7-hydroxytryptophan (7-OH-Trp) residues in preMADH; hydroxylation of the 7-OH-Trp at position 6; and dehydrogenation of the cross-linked unit to a quinone. Each step is a two-electron oxidation. MauG can use hydrogen peroxide (H_2O_2) or dioxygen (O_2) as the oxidizing cosubstrate (*6*).

When a surgeon-enzyme such as MauG catalyzes cofactor construction, site access becomes important, because the amino acids to be cut and sutured may be buried in the patient's interior. Protein-protein interactions can drive conformational changes that permit direct access. Before the structural studies of Jensen *et al*., one might have surmised that MauG would perform such an "open" procedure on preMADH. MauG can form a unique intermediate containing one Fe(IV)-oxo (ferryl) site and one non-ferryl Fe(IV); this Fe(IV)/Fe(IV)=O complex oxidizes MADH in the synthesis of TTQ (*7*). Ferryl hemes in other enzymes are known to effect both hydroxylations and radical couplings on aromatic substrates. One might thus have anticipated that engagement of preMADH and MauG would permit the ferryl heme in MauG to directly access the Trp residues in MADH.

Jensen *et al*.'s structures of the (pre)MADH•MauG complexes defy these expectations. Binding of MauG positions its ferryl-forming heme away from the MADH interface, ~40 Å from the target Trp and 7-OH-Trp residues! MauG bound to preMADH in this way can complete TTQ construction upon exposure of the crystals to H_2O_2, and the resultant structural changes are essentially localized to the cofactor region. The structures thus imply that TTQ construction is more akin to keyhole surgery, with MauG extracting electrons from MADH sequentially from a long distance, likely generating radical intermediates, until cofactor synthesis is complete.

The structures shed light on several prior mechanistic observations, including the stability of the unique Fe(IV)/Fe(IV)=O intermediate in MauG. On the basis of its Mössbauer spectra, one of the Fe(IV)-hemes had been assigned as having two axial ligands from the protein (*8*), a previously unknown complex. The structures identify the ligands as a histidine and tyrosine, an unprecedented combination for a c-type heme. Bacterial two-heme cytochrome c peroxidases—which are similar to MauG in overall structure, have nearly identical two-heme cofactor regions, and catalyze similar reactions involving H_2O_2, but do not form the Fe(IV)/Fe(IV)=O intermediate—have a histidine or methionine residue at the position of the MauG tyrosine (*9*). Thus, the tyrosine ligand to the central heme may be a crucial surgical instrument of MauG. Substitution of this tyrosine with other residues could be used to test this idea.

The structures also offer new mechanistic insights and suggest approaches for further dissection of the surgical mechanism. Having ruled out direct access of MauG to the MADH Trp residues, the authors envisage the sequential extraction of six electrons by the Fe(IV) hemes, most likely in three rounds of the MauG reaction cycle. The hemes are ~15 Å to ~35 Å from the two Trps—a long distance for the electrons to travel. The surgeon uses the enzyme equivalent of a scope, positioning at its MADH interface a Trp residue that most likely relays electrons from the incipient TTQ to its closer, six-coordinate Fe(IV)-heme and a second Trp almost centrally between the two hemes that probably relays electrons between them (*10*). Variants in which the electron-relay Trp residues are substituted by other residues might provide useful probes of the electron-transfer and TTQ-assembly mechanisms.

Jensen *et al*.'s study leaves at least two key questions unan-

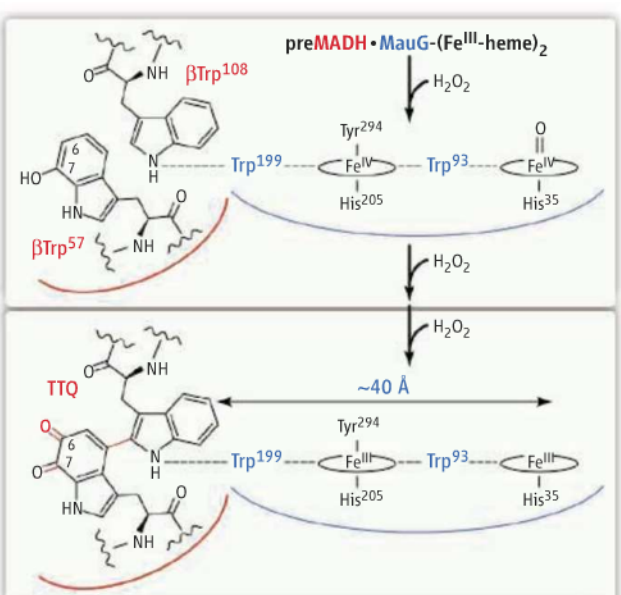

Schematic representation of the MADH•MauG complex and synthesis of the TTQ cofactor therein. Bonds of the cofactor installed by MauG are shown in red and residues that are part of the surgeon's "scope" in blue.

Department of Chemistry, Pennsylvania State University, University Park, PA 16802, USA. E-mail: jmb21@psu.edu

swered. First, it is unclear how the C7 hydroxyl group already present on Trp^{57} in preMADH (*11*, *12*) is incorporated. The gene encoding the β subunit specifies Trp at this position, and no surgeon specializing in the initial 7-hydroxylation of Trp^{57} has been identified (*6*).

Second, although the structures provide crucial insight into the fundamental nature of the individual oxidation steps [long-distance electron transfers with Trp relays (*10*)], they do not reveal the identities of partially assembled intermediates and thus do not resolve the full reaction sequence. Elucidation of this sequence remains a daunting challenge, especially because the oxidation steps are apparently processive (*2*). Variant proteins designed with the aid of these structures may permit strategic disruption of the process and accumulation of intermediate forms for kinetic and structural characterization.

Is the remote nature of the posttranslational active-site surgery by MauG on preMADH unique to this system? The answer appears to be "no." A recent paper by Cotruvo and Stubbe examining the class Ib ribonucleotide reductase from *Escherichia coli* implies that the protein NrdI acts as a remote enzyme-surgeon in this system (*13*). As the Jensen *et al*. study so beautifully illustrates, structures of surgeon-patient complexes should reveal important details of this and other remote enzyme surgeries.

References

1. L. Xie, W. A. van der Donk, *Proc. Natl. Acad. Sci. U.S.A.* **98**, 12863 (2001).
2. L. M. R. Jensen *et al.*, *Science* **327**, 1392 (2010).
3. Y. Wang *et al.*, *Biochemistry* **42**, 7318 (2003).
4. W. S. McIntire, D. E. Wemmer, A. Chistoserdov, M. E. Lidstrom, *Science* **252**, 817 (1991).
5. Y. Wang *et al.*, *J. Am. Chem. Soc.* **127**, 8258 (2005).
6. C. M. Wilmot, V. L. Davidson, *Curr. Opin. Chem. Biol.* **13**, 469 (2009).
7. X. Li *et al.*, *Proc. Natl. Acad. Sci. U.S.A.* **105**, 8597 (2008).
8. L. Chen *et al.*, *J. Mol. Biol.* **276**, 131 (1998).
9. G. W. Pettigrew, A. Echalier, S. R. Pauleta, *J. Inorg. Biochem.* **100**, 551 (2006).
10. J. M. Bollinger Jr., *Science* **320**, 1730 (2008).
11. A. R. Pearson *et al.*, *Biochemistry* **43**, 5494 (2004).
12. A. R. Pearson, S. Marimanikkuppam, X. Li, V. L. Davidson, C. M. Wilmot, *J. Am. Chem. Soc.* **128**, 12416 (2006).
13. J. A. Cotruvo Jr, J. Stubbe, *Biochemistry* **49**, 1297 (2010).

10.1126/science.1187421

PLANETARY SCIENCE

Revealing Titan's Interior

Gravity field measurements by the Cassini spacecraft suggest that Titan's interior was too cold for the primordial mixture of ice and rock to melt and fully separate.

Frank Sohl

The interior structure and composition of solar system bodies are key to understanding their origin and evolution. Saturn's largest icy moon, Titan, and the jovian moons, Ganymede and Callisto, are of similar size, mean density, and primordial ice-rock fraction from which the satellites formed. Titan is distinct due to its dense nitrogen atmosphere, with methane as the next most abundant constituent, which precludes direct observations of the surface. Before the arrival of the Cassini-Huygens spacecraft to study the Saturn system in 2004, little was known about the nature of Titan's interior—information as to its origin, evolution, and the rate at which it degasses was limited. On page 1367 of this issue, Iess *et al*. (*1*) report evidence based on the analysis of its gravitational field that the interior was much colder than previously thought, and thereby impeded substantial melting and subsequent separation of the primordial ice-rock mixture.

The Cassini-Huygens mission has revealed a remarkable diversity of Titan's icy landscapes, such as branching riverbeds, liquid methane and/or ethane pooled in polar lakes, and wind-blown equatorial dune fields of complex organic material settled from high altitude (*2*). A variety of cryovolcanic surface features can be attributed to Titan's recent internal activity (*3*). The isotopic signature of carbon and nitrogen and the presence of ^{40}Ar in Titan's atmosphere suggests relatively late formation of at least part of Titan's atmosphere by cryovolcanic degassing of the ice-rock interior (*4*, *5*).

Titan and most other satellites are in synchronous rotation and subject to tidal forces exerted by their primaries. The nonspherical part of their gravity fields is predominated by the spin and tidal contributions, which can be determined from the polar oblateness and equatorial ellipticity of the gravity field, respectively. Iess *et al*. determine both contributions by using different flyby geometries. Titan's ratio of the spin and tidal coefficients is close to 10:3, a value consistent with theoretical predictions for a synchronously rotating satellite in hydrostatic equilibrium. This allows Iess *et al*. to deduce Titan's axial moment of inertia with great precision, thereby providing a measure for the concentration of mass toward the center. Taken together with the satellite's known mean density, interior structure models can then be constructed. The new results imply that Titan's state of internal differentiation (see the figure) is an intermediate between partly differentiated (or separated) Callisto and Ganymede. The latter is strongly differentiated into an iron-rich liquid core, surrounded by a silicate rock mantle and overlain by a water ice/liquid shell and possesses a self-sustained, dipolar magnetic field (*6*).

The interpretation of Titan's gravitational field in terms of interior structure leads Iess *et al*. to conclude that either incomplete separation of the primordial mixture of ice and rock from which Titan formed or the presence of a substantially hydrated rock-rich central core could explain the inferred axial moment of inertia. Both interpretations differ from interior models considered previously (*5*, *7*–*9*), with strong implications for Titan's thermal history. The implication is that Titan's interior may have failed to get sufficiently hot for melting of a substantial portion of the primordial ice-rock mixture to occur and separation of ice from rock to proceed. There is notable discrepancy between the (hydrostatic) gravity field and the large-scale topography of Titan, as deduced from Cassini radar altimetry (*10*). Titan is slightly oblate, so that its poles have lower elevations than the equator, causing associated gravity anomalies which are attributed by Iess *et al*. to the presence of warm ice below. Thermodynamic models (*5*, *7*–*9*) suggest the present existence of a subsurface water ocean, sandwiched between a stagnant, floating ice shell and the dense interior, similar to those proposed for Ganymede and Callisto. Nonpolar solutes like ammonia and methanol and dilute salty impurities would lead to an appreciable melting point depression of the ice, resulting in even thicker and colder subsurface oceans. It is an open issue, however, how such oceans could have survived on cold and incompletely differentiated icy satellites such as Callisto and, as we now know, Titan.

The results obtained by Iess *et al*. facilitate comparison between Titan, Ganymede, and Callisto and indicate that satellites of similar size and composition in terms of their primor-

Institute of Planetary Research, German Aerospace Center (DLR), Rutherfordstrasse 2, 12489 Berlin, Germany. E-mail: frank.sohl@dlr.de

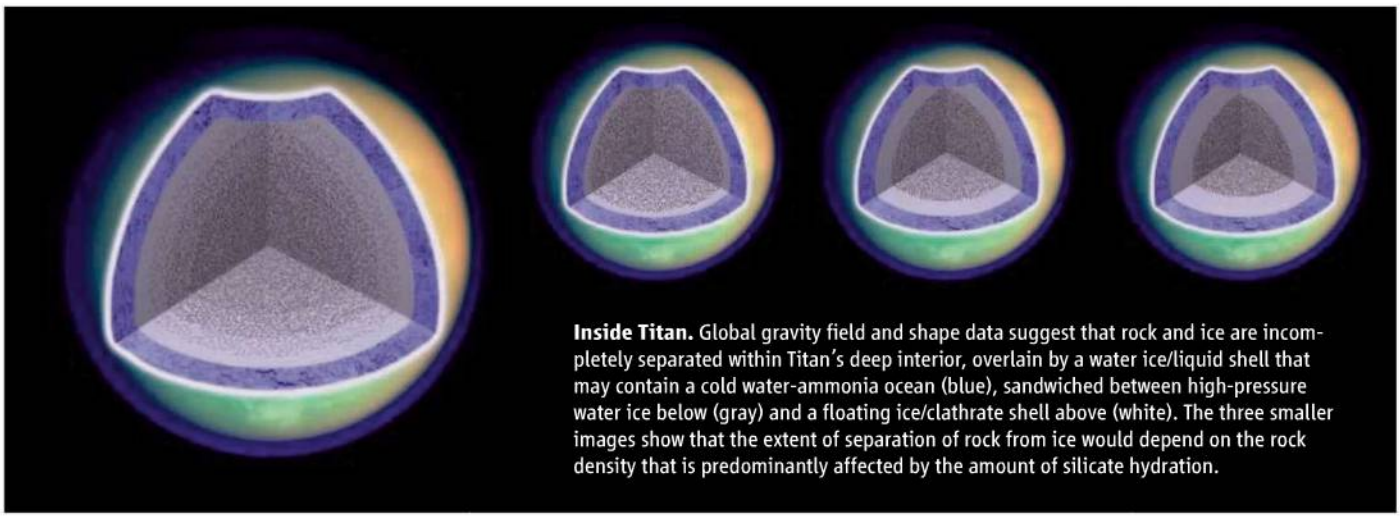

Inside Titan. Global gravity field and shape data suggest that rock and ice are incompletely separated within Titan's deep interior, overlain by a water ice/liquid shell that may contain a cold water-ammonia ocean (blue), sandwiched between high-pressure water ice below (gray) and a floating ice/clathrate shell above (white). The three smaller images show that the extent of separation of rock from ice would depend on the rock density that is predominantly affected by the amount of silicate hydration.

dial ice-rock mixtures may display distinct degrees of internal differentiation. Impact-induced melting and/or intense tidal heating of Ganymede, locked in orbital resonances with the inner neighboring satellites Io and Europa, may have triggered runaway differentiation, but Callisto farther out from Jupiter remained unaffected (*11*). Titan's interior must have stayed relatively cold and less dissipative to avoid tidal heating and damping of Titan's notable orbital eccentricity (*12*). Prolonged accretion times farther away from their primaries and gradual unmixing of ice and rock may also play a role for incomplete differentiation of icy satellites.

References and Notes

1. L. Iess *et al.*, *Science* **327**, 1367 (2010).
2. R. Jaumann *et al.*, in *Titan from Cassini-Huygens*, R.H. Brown, J.-P. Lebreton, J. Hunter Waite, Eds. (Springer, New York, 2009), pp. 75–140.
3. R. M. C. Lopes *et al.*, *Icarus* **186**, 395 (2007).
4. J. Lunine *et al.*, in *Titan from Cassini-Huygens*, R. H. Brown, J.-P. Lebreton, J. Hunter Waite, Eds. (Springer, New York, 2009), pp. 35–59.
5. G. Tobie *et al.*, *Nature* **440**, 61 (2006).
6. G. Schubert *et al.*, in *Jupiter*, F. Bagenal, T. Dowling, W. McKinnon, Eds. (Cambridge Univ. Press, Cambridge, 2004), pp. 281–306.
7. F. Sohl *et al.*, *J. Geophys. Res.* **108**, 5130 (2003).
8. A. D. Fortes *et al.*, *Icarus* **188**, 139 (2007).
9. O. Grasset *et al.*, *Planet. Space Sci.* **48**, 617 (2000).
10. H. A. Zebker *et al.*, *Science* **324**, 921 (2009).
11. A. C. Barr, R. M. Canup, *Nat. Geosci.* **3**, 164 (2010).
12. F. Sohl *et al.*, *Icarus* **115**, 278 (1995).

13. Supported by the Helmholtz Association through the research alliance "Planetary Evolution and Life." I am grateful to M. Weiland and R. Ziethe for technical support and additional computations supplementing construction of the figure.

10.1126/science.1186255

OCEANS

Interesting Times for Marine N_2O

Changes in ocean chemistry could exacerbate global warming by raising the atmospheric concentration of nitrous oxide, a potent greenhouse gas.

Louis A. Codispoti

Although present in minute concentrations in Earth's atmosphere, nitrous oxide (N_2O) is a highly potent greenhouse gas (*1*). It is also becoming a key factor in stratospheric ozone destruction (*2*). For the past ~400,000 years, changes in atmospheric N_2O appear to have roughly paralleled changes in CO_2 and to have had modest impacts on climate (*1*), but this may change. Human activities may be causing an unprecedented rise in the terrestrial N_2O source (*2*). Marine N_2O production may also rise substantially as a result of eutrophication, warming, and ocean acidification. Because the marine environment is a net producer of N_2O, much of this production will be lost to the atmosphere, thus further intensifying N_2O's climatic impact.

University of Maryland Center for Environmental Science, Horn Point Laboratory, Cambridge, MD 21613, USA. E-mail: codispot@umces.edu

Crucial to this discussion are the relationships between dissolved oxygen levels and their variability, and the production of N_2O. Under well-oxygenated conditions, microbes produce N_2O at low rates as a side product during the first step of nitrification ($NH_4^+ \rightarrow NO_2^-$). At low oxygen concentrations, nitrifiers may also reduce NO_2^- to N_2O, a process referred to as nitrifier denitrification (*3*). Overall, the fraction of N_2O produced by nitrifiers relative to NO_2^- increases as oxygen concentrations decrease, such that the yield at ~1% oxygen saturation is ~20 times greater than at 100% saturation (*4*).

These relationships favor high N_2O production by nitrification in hypoxic waters ($O_2 > 1\%$ and $< 30\%$ saturation). Under suboxic conditions ($O_2 < 1\%$ saturation), denitrifying bacteria that use oxidized nitrogen to support respiration can be net producers or net consumers of N_2O. N_2O concentrations are high at the boundaries and low in the center of quasi-stable suboxic zones (*5*). These zones account for 0.1 to 0.2% of the ocean volume (*3*), but are surrounded by much larger volumes of hypoxic waters (~10% of the ocean volume). Studies of N_2O production in regions containing suboxic waters suggest that these regions are strong net producers (*5*, *6*).

Generally, then, N_2O yields are high when O_2 concentrations are low. N_2O production rates should be particularly high in shallow suboxic and hypoxic waters, because respiration and biological turnover rates are higher near the sunlit waters where phytoplankton produce the fuel for respiration.

When denitrifiers switch from oxic to nitrogen respiration, they experience a lag in their ability to reduce N_2O to N_2. Conditions are thus particularly favorable for N_2O production when suboxia occurs close

CREDIT: (MONTAGE) MARIANNE WEILAND/DLR-RPIF

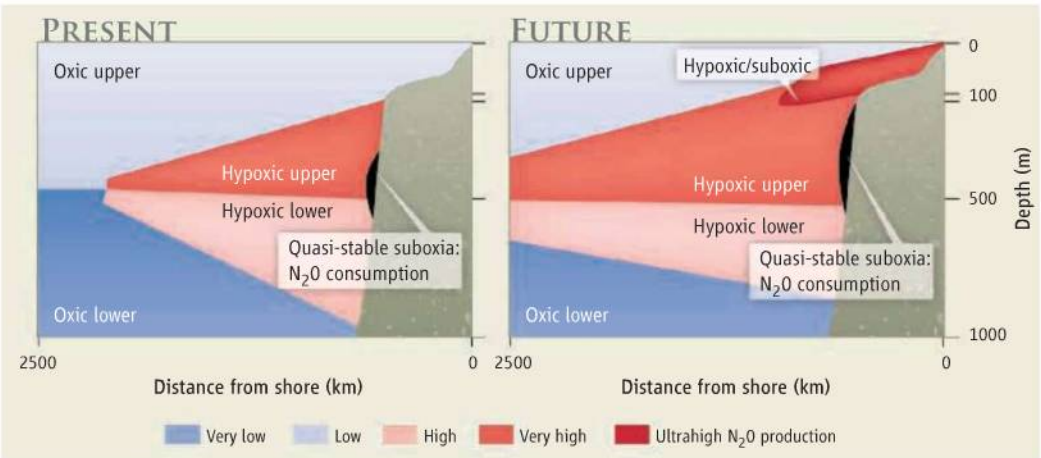

A generic eastern boundary in present-day and future oceans. Suboxia can extend further offshore than shown here, but is absent from a large portion of the oceanic eastern boundary.

enough to the sea surface to permit periodic O_2 injections. The highest N_2O concentrations observed in the open ocean (~800 nM, compared with 100%-saturation values of ~10 nM) occurred over the West Indian Shelf during the southwest monsoon (*6*). At this time, productive upwelling waters were capped by low-salinity waters diluted by the high runoff that occurs during the monsoon, and hypoxic and suboxic waters occurred at depths < 50 m. Under these conditions, shallow but unstable suboxia enabled denitrifiers to be strong net N_2O producers (*6*). Maximum production rates were ~10,000 times greater than the ocean average (*7*).

Net N_2O production in the open ocean is ~1.4×10^{11} mol (6 Tg of N) per year. About half of this production occurs in hypoxic and suboxic waters, and the rest in more oxygenated waters. Another ~0.7×10^{11} mol per year is produced in estuaries (*4*–*6*). Hypoxia is enhanced along oceanic eastern boundaries (see the figure) and in the northern Indian Ocean. This uneven distribution, combined with the massive rate increases that can occur under favorable conditions, raises the possibility that modest changes in key areas could greatly amplify marine N_2O production.

The marine N_2O source thus depends critically on what will happen to the ~10% of the ocean volume that is hypoxic and suboxic. Important subsets of this volume are the shallow portions that occur in productive upwelling regions and estuaries, where respiration is high and increases toward the sea surface, and where shallow denitrification (< 100 m) promotes net N_2O production.

Recent observations and models suggest that marine hypoxic and suboxic regions are likely to expand and shoal (become shallower) (*7*–*9*). For example, O_2 solubility will decrease with warmer water temperatures, thereby decreasing the supply of oxygen from the atmosphere and encouraging hypoxia. In addition, anthropogenic nutrient inputs have increased the incidence of hypoxia in coastal waters and estuaries (*6*).

Shifts in respiration that favor the upper 1000 m of the 4000-m-deep oceanic water column may be particularly important, because the lowest oxygen concentrations occur in the upper 1000 m and a substantial fraction of this water is already on the verge of hypoxia. Such a change could result from reduced sinking velocity of particulates in the ocean. For example, ocean acidification as a result of fossil fuel consumption (*10*) may decrease the production of calcium carbonate "ballast" that enhances the sinking rates of organic matter (*11*), as may impoundments that trap minerals that would otherwise reach the ocean.

There are indications that the proportion of carbon, relative to elements such as nitrogen, phosphorus, and iron that limit primary production of organic matter by phytoplankton, is increasing (*9*). Such a change could maintain production of the labile organic matter that fuels N_2O production, even if the supply of limiting nutrients to the sunlit layers that support phytoplankton decreases.

The Gulf of California provides an interesting case study. Here, phytoplankton blooms correlate with runoff from terrestrial fertilizer applications (*12*) and occur over a well-developed oxygen minimum zone (mid-depth layer with minimum oxygen). The resulting increase of subsurface respiration should lead to expansion and shoaling of this minimum, causing the high-yield part of the N_2O production system to "climb" the steep respiration gradient that increases toward the sea surface.

An increase in horizontal respiration rate gradients toward low-oxygen oceanic eastern boundaries could also increase N_2O production. Some models predict a deeper thermocline (lower respiration) as a result of global warming; others suggest the opposite (*13*). Observations (*14*, *15*) suggest an increase in eastern boundary upwelling and thermocline shoaling.

Factors such as sediments, atmospheric nutrient inputs, and intentional iron fertilization are not discussed in detail here but, in the main, would bolster the notion of an impending and substantial increase in marine N_2O production. Given that N_2O studies in the sea began in earnest only ~30 years ago (*16*), caution is in order when predicting future changes, but the marine N_2O production rate is clearly worthy of increased attention. Future experiments should focus on the controls for marine N_2O production and on potential N_2O production "hotspots."

References and Notes

1. P. Forster *et al.*, in *Climate Change 2007: The Physical Science Basis. Contribution of Working Group I to the Fourth Assessment Report of the Intergovernmental Panel on Climate Change*, S. Solomon *et al.*, Eds. (Cambridge Univ. Press, Cambridge, 2007), pp. 129–234.
2. D. J. Wuebbles, *Science* **326**, 56 (2009).
3. L. A. Codispoti, T. Yoshinari, A. H. Devol, in *Respiration in Aquatic Ecosystems*, P. A. del Giorgio, P. J. LeB. Williams, Eds. (Oxford Univ. Press, Oxford, 2005), pp. 225–247.
4. P. Suntharalingam, J. L. Sarmiento, J. R. Toggweiler, *Global Biogeochem. Cycles* **14**, 1353 (2000).
5. H. W. Bange, in *Nitrogen in the Marine Environment*, D. Capone *et al.*, Eds. (Elsevier, Amsterdam, 2008), chap. 2, pp. 51–94.
6. S. W. A. Naqvi *et al.*, *Biogeosciences Discuss.* **6**, 9455 (2009).
7. The concentration of 800 nM built up over a period of several months. Assuming an increase of 600 nM over 3 months yields a monthly production rate of 200 nM. The total open-ocean net N_2O rate of 1.4×10^{11} mol $year^{-1}$ divided by the volume of the ocean yields a rate of 0.01 nM $month^{-1}$.
8. L. Stramma, G. C. Johnson, J. Sprintall, V. Mohrholz, *Science* **320**, 655 (2008).
9. A. Oschlies *et al.*, *Global Biogeochem. Cycles* **22**, GB4008 (2008).
10. L. R. Kump, T. J. Bralower, A. Ridgwell, *Oceanography (Wash. D.C.)* **22**, 94 (2009).
11. M. Hofmann, H.-J. Schellnhuber, *Proc. Natl. Acad. Sci. U.S.A.* **106**, 3017 (2009).
12. J. M. Beman, K. R. Arrigo, P. A. Matson, *Nature* **434**, 211 (2005).
13. G. A. Vecchi, A. Clement, B. J. Soden, *EOS* **89**, 81 (2008).
14. F. Chan *et al.*, *Science* **319**, 920 (2008).
15. H. V. McGregor, M. Dima, H. W. Fischer, S. Mulitza, *Science* **315**, 637 (2007).
16. T. Yoshinari, *Mar. Chem.* **4**, 189 (1976).

17. I thank V. Coles, R. Alley, G. Strother, S. W. A. Naqvi, H. Bange, and J. Elkins for helpful advice. H. Garcia calculated the volume of hypoxic ocean water.

10.1126/science.1184945

Altruism, Spite, and Greenbeards

Stuart A. West* and Andy Gardner*

Hamilton's theory of inclusive fitness showed how natural selection could lead to behaviors that decrease the relative fitness of the actor and also either benefit (altruism) or harm (spite) other individuals. However, several fundamental issues in the evolution of altruism and spite have remained contentious. Here, we show how recent work has resolved three key debates, helping clarify how Hamilton's theoretical overview links to real-world examples, in organisms ranging from bacteria to humans: Is the evolution of extreme altruism, represented by the sterile workers of social insects, driven by genetics or ecology? Does spite really exist in nature? And, can altruism be favored between individuals who are not close kin but share a "greenbeard" gene for altruism?

Darwin's (*1*) theory of natural selection explains both the process and the purpose of adaptation (Fig. 1). The process is that heritable characters associated with greater reproductive success will be selected for and accumulate in natural populations. This leads to the apparent purpose of adaptation: characters appearing as if designed to maximize the individual's reproductive success (fitness).

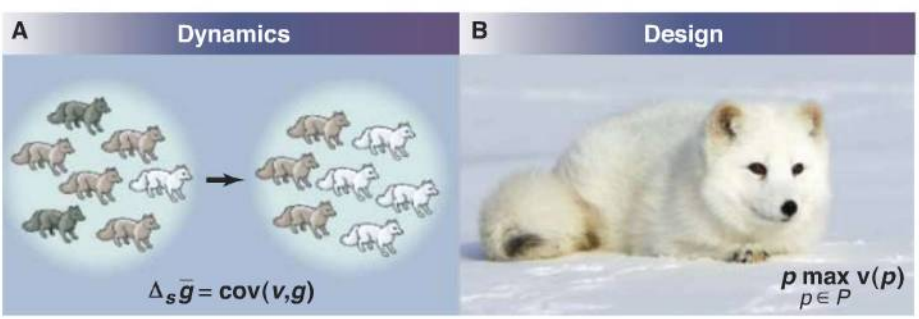

Fig. 1. Darwinian adaptation—dynamics and design. **(A)** Natural selection is the genetic change in the population owing to differential reproductive success of individual organisms. For example, among ancestral Arctic foxes, individuals with pale fur left more descendants than individuals with dark fur so that genes for pale fur accumulated in the population. Price's (*35*) equation formalizes this, stating that the change in the heritable portion of any character ascribable to natural selection ($\Delta_S \bar{g}$) is equal to the covariance between an individual's genetic ("breeding") value for the trait (g) and its relative fitness (v). **(B)** As a consequence of past natural selection, today's Arctic foxes look "designed" to fit their environment. This is captured by an optimization program, which states that the phenotype (p) of the organism is functioning as if to maximize the individual's relative fitness (v; more generally, its inclusive fitness) (*6*, *7*). [Credit: Biosphoto/Cordier Sylvain/Peter Arnold Inc.]

Fisher (*2*) united Darwinism with Mendelian genetics by describing natural selection in terms of changes in gene frequencies. Genes associated with greater individual fitness are predicted to increase in frequency, leading to an increase in mean fitness. This "fundamental theorem of natural selection" was intended to capture the process (natural selection) and the purpose (maximization of individual fitness) of adaptation.

Altruism, Spite, and Inclusive Fitness

In the 1960s, Hamilton (*3*, *4*) realized that maximization of individual fitness could not explain altruistic or spiteful traits, which are costly to the individuals that perform them. The paragon of altruism is the sterile worker caste within social-insect colonies, which help rear the offspring of their queen. An equally extreme example are slime mold cells that altruistically give up their own survival to become the nonviable stalk of a fruiting body, helping other cells to disperse in the form of spores (*5*). The problem is that such altruism reduces the reproductive success of the altruist—so why is it not weeded out by natural selection?

Hamilton (*3*) showed that genes can spread not only through their direct impact on their own transmission but also through their indirect impact on the transmission of copies present in other individuals. Consequently, altruistic behaviors can be favored if the benefits are directed toward other individuals who share genes for altruism (Fig. 2). This is encapsulated by Hamilton's rule (*3*), which states that a trait will be favored by selection when $rb - c > 0$, where c is the fitness cost to the actor, b is the fitness benefit to the recipient, and r is their genetic relatedness. This form of Hamilton's rule emphasizes interactions between two individuals, but it can be extended to allow for interactions with multiple individuals [supporting online material (SOM) text and table S1].

Hamilton's general point was that natural selection leads organisms to appear designed as if to maximize their inclusive fitness, which is the sum of fitness gained through producing offspring (direct fitness) and through affecting the fitness of related individuals (indirect fitness). The easiest way in which indirect fitness can be obtained is through interactions with close kin, in which case genes are identical by descent (from a common ancestor), and so this is usually referred to as "kin selection." However, inclusive fitness is not simply a concept that relates to interactions between relatives; it is our modern interpretation of Darwinian fitness, providing a general theory of adaptation (*6*, *7*).

Extreme Altruism and the Haplodiploidy Hypothesis

The sterile workers of the social insects are extreme altruists, who give up any chance of independent reproduction in order to help others. In the Hymenoptera (ants, bees, and wasps) and termites, this extreme altruism has led to a division of labor between individuals and the evolution of the highest level of social organization, termed eusociality. Depending upon how eusociality is defined, it has evolved 3 to 11 times in the Hymenoptera, as well as in termites, thrips, aphids, spiders, beetles, shrimps, and mole rats (*8*, *9*).

A major topic of debate has been whether eusociality has evolved multiple times in hymenopterans because of their haplodiploid genetics or their ecology. Under haplodiploidy, fertilized eggs develop into (diploid) females, and unfertilized eggs develop into (haploid) males. Hamilton (*3*) suggested that because haplodiploidy leads to a female being more related to her sisters ($r = 0.75$, assuming an outbred population in which females mate once) than her own offspring ($r = 0.5$), this makes it easier for Hamilton's rule to be satisfied (Fig. 3A).

However, haplodiploidy also leads to a female being less related to a brother ($r = 0.25$), exactly canceling the benefit of increased relatedness to sisters (*10*). The haplodiploidy hypothesis is not rescued if the population sex ratio is biased toward females because this bias also reduces the relative reproductive value of females, exactly canceling any relatedness benefits (*11*). Numerous studies have examined whether certain life histories could rescue Hamilton's haplodiploidy hypothesis by making the average relatedness to siblings $r > 0.5$, but none appears generally applicable (SOM text). In contrast, others have argued that what is special about the hymenopterans is that their natural history leads to a relatively high benefit of helping (high b/c ratio), such as advanced parental care and a powerful sting that facilitates group defense (*12*).

The Monogamy Hypothesis

Recent work (*8*, *13*) has suggested a possible resolution to this debate, arguing that strict lifetime monogamy, in which females only mate with

Department of Zoology, Oxford University, South Parks Road, Oxford OX1 3PS, UK.

*To whom correspondence should be addressed. E-mail: stuart.west@zoo.ox.ac.uk (S.A.W); andy.gardner@zoo.ox.ac.uk (A.G.)

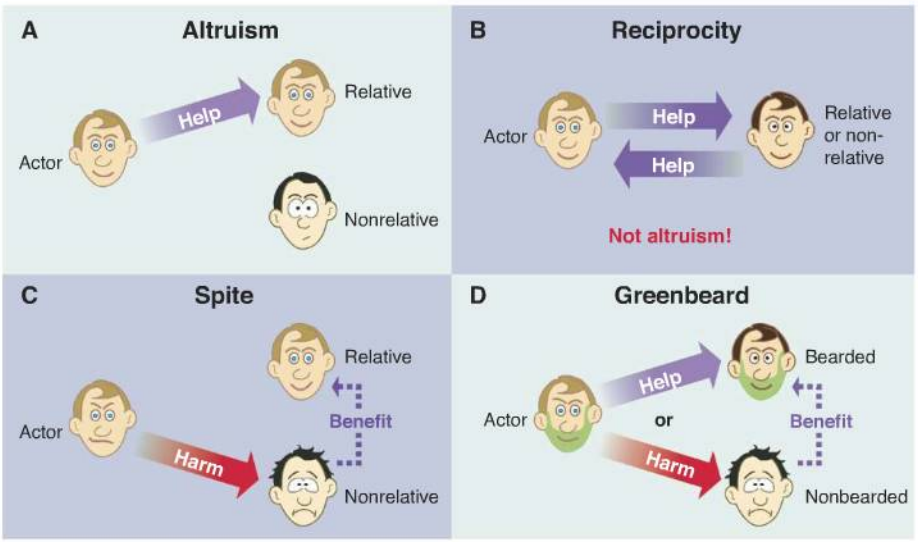

Fig. 2. Mechanisms for altruism, spite, and reciprocity. **(A)** Altruism can be favored if it is preferentially directed toward relatives. **(B)** Reciprocity is favored when it makes the actor more likely to receive help in the future. Reciprocity relies upon a future direct fitness benefit for cooperation and so is not altruistic. **(C)** Spite can be favored if it is preferentially directed toward relatively unrelated individuals, whose loss improves the fitness of relatives. **(D)** Greenbeards are favored by directing altruism toward fellow greenbeard individuals or spite toward nonbearded individuals.

one male in their entire life, is crucial for the evolution of eusociality. Monogamy leads to a potential worker being equally related ($r = 0.5$) to her own offspring and to the offspring of her mother (siblings). In this case, any small efficiency benefit for rearing siblings over their own offspring ($b/c > 1$) will favor eusociality (Fig. 3B).

In contrast, even a low probability of multiple mating means that potential workers would be more related to their own offspring. In this case, costly helping would require a significant efficiency advantage to rearing siblings over own offspring (Fig. 3C). Until group living is established, allowing the evolution of specialized cooperative behavior and division of labor, the ratio b/c cannot be expected to greatly exceed 1. For example, feeding a sibling is unlikely to be hugely more beneficial than feeding an offspring by the same amount. Consequently, in the absence of strict monogamy the population cannot even get started on the road to eusociality.

In support of this hypothesis, comparative studies have found monogamy to be the ancestral state in all the independent origins of eusociality studied (*9*, *14*). Monogamy originated first, giving a high relatedness, and then when ecological conditions led to a high enough b/c, eusociality evolved (SOM text). Important ecological conditions include "life insurance" benefits of allowing helpers to complete parental care after the death of the mother (for example, ants, bees, and wasps), and "fortress defense" benefits of remaining to help use or defend a food source, when opportunities for successful migration are low (for example, aphids, beetles, termites, thrips, and shrimps) (*12*, *14*).

There are some eusocial species in which queens mate multiply. However, this is a derived condition that has evolved after workers have already lost the ability to mate and realize full reproductive potential (*9*). Furthermore, these species have had the time to evolve division of labor and specialized helping behaviors, giving a substantial b/c.

The beauty of the monogamy hypothesis is that it simplifies our understanding of how eusociality evolved, emphasizing that the interaction between kinship and ecology is fundamental and that they are not competing explanations (*8*, *13*). For example, the search for how to increase relatedness to siblings ($r > 0.5$) has been a red herring; what is key is that average relatedness stays at 0.5. Other red herrings include the possibility for eusociality to have evolved via cooperation between sisters (the parasocial route) because that would lead to $r < 0.5$ (*8*) and the suggestion that high relatedness is a consequence rather than a cause of eusociality (*15*), in which case the observed correlation with monogamy would not be predicted (*9*). Finally, the monogamy hypothesis suggests that factors that facilitate monogamy, such as lifetime storage of sperm by females, are also important in explaining the distribution of eusociality.

Get the Right Spite

Inclusive-fitness theory explains altruism but also has a darker side. Spiteful traits, which are harmful to both actor and recipient, may be favored (*4*). Considering the classic two-party version of Hamilton's rule, if c is positive (which is costly to the actor), and b is negative (which is costly to the recipient), then $rb - c > 0$ can be satisfied if relatedness (r) is negative. Negative relatedness may seem a bizarre concept, but it simply means that the recipient is less related to the actor than is an average member of the population (SOM text).

Another way to think about spite is to distinguish between the primary recipient of the harming behavior (the individual physically attacked) and those secondarily influenced as a byproduct of this (those experiencing reduced competition from the harmed individual) (*16*, *17*). From this perspective, spite can be favored if the actor is more related to the secondary recipients (who benefit) than to the primary recipients (who are harmed). Spite can therefore be thought of as altruism toward the secondary recipients: Harming an individual can be favored if this provides a

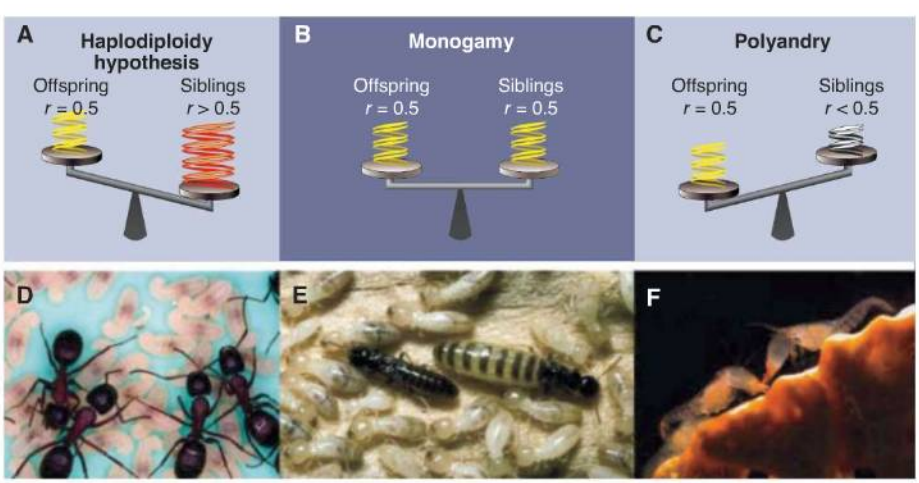

Fig. 3. Monogamy paves the way to eusociality. **(A)** The haplodiploidy hypothesis relies on individuals being more related to siblings than offspring, making siblings worth more than offspring. As originally envisioned, this appears to have been a red herring. **(B)** The monogamy hypothesis emphasizes that if an individual is equally related to its siblings and its offspring, even a very slight efficiency benefit for raising siblings translates into a selective advantage for helping. **(C)** Without strict monogamy, individuals are more related to their offspring than they are to their siblings so that a large efficiency benefit is required in order for sibling-rearing to be favored. **(D)** Sterile workers caring for brood in the ant *Camponotus herculeanus*. **(E)** A lifetime monogamous pair from the termite *Reticulitermes flavipes*. **(F)** Nonbreeding workers in the shrimp *Synalpheus regalis*. [Photos provided by David Nash, Barbara Thorne, and Emmett Duffy]

benefit to closer relatives (Fig. 2C). These two different encapsulations of spite are different ways of looking at the same thing, using either a two- or three-party Hamilton's rule (SOM text) (*16*, *17*). If the actor is more closely related to the secondary recipients than the primary recipients in a three-party rule, then this leads to a negative relatedness in the two-party rule.

Although many behaviors have been suggested as spiteful, they are usually explained as selfish behaviors that are costly to the recipient but provide a benefit to the actor ($c < 0$) (Table 1). This benefit is often a reduction in future competition for resources, for the actor or their offspring, with confusion arising because the direct fitness consequences were only considered in the short term and not over the lifetime of the actor (SOM text) (*18*). What matters for natural selection are fitness consequences over the entire lifetime and not some arbitrary period. For example, herring gulls kill the chicks at neighboring nests, but this reduces the future competition over resources for both themselves and their offspring. Furthermore, there is no evidence that such examples involve a sufficient secondary benefit to relatives. Indeed, it has even been suggested that the conditions required are so restrictive that spite would be rare or nonexistent (*11*, *12*).

However, recent theory has shown that a positive relatedness to secondary recipients can be obtained more easily than previously thought, suggesting that at least from a theoretical perspective spite is plausible (*19*) if there is (i) large variance in relatedness between competitors; (ii) kin discrimination, with harming behaviors aimed at individuals to whom the actor is relatively unrelated (making the actor relatively more related to the secondary recipients); or (iii) strong local competition so that harming the primary recipient provides appreciable benefits to secondary recipients. When these conditions are met, spiteful behaviors can be favored so as to reduce competition for relatives. Consider the extreme example of when two genetically identical (clonal) individuals are competing with a nonrelative to whom they are unrelated. One of the clone-mates could be selected to harm the nonrelative, at a cost to itself, if this harming reduces the nonrelative's ability to compete for resources and hence benefits the other clone-mate.

Table 1. Not spite: examples of traits that have been suggested as spiteful but actually provide a direct benefit to the actor and hence are selfish (table S2).

Taxa	Suggested spiteful traits	Why selfish, not spiteful
Birds	Protection of territories, siblicide at neighboring nests.	Decreased competition for resources, for self or offspring
Fish	Egg cannibalism	Decreased competition for resources, for offspring
Humans	Punishment and rejection of low offers in economic games	Leads to increased cooperation in the long term
Mammals	Infanticide, harassment of nondescendant juveniles and injured males	Decreased competition, for offspring or mates

Real Spite

To demonstrate spite, it must be shown that a trait is costly to the actor (positive c) and costly to the recipient (negative b). In addition, for spite to have evolved by means of natural selection, the actor must be more closely related to the secondary recipients (beneficiaries) than to the primary recipient that they harm (Fig. 2C). The sterile soldier caste in polyembryonic parasitoid wasps satisfies all these conditions (*17*). Females lay their eggs on the eggs of moth caterpillars, after which the wasp eggs divide asexually and consume the growing caterpillar from the inside (*20*). Although most larvae develop normally, a fraction become a soldier morph. Developing as a soldier is costly to the actor, because the soldiers are sterile, and costly to the recipient, because the soldiers seek out and kill other larvae within the host. Finally, soldiers preferentially kill larvae to which they are less related (those that have developed from other eggs), freeing up resources for their clone-mates.

Another example of spite is provided by the production of antimicrobial bacteriocins by many bacteria (*21*). These compounds are lethal to conspecifics that lack an immunity gene (*22*). In some cases, cell death is required to release the bacteriocins into the environment, and so it is clearly a costly trait (positive c). In addition, there is genetic linkage between the bacteriocin production and immunity genes so that close relatives both produce and are immune to a particular bacteriocin (*22*). Consequently, the release of bacteriocins kills nonrelatives, freeing up resources for clone-mates. Experimental work on bacteriocins has also supported the prediction that the relative advantage of spite is greater when variance in relatedness is higher (giving an intermediate mean relatedness) because this leads to interactions with both close relatives and nonrelatives, allowing a relatively higher relatedness to the secondary beneficiaries (Fig. 4) (*21*, *23*).

Spiteful Words

As discussed above, spite can be considered a form of altruism. Consequently, it is useful to ask whether we gain anything by distinguishing spite from altruism. At one level, it can be useful to emphasize the similarities, that both are favored because they lead to an increase in the inclusive fitness of the actor through indirect fitness consequences. This will also help avoid debates over whether certain traits should be classed as altruism or spite because the mathematics of any

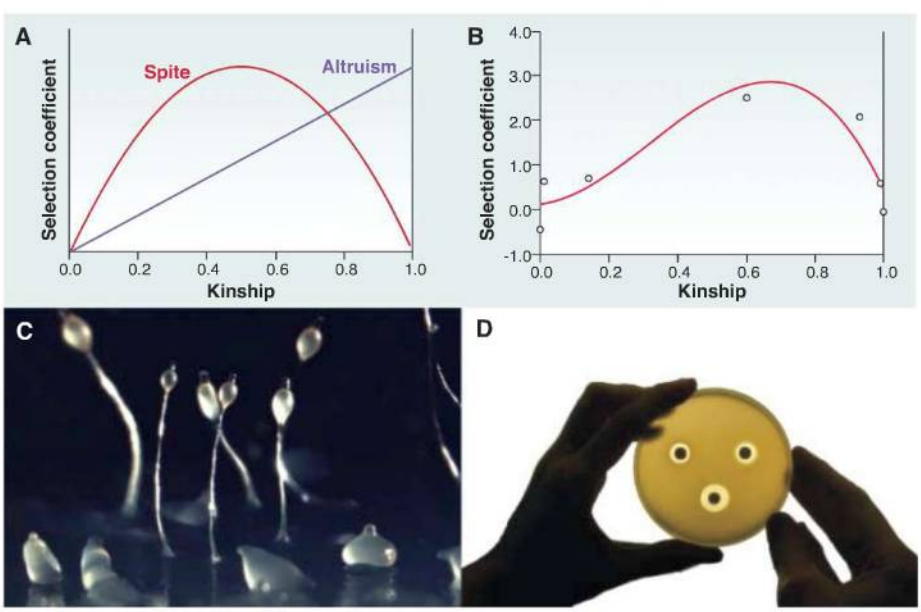

Fig. 4. Population structure, altruism, and spite. (**A**) Theory predicts that as relatedness within a patch increases, there is an increase in altruistic traits and a domed relationship with spiteful traits (*3*, *15*). (**B**) As predicted, the relative benefit of bacteriocin production in *Pseudomonas aeruginosa* shows a domed relationship with relatedness (*23*) (**C**) Altruism: a fruiting body of the slime mold *Dictyostelium discoideum*. (**D**) Spite: A piece of filter paper soaked with a bacteriocin (left spot) causes an inhibition zone where bacteria cannot grow, in the same way as a traditional antibiotic (right spot; bottom spot shows both in combination). [Photos provided by Owen Gilbert, Margaret Riley, and Sara Cody]

case can be rearranged so as to make a spiteful or altruistic two-party rule (*16*, *17*).

However, there are also a number of reasons why it is useful to distinguish spite from altruism (*17*). From a behavioral perspective, there is a clear difference between helping and harming. Additionally, there are biologically interesting differences between altruism and spite. For example, local competition for resources typically selects for spite and against altruism (*21*); altruistic traits are predicted to show a positive relationship with relatedness (*3*), whereas spiteful traits are predicted to show a domed relationship (Fig. 4) (*19*, *21*); and kin discrimination is key in the examples of spite, whereas altruism can often evolve without kin discrimination when limited dispersal keeps relatives together (*3*).

Spite can also be defined from a mechanistic or psychological perspective in primates and humans as a behavior that harms another or arises from a desire to harm another (*24*, *25*). In these cases, harming is likely to be favored because on average it provides a direct benefit to the actor ($c < 0$) and is selfish, not spiteful. It is crucial not to mix definitions of spite by raising the problem and rarity of evolutionary spite then going on to examine a harming behavior that provides a direct benefit to the actor, and therefore is not evolutionary spiteful. The specific conditions required to favor evolutionary spite might make it relatively unlikely in humans and other primates. Indeed, spite may be rare in general because it is hard to obtain situations in which populations are structured so that harming nonrelatives is an efficient way of helping relatives.

Greenbeards

Hamilton (*3*, *26*) pointed out that indirect-fitness benefits require genetic relatedness per se and not kinship. Imagine a gene (or cluster of tightly-linked genes) that gives rise to a conspicuous phenotype, uses this phenotype to discriminate between carriers and noncarriers of the gene, and leads to costly helping toward other carriers of the gene (Fig. 2D). This gene could be favored by natural selection, even if carriers share no other genes in common. Thus, the crucial requirement for altruism is genetic relatedness at the altruism locus and not genealogical relationship over the whole genome.

Dawkins proposed the hypothetical example of a gene that gives rise to a green beard while simultaneously prompting individuals with green beards to direct cooperation toward other green-bearded individuals (*27*). However, this "greenbeard" mechanism can also occur without a visible tag. What is required more generally is a single gene (or a number of tightly-linked genes) encoding both the cooperative behavior and causing cooperators to associate (*26*, *28*). Greenbeards are one of the two ways in which natural selection can favor altruistic behavior, with the other being interactions with genealogical kin (*3*). However, despite this fundamental position it has been assumed that greenbeards would not occur in nature because they could be easily invaded by "falsebeards" (cheats) that displayed the beard without also performing the behavior (*27*).

This assumption has been overturned by the discovery of a number of altruistic greenbeards. In the slime mold *Dictyostelium discoideum*, individuals with the *csa* gene adhere to each other in aggregation streams and cooperatively form fruiting bodies while excluding noncarriers of the gene (*5*). Other examples have been found in yeast, a bacterial plant pathogen, and a lizard (SOM text). In addition, spiteful greenbeards have been discovered, including the *Gp*-9 gene of the fire ant *Solenopsis invicta* (*29*). Workers with the *b* allele at this locus use odor to determine whether prospective queens also carry this allele, dismembering them if they do not. Another example is provided by bacteriocin production, in which the bacteriocin-encoding gene and the immunity gene are tightly linked (*22*).

Theoretical work has clarified when we would expect greenbeards to occur (*30*). Greenbeards can be categorized into four groups, with different evolutionary dynamics, according to whether they are altruistic (helping) or spiteful (harming) and always expressed (obligate; for example, bacteriocins) or only expressed in response to the presence of the greenbeard in others (facultative; for example, *Gp*-9). For all cases except the facultative altruistic greenbeard, the greenbeard is selected against at low frequencies and only favored when it has established itself to a certain frequency. Population structure can solve this problem by keeping individuals with greenbeards together. The best place to look for new greenbeards may be in microbes, in which asexual growth can lead to extreme population structuring; the relatively simple link between genotype and phenotype may prevent a decoupling of beard and social trait (falsebeards), and genetic knockouts facilitate the detection of greenbeards (*30*).

Some models for altruism in humans (*31*–*34*) and social insects (*15*) implicitly invoke greenbeard mechanisms without realizing this, such as the suggestion that altruistic individuals differ from individuals who are not altruistic in some observable characteristic [such as being more likely to smile and laugh (*31*, *32*)] or models of "strong reciprocity" that assume punishment and altruism to be genetically linked (*33*, *34*). However, there is no reason to suspect that traits such as smiling or punishment will be encoded by the same gene or closely linked genes as those that lead to altruism. Consequently, falsebeards could arise, and these proposed explanations for altruism would not be evolutionarily stable (*30*).

Conclusions

A unifying theme in all the issues that we have discussed here is the importance of the interplay between theory and data. The monogamy hypothesis cuts through the superfluous details by focusing on a key aspect of the underlying biology. Theoretical work on spite and greenbeards was spurred by biological examples but then led to a unifying framework that illuminated detection problems and suggested where to look for further examples. All of these examples illustrate that the distinction between genetics (r) and ecology (b/c) is both artificial and unhelpful. What really matters is how they interact, as has always been emphasized by Hamilton's rule.

References and Notes

1. C. Darwin, *On the Origin of Species by Means of Natural Selection, or, the Preservation of Favoured Races in the Struggle for Life* (John Murray, London, UK, 1859).
2. R. A. Fisher, *The Genetical Theory of Natural Selection* (Clarendon, Oxford, 1930).
3. W. D. Hamilton, *J. Theor. Biol.* **7**, 1 (1964).
4. W. D. Hamilton, *Nature* **228**, 1218 (1970).
5. D. C. Queller, E. Ponte, S. Bozzaro, J. E. Strassmann, *Science* **299**, 105 (2003).
6. A. Grafen, *J. Evol. Biol.* **20**, 1243 (2007).
7. A. Gardner, *Biol. Lett.* **5**, 861 (2009).
8. J. J. Boomsma, *Philos. Trans. R. Soc. Lond. B Biol. Sci.* **364**, 3191 (2009).
9. W. O. H. Hughes, B. P. Oldroyd, M. Beekman, F. L. W. Ratnieks, *Science* **320**, 1213 (2008).
10. R. L. Trivers, H. Hare, *Science* **191**, 249 (1976).
11. R. Craig, *Evolution* **33**, 319 (1979).
12. J. E. Strassmann, D. C. Queller, *Proc. Natl. Acad. Sci. U.S.A.* **104** (suppl 1), 8619 (2007).
13. J. J. Boomsma, *Curr. Biol.* **17**, R673 (2007).
14. J. E. Duffy, K. S. Macdonald, *Proc. Biol. Sci.* **277**, 575 (2010).
15. E. O. Wilson, B. Hölldobler, *Proc. Natl. Acad. Sci. U.S.A.* **102**, 13367 (2005).
16. L. Lehmann, K. Bargum, M. Reuter, *J. Evol. Biol.* **19**, 1507 (2006).
17. A. Gardner, I. C. W. Hardy, P. D. Taylor, S. A. West, *Am. Nat.* **169**, 519 (2007).
18. K. R. Foster, T. Wenseleers, F. L. W. Ratnieks, *Ann. Zool. Fenn.* **38**, 229 (2001).
19. A. Gardner, S. A. West, *J. Evol. Biol.* **17**, 1195 (2004).
20. D. Giron, D. W. Dunn, I. C. W. Hardy, M. R. Strand, *Nature* **430**, 676 (2004).
21. A. Gardner, S. A. West, A. Buckling, *Proc. Biol. Sci.* **271**, 1529 (2004).
22. M. A. Riley, J. E. Wertz, *Annu. Rev. Microbiol.* **56**, 117 (2002).
23. R. F. Inglis, A. Gardner, P. Cornelis, A. Buckling, *Proc. Natl. Acad. Sci. U.S.A.* **106**, 5703 (2009).
24. M. Hauser, K. McAuliffe, P. R. Blake, *Philos. Trans. R. Soc. Lond. B Biol. Sci.* **364**, 3255 (2009).
25. K. Jensen, J. Call, M. Tomasello, *Proc. Natl. Acad. Sci. U.S.A.* **104**, 13046 (2007).
26. W. D. Hamilton, in *Biosocial Anthropology*, R. Fox, Ed. (Wiley, New York, 1975), pp. 133–155.
27. R. Dawkins, *The Selfish Gene* (Oxford Univ. Press, Oxford, 1976).
28. L. Lehmann, L. Keller, *J. Evol. Biol.* **19**, 1365 (2006).
29. L. Keller, K. G. Ross, *Nature* **394**, 573 (1998).
30. A. Gardner, S. A. West, *Evolution* **64**, 25 (2010).
31. R. H. Frank, *Am. Econ. Rev.* **77**, 593 (1987).
32. M. J. Owren, J.-A. Bachorowski, in *Emotions: Current Issues and Future Directions*, T. J. Mayne, G. A. Bonanno, Eds. (Guilford, New York, 2001), pp. 152–191.
33. H. Gintis, *J. Theor. Biol.* **206**, 169 (2000).
34. S. Bowles, H. Gintis, *Theor. Popul. Biol.* **65**, 17 (2004).
35. G. R. Price, *Nature* **227**, 520 (1970).

36. We thank J. Alpedrinha, K. Boomsma, A. Griffin, M. Hauser, K. Jensen, L. Keller and P. Taylor for comments and the Royal Society, European Research Council, and Leverhulme Trust for funding.

Supporting Online Material

www.sciencemag.org/cgi/content/full/327/5971/1341/DC1
SOM Text
Tables S1 and S2
References

10.1126/science.1178332

Identification of a Primary Target of Thalidomide Teratogenicity

Takumi Ito,[1]* Hideki Ando,[2]* Takayuki Suzuki,[3,4] Toshihiko Ogura,[3] Kentaro Hotta,[2] Yoshimasa Imamura,[5] Yuki Yamaguchi,[2] Hiroshi Handa[1,2]†

Half a century ago, thalidomide was widely prescribed to pregnant women as a sedative but was found to be teratogenic, causing multiple birth defects. Today, thalidomide is still used in the treatment of leprosy and multiple myeloma, although how it causes limb malformation and other developmental defects is unknown. Here, we identified cereblon (CRBN) as a thalidomide-binding protein. CRBN forms an E3 ubiquitin ligase complex with damaged DNA binding protein 1 (DDB1) and Cul4A that is important for limb outgrowth and expression of the fibroblast growth factor Fgf8 in zebrafish and chicks. Thalidomide initiates its teratogenic effects by binding to CRBN and inhibiting the associated ubiquitin ligase activity. This study reveals a basis for thalidomide teratogenicity and may contribute to the development of new thalidomide derivatives without teratogenic activity.

During the late 1950s and early 1960s, thalidomide was sold as a sedative in over 40 countries and was often prescribed to pregnant women as a treatment for morning sickness. Before its teratogenic activity came to light and its use was discontinued, ~10,000 affected children were born from women taking thalidomide during pregnancy (*1*–*3*). Use of thalidomide during weeks 3 to 8 of gestation causes multiple birth defects such as limb, ear, cardiac, and gastrointestinal malformations (*1*–*3*). The limb malformations, known as phocomelia and amelia, are characterized, respectively, by severe shortening or complete absence of legs and/or arms, whereas the ear malformations lead to anotia, microtia, and hearing loss. Despite considerable effort, little is known about how these developmental defects are caused. Previous studies have suggested thalidomide-induced oxidative stress and its antiangiogenic action as a possible cause of teratogenicity (*4*, *5*). However, several important questions remain unanswered, such as what are direct targets of thalidomide and how the target molecules mediate its teratogenic effects.

Recently, thalidomide use has increased for the treatment of multiple myeloma and erythema nodosum leprosum, a painful complication of leprosy (*2*, *3*, *6*, *7*). Owing to its teratogenicity, however, thalidomide is used under strict control (*8*), and removal of its side effects is desirable for wider applications of this potentially useful drug. It is important to elucidate the molecular mechanism of thalidomide teratogenicity, especially to identify its molecular target(s), because such knowledge might allow rapid screening for potentially useful related compounds devoid of teratogenic activity. In this regard, we have been developing high-performance affinity beads that allow single-step affinity purification of drug target proteins from crude cell extracts (*9*). Here we show that cereblon (CRBN), a protein encoded by a candidate gene for mild mental retardation, is a primary target of thalidomide teratogenicity.

Binding of thalidomide to CRBN and DDB1. To purify thalidomide-binding proteins, we performed affinity purification using ferrite-glycidyl methacrylate (FG) beads (*9*). The carboxylic thalidomide derivative FR259625 was covalently conjugated to the beads (fig. S1) and incubated with human HeLa cell extracts (*10*). After extensive washing, bound proteins were eluted with free thalidomide, and the eluate fractions were subjected to SDS gel electrophoresis and silver staining. Two polypeptides were specifically eluted (Fig. 1A, lane 3). When free thalidomide was added to extracts before incubation with the beads, the yields of these proteins were reduced (Fig. 1A, lane 4), which suggested that these proteins specifically interact with thalidomide. The 127- and 55-kD proteins were therefore subjected to proteolytic digestion and tandem mass spectrometry and were identified as CRBN and damaged DNA binding protein 1 (DDB1), respectively (table S1). Identities of these proteins were confirmed by immunoblotting (Fig. 1A). CRBN and DDB1 were isolated similarly as thalidomide-binding proteins from various cell types (fig. S2). To determine whether this interaction is direct, we used purified recombinant proteins. FLAG-tagged CRBN, but not V5 (GKPIPNPLLGLDST) (*11*) epitope- and histidine (His)–tagged DDB1, bound to thalidomide beads (Fig. 1B). We therefore asked whether DDB1 binds to thalidomide beads through its interaction with CRBN. As expected, DDB1 was coprecipitated with FLAG- and hemagglutinin (HA) epitope–tagged (FH-) CRBN (Fig. 1C) and was not affinity-purified from CRBN-depleted 293T cells (fig.

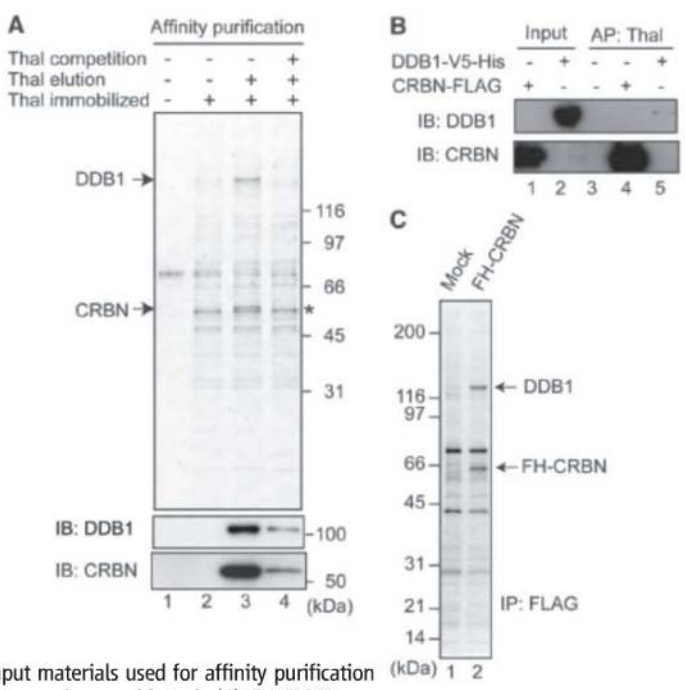

Fig. 1. Thalidomide binds to CRBN and DDB1. **(A)** Thalidomide (Thal)-binding proteins were purified from HeLa cell extracts by using thalidomide-immobilized (+) or control (–) beads. Where indicated, bound proteins were eluted with free thalidomide. As indicated, 0.3 mM thalidomide was added to extracts before incubation with the beads. Eluted proteins were analyzed by silver staining (top) or immunoblotting (IB) (bottom). Asterisk indicates nonspecific signal. **(B)** Purified recombinant CRBN-FLAG and DDB1-V5-His were, respectively, incubated with thalidomide beads. Input materials used for affinity purification (AP) and bound materials were immunoblotted. **(C)** FH-CRBN was immunoprecipitated (IP) from 293T cells stably expressing FH-CRBN or from control cells, followed by SDS gel electrophoresis and silver staining.

[1]Integrated Research Institute, Tokyo Institute of Technology, Yokohama 226-8503, Japan. [2]Graduate School of Bioscience and Biotechnology, Tokyo Institute of Technology, Yokohama 226-8501, Japan. [3]Institute of Development, Aging and Cancer, Tohoku University, Sendai 980-8575, Japan. [4]Precursory Research for Embryonic Science and Technology, Japan Science and Technology Agency (JST), Saitama 332-0012, Japan. [5]Drug Discovery Research, Astellas Pharma Inc., Ibaraki 305-8585, Japan.

*These authors contributed equally to this work.
†To whom correspondence should be addressed. E-mail: handa.h.aa@m.titech.ac.jp

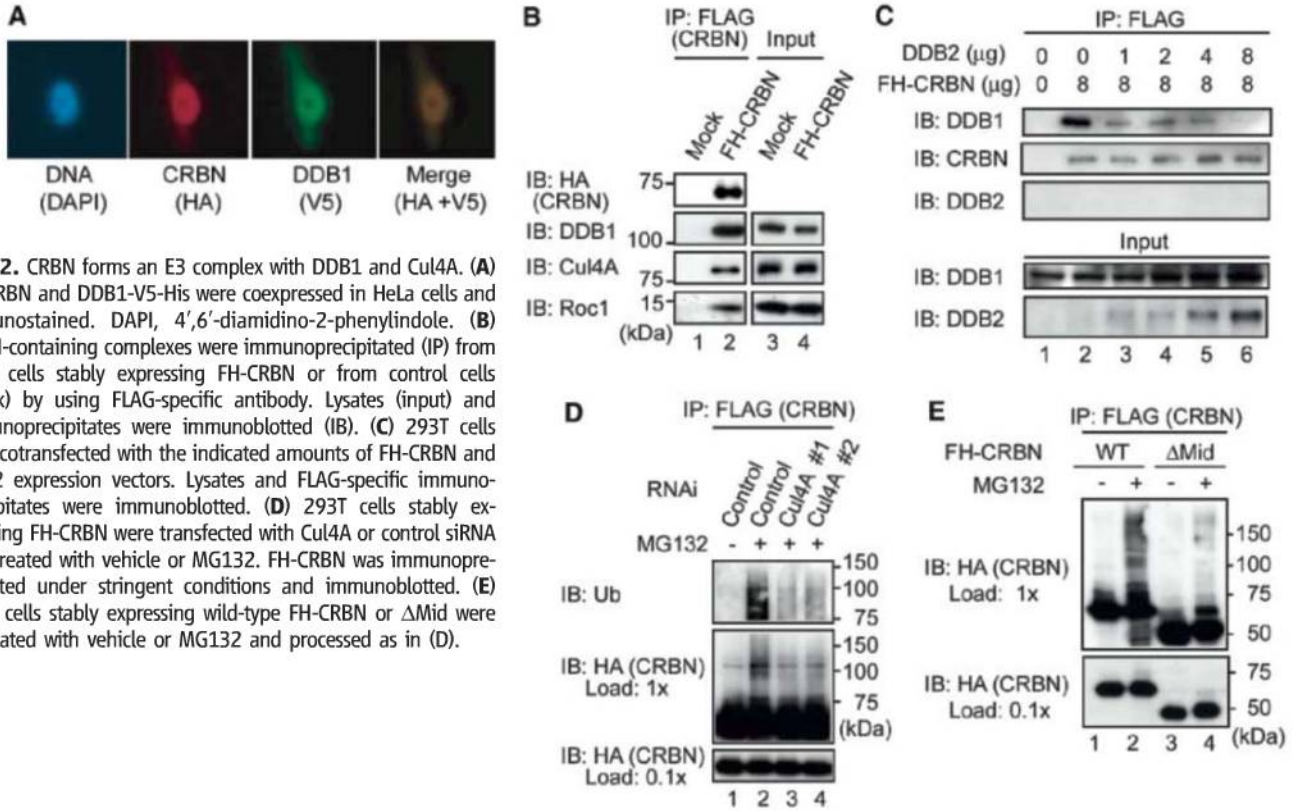

Fig. 2. CRBN forms an E3 complex with DDB1 and Cul4A. **(A)** FH-CRBN and DDB1-V5-His were coexpressed in HeLa cells and immunostained. DAPI, 4′,6′-diamidino-2-phenylindole. **(B)** CRBN-containing complexes were immunoprecipitated (IP) from 293T cells stably expressing FH-CRBN or from control cells (mock) by using FLAG-specific antibody. Lysates (input) and immunoprecipitates were immunoblotted (IB). **(C)** 293T cells were cotransfected with the indicated amounts of FH-CRBN and DDB2 expression vectors. Lysates and FLAG-specific immunoprecipitates were immunoblotted. **(D)** 293T cells stably expressing FH-CRBN were transfected with Cul4A or control siRNA and treated with vehicle or MG132. FH-CRBN was immunoprecipitated under stringent conditions and immunoblotted. **(E)** 293T cells stably expressing wild-type FH-CRBN or ΔMid were incubated with vehicle or MG132 and processed as in (D).

S3A), which led us to conclude that thalidomide interacts directly with CRBN and indirectly with DDB1 through its interaction with CRBN. The equilibrium dissociation constant of the CRBN-thalidomide interaction was calculated to be 8.5 nM (*10*). Moreover, CRBN did not bind to phthalimide, a nonteratogenic analog of thalidomide (*12*), which substantiated the high affinity and specificity of the CRBN-thalidomide interaction (fig. S3B).

Formation of an E3 complex by CRBN, DDB1, and Cul4A. Human *CRBN* was originally identified as a candidate gene for autosomal recessive mild mental retardation and encodes a 442–amino acid protein that is highly conserved from plants to humans (*13*). Although CRBN was reported to interact with DDB1 in a recent proteomic analysis (*14*), the functional relevance of this interaction remains unclear. Consistent with the apparently stoichiometric interaction of CRBN and DDB1 (Fig. 1C), these proteins are colocalized mainly in the nucleus, but also in the cytoplasm (Fig. 2A). DDB1 is a component of E3 ubiquitin ligase complexes containing Cullin 4 (Cul4A or Cul4B), regulator of cullins 1 (Roc1), and a substrate receptor (*15*, *16*). In principle, the function of E3 ubiquitin ligases is to direct the polyubiquitination of substrate proteins by a specifically interacting ubiquitin-conjugating enzyme (E2) (*17*, *18*). Cul4 is thought to play a scaffold function, whereas Roc1 has a RING finger domain that associates with the E2 ubiquitin-conjugating enzyme. Substrate receptors, such as DDB2, CSA, and CDT2, directly bind to specific substrates and mediate their ubiquitination (*15*, *19*, *20*). We examined whether CRBN interacts with other components of the E3 complex and found that Cul4A and Roc1 were indeed coprecipitated with FH-CRBN (Fig. 2B). If CRBN functions as a substrate receptor of a Cul4-DDB1 E3 complex, it would be expected to compete for binding to DDB1 with other substrate receptor subunits, such as DDB2. Consistent with this, the amount of DDB1 coprecipitated with FH-CRBN was reduced in the presence of increasing amounts of coexpressed DDB2 (Fig. 2C). Although thalidomide can induce oxidative DNA damage (*4*), CRBN is likely to function independently of the DDB2-mediated DNA damage response pathway [see supporting online material (SOM) text].

We then examined whether the CRBN complex actually has E3 ubiquitin ligase activity. Because substrate receptors and Cul4 are known to undergo autoubiquitination in vitro in the absence of their specific substrates (*15*, *16*), in vitro ubiquitination assays were performed using purified protein components. Indeed, intrinsic ubiquitination activity was observed in the presence of the CRBN complex (fig. S4). We then examined whether CRBN is autoubiquitinated in cells. For this, CRBN was affinity-purified from 293T cells expressing FH-CRBN in the presence or absence of the proteasome inhibitor MG132. Autoubiquitination of FH-CRBN was detected in the presence of MG132, and its ubiquitination was abrogated by small interfering RNA (siRNA)–mediated depletion (knockdown) of Cul4A (Fig. 2D, fig. S5A, and table S2). Knockdown of DDB1 led to a substantial reduction of the CRBN protein level (fig. S5B), and it was not possible to determine the effect of DDB1 knockdown on CRBN ubiquitination. Nevertheless, this finding suggests that DDB1 and CRBN are functionally linked.

To further investigate the role of DDB1 in CRBN function, we obtained a CRBN mutant deficient in DDB1 binding. Mutational analysis revealed that deletion of amino acids 187 to 260 of CRBN (ΔMid) abolishes its interaction with DDB1 (fig. S6). ΔMid was therefore stably expressed in 293T cells and examined for its ubiquitination after MG132 treatment. Ubiquitination of ΔMid was reduced compared with wild-type CRBN (Fig. 2E). Collectively, these findings suggest that CRBN is a subunit of a functional E3 ubiquitin ligase complex and undergoes autoubiquitination in a Cul4A- and DDB1-dependent manner.

Inhibition of CRBN function by thalidomide. To investigate the structural basis of the CRBN-thalidomide interaction and its functional significance, we wished to obtain a CRBN point mutant that does not bind to thalidomide but is assembled into a functional E3 complex. Using a series of deletion mutants, we mapped its thalidomide-binding region to the C-terminal 104 amino acids, which corresponds to the most highly conserved region of the protein (figs. S7 and S8). Assuming that evolutionarily conserved residues may be important for thalidomide binding, we constructed a series of point mutants, and two point

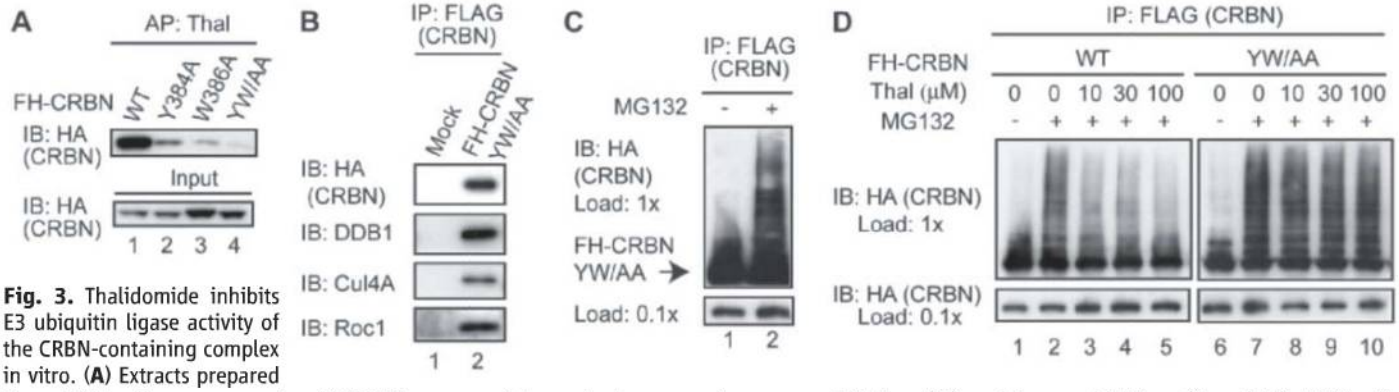

Fig. 3. Thalidomide inhibits E3 ubiquitin ligase activity of the CRBN-containing complex in vitro. (**A**) Extracts prepared from 293T cells overexpressing FH-CRBN or one of its mutants were incubated with thalidomide-immobilized beads, and lysates (input) and affinity-purified (AP) materials were immunoblotted (IB). (**B**) 293T cells stably expressing FH-CRBN$^{YW/AA}$ were subjected to FLAG-specific antibody immunoprecipitation (IP) and immunoblotting. (**C** and **D**) 293T cells stably expressing FH-CRBN or FH-CRBN$^{YW/AA}$ were processed as in Fig. 2E. In (D), cells were treated with the indicated concentrations of thalidomide for 4 hours before harvest.

mutants, Y384A and W386A, were found to be defective for thalidomide binding (Fig. 3A) (*11*). Moreover, the double point mutant Y384A/W386A (CRBN$^{YW/AA}$) had extremely low thalidomide-binding activity. We then asked whether CRBN$^{YW/AA}$ is functionally active in cells. The subcellular localization of the mutant was indistinguishable from wild-type CRBN (fig. S7C). Moreover, CRBN$^{YW/AA}$ was coprecipitated with DDB1, Cul4A, and Roc1 (Fig. 3B) and was autoubiquitinated after MG132 treatment (Fig. 3C), which demonstrated that CRBN$^{YW/AA}$ is assembled into a complete E3 ubiquitin ligase complex.

We examined possible effects of thalidomide on ubiquitination by treating 293T cells stably expressing FH-CRBN or FH-CRBN$^{YW/AA}$ with MG132 and thalidomide at similar or higher concentrations relative to the therapeutic doses used in humans (*21*). Autoubiquitination of wild-type CRBN was inhibited by thalidomide in a concentration-dependent manner, whereas autoubiquitination of CRBN$^{YW/AA}$ was not affected by thalidomide even at the highest concentration used (Fig. 3D). Together, these results suggest that thalidomide inhibits E3 function of the CRBN-containing complex by directly binding to CRBN.

CRBN as an in vivo target of thalidomide. Next, we investigated a possible role of CRBN in thalidomide teratogenicity in animal models. Thalidomide is teratogenic in rabbits and chicks, but not in mice and rats (*1*–*3*). We first used zebrafish as a model system because (i) the rapid progress of development of zebrafish can be monitored in real time because of the transparency of the embryo, (ii) knockdown of genes of interest can be carried out easily (*22*), and (iii) zebrafish are suitable for pharmacotoxicological studies (*23*). Given that thalidomide was recently shown to inhibit angiogenesis in zebrafish embryos (*24*), we reasoned that zebrafish might be susceptible to other activities of thalidomide.

To examine the effects of thalidomide on zebrafish development, we transferred dechorionated embryos to media containing different concentrations of thalidomide at 2 hours post fertilization (hpf) and allowed them to develop for 3 days. It was immediately apparent that in thalidomide-treated embryos, development of pectoral fins and otic vesicles was disturbed, whereas other aspects of development were not generally affected (Fig. 4, A and B, and fig. S9). More specifically, formation of the proximal endoskeletal disc of the pectoral fin was severely inhibited at 75 hpf (Fig. 4A), and otic vesicle size was significantly reduced at 30 hpf (Fig. 4B and fig. S11). Pectoral fin malformations were already apparent at 48 hpf (Fig. 5, C and D). More detailed phenotypes induced by thalidomide are described in the SOM text. Recent studies have suggested that development of pectoral fins and otic vesicles in teleosts share common molecular pathways with that of tetrapod limbs and ears (*25*–*27*).

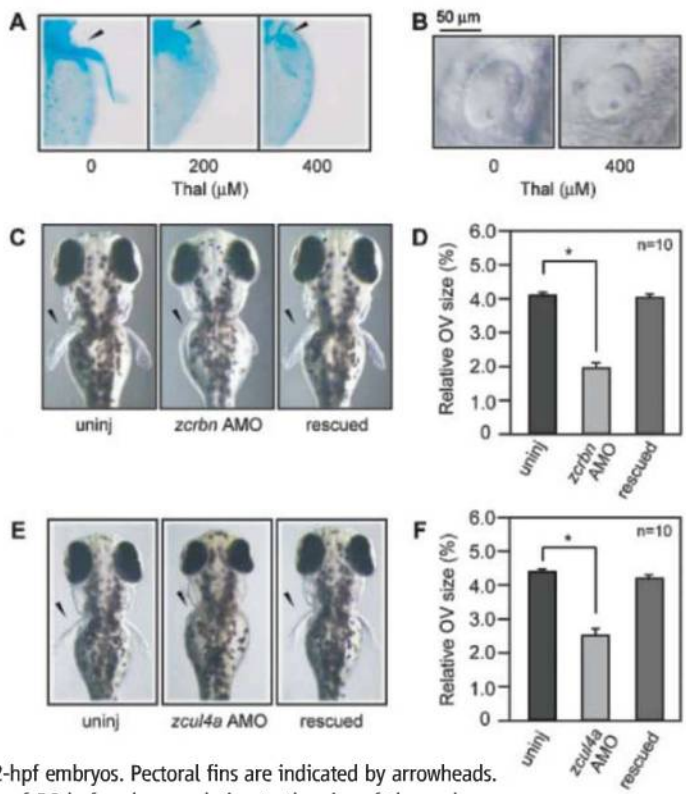

Fig. 4. Thalidomide treatment or down-regulation of the CRBN complex causes similar developmental defects in zebrafish. (**A** and **B**) Zebrafish embryos were allowed to develop in media containing the indicated concentrations of thalidomide. (A) Embryos at 75 hpf were fixed and stained with Alcian blue. Pectoral fins are indicated by arrowheads. (B) Close-up view of otic vesicles of 30-hpf live embryos. (**C** and **D**) Where indicated, *zcrbn* AMO was injected with (rescued) or without *zcrbn* mRNA into one-cell stage embryos. (**E** and **F**) Where indicated, *zcul4a* AMO was injected with or without *zcul4a* mRNA into one-cell stage embryos. (C and E) Dorsal views of pectoral fins of 72-hpf embryos. Pectoral fins are indicated by arrowheads. (D and F) Otic vesicle size of 30-hpf embryos relative to the size of the embryo. Representative raw data are shown in fig. S14. *$P < 0.001$. uninj, uninjected.

Zebrafish have a *CRBN* orthologous gene which we call *zcrbn*, whose product has ~70% identity to human CRBN (fig. S8). We first examined the expression pattern of *zcrbn* mRNA and found that the gene is highly expressed in the brain, head vasculature, otic vesicles, and developing pectoral fins at 30 and 48 hpf (fig. S12). zCrbn interacts with DDB1 and is affinity-purified from zebrafish embryos as a major interactor with thalidomide (fig.

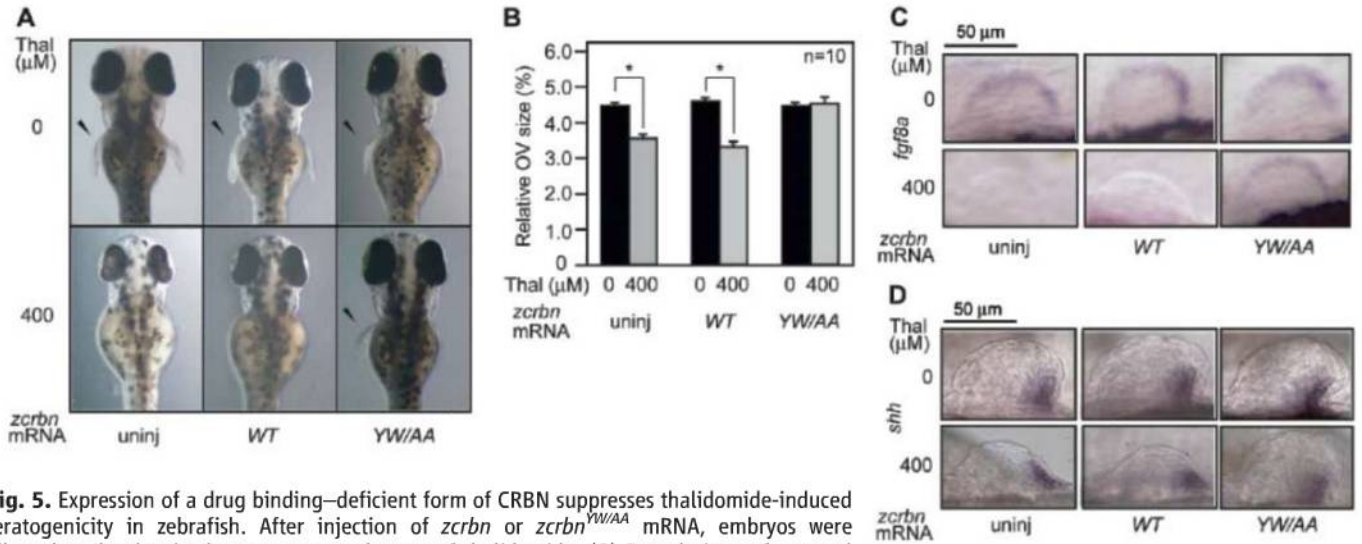

Fig. 5. Expression of a drug binding–deficient form of CRBN suppresses thalidomide-induced teratogenicity in zebrafish. After injection of *zcrbn* or *zcrbn*$^{YW/AA}$ mRNA, embryos were allowed to develop in the presence or absence of thalidomide. (**A**) Dorsal views of pectoral fins of 72-hpf embryos. Fins are indicated by arrowheads. (**B**) Otic vesicle size of 30-hpf embryos relative to the size of the embryo. *$P < 0.001$. (**C** and **D**) Embryos at 48 hpf were subjected to hybridization with antisense probes for *fgf8a* or *shh*. Close-up views of fin buds are shown. uninj, uninjected.

S13), which suggests that the findings of our cell culture studies are valid in zebrafish. Hence, the function of zCrbn during early development was examined. Embryos injected with an antisense morpholino oligonucleotide (AMO) for *zcrbn* exhibited specific defects in fin and otic vesicle development (Fig. 4, C and D, and figs. S9 to S11 and S14), phenotypes similar to those of thalidomide-treated embryos. For example, the size of otic vesicles was reduced by half in the knockdown embryos (Fig. 4D). These defects were rescued by coinjection of *zcrbn* mRNA (Fig. 4, C and D, and figs. S9 to S11 and S14).

The above findings suggested an interesting possibility that thalidomide exerts teratogenic effects by inhibiting zCrbn function. If so, its teratogenic effects might be reversed by overexpression of a functionally active, thalidomide binding–defective form of zCrbn. To test this idea, we used zCrbn carrying Y374A and W376A mutations, which correspond to Y384A and W386A mutations in human CRBN. zCrbn$^{YW/AA}$ had extremely low thalidomide-binding activity (fig. S13C). In the absence of thalidomide, overexpression of zCrbn or zCrbn$^{YW/AA}$ had no discernible effect on fin and otic vesicle development (Fig. 5 and figs. S9 to S11). As we have already seen in Fig. 4, thalidomide treatment significantly reduced otic vesicle size ($P < 0.001$, Mann-Whitney U test) (Fig. 5B and fig. S11). Thalidomide treatment of embryos overexpressing wild-type zCrbn similarly reduced otic vesicle size ($P < 0.001$). However, thalidomide treatment of embryos overexpressing zCrbn$^{YW/AA}$ did not affect otic vesicle size significantly ($P = 0.59$). Thalidomide-induced pectoral fin malformations were also rescued by overexpression of zCrbn$^{YW/AA}$ (Fig. 5A and fig. S10), which demonstrated that thalidomide exerts teratogenic effects by binding to CRBN and inhibiting its function.

Molecular mechanism of thalidomide teratogenicity. As the connection between thalidomide and CRBN was established, we then examined whether the CRBN-containing E3 complex is involved in thalidomide teratogenicity, by down-regulating the zebrafish homolog of Cul4A (zCul4a). *zcul4a* mRNA is abundantly expressed in the brain and pectoral fins (fig. S12). As expected, microinjection of AMO for *zcul4a* caused similar defects in otic vesicles and pectoral fins, and these phenotypes were rescued by coinjection of *zcul4a* mRNA (Fig. 4, E and F, and figs. S9 to S11 and S14). Nevertheless, phenotypic similarities between zCrbn and zCul4A knockdown embryos may be just coincidental. To rule out this possibility, we examined the importance of the physical interaction between CRBN and DDB1 in vivo, by using zCrbn$^{\Delta Mid\ YW/AA}$. As expected, DDB1 and thalidomide did not bind to this mutant, and thalidomide-induced developmental defects were not rescued by its overexpression (fig. S15). These results suggest that the CRBN-containing E3 ubiquitin ligase complex plays a crucial role in fin and otic vesicle development and is a target of thalidomide.

To obtain a clue to the pathway(s) downstream of thalidomide and CRBN, we examined expression of key signaling molecules during pectoral fin development. Sonic hedgehog (Shh) is expressed in the zone of polarizing activity (ZPA) and is responsible for anteroposterior patterning of limbs (*28*), whereas fibroblast growth factor (fgf) 8 is expressed in the apical ectodermal ridge (AER) of limbs and is responsible for limb outgrowth along the proximodistal axis (*29*, *30*). In thalidomide-treated 48-hpf embryos, *fgf8a* expression in the AER was severely reduced or absent (Fig. 5C), whereas *shh* expression in the ZPA was affected negligibly (Fig. 5D). In addition, *fgf8a* expression was restored by injection of *zcrbn*$^{YW/AA}$ mRNA (Fig. 5C). Knockdown of zCrbn or zCul4a also resulted in a reduction of *fgf8a* expression in the AER, whereas it had little effect on *shh* expression in the ZPA (fig. S14). Thus, an inhibitor of fgf8 production is a possible downstream target of thalidomide and the CRBN-containing E3 complex.

Conserved role for CRBN in zebrafish and chicks. Finally, in order to validate our findings, we used chicks, well-established model organisms for studying thalidomide teratogenicity. As reported previously (*12*, *31*), exposure to thalidomide resulted in the complete absence of a forelimb at a high incidence (Fig. 6A and fig. S16). Overexpression of human CRBN$^{YW/AA}$, but not wild-type CRBN, in the forelimb field remarkably reduced thalidomide sensitivity (Fig. 6A and fig. S16). Expression of *fgf8* and *fgf10* was then examined. Fgf10 is also an important regulator of proximodistal limb patterning and is normally expressed in the mesoderm beneath the AER (Fig. 6B). Thalidomide down-regulated *fgf10* expression in the mesoderm and, perhaps to a lesser extent, *fgf8* expression in the AER, and their expression was restored by overexpression of CRBN$^{YW/AA}$ (Fig. 6B). These results, together with the finding that chick CRBN binds to thalidomide and DDB1 (fig. S17), suggest that the developmental role of CRBN is conserved in fins and limbs.

Discussion. The mechanism of action of thalidomide appears to be multifaceted, but is not fully understood. The immunomodulatory and antiangiogenic activities of thalidomide have been proposed to be partly responsible for its teratogenic activity, as well as its therapeutic value in the treatment of leprosy and multiple myeloma (*2*, *3*, *6*, *7*). In this respect, thalidomide is known to inhibit the production of some cytokines such as tumor necrosis factor–α and vascular endothelial growth factor (*32*, *33*). Thalidomide is also capable of inducing apoptosis and producing reactive oxygen species (*3*, *4*). Despite such accumulating data, little is known about direct

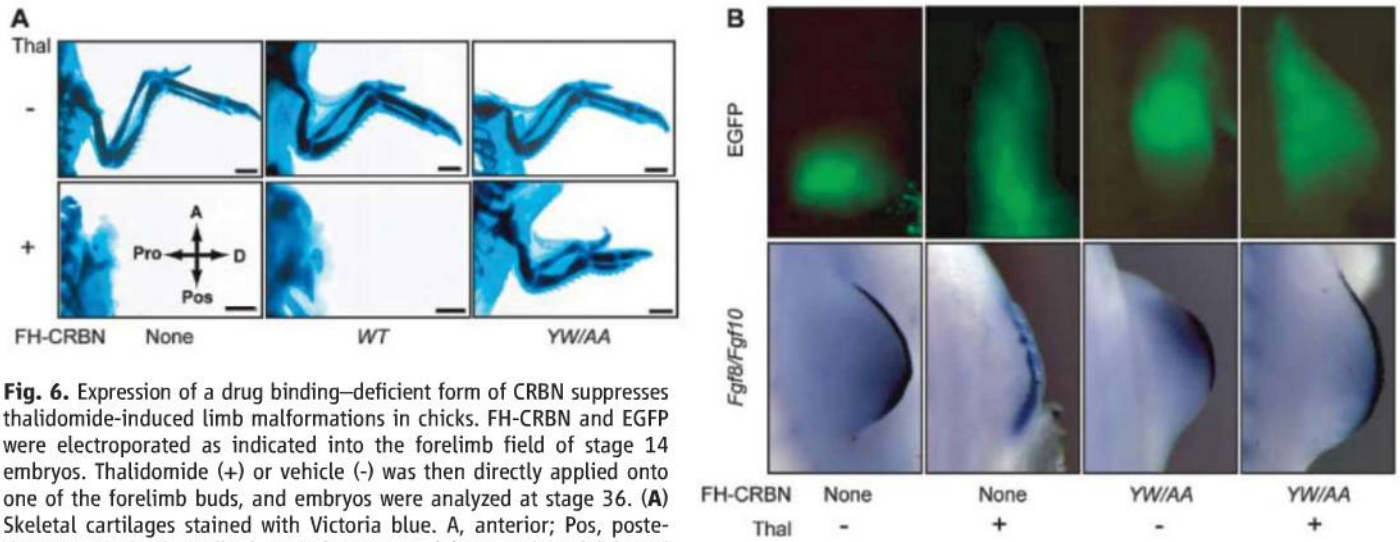

Fig. 6. Expression of a drug binding–deficient form of CRBN suppresses thalidomide-induced limb malformations in chicks. FH-CRBN and EGFP were electroporated as indicated into the forelimb field of stage 14 embryos. Thalidomide (+) or vehicle (-) was then directly applied onto one of the forelimb buds, and embryos were analyzed at stage 36. (**A**) Skeletal cartilages stained with Victoria blue. A, anterior; Pos, posterior; Pro, proximal; D, distal. Scale bar, 1 mm. (**B**) Expression of *fgf8* and *fgf10* visualized by in situ hybridization. EGFP marks area of electroporation.

molecular targets of thalidomide. Here we provided several lines of evidence that CRBN is a primary target of thalidomide teratogenicity. Because overexpression of the thalidomide-insensitive form of CRBN rescued the effects of thalidomide largely, if not entirely, in zebrafish and chicks, CRBN is thought to play an important role as an upstream mediator of thalidomide action at least in these species. Whereas CRBN is ubiquitously expressed in humans, thalidomide exerts tissue-specific effects. Evidently, CRBN is necessary, but not sufficient, for thalidomide teratogenicity, and downstream components are likely to contribute to the tissue-specific effects of thalidomide (see SOM text).

The finding that fgf8 is a downstream target of thalidomide and CRBN fits well with a previous report, in which a similar effect of thalidomide on *fgf8* expression was described in rabbits, another sensitive species (*34*). In developing chick limb buds, thalidomide was shown to up-regulate expression of a subset of bone morphogenetic protein (BMP) family genes and to induce apoptosis (*12*). Coincidentally, mouse BMPs were shown to inhibit *fgf8* expression and to induce apoptosis in the AER (*35*). Thus, CRBN appears to be a missing link between thalidomide and these key developmental regulators.

However, this study does not rule out other mechanisms of thalidomide action, particularly in mammals. Thalidomide-induced oxidative stress is thought to occur through the direct formation of reactive oxygen species (*4*) and is therefore clearly a CRBN-independent process. Second, a recent study suggested antiangiogenic activity of thalidomide as a primary cause of chick limb malformations, demonstrating that thalidomide-induced inhibition of vasculogenesis precedes inhibition of *fgf8* expression and cell death in limb buds (*31*). By contrast, our data suggest that, in zebrafish, inhibition of vasculogenesis follows thalidomide-induced morphological and transcriptional changes in pectoral fin buds (fig. S18 and SOM text), which implies that the sequence of events induced by thalidomide is different in these organisms. These observations are concordant with the common view of species differences in thalidomide action (see SOM for further discussion on the species differences). Another point to consider is the fact that thalidomide is rapidly hydrolyzed or metabolized to more than a dozen products in vitro and in vivo (*2*, *21*, *36*). Thalidomide and its products may have the same or different molecular target(s) (see SOM text).

Our findings suggest that thalidomide exerts teratogenic effects, at least in part, by binding to CRBN and inhibiting the associated ubiquitin ligase activity (fig. S19). We speculate that control of ubiquitin-dependent proteolysis by thalidomide and CRBN leads to abnormal regulation of the BMP and fgf8 signaling pathways and of developmental programs that require their normal functions. Incidentally, many E3 ubiquitin ligases are known to target developmental and/or transcriptional regulators and to control developmental programs (*37*, *38*). There are, however, a number of unanswered questions, such as: What are the substrates of CRBN E3 ubiquitin ligase? How does thalidomide inhibit the ubiquitination of CRBN in the ligase complex? How might this pathway be interconnected to the other pathways targeted by thalidomide? These issues need to be addressed to fully appreciate the model. Last, but not least, because thalidomide is now used for the treatment of multiple myeloma and leprosy, identification of its direct target may allow rational design of more effective thalidomide derivatives without teratogenic activity (see SOM text).

References and Notes

1. M. T. Miller, K. Strömland, *Teratology* **60**, 306 (1999).
2. M. Melchert, A. List, *Int. J. Biochem. Cell Biol.* **39**, 1489 (2007).
3. J. Knobloch, U. Rüther, *Cell Cycle* **7**, 1121 (2008).
4. T. Parman, M. J. Wiley, P. G. Wells, *Nat. Med.* **5**, 582 (1999).
5. R. J. D'Amato, M. S. Loughnan, E. Flynn, J. Folkman, *Proc. Natl. Acad. Sci. U.S.A.* **91**, 4082 (1994).
6. J. Sheskin, *Clin. Pharmacol. Ther.* **6**, 303 (1965).
7. S. Singhal *et al.*, *N. Engl. J. Med.* **341**, 1565 (1999).
8. J. B. Zeldis, B. A. Williams, S. D. Thomas, M. E. Elsayed, *Clin. Ther.* **21**, 319 (1999).
9. S. Sakamoto, Y. Kabe, M. Hatakeyama, Y. Yamaguchi, H. Handa, *Chem. Rec.* **9**, 66 (2009).
10. Materials and methods and additional text are available as supporting information on *Science* Online.
11. Single-letter abbreviations for the amino acid residues used in this research article are as follows: A, Ala; C, Cys; D, Asp; E, Glu; F, Phe; G, Gly; H, His; I, Ile; K, Lys; L, Leu; M, Met; N, Asn; P, Pro; Q, Gln; R, Arg; S, Ser; T, Thr; V, Val; W, Trp; and Y, Tyr.
12. J. Knobloch, J. D. Shaughnessy Jr., U. Rüther, *FASEB J.* **21**, 1410 (2007).
13. J. J. Higgins, J. Pucilowska, R. Q. Lombardi, J. P. Rooney, *Neurology* **63**, 1927 (2004).
14. S. Angers *et al.*, *Nature* **443**, 590 (2006).
15. R. Groisman *et al.*, *Cell* **113**, 357 (2003).
16. F. Ohtake *et al.*, *Nature* **446**, 562 (2007).
17. C. M. Pickart, *Cell* **116**, 181 (2004).
18. M. D. Petroski, R. J. Deshaies, *Nat. Rev. Mol. Cell Biol.* **6**, 9 (2005).
19. K. Sugasawa *et al.*, *Cell* **121**, 387 (2005).
20. J. Jin, E. E. Arias, J. Chen, J. W. Harper, J. C. Walter, *Mol. Cell* **23**, 709 (2006).
21. M. E. Franks, G. R. Macpherson, W. D. Figg, *Lancet* **363**, 1802 (2004).
22. A. Nasevicius, S. C. Ekker, *Nat. Genet.* **26**, 216 (2000).
23. M. B. Veldman, S. Lin, *Pediatr. Res.* **64**, 470 (2008).
24. T. Yabu *et al.*, *Blood* **106**, 125 (2005).
25. M. Tanaka *et al.*, *Nature* **416**, 527 (2002).
26. M. C. Davis, R. D. Dahn, N. H. Shubin, *Nature* **447**, 473 (2007).
27. A. Streit, *J. Anat.* **199**, 99 (2001).
28. R. D. Riddle, R. L. Johnson, E. Laufer, C. Tabin, *Cell* **75**, 1401 (1993).
29. A. M. Moon, M. R. Capecchi, *Nat. Genet.* **26**, 455 (2000).
30. M. Lewandoski, X. Sun, G. R. Martin, *Nat. Genet.* **26**, 460 (2000).
31. C. Therapontos, L. Erskine, E. R. Gardner, W. D. Figg, N. Vargesson, *Proc. Natl. Acad. Sci. U.S.A.* **106**, 8573 (2009).
32. A. L. Moreira *et al.*, *J. Exp. Med.* **177**, 1675 (1993).
33. D. Gupta *et al.*, *Leukemia* **15**, 1950 (2001).
34. J. M. Hansen, S. G. Gong, M. Philbert, C. Harris, *Dev. Dyn.* **225**, 186 (2002).
35. S. Pajni-Underwood, C. P. Wilson, C. Elder, Y. Mishina, M. Lewandoski, *Development* **134**, 2359 (2007).
36. F. Chung *et al.*, *Clin. Cancer Res.* **10**, 5949 (2004).

37. Y. Cang *et al.*, *Cell* **127**, 929 (2006).
38. Y. Cang *et al.*, *Proc. Natl. Acad. Sci. U.S.A.* **104**, 2733 (2007).
39. We thank T. Wada, S. Sakamoto, and S. Ishihara for discussions; P. Raychaudhuri, T. Matsunaga, S. Krauss, B. Thisse, A. Kawakami, S. Noji, J. Izpisua-Belmonte, K. Kawakami, and J. Yamauchi for valuable reagents; Y. Tsuboi for technical support; and P. Sharp and A. Berk for comments on this manuscript. This work was supported by Special Coordination Funds for Promoting Science and Technology from JST, by the Global COE (Center of Excellence) Program from the Japan Ministry of Education, Culture, Sports, Science, and Technology (MEXT), and by a grant for Research and Development Projects in Cooperation with Academic Institutions from the New Energy and Technology Development Organization (H.H. and H.A.). This work was also supported by grants-in-aid for Scientific Research (20370084 to T.O.) and for Young Scientists (21770226 to T.S.) from MEXT and by the Precursory Research for Embryonic Science and Technology program from JST (T.S.). T.I. was a Japan Society for the Promotion of Science Research Fellow. An application for a patent has been filed in the Japan Patent Office.

Supporting Online Material
www.sciencemag.org/cgi/content/full/327/5971/1345/DC1
Materials and Methods
SOM Text
Figs. S1 to S19
Tables S1 and S2
References

5 June 2009; accepted 10 February 2010
10.1126/science.1177319

REPORTS

Variations in the Sun's Meridional Flow over a Solar Cycle

David H. Hathaway[1]* and Lisa Rightmire[2]

The Sun's meridional flow is an axisymmetric flow that is generally directed from its equator toward its poles at the surface. The structure and strength of the meridional flow determine both the strength of the Sun's polar magnetic field and the intensity of sunspot cycles. We determine the meridional flow speed of magnetic features on the Sun using data from the Solar and Heliospheric Observatory. The average flow is poleward at all latitudes up to 75°, which suggests that it extends to the poles. It was faster at sunspot cycle minimum than at maximum and substantially faster on the approach to the current minimum than it was at the last solar minimum. This result may help to explain why this solar activity minimum is so peculiar.

The Sun's meridional flow has been difficult to measure (*1*). Its amplitude (10 to 20 m s^{-1}) is more than an order of magnitude weaker than that of the other major flows on the surface of the Sun (granulation ~3000 m s^{-1}, supergranulation ~300 m s^{-1}, and differential rotation ~170 m s^{-1}). In the past, this has led to reports of vastly different flow speeds and directions (*2*–*5*). Despite its weakness, the meridional flow plays a key role in the magnetic evolution of the Sun's surface. It transports magnetic elements that, when carried to the poles, reverse the magnetic polarity of the poles and build up polar fields of opposite polarity after each sunspot cycle maximum. Models of this magnetic flux transport process (*6*–*8*) have employed a variety of substantially different flow profiles. The fidelity of these flux transport models is important because they are used in climate change studies (*9*, *10*) to estimate the total irradiance of the Sun over the past century. The meridional flow is also key to flux transport dynamo models that have been used to predict the amplitude of Solar Cycle 24 (*11*, *12*). An obvious conflict between the surface flux transport models (*6*–*10*) and the flux transport dynamo models (*11*, *12*) is found in their sensitivity to the strength of the meridional flow. A stronger meridional flow produces weaker polar fields in the surface flux transport models, whereas the same flow produces stronger polar fields (and shorter sunspot cycles) in the flux transport dynamos. Solar Cycle 23 (1996 to 2008) provides an interesting problem for all of these models. The strength of the polar fields produced after cycle maximum in 2000–2001 was only about half that seen in the previous three solar cycles (*13*). Furthermore, cycle 24 started much later than average. The late start for cycle 24 has left behind a long quiet minimum unlike any in the past 100 years.

We measured the Sun's meridional flow to determine its variability over Solar Cycle 23 by following the motions of the small magnetic elements that populate the entire surface of the Sun. These are precisely the elements whose motions are modeled in both the surface flux transport models and the flux transport dynamo models. Motions of sunspots, and even the plasma at the surface, are known to differ from those of the small magnetic elements (*1*–*5*). The data we used have been acquired by the Michelson Doppler Imager (MDI) on the European Space Agency (ESA)/National Aeronautics and Space Administration (NASA) Solar and Heliospheric Observatory (SOHO). MDI produces images of the line-of-sight magnetic field across the visible solar disc every 96 min. This is done by measuring differences in circular polarization on either side of a spectral absorption line caused by traces of nickel in the Sun's atmosphere (*14*). We measured the displacement of the magnetic elements by comparing their positions at 8-hour (5-image) intervals from May 1996 to June 2009. The 1024-by-1024 pixel magnetic images were mapped onto a 1024-by-1024 grid in heliographic latitude and longitude from the central meridian. This mapping accounts for changes in the position angle of the Sun's rotation axis relative to the spacecraft's vertical axis, changes in the tilt angle of the Sun's rotation axis toward or away from the spacecraft, and changes in perspective at different distances from the Sun. Because sunspots have very different proper motions (*4*) and produce localized outflows (*15*), we removed sunspots and their immediate surroundings by masking all pixels with measured absolute field strengths greater than 500 Gauss and all contiguous pixels of the same polarity with absolute field strengths above 100 Gauss. Displacements in longitude and

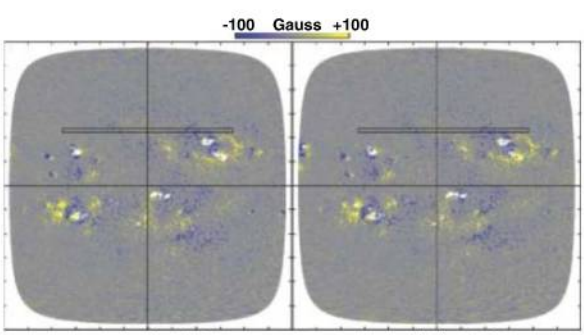

Fig. 1. Magnetic element motion. A pair of masked magnetic maps from 5 June 2001 that were obtained 8 hours apart are shown here with blue representing negative magnetic polarity and yellow representing positive magnetic polarity. The tick marks around the borders are at 15° intervals in latitude and in longitude from the central meridian. The masked-out sunspot areas are evident as white patches. The strongest correlation for the outlined strip of pixels in the earlier map (**left**) is calculated to occur for a shift of 23.7 pixels in longitude and 0.4 pixels in latitude for a similar strip in the later map (**right**).

[1]NASA Marshall Space Flight Center, Huntsville, AL 35812, USA. [2]University of Memphis, Memphis, TN 38152, USA.
*To whom correspondence should be addressed. E-mail: david.hathaway@nasa.gov

latitude were determined for strips (11 pixels high in latitude and 600 pixels long in longitude) by finding the maximum in the cross-correlation with similar strips from the magnetic image acquired 8 hours later (Fig. 1). These calculations were done at 860 latitude positions between ±75° for more than 60,000 image pairs. The meridional flow velocities from these measurements were averaged over individual 27-day rotations of the Sun to extract the axisymmetric signals for each of 167 rotations in the time interval.

The MDI instrument has several known imaging problems (*16*). Our own measurements were most sensitive to the misalignment of the instrument with respect to the star trackers. A small misalignment rotates the 2000 m s^{-1} solar rotation signal into an apparent meridional flow from one hemisphere to the other. Although north-south asymmetries in solar activity do frequently occur, they are usually highly variable and never persist for very long (*17*). We found that a position angle correction of 0.21° counterclockwise [consistent with previous estimates (*16*)] minimized this signal but left a weak trend (from 0.7 m s^{-1} south-to-north in 1996 to 0.7 m s^{-1} north-to-south in 2009). This correction also revealed a significant annual variation (Fig. 2). We attribute this variation to a 0.08° decrease in the accepted tilt of the Sun's equatorial plane relative to the plane of Earth's orbit. This was indicated in a previous study (*18*) based on data from 1996 to 2001 but has not been adopted by the community.

We have constructed the average meridional flow profile (Fig. 3) from those obtained for the individual solar rotations after removing the cross-equatorial signal caused by the annual variation in the error in the tilt angle of the Sun's equatorial plane. This average profile is slightly asymmetric, with a peak velocity of about 12 m s^{-1} in the south and 10 m s^{-1} in the north. The average meridional flow is still poleward at 75° latitude in each hemisphere. This observed profile differs substantially at some latitudes when compared with profiles used in surface flux transport models (*6*–*10*). These discrepancies, if they exist, represent a challenge for understanding the meridional flow and its effect on the polar fields. An earlier study of the magnetic element motions (*5*) and measurements with helioseismic methods (*19*–*21*) had suggested this poleward extension, but all of those measurements were confined to latitudes below 60°. Our measurements show that the meridional flow extends well beyond 75° latitude in each hemisphere.

We fit the individual meridional flow profiles with associated Legendre polynomials (*1*) to extract the flow components. By far, the dominant component is that associated with $P_2^1(\theta) = 2\sin\theta\cos\theta$, where θ is the colatitude measured southward from the north pole. The amplitude of this component (Fig. 4) is well determined for each solar rotation and shows a systematic variation over the solar cycle—fast flow at minimum and slow flow at maximum. The flow speed was 11.5 m s^{-1} at Cycle 23 minimum in 1996–1997. It dropped to 8.5 m s^{-1} at Cycle 23 maximum in 2000–2001 and then increased to 13.0 m s^{-1} in 2004 and has maintained that speed. The slowing of the meridional flow from minimum to maximum seems to be a regular occurrence. This was seen in previous solar cycles (*5*), but with less certainty and poorer time resolution. The variations seen from 1996 to 2009 also indicate a difference between Cycle 23 minimum (1996–1997) and Cycle 24 minimum (2008–2009)—the meridional flow has been substantially faster since 2004 than it was during the Cycle 23 minimum. This is consistent with the observed weaker polar fields (*13*) in the surface flux transport models (*6*–*10*) but leads to conflicts with the flux transport dynamos (*11*, *12*). This fast meridional flow should produce stronger polar fields and a short cycle in the flux transport dynamo models, whereas the observations indicate weak polar fields and a long solar cycle.

The source of the disagreement between the surface flux transport models (*6*–*10*) and the flux transport dynamo models (*11*, *12*) can be seen in the latitudinal distribution of magnetic polarities in these models. The dynamo models have fields of one polarity centered on the sunspot latitudes, whereas the surface models have bands of opposite magnetic polarity on either side of the sunspot latitudes, as is observed. A fast meridional flow in the dynamo models carries elements of only one polarity to the poles. This rapidly erodes the old polar fields and produces strong polar fields of the opposite polarity. A fast meridional flow in the surface models inhibits opposite polarities from canceling each other across the equator and carries elements of both polarities to the poles (with a slight excess of elements with the polarity of the poleward side of the sunspot latitudes). This requires a longer time to reverse the old polar fields and builds up weaker polar fields of the opposite polarity. The variations we observe in the strength of the poleward meridional flow help the surface flux transport models explain (*22*, *23*) the production of weaker polar fields (*13*) and this long quiet minimum based on the faster meridional flow found after 2004.

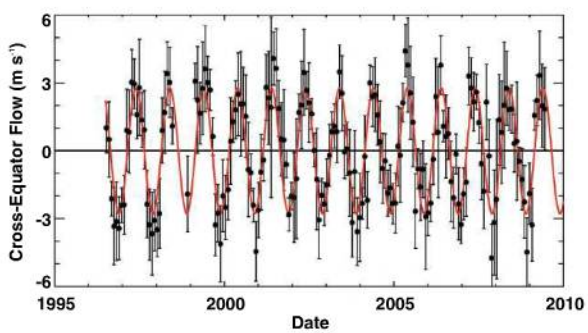

Fig. 2. Annual variation in the cross-equatorial flow. The measured cross-equatorial flow component for each of 167 rotations of the Sun is shown by the filled circles with 2σ error bars. The signal is well fit (red line), with an annual variation produced by a 0.08° decrease in the accepted tilt of the Sun's equatorial plane to the plane of the Earth's orbit. Using the accepted value of 7.25° projects the Sun's rotational velocity into a south-to-north flow in the spring and a north-to-south flow in the fall.

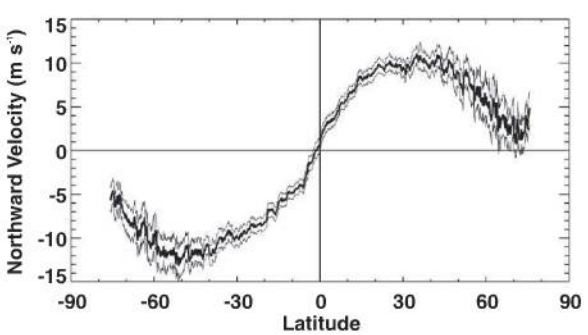

Fig. 3. The average meridional flow profile from 167 rotations of the Sun between May 1996 and June 2009 is shown with the thick line for 860 latitude positions between ±75°. The 2σ error range is indicated by the thin lines.

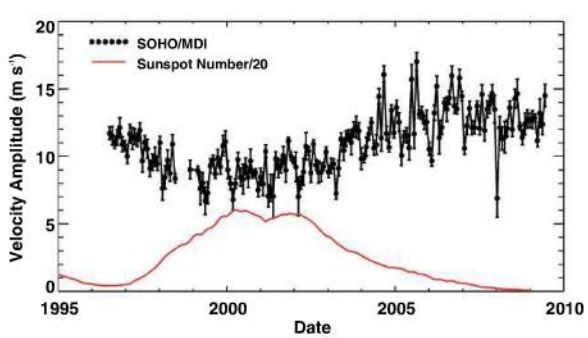

Fig. 4. Meridional flow amplitude variation from May 1996 to June 2009. The amplitude of the primary component of the meridional flow is plotted as dots with 2σ error bars for each solar rotation. The dots are connected except across the SOHO "summer vacation" in 1998. The scaled (by 1/20) smoothed sunspot number is shown in red to indicate the phases of the solar activity cycle.

References and Notes

1. D. H. Hathaway, *Astrophys. J.* **460**, 1027 (1996).
2. K. Topka, R. Moore, B. J. LaBonte, R. Howard, *Sol. Phys.* **79**, 231 (1982).
3. E. Ribes, P. Mein, A. Mangeney, *Nature* **318**, 170 (1985).
4. M. A. Kambry, J. Nishikawa, T. Sakurai, K. Ichimoto, E. Hiei, *Sol. Phys.* **132**, 41 (1991).
5. R. W. Komm, R. F. Howard, J. W. Harvey, *Sol. Phys.* **147**, 207 (1993).
6. C. R. DeVore, N. R. Sheeley Jr., *Sol. Phys.* **108**, 47 (1987).
7. A. A. van Ballegooijen, N. P. Cartledge, E. R. Priest, *Astrophys. J.* **501**, 866 (1998).
8. C. J. Schrijver, A. M. Title, *Astrophys. J.* **551**, 1099 (2001).
9. Y.-M. Wang, J. L. Lean, N. R. Sheeley Jr., *Astrophys. J.* **625**, 522 (2005).
10. J. L. Lean, D. H. Rind, *Geophys. Res. Lett.* **35**, L18701 (2008).
11. M. Dikpati, G. de Toma, P. A. Gilman, *Geophys. Res. Lett.* **33**, L05102 (2006).
12. A. R. Choudhuri, P. Chatterjee, J. Jiang, *Phys. Rev. Lett.* **98**, 131103 (2007).
13. L. Svalgaard, E. W. Cliver, Y. Kamide, *Geophys. Res. Lett.* **32**, L01104 (2005).
14. P. H. Scherrer *et al.*, *Sol. Phys.* **162**, 129 (1995).
15. N. R. Sheeley Jr., *Sol. Phys.* **9**, 347 (1969).
16. MDI Calibration Notes and Known Problems, http://soi.stanford.edu/data/cal
17. D. H. Hathaway, R. M. Wilson, *Sol. Phys.* **224**, 5 (2004).
18. J. G. Beck, P. Giles, *Astrophys. J.* **621**, L153 (2005).
19. P. M. Giles, T. L. Duvall Jr., P. H. Scherrer, R. S. Bogart, *Nature* **390**, 52 (1997).
20. J. Schou, R. S. Bogart, *Astrophys. J.* **504**, L131 (1998).
21. I. González Hernández *et al.*, *Astrophys. J.* **638**, 576 (2006).
22. C. J. Schrijver, Y. Liu, *Sol. Phys.* **252**, 19 (2008).
23. Y.-M. Wang, E. Robbrecht, N. R. Sheeley Jr., *Astrophys. J.* **707**, 1372 (2009).

24. The SOHO/MDI project is supported by NASA grant NAG5-10483 to Stanford University. SOHO is a project of international cooperation between ESA and NASA. L.R. was supported as a summer intern at NASA/Marshall Space Flight Center through the Marshall Space Grant Research Internship Project.

15 September 2009; accepted 13 January 2010
10.1126/science.1181990

Cavity Quantum Electrodynamics with Anderson-Localized Modes

Luca Sapienza,* Henri Thyrrestrup, Søren Stobbe, Pedro David Garcia, Stephan Smolka, Peter Lodahl*

A major challenge in quantum optics and quantum information technology is to enhance the interaction between single photons and single quantum emitters. This requires highly engineered optical cavities that are inherently sensitive to fabrication imperfections. We have demonstrated a fundamentally different approach in which disorder is used as a resource rather than a nuisance. We generated strongly confined Anderson-localized cavity modes by deliberately adding disorder to photonic crystal waveguides. The emission rate of a semiconductor quantum dot embedded in the waveguide was enhanced by a factor of 15 on resonance with the Anderson-localized mode, and 94% of the emitted single photons coupled to the mode. Disordered photonic media thus provide an efficient platform for quantum electrodynamics, offering an approach to inherently disorder-robust quantum information devices.

The interaction between a single photon and a single quantized emitter is the core of cavity quantum electrodynamics (QED) and constitutes a node in a quantum information network (*1*, *2*). So far, cavity QED experiments have been realized with a wide range of two-level systems, including atoms (*3*), ions (*4*), Cooper-pair boxes (*5*), and semiconductor quantum dots (*6*–*8*) coupled to photons confined in a cavity. A common requirement for all these implementations is highly engineered cavities, in some cases requiring nanometer-scale accuracy (*9*). Surprisingly, multiple scattering of photons in disordered dielectric structures offers an alternative route to light confinement. If the scattering is very pronounced, Anderson-localized modes form spontaneously. Anderson localization (*10*) is a multiple-scattering wave phenomenon that has been observed for, e.g., light (*11*), acoustic waves (*12*), and atomic Bose-Einstein condensates (*13*). We have demonstrated cavity QED with Anderson-localized modes by efficiently coupling a single quantum dot (QD) to a disorder-induced cavity mode (*14*) in a photonic crystal waveguide.

DTU Fotonik, Department of Photonics Engineering, Technical University of Denmark, Ørsteds Plads 343, DK-2800 Kgs. Lyngby, Denmark.

*To whom correspondence should be addressed. E-mail: lucs@fotonik.dtu.dk (L.S.); pelo@fotonik.dtu.dk (P.L.)

Photonic crystals are composite nanostructures in which a periodic modulation of the refractive index forms a photonic band gap of frequencies where light propagation is fully suppressed. By deliberately introducing a missing row of holes in a two-dimensional photonic crystal membrane, the periodicity is broken locally and light is guided (Fig. 1A). Such photonic crystal waveguides are strongly dispersive, i.e., light propagation depends sensitively on the optical frequency and can be slowed down. Engineering the photonic crystal waveguide enables the enhancement of light-matter interaction, which is required for high-efficiency single-photon sources (*15*) for quantum information technology (*1*, *16*). In the slow-light regime of photonic crystal waveguides, light propagation is very sensitive to unavoidable structural imperfections (*17*, *18*) and multiple-scattering events randomize propagation (*19*). Although multiple scattering is commonly considered a nuisance for a device, leading to optical losses, here the influence of wave interference in multiple scattering stops light propagation and forms strongly confined Anderson-localized modes (*10*) (Fig. 1B). Anderson-localized modes in a photonic crystal waveguide appear as a result of the primarily one-dimensional nature of the propagation of light provided that the localization length is shorter than the length of the waveguide (*20*).

We deliberately created Anderson-localized modes by fabricating photonic crystal waveguides with a lithographically controlled amount of disorder (Fig. 1B). The hole positions in three rows above and below the waveguide were randomly perturbed with a standard deviation varying between 0 and 6% of the lattice parameter. We investigated the Anderson-localized modes by recording QD photoluminescence spectra under high-excitation power where the feeding from multiple QDs makes Anderson-localized modes appear as sharp spectral resonances (Fig. 1C). The observation of spectrally separated random resonances is a signature of Anderson localization of light (*14*), while the detailed statistics of the intensity fluctuations unambiguously verifies localization even in the presence of absorption (*21*). Figure 1D shows the intensity distribution from spectra recorded at different spatial and spectral positions, which allow us to average over different realizations of disorder. Clear deviations from the Rayleigh distribution predicted for non-localized waves are observed. Light is localized if the variance of the normalized intensity fluctuations exceeds the critical value of 7/3 (*21*), and we extract a variance of 5.3, which proves Anderson localization.

Examples of Anderson-localized modes are shown in Fig. 2 as peaks appearing at random spectral positions, although limited to the slow-light regime of the photonic crystal waveguide. The latter property is due to the strongly dispersive behavior of the localization length that is considerably shortened in the slow-light regime. We tuned the spectral range of Anderson-localized modes by controlling the amount of disorder. Even in samples without engineered disorder, intrinsic and thus unavoidable imperfections, such as surface roughness, are sufficient to localize light (*22*).

The important cavity figures-of-merit are the mode volume V and the Q factor. Decreasing V leads to an enhancement of the electromagnetic field and thus improves light-matter coupling. The Q factor is proportional to the cavity storage time of a photon that needs to be increased for cavity QED applications. High Q factors ranging between 3000 and 10,000 are obtained for different degrees of disorder (Fig. 2) and are comparable to state-of-the-art values obtained for traditional photonic crystal nanocavities containing QDs (*7*).

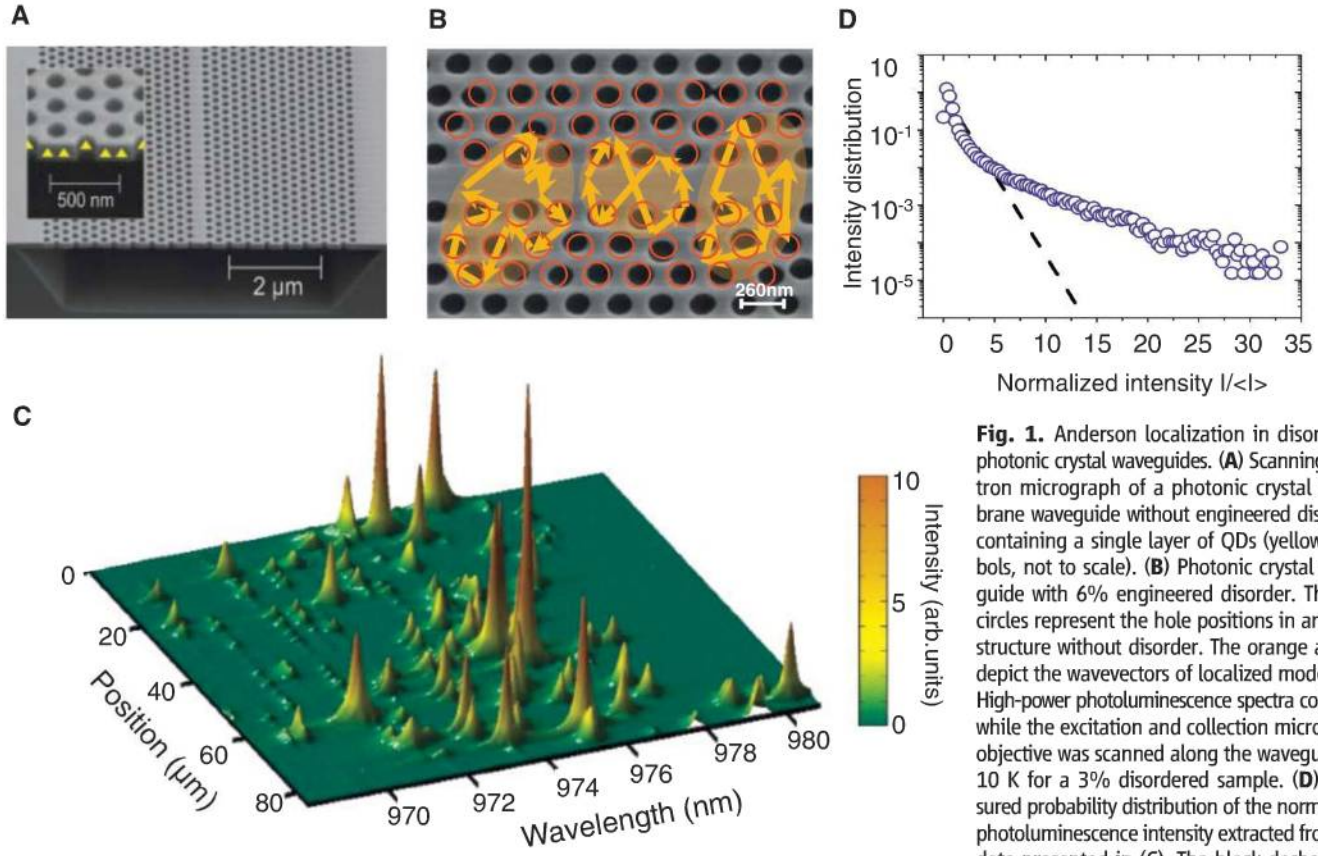

Fig. 1. Anderson localization in disordered photonic crystal waveguides. **(A)** Scanning electron micrograph of a photonic crystal membrane waveguide without engineered disorder, containing a single layer of QDs (yellow symbols, not to scale). **(B)** Photonic crystal waveguide with 6% engineered disorder. The red circles represent the hole positions in an ideal structure without disorder. The orange arrows depict the wavevectors of localized modes. **(C)** High-power photoluminescence spectra collected while the excitation and collection microscope objective was scanned along the waveguide at 10 K for a 3% disordered sample. **(D)** Measured probability distribution of the normalized photoluminescence intensity extracted from the data presented in (C). The black dashed line represents the Rayleigh distribution.

Anderson-localized cavities thus offer a fundamentally new route to cavity QED that is inherently robust to fabrication imperfections, as opposed to traditional cavities (*9*).

Pumping the sample at low-excitation power allowed us to resolve single QD lines and therefore to enter the regime of cavity QED. Figure 3A shows an example of a photoluminescence spectrum displaying single QD peaks and Anderson-localized cavities. QDs and cavity peaks can be easily distinguished from their different temperature dependences (Fig. 3B) that also enable the spectral tuning of single QDs into resonance with an Anderson-localized cavity. Figure 3C displays the crossing between a QD and an Anderson-localized cavity, demonstrating that the cavity-QD system is in the Purcell regime where the cavity promotion of vacuum fluctuations enhances the QD decay rate (*6*).

The Purcell enhancement is studied by means of time-resolved photoluminescence spectroscopy: A QD is repeatedly excited with a short optical pulse and the emission time is measured. Collecting many single-photon events allowed us to record a decay curve representing a histogram of detection events versus time. Two examples of decay curves for the QD tuned on- and off-resonance with an Anderson-localized cavity are presented in Fig. 4A. Off resonance, the QD decay rate is inhibited due to the two-dimensional photonic band gap, leading to an emission rate of 0.5 ns^{-1}. A pronounced enhancement by a factor of 15 is observed on resonance where a fast decay rate of 7.9 ns^{-1} is extracted. An important figure-of-merit for, e.g., single-photon sources or nanolasers is the β factor, which expresses the fraction of photons emitted into a cavity mode. By comparing the emission rates on and off resonance, we extract β = 94%, which represents a lower bound because even for large detuning, residual coupling to the waveguide can persist. The high β factor competes with results obtained on standard photonic crystal nanocavities with carefully optimized cavity design and QD density (*7*). Our results demonstrate that distributed photonic dis-

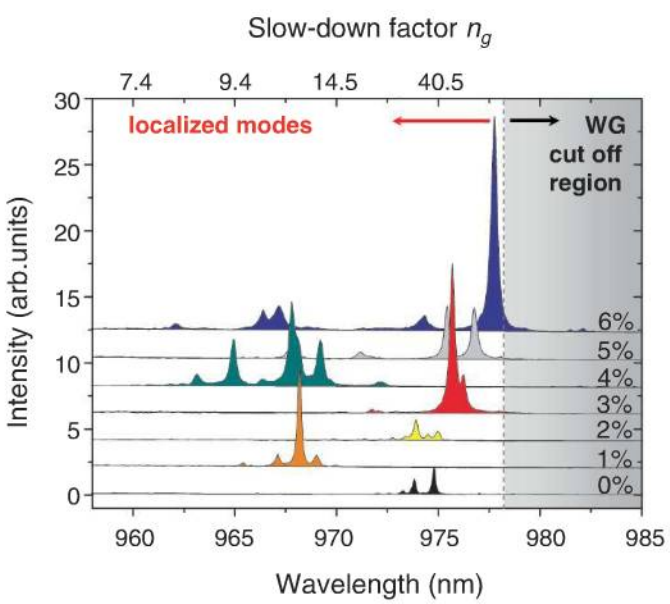

Fig. 2. Spectral signature of Anderson-localized modes. Photoluminescence spectra collected as in Fig. 1C, for various degrees of engineered disorder. Each spectrum was collected with the excitation and collection microscope objective at a fixed position on the waveguide and was vertically shifted for visual clarity. The gray area highlights the calculated waveguide (WG) cut-off region, assuming a refractive index of GaAs of 3.44. $n_g = \frac{c}{\partial\omega/\partial k}$ is the calculated group velocity slow-down factor for an ideal structure without disorder, where c is the vacuum light speed, ω is the frequency, and k is the wave number.

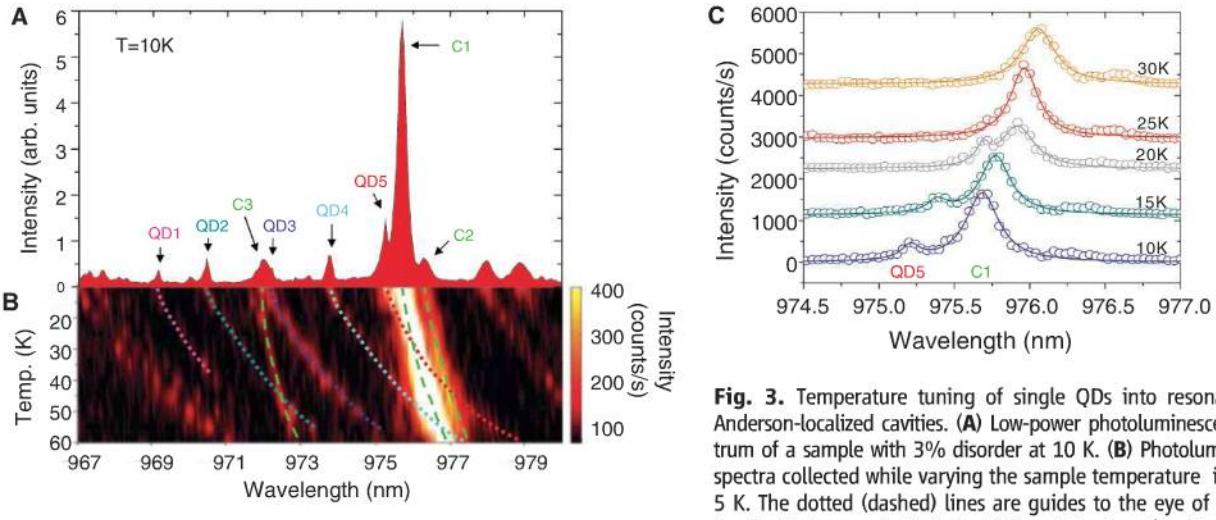

Fig. 3. Temperature tuning of single QDs into resonance with Anderson-localized cavities. (**A**) Low-power photoluminescence spectrum of a sample with 3% disorder at 10 K. (**B**) Photoluminescence spectra collected while varying the sample temperature in steps of 5 K. The dotted (dashed) lines are guides to the eye of the wavelength displacement of selected QD emission lines (localized modes). (**C**) Enlargement of the spectra displaying the QD-cavity crossing. The spectra are fitted to two Lorentzians (solid lines) representing the QD and the cavity peak.

order provides a powerful way of enhancing the interaction between light and matter, enabling cavity QED.

The decay rates of two individual QDs tuned across an Anderson-localized cavity are plotted in Fig. 4B. Different enhancement factors (15 and 9 at temperature $T = 25$ and 55 K, respectively) are observed on resonance due to the different positions and dipole orientations of the QDs that influence their coupling to the cavity mode. The presence of an additional Anderson-localized cavity gives rise to the asymmetric detuning dependence of the decay rate. Assuming a perfect spatial match between the QD and the cavity mode, we can extract an upper bound on the mode volume of the Anderson-localized cavity of $V \sim 1\ \mu m^3$ from the observed rate on resonance. By estimating the extension of the localized modes in the two directions orthogonal to the waveguide (*23*), we derive a cavity length of 25 μm for cavity C1. Establishing the fundamental lower limit of the cavity length relates to the fundamental question of determining the localization length of Anderson-localized modes. It is predicted that the localization length can be reduced below the wavelength of light, and it was even suggested that no fundamental lower boundary exists (*24*). Consequently, engineered disorder might pave a way to subwavelength confinement of light in dielectric structures.

Figure 4B shows that Purcell enhancement is observed mainly within the cavity linewidth, which is opposed to the surprisingly far-reaching coupling reported for standard photonic crystal cavities under nonresonant excitation (*7*). Consequently, the extracted QD decay rates are sensitive probes of the local photonic environment of disordered photonic crystal waveguides. Photon emission in disordered photonic structures was predicted to lead to a new class of infinite-range correlations manifested as fluctuations in the decay rate of embedded emitters (*25*). Thus, the Purcell enhancement stems from the local enhancement of the photonic density of states in the Anderson-localized regime that promotes spontaneous emission of photons.

QDs detuned from Anderson-localized cavities may couple to the slowly propagating mode of the photonic crystal waveguide. In this case, the QD decay rate is expected to scale proportional to the group velocity slow-down factor n_g (*26*). This behavior is observed for three different QDs at large detunings Δ from the dominating Anderson-localized cavity mode (Fig. 4C), i.e., here the radiative coupling is well described by the local photonic density of states of the unperturbed photonic crystal waveguide. This interesting coexistence of ordered and disordered properties occurs because relatively few periods of the photonic crystal lattice are required to build up the local environment determining the QD decay rate. Thus, the length scale on which the local photonic density of states builds up is mostly shorter than the localization length, which accounts for the success of photonic crystals despite ubiquitous disorder for, e.g., nanocavities (*9*), single-photon sources (*15*), or spontaneous emission control (*27*).

Our experiments demonstrate that disorder is an efficient resource for confining light in nanophotonic structures, thereby opening a new avenue to all-solid-state cavity QED that exploits disorder as a resource rather than a nuisance. Exploring disorder to enhance light-matter interaction and establishing the ultimate boundaries for this new technology provide exciting research challenges for the future, of relevance to not only QED but also other research fields that rely on enhanced light-matter interaction, such as energy harvesting or biosensing (*28*). Coupling several cavities is a potential way of scaling cavity QED for quantum information technology and represents one of the major challenges for engineered nanocavities. Controlled disorder might offer an interesting route to coherently couple cavities using so-called necklace states that are naturally occurring coupled Anderson-localized modes (*29*, *30*).

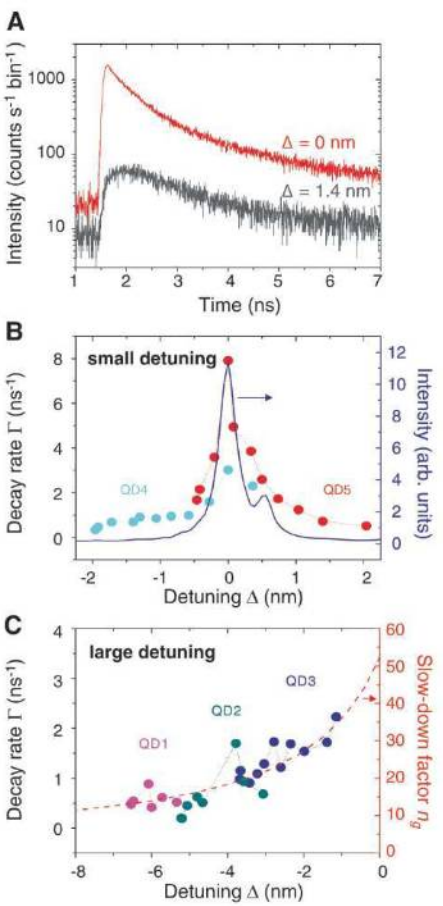

Fig. 4. Detuning dependence of single QD decay rates. (**A**) Decay curves of QD5 for two values of detuning Δ relative to the localized mode C1. (**B**) Decay rates of QD4 and QD5 versus detuning and cavity emission spectrum. (**C**) Decay rates of QD1, QD2, QD3 versus detuning. The dashed line is the calculated slow-down factor for the unperturbed photonic crystal waveguide. The enhancement at $\Delta = -4$ nm stems from the coupling of QD2 to a weak Anderson-localized cavity mode (C3 in Fig. 3A).

References and Notes

1. H. J. Kimble, *Nature* **453**, 1023 (2008).
2. T. Wilk, S. C. Webster, A. Kuhn, G. Rempe, *Science* **317**, 488 (2007).
3. J. M. Raimond, M. Brune, S. Haroche, *Rev. Mod. Phys.* **73**, 565 (2001).
4. H. Häffner, C. F. Roosa, R. Blatt, *Phys. Rep.* **469**, 155 (2008).
5. A. Wallraff *et al.*, *Nature* **431**, 162 (2004).
6. J. M. Gérard *et al.*, *Phys. Rev. Lett.* **81**, 1110 (1998).
7. K. Hennessy *et al.*, *Nature* **445**, 896 (2007).
8. I. Fushman *et al.*, *Science* **320**, 769 (2008).
9. Y. Akahane, T. Asano, B.-S. Song, S. Noda, *Nature* **425**, 944 (2003).
10. P. W. Anderson, *Phys. Rev.* **109**, 1492 (1958).
11. D. S. Wiersma, P. Bartolini, A. Lagendijk, R. Righini, *Nature* **390**, 671 (1997).
12. H. Hu, A. Strybulevych, J. H. Page, S. E. Skipetrov, B. A. van Tiggelen, *Nat. Phys.* **4**, 945 (2008).
13. J. Billy *et al.*, *Nature* **453**, 891 (2008).
14. J. Topolancik, B. Ilic, F. Vollmer, *Phys. Rev. Lett.* **99**, 253901 (2007).
15. T. Lund-Hansen *et al.*, *Phys. Rev. Lett.* **101**, 113903 (2008).
16. E. Knill, R. Laflamme, G. J. Milburn, *Nature* **409**, 46 (2001).
17. S. Hughes, L. Ramunno, J. F. Young, J. E. Sipe, *Phys. Rev. Lett.* **94**, 033903 (2005).
18. S. John, *Phys. Rev. Lett.* **58**, 2486 (1987).
19. A. F. Koenderink, A. Lagendijk, W. L. Vos, *Phys. Rev. B* **72**, 153102 (2005).
20. S. Mazoyer, J. P. Hugonin, P. Lalanne, *Phys. Rev. Lett.* **103**, 063903 (2009).
21. A. A. Chabanov, M. Stoytchev, A. Z. Genack, *Nature* **404**, 850 (2000).
22. J. Topolancik, F. Vollmer, B. Ilic, *Appl. Phys. Lett.* **91**, 201102 (2007).
23. Materials and methods are available as supporting material on *Science* Online.
24. A. Lagendijk, B. van Tiggelen, D. S. Wiersma, *Phys. Today* **62**, 24 (2009).
25. B. Shapiro, *Phys. Rev. Lett.* **83**, 4733 (1999).
26. V. S. C. Manga Rao, S. Hughes, *Phys. Rev. B* **75**, 205437 (2007).
27. P. Lodahl *et al.*, *Nature* **430**, 654 (2004).
28. R. C. Somers, M. G. Bawendi, D. G. Nocera, *Chem. Soc. Rev.* **36**, 579 (2007).
29. J. B. Pendry, *J. Phys. C* **20**, 733 (1987).
30. J. Bertolotti, S. Gottardo, D. S. Wiersma, M. Ghulinyan, L. Pavesi, *Phys. Rev. Lett.* **94**, 113903 (2005).

31. We gratefully acknowledge T. Schlereth and S. Höfling for quantum dot growth, J.M. Hvam for discussions, and the Council for Independent Research (Technology and Production Sciences and Natural Sciences) and the Villum Kann Rasmussen Foundation for financial support.

Supporting Online Material

www.sciencemag.org/cgi/content/full/327/5971/1352/DC1
Materials and Methods
References

24 November 2009; accepted 20 January 2010
10.1126/science.1185080

Light-Controlled Self-Assembly of Semiconductor Nanoparticles into Twisted Ribbons

Sudhanshu Srivastava,[1] Aaron Santos,[1] Kevin Critchley,[1,2] Ki-Sub Kim,[1,3] Paul Podsiadlo,[1,4] Kai Sun,[5] Jaebeom Lee,[1,7] Chuanlai Xu,[1,8] G. Daniel Lilly,[1] Sharon C. Glotzer,[1,6]* Nicholas A. Kotov[1,5,6,7]*

The collective properties of nanoparticles manifest in their ability to self-organize into complex microscale structures. Slow oxidation of tellurium ions in cadmium telluride (CdTe) nanoparticles results in the assembly of 1- to 4-micrometer-long flat ribbons made of several layers of individual cadmium sulfide (CdS)/CdTe nanocrystals. Twisting of the ribbons with an equal distribution of left and right helices was induced by illumination with visible light. The pitch lengths (250 to 1500 nanometers) varied with illumination dose, and the twisting was associated with the relief of mechanical shear stress in assembled ribbons caused by photooxidation of CdS. Unusual shapes of multiparticle assemblies, such as ellipsoidal clouds, dog-bone agglomerates, and ribbon bunches, were observed as intermediate stages. Computer simulations revealed that the balance between attraction and electrostatic repulsion determines the resulting geometry and dimensionality of the nanoparticle assemblies.

Spirals, helicoids, helices, twisted ribbons (TRs), and other helical structures present fascinating geometries from the perspectives of mathematics, biology, optics, and mechanics. The formation of helices from nanoparticles (NPs) will make possible exploitation of the unusual properties of helices arising from quantum confinement (*1*, *2*) within NPs, as well as expand the design space (*3*, *4*) and offer new means of controlling the pitch and/or chirality of the helical structures. To achieve self-organization of such intricate objects, it is necessary to fine-tune the overall balance of forces, including anisotropy of interactions that drive assembly of NPs into larger structures. Control of these processes will require the discovery of many-body interactions at the nanoscale, as well as understanding their dynamics and capabilities of formation of complex self-organized patterns transitioning from nano- to microscale.

As a model system for realizing these goals, we used an aqueous dispersion of CdTe (*5*) NPs (emission maximum at 550 nm) prepared (*6*) with thioglycolic acid (TGA) as a stabilizer with the TGA-to-Cd^{2+} ratio close to 1.0, rather than the traditional value of 2.4 (*7*). Based on the variety of existing data (*1*, *6*, *8*), these NPs exhibit strong anisotropy due to permanent dipoles on them (*1*, *8*). The strongly reduced concentration of TGA is expected to lead to the elimination of tetrahedral apices, where the local concentration of TGA is the highest, and an increase of the average value of dipole on NPs. It also increases chemical reactivity of the NPs, which intricately interplays with the interparticle forces. After preparation, the CdTe NPs are precipitated by addition of methanol and centrifuged for 20 min, followed by redispersion in deionized water at pH = 9 (adjusted by addition of NaOH). The orange color of the NP solution turns dark green within ~72 hours, indicating that NP self-assembly has occurred.

TRs with distinctive helicity (Fig. 1, A, B, and D to F), were the primary product of the aging process (Fig. 1) (*6*). The length of the TRs made from CdTe typically ranged from 0.8 to 2 μm, but can be as long as 8 μm (Fig. 1). Some straight nanowires (NWs) were also produced as a secondary product (Fig. 1C) and were identified as well-studied single crystalline Te wires (fig. S1) (*7*). Unlike these NWs or other NP assemblies (*6*), the TRs were made from individual NPs layered on top of each other (Fig. 1, G to I). Their thickness, as determined by atomic force microscopy (AFM), was 10 to 12 nm and corresponds to three to four NP layers. The pitch of the CdTe TRs averaged ~350 nm (Fig. 1, E and F). The distribution between right- and left-handed twisting was approximately equal: 52% right and 48% left, which indicates a nearly racemic mixture of chiral isomers (fig. S2) (*7*). Remarkably, the helical ribbons form bundles in which all TRs have the same chirality. Instead of the typical red shift of optical features found in previous studies of NP assemblies (*6*, *9*, *10*), a gradual blue shift of the luminescence and absorption peaks was observed during formation of TRs (Fig. 2A). This observation normally would have indicated the decrease in delocalization volume of excitons in CdTe and, hence, a wholly different process is taking place than that previously reported. This phenomenon is rather unusual but can be understood when the entire process of transformation of NPs to helicoidal structures is discussed.

We first characterized the composition of the products with x-ray energy dispersive spectroscopy (XEDS). The atomic percent Cd:Te:S ratio for TRs and original CdTe NPs was 46:10:44 and 43:38:19, respectively. The assembly process is associated with considerable loss of Te and transition to CdS/CdTe NPs, in which the CdS phase is strongly dominant. This substantial change of

[1]Department of Chemical Engineering, University of Michigan, Ann Arbor, MI 48109, USA. [2]School of Physics and Astronomy, University of Leeds, Leeds LS2 9JT, UK. [3]Department of Chemical and Biological Engineering, Chungju National University, 72 Daehak-ro, Chungju, Chungbuk 380-702, Republic of Korea. [4]Center for Nanoscale Materials, Argonne National Laboratory, Argonne, IL 60439, USA. [5]Department of Materials Science and Engineering, University of Michigan, Ann Arbor, MI 48109, USA. [6]Department of Biomedical Engineering, University of Michigan, Ann Arbor, MI 48109, USA. [7]Department of Nanomedical Engineering, College of Nanoscience and Nanoengineering, Pusan National University, Miryang 627-706, Republic of Korea. [8]School of Food Science and Technology, Jiangnan University, Wuxi, Jiangsu 214122, China.

*To whom correspondence should be addressed. E-mail: sglotzer@umich.edu (S.C.G.); kotov@umich.edu (N.A.K.)

the composition can be observed in high-resolution transmission electron microscopy (HRTEM) images (Fig. 2, C and D). The lattice spacing for {111} planes for as-prepared CdTe NPs is 0.384 nm but is shorter for NPs in TRs: 0.344 nm (Fig. 2C), as expected for CdS particles. Selected-area electron diffraction (SAED) patterns of the TRs showed the presence of characteristic diffraction patterns for both CdTe (111) (d = 0.38 nm), (220) (d = 0.22 nm), and CdS (100) (d = 0.34 nm), (101) (d = 0.31 nm), and (110) (d = 0.19 nm) planes (*11*) (Fig. 2, E and F). These data and the presence of Te NWs indicate that the process of oxidation Te^{2-} to Te^0 takes place.

To gain better knowledge about the transformation of NPs into TR, dynamics of multiparticle assembly, and driving forces of this process, we investigated the intermediate stages of

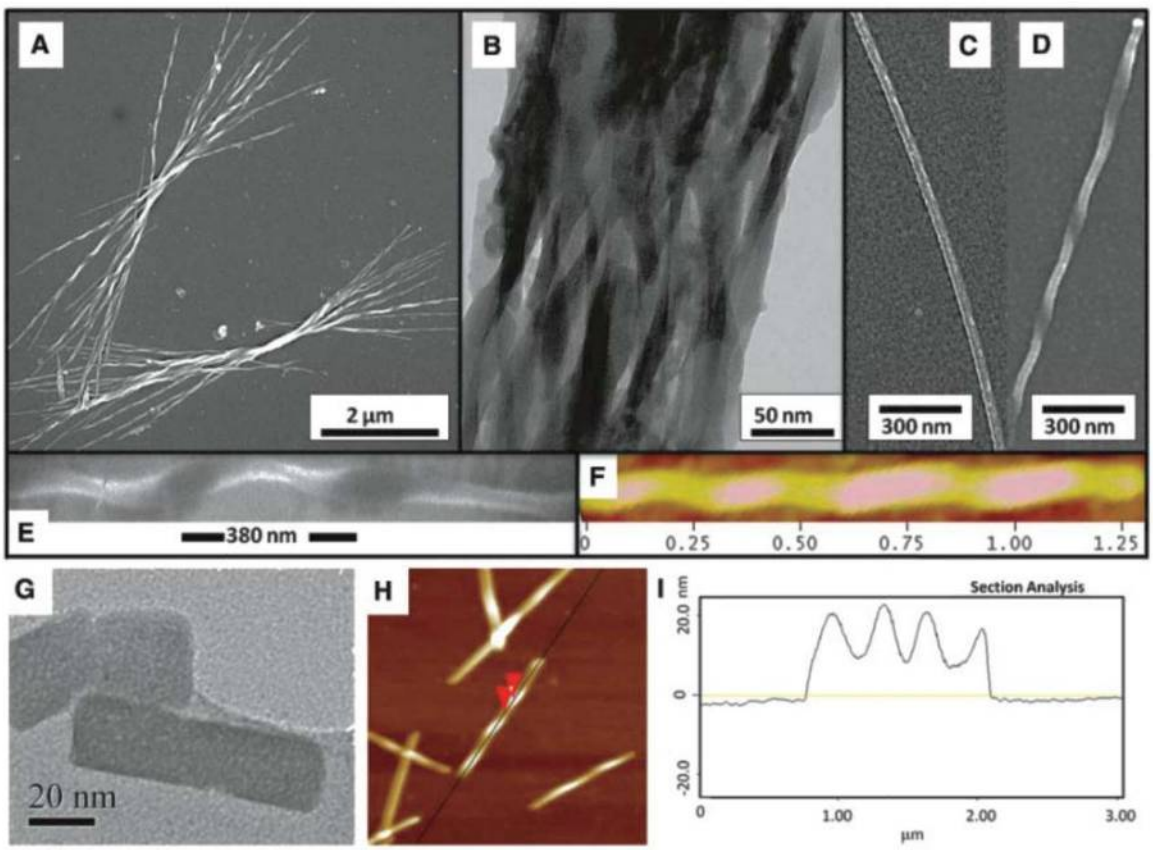

Fig. 1. (**A** and **B**) SEM (A) and TEM (B) images of bundles of TRs. (**C** and **D**) Individual straight Te NWs (C) and CdTe/CdS TRs (D). (**E** and **F**) SEM (E) and AFM images (F) of individual TRs with pitch lengths of 380 (E) and 400 nm (F). (**G**) TEM image of a cross section of TRs (the cutting plane may not be perpendicular to the TR axis). (**H** and **I**) AFM image and cross-sectional analysis of TRs.

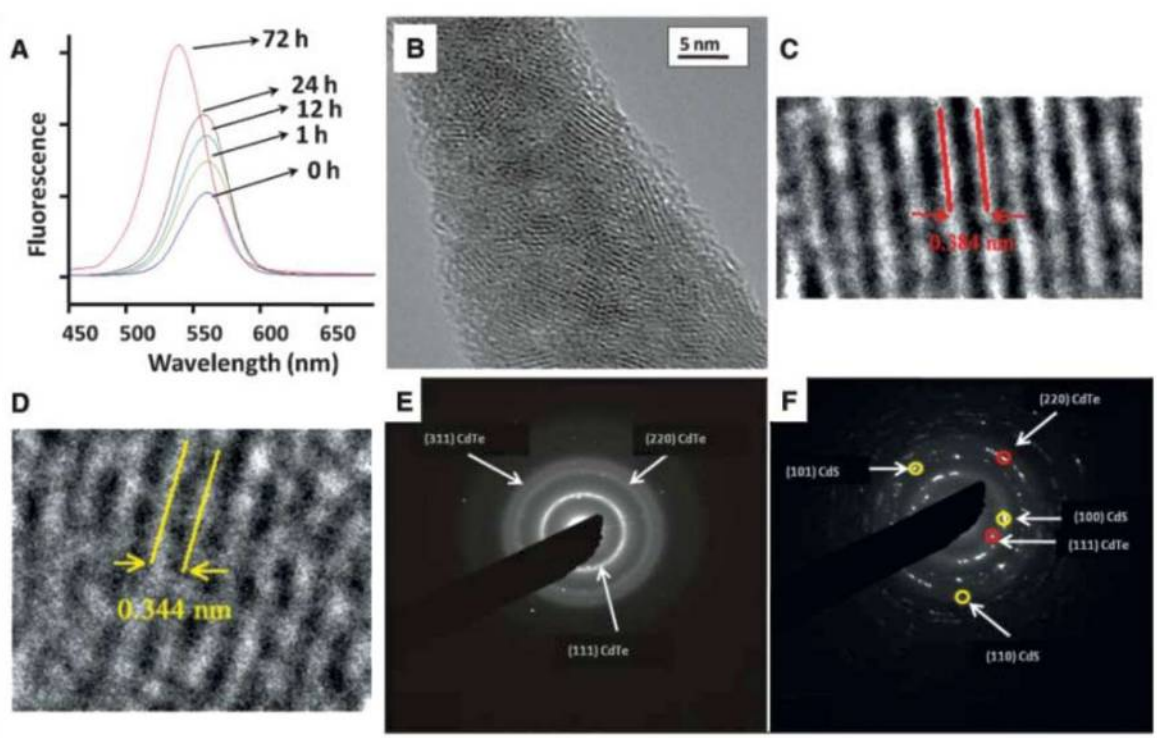

Fig. 2. (**A**) Evolution of fluorescence spectra for the self-organization of NPs into TRs. (**B**) HRTEM images for CdTe TRs taken in the "twist region." (**C** and **D**) Lattice fringes for {111} planes for the as-prepared NPs (C) and those in TR (D). (**E** and **F**) SAED patterns from CdTe NPs (E) and TR (F) with diffraction rings characterizing CdTe and CdS marked in red and yellow, respectively.

particle self-organization with corresponding trends in atomic composition. Both CdTe and CdS are light-sensitive (*12*), so subsequent studies were carried out both in dark and light conditions.

Examination of 1, 12, 24, and 72 hours time points of samples assembled under ambient light by scanning electron microscopy (SEM) and TEM revealed an interesting evolution of shapes of the multiparticle assemblies. Small spherical agglomerates were the starting point of the NP-to-TR transition and were exclusively present at the 1-hour time point after redispersion. By 12 hours, they transformed into much larger spheroids with complex elongated shapes (Fig. 3A) and then evolved into dog-bone–shaped NP systems by 24 hours (Fig. 3B). At 48 hours from the beginning of the self-assembly process, the dog-bone agglomerates reorganized themselves by stretching along a specific axis, resulting in fairly thick NWs (Fig. 3C) (*13*). At 72 hours, the thicker linear assemblies lead to thinner ones: On closer examination, they were the bunches of NWs or ribbons that unravel as "bouquets" of TRs of the same chirality (Fig. 3D and fig. S2) (*7*). The transition of spherical agglomerates to dog-bone–shaped assemblies is associated with a drastic reduction of Te content, which subsequently increased only slightly.

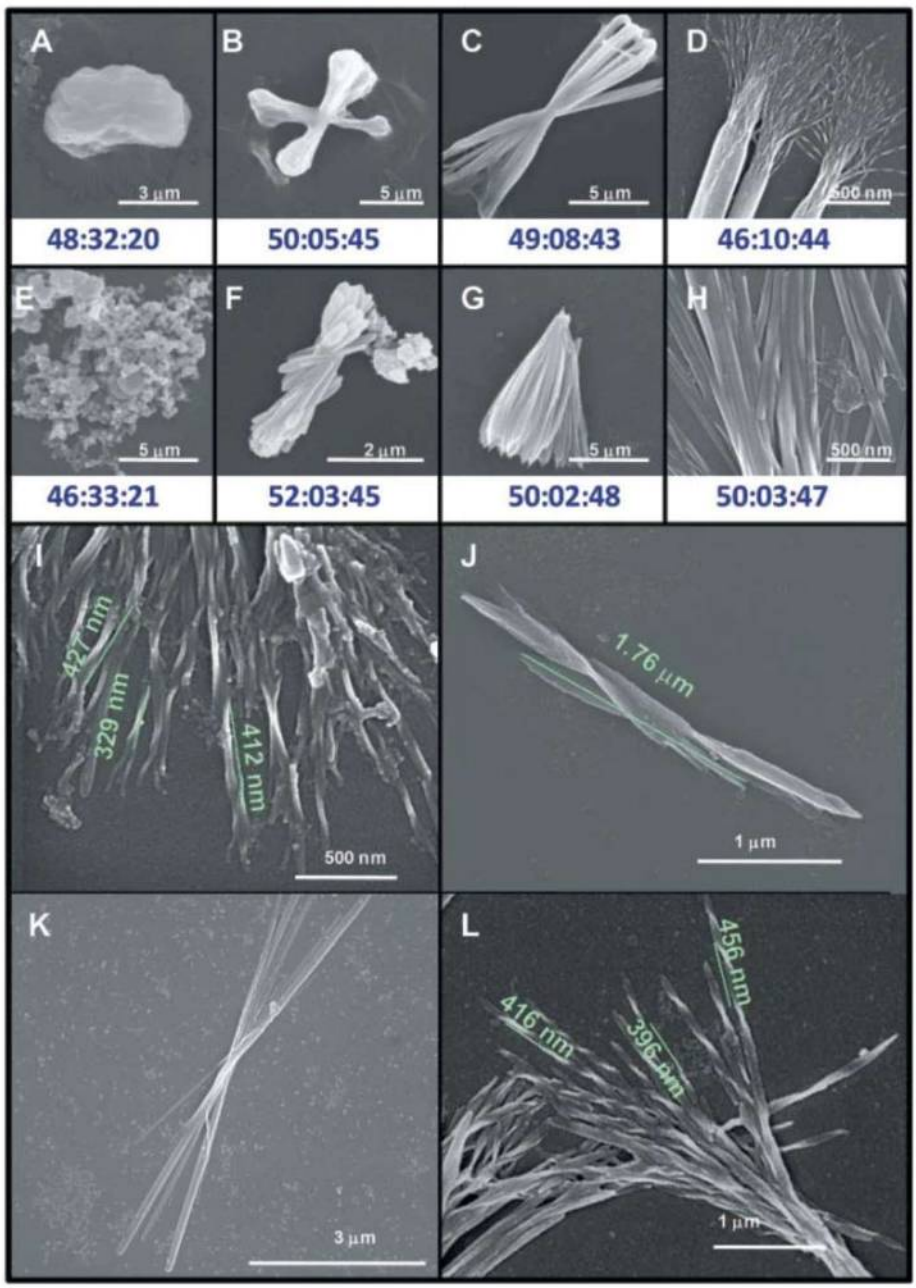

Fig. 3. Intermediate stages of TR formation and control of the twisting pitch. (**A** to **H**) SEM images of the ribbons assembled in ambient light (A) 12, (B) 24, (C) 48, and (D) 72 hours after redispersion of stabilizer-depleted particles. The ribbons assembled in dark conditions at the same time points: (E) 12, (F) 24, (G) 48, and (H) 72 hours. The XEDS Cd:Te:S atomic ratios for the particle assemblies are given below the corresponding images. (**I** and **J**) TRs prepared at different light intensities: (I) 61 and (J) 21 μW. (**K** and **L**) SEM images of ribbons after 52 hours in dark assembly (K) and then illuminated by the ambient light (61 μW) for 24 hours (L). NP concentration, 5 μM.

When the concentration of NPs was reduced from the beginning of the reaction, the dog-bone stage disappeared, individual nanoribbons were formed as an intermediate stage, and the TRs emerged at ~24 hours, followed by their bundling together at 72 hours (fig. S4) (*7*). These results indicated that ribbons represent an important intermediate product of the NP-to-TR transition, regardless of whether they are individual or associated into bunches.

When assembly takes place in the dark, after 1 hour, the NPs form loosely associated agglomerates that, again, exhibit a tendency to consolidate by 12 hours (Fig. 3E). No intermediate dog-bone–shaped structures were observed; their presence must be associated with a larger number of more strongly interacting particles. Instead, the NPs transformed into straight, multiparticle ribbons in 24 hours, which were also bunched together (Fig. 3F). These ribbons exhibited the propensity to debundle and become thinner after 48 hours (Fig. 3G). Eventually, the reaction in the dark resulted in distinct long, straight ribbons (Fig. 3H) in 72 hours with no twisting, which confirmed the importance of (i) straight ribbons as an intermediate stage and (ii) light as a stimulus for the transition of straight ribbons into twisted ones. It also offered a new means of control over helical NP assemblies.

XEDS data (Fig. 3, A to H, and fig. S6) (*7*) for all of the complex intermediate stages in both light and dark conditions reveal important points about the nature of the processes taking place and the origin of the unusual twisted morphology. The oxidation of Te^{2-} takes place in both light and dark. After 24 hours (i.e., at the dog-bone stage for light and the bunched-nanoribbons stage for dark conditions), the NPs are predominantly made from CdS, with only 3 to 5% of Te atoms. The amount of S in illuminated samples is consistently lower than that in NPs made in dark, and photocorrosion of CdS must be associated with the appearance of the twisted geometry. The conclusion can also be confirmed by the larger {111} lattice spacing observed in the assemblies obtained in light conditions, rather than in the dark (fig. S13) (*7*). Photooxidation of Te^{2-} leads to the strong change of chemical make-up of the NPs and accompanies the general assembly in ribbons, but it alone cannot be responsible for the appearance of helical assemblies.

The photooxidation of CdS in CdS/CdTe NPs before the complete removal of Te^{2-} centers may seem counterintuitive. However, the particles assembling into the ribbons and undergoing the twisting process are primarily made from CdS already (95 to 97%). The preference for oxidation of CdS over CdTe originates most likely from the gradient core-shell structure of the NPs obtained by the replacement of Te with S during the Te^{2-}

oxidation stage (*7*). SAED patterns indicate the presence of both CdTe and CdS phases (Fig. 2F), consistent with core-shell morphology. The surface of the NPs is likely to be pure CdS, whereas the Te atoms concentrated in the core become shielded from the photoreaction with dissolved oxygen. Also, the areas of delocalization of hole and electron tend to separate in NPs with CdTe/CdS heterojunctions, increasing the probability of interfacial photocorrosion.

We further explored the effects of illumination on NP-to-TR transitions. As such, TRs (~50 nm wide) prepared under 61 (ambient), 45, 38, and 21 μW showed pitch lengths of ~250 to 400 (Fig. 3I), ~500 to 600, ~1000, and ~1500 nm (Fig. 3J), respectively (fig. S7) (*7*). At all light intensities, HRTEM demonstrated the same polycrystalline nature composed of CdTe/CdS NPs. The dependence of the pitch length of TRs on light can also be traced in the dose of photons. A sample was aged in dark conditions for more than 2 days to form straight ribbons (Fig. 3K) and then was illuminated by ambient light (61 μW). The SEM images showed sequential change, and the pitch length was ~400-nm pitch length after 24 hours in light conditions (Fig. 3L).

The series of transformations of NPs and the subsequent structures observed are different from the reactions reported in previous organic or inorganic helical systems (*14*) or other NP assemblies (*15*, *16*). This necessitates gaining further insight into the balance of forces behind the TR formation. Typical helical structures originate from either specific crystal lattice distortions (*17*), mechanical strains (*18*), or chiral building blocks and form directly from the constituents. Helical structures can be formed because of mechanical stress or mismatch of the crystal lattice planes. The truncated tetrahedral structures of cubic II-VI semiconductor NPs can potentially be chiral, but we obtained no experimental evidence for chirality of individual NP involved in the NP-to-TR transition. The polycrystalline nature and the existence of two distinct crystalline phases in the TRs (CdTe and CdS) made the possibility of oriented attachment (*19*) and screw axis dislocations (*20*) in the extended crystal lattice as sources of helicity highly unlikely. Moreover, both of these mechanisms of helix formation at the nanoscale typically result in much shorter (by one to two orders of magnitude) pitch lengths than those observed in Fig. 1.

Therefore, we propose the following model for TR formation: Initially, between 1 and 24 hours, in both light and dark conditions, the attraction between the NPs is relatively weak, and dynamic aggregates with fairly spherical shapes are produced (Fig. 3, A and E). The same period of time overlaps with the completion of Te replacement with CdS. This change to CdS-dominant NPs prevents them from recrystallizing into CdTe thin, cylindrical NWs that have been observed before (*6*), because CdS has a greater activation barrier of recrystallization (*6*).

The forces between NPs are substantially stronger for light conditions, and the spheroids are larger and denser (Fig. 3A) than in dark conditions. We hypothesize that the multiparticle spheroids evolve into the dog-bone–shaped structures (Fig. 3B) because of gradual increase of anisotropic dipolar NP-NP interactions and the tendency of electric dipoles to align (*6*). The thin center part of the dog-bone and its conical apexes pointing to each other from each "pole" form through NP reorganization caused by forces that favor axial distribution. The potential origins of the greater dipolar interactions in the illuminated NPs are the entrapment of photogenerated charges at the interfacial states and unequal photoetching, which increases the value of the dipole moment (*21*). The reorganization continues until the round "clouds" become separated and eventually reorganize by stretching and producing ribbons and their bundles (Fig. 3, C and D).

Unlike the initial round agglomerates, the layers of NPs in the ribbons are well connected to each other (Fig. 2B) by short-range van der Waals interactions and hydrophilic or hydrophobic, dipole-dipole, and charge-dipole forces. In such objects, twisting can be produced as a result of internal shear strain between different NP layers, which can be partially relieved by acquiring the helical shape with uniform pitch length, despite some increase of elastic energy stored in the ribbon as a whole upon twisting. This is a common property of many ribbon-like structures (*22*) and was also observed in ribbons from multiwalled carbon nanotubes that acquire a twisted conformation to gain better registry between interacting graphene sheets (*23*). The source of internal strain in our ribbons is light-induced photocorrosion (*24*, *25*) of individual NP units, which results in reorganization of the bonded NPs trying to attain better and/or different packing because of the change of charge and/or dipole moment.

In the dark, no strain is generated, and the ribbons remain straight (Fig. 3, H and K) but tend to bunch. When light is on, photocorrosion of CdS results in the increase of charge/dipole in the already assembled ribbons, the stress between the layers of NPs gradually builds up with increasing the time or intensity of illumination, and twisting occurs. A greater degree of photoetching results in greater strain in the ribbons, and hence, stronger twisting (Fig. 3, I and J). The overall dose of illumination is most important in this respect; thus, the twisting can be controlled by both intensity (Fig. 3, I and J) and the time of light exposure (Fig. 3L).

Different experimental results, such as TEM/SEM images, XEDS, x-ray photoelectron spectroscopy (XPS), and dynamic light scattering data (Figs. 1 to 3) (*7*) support this mechanism of NP assembly into TRs. Changes in atomic percent composition seen in XEDS (Fig. 3, A to H, and fig. S6) (*7*) and XPS data (figs. S8 to S11) (*7*) confirmed photoinduced oxidation of CdS. There are two additional pieces of evidence for this mechanism that are particularly revealing. The key role of oxidation in TR formation can be confirmed by performing the NP self-organization reaction in an inert atmosphere. Even under light, no twisting was observed (fig. S12) (*7*) when oxygen was excluded from the reaction. Additionally, the steady increase of the zeta potential of NPs (fig. S15) from –10 to –50 mV clearly indicated that photoreaction results in a great increase in particle charge. This finding confirms the generation of a strong long-distance strain in the ribbons upon illumination. Alternatively, chemical oxidation with H_2O_2 fails to generate high zeta potential (always below –25 mV and eventually drops to zero) and, thus, fails to produce TRs (fig. S18) (*7*).

To further understand the assembly process, we carried out computer simulations to ascertain why the NPs under these conditions produce ribbons as the key precursors to TRs in light and dark conditions, and not chains (*8*) or sheets (*1*), as previously found for the same NPs under different conditions. This is also important from the perspective of understanding and controlling the forces between the NPs, so that the design of twisted and other self-organized microstructures can be done at the NP level. To describe the self-organization process of NPs, we used the same coarse-grained simulation model as did Tang *et al.* and Zhang *et al.* (*1*, *8*, *26*), with

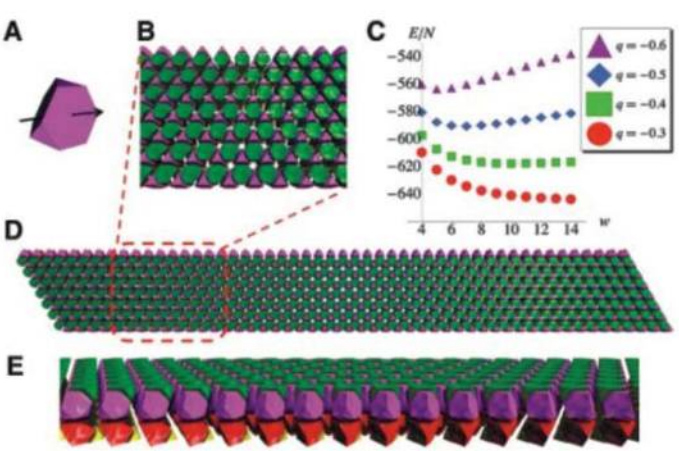

Fig. 4. **(A)** A truncated tetrahedron particle used in the simulations. **(B)** Close-up of the hexagonal packing structure obtained from BUBBA. **(C)** Plot of the energy per particle (*E*/*N*) measured in kilojoules per mole versus the width (*w*) of a ribbon measured in particles. **(D** and **E)** Top and side views, respectively, of straight ribbons. Pink and yellow tetrahedra point up; green and red tetrahedra point down. The arrow indicates the direction of the dipole moment.

modified parameters (*7*) to account for the present experimental conditions. Our choice of parameters reflects the reduced amount of TGA per CdTe, resulting in a net decrease of the charge, an increase of the face-face attraction energy, and a change in the direction of the dipole moment as compared with the conditions under which chains are obtained.

We used a recently developed technique for predicting ordered assemblies of building blocks with strong interactions via bottom-up building block assembly (BUBBA) (*26*) to determine the preferred local packing structure of tetrahedrons within ribbons. Then, Monte Carlo simulations were used to calculate the energy as a function of ribbon width to ascertain whether, and under what conditions, ribbons of finite width (rather than chains or sheets) (*1*, *8*) were the minimum energy structures. We found that NPs form four interdigitated layers grouped in two bilayers with tetrahedrons arranged hexagonally and inverted in alternate layers for denser packing (Fig. 4), which is consistent with TEM and SEM observations (Figs. 1, G to I, and 2B), albeit without the packing perfection seen in the simulations. The energy of the ribbon is minimized for a range of widths of ~18 to 110 nm, which matches structural parameters of TRs very well (Figs. 1 to 3). Increasing the charge resulted in more narrow ribbons, whereas decreasing the charge resulted in wider ribbons.

Overall, the multiparticle behavior and transition from packing into chains, ribbons, and sheets can be understood in terms of a competition between the face-face attraction and the charge-charge repulsion. For low charge and strong face attraction, as was the case in previous studies (*1*), particles pack very densely and would, if constrained to the same packing structure, form infinite two-dimensional sheets. By increasing the amount of charge, an infinite sheet becomes energetically unfavorable because of the long-range electrostatic repulsion, and NPs assemble as ribbons. Further increase of particle charge will eventually result in chains, as was observed for higher concentrations of TGA (*6*, *8*). Note that this concerns the effect of NP charge before the assembly. Once a larger NP system is assembled and held together by strong interparticle interactions, it may not be able to transition freely from sheets to ribbons of smaller width and then to chains. However, if there are structural units more loosely attached to each other, such as ribbons in bunches, they do separate, as can be seen by the unraveling of the bouquets of TRs (Fig. 3D and fig. S14).

The notion of evolving NP assemblies and better understanding of parameters controlling behavior of large numbers of nanoscale particles as a whole will be useful for many other nanocolloid systems. This study demonstrates that light can induce microscale twisting of the matter due to strong effect on the mutual interactions of nanoscale building blocks in a multibody system. The modulation in the pitch length for the TRs under different light intensities creates a new approach in the synthesis of nanostructures and new opportunities to generate nanomaterials with controlled circular dichroism and other optical, electronic, and mechanical properties.

References and Notes

1. Z. Tang, Z. Zhang, Y. Wang, S. C. Glotzer, N. A. Kotov, *Science* **314**, 274 (2006).
2. R. S. Yang, Z. L. Wang, *J. Am. Chem. Soc.* **128**, 1466 (2006).
3. S. C. Glotzer, M. J. Solomon, N. A. Kotov, *AIChE J.* **50**, 2978 (2004).
4. S. C. Glotzer, M. J. Solomon, *Nat. Mater.* **6**, 557 (2007).
5. C. Li, N. Murase, *Chem. Lett.* **34**, 92 (2005).
6. Z. Tang, N. A. Kotov, M. Giersig, *Science* **297**, 237 (2002).
7. See supporting material on *Science* Online.
8. Z. Zhang, Z. Tang, N. A. Kotov, S. C. Glotzer, *Nano Lett.* **7**, 1670 (2007).
9. W. W. Yu, L. H. Qu, W. Z. Guo, X. G. Peng, *Chem. Mater.* **15**, 2854 (2003).
10. J. Guo, W. Yang, C. Wang, *J. Phys. Chem. B* **109**, 17467 (2005).
11. K. V. K. Rao, S. V. N. Naidu, L. Iyengar, *J. Am. Ceram. Soc.* **51**, 467 (1968).
12. M. T. S. Nair, P. K. Nair, R. A. Zingaro, E. A. Meyers, *J. Appl. Phys.* **75**, 1557 (1994).
13. S. Busch *et al.*, *Eur. J. Inorg. Chem.* **1999**, 1643 (1999).
14. M. J. Bierman, Y. K. A. Lau, A. V. Kvit, A. L. Schmitt, S. Jin, *Science* **320**, 1060 (2008); published online 1 May 2008 (10.1126/science.1157131).
15. Y. Zhou, Q. M. Ji, M. Masuda, S. Kamiya, T. Shimizu, *Chem. Mater.* **18**, 403 (2006).
16. T. Vossmeyer *et al.*, *Science* **267**, 1476 (1995).
17. K. S. Cho, D. V. Talapin, W. Gaschler, C. B. Murray, *J. Am. Chem. Soc.* **127**, 7140 (2005).
18. L. S. Li, H. Z. Jiang, B. W. Messmore, S. R. Bull, S. I. Stupp, *Angew. Chem. Int. Ed.* **46**, 5873 (2007).
19. D. V. Talapin, H. Yu, E. V. Shevchenko, A. Lobo, C. B. Murray, *J. Phys. Chem. C* **111**, 14049 (2007).
20. X. D. Han *et al.*, *Nano Lett.* **7**, 452 (2007).
21. Y. Wang, Z. Tang, M. A. Correa-Duarte, L. M. Liz-Marzán, N. A. Kotov, *J. Am. Chem. Soc.* **125**, 2830 (2003).
22. T. McMillen, A. Goriely, *J. Nonlinear Sci. E* **12**, 241 (2002).
23. M.-F. Yu *et al.*, *Phys. Rev. B* **64**, 241403 (2001).
24. S. Yang *et al.*, *J. Am. Chem. Soc.* **128**, 10460 (2006).
25. A. Goriely, P. Shipman, *Phys. Rev. E* **61**, 4508 (2000).
26. E. Jankowski, S. C. Glotzer, *J. Chem. Phys.* **131**, 104104 (2009).

27. We acknowledge joint financial support by the Air Force Office of Scientific Research under Multiuniversity Research Initiative grant FA9550-06-1-0337. P.P. thanks the Fannie and John Hertz Foundation for support of his work through a graduate fellowship. This research was supported by the World Class University program through the Korea Science and Engineering Foundation funded by the Ministry of Education, Science and Technology (grant R33-2008-000-10021-0). We thank J. Kim (Univ. of Michigan) for helpful suggestions and discussions and W. Chen (JiangNan University) for assistance with some TEM data. P.P.'s work at the Center for Nanoscale Materials was supported by the Office of Science, Office of Basic Energy Sciences, of the U.S. Department of Energy under contract no. DE-AC02-06CH11357. P.P. acknowledges the support of the Willard Frank Libby postdoctoral fellowship from Argonne National Laboratory. The transmission electron microscope used in the study was supported by NSF grant DMR-9871177, and the scanning electron microscope used was supported by NSF grant DMR-0320740. S.C.G. and A.S. acknowledge the support of the J. S. McDonnell Foundation for the development of BUBBA. K.C. thanks Marie Curie Actions MOIF-CT-2006-039636 for financial support.

Supporting Online Material

www.sciencemag.org/cgi/content/full/science.1177218/DC1
Materials and Methods
SOM Text
Figs. S1 to S22
References

3 June 2009; accepted 2 February 2010
Published online 11 February 2010;
10.1126/science.1177218
Include this information when citing this paper.

The Near-Tip Fields of Fast Cracks

Ariel Livne, Eran Bouchbinder,* Ilya Svetlizky, Jay Fineberg†

In a stressed body, crack propagation is the main vehicle for material failure. Cracks create large stress amplification at their tips, leading to large material deformation. The material response within this highly deformed region will determine its mode of failure. Despite its great importance, we have only a limited knowledge of the structure of this region, because it is generally experimentally intractable. By using a brittle neo-Hookean material, we overcame this barrier and performed direct and precise measurements of the near-tip structure of rapid cracks. These experiments reveal a hierarchy of linear and nonlinear elastic zones through which energy is transported before being dissipated at a crack's tip. This result provides a comprehensive picture of how remotely applied forces drive material failure in the most fundamental of fracture states: straight, rapidly moving cracks.

Material failure occurs at small scales in the immediate vicinity of the tip of a crack. The existence of a crack in an otherwise perfect material dramatically amplifies applied stresses to values that approach a mathematical singularity at the crack's tip (*1*). The stress fields formed by a crack transport remotely applied elastic energy to the crack's tip, where the energy is dissipated by material fracture. Even small external stresses can generate sufficiently large stresses within this small microscopic region to initiate fracture. Linear elastic fracture mechanics (LEFM) provides the theoretical framework for understanding this stress amplification. LEFM assumes that the material under stress obeys linear elasticity (that is, Hooke's law) at every point up to the very near vicinity of a crack's tip. All of the complex dissipative and nonlinear processes that are involved in fracture and not described by LEFM are assumed to occur within a sufficiently small region around the tip. Nevertheless, this

Racah Institute of Physics, Hebrew University of Jerusalem, Jerusalem 91904, Israel.

*Present address: Department of Chemical Physics, Weizmann Institute of Science, Rehovot 76100, Israel.
†To whom correspondence should be addressed. E-mail: jay@vms.huji.ac.il

theory is very successful in describing the motion of a single straight crack in brittle materials (*2*).

Material failure, however, does not always occur via the propagation of individual straight cracks; propagating cracks are known to either microscopically branch or spontaneously oscillate if their propagation speed is sufficiently rapid (*3*, *4*). Moreover, how stresses are distributed and regularized near a crack's tip will determine the mode of failure (for example, brittle or ductile) and may hold the key to resolving important open questions about issues such as crack stability and path selection. Thus, the key to understanding these effects may lie in the structure of the near-tip region (*5*, *6*), where strains become so large that the linear stress-strain response underpinning LEFM must break down.

Progress in understanding the structure of this critical region has been, on the whole, limited by our lack of hard data describing the detailed physical processes that occur within. Due to the microscopic size and near–sound speed velocity of the near-tip region, direct measurements are very difficult, with numeric or atomistic calculations being the only means to assess it (*7*–*9*). As a result, attempts to understand the near-tip region have been largely empirical (*10*–*23*), using a wide variety of approaches. Many of these approaches assume that the material response is linearly elastic down to the immediate vicinity of the crack tip, where energy is dissipated. However, because of the large strains that always exist near a crack's tip, nonlinear elastic contributions must occur.

We studied the near-tip structure by using polyacrylamide gels (*24*). Their measured elastic response (up to strains of ~100%) is neo-Hookean (*24*), which is an extension of Hooke's law to large deformations (*25*). This constitutive relation has a well-founded statistical thermodynamic origin and is inherently nonlinear at large strains (*26*). These brittle materials provide a means to directly observe the detailed dynamics of rapid fracture, by slowing crack propagation velocities by nearly three orders of magnitude (typical crack speeds of 1200 m/s in glass correspond to 2 m/s in gels). Experiments have demonstrated that the dynamics of tensile cracks propagating in these gels are identical to those of other amorphous brittle materials (*27*). These include both single-crack dynamics (*1*, *28*) and crack instabilities (*3*, *27*) that occur at high propagation velocities v. Here, only single-crack modes for $v < 0.9c_S$ (where c_S is the shear wave speed) are considered, because crack instabilities were suppressed (*4*).

We studied the structure of the deformation fields of dynamic cracks at scales ranging from the system size (Fig. 1A) to those well within the region where nonlinear elasticity becomes important. We do this by tracking a passive tracer field imprinted on the gel faces with a fast high-resolution camera (Fig. 1B) (*24*). Comparison of each photograph with the undeformed tracer field provides the full displacement field, $\mathbf{u}(\mathbf{r}, t)$, surrounding the crack tip (Fig. 2A, inset), where $\mathbf{r}$ is the distance from the tip and t is time. Differentiation of $\mathbf{u}(\mathbf{r}, t)$ yields the strain fields (for example, Fig. 1B), so this method provides a precise measurement of all of the fields that locally drive a moving crack.

Crack advance is understood as a balance between the energy influx from the surrounding elastic fields and the energy dissipated at the crack's tip (fracture energy). In brittle materials, all dissipative processes occur near a crack's tip and include plastic deformation and bond breaking. The extent of the dissipative region may be determined by considering the energy flux through different contours surrounding the crack tip (Fig. 2A). At all scales beyond the dissipative region, the driving energy flux should be constant for steady-state propagation. The rate of energy per unit of sample width flowing through any closed contour, C, surrounding the crack tip is provided by the J integral (*1*)

$$J = \int_C [(U + \tfrac{1}{2}\rho\partial_t u_i \partial_t u_i)\nu n_x + s_{ij} n_j \partial_t u_i] dC \quad (1)$$

Here, $\mathbf{n}$ is an outward unit vector on C, ρ is the density of the undeformed material, U is a functional describing the material's elastic energy per unit of undeformed volume. For the incompressible neo-Hookean material described here, $U = \mu/2\ [F_{ij}F_{ij} + \det(\mathbf{F})^{-2} - 3]$, where μ is the shear modulus and $F_{ij} \equiv \delta_{ij} + \partial_j u_i$ (*29*). The stress tensor $s_{ij} = \partial_{F_{ij}} U$ defines the material's constitutive law, where i and j run over the crack propagation direction x and the loading direction y in the undeformed (two-dimensional) frame. Their counterparts are x' and y' in the deformed (laboratory) frame. We consider steady-state propagation, so $\partial_t = -v\partial_x$ in Eq. 1. Under these conditions, the J integral is independent of the contour C if no dissipative regions (other than the immediate crack-tip region) are enclosed within.

The energy flux $G = J/v$ is the amount of energy flowing into C per unit of crack extension. Using the measured deformation field, G was computed for different contours about dynamic crack tips, with the encompassed area ranging from ~100 mm^2 down to ~500 μm^2 (Fig. 2A). At all measured scales, the energy flux computed for the neo-Hookean constitutive law is constant (Fig. 2A). This explicit demonstration of the path independence of the J integral has several important implications. Foremost, no bulk dissipation is observed down to the smallest measured contour, ~500 μm^2, implying a purely elastic response (that is, no irreversible deformation) on these scales. Furthermore, the constant G implies that the neo-Hookean description of the gels' elasticity, which is inferred from large-scale measurements and moderate strains, holds up in the

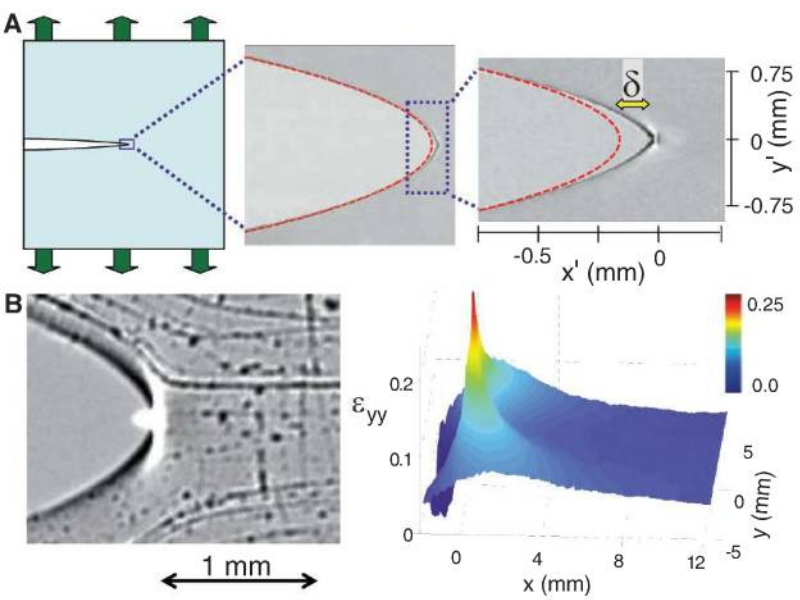

Fig. 1. (**A**) The tip [at $(x',y') = 0$] of a rapidly moving tensile crack ($v = 0.7c_S$) as seen at different scales. (Left) A schematic representation of the crack at the system size. (Center) A photograph of the crack's tip at a 5.2 × 5.4–mm scale demonstrating that its shape is close to the characteristic parabolic shape (dashed line) predicted by LEFM. (Right) A closeup of the same crack shows deviations from the parabolic crack-tip opening profile as the crack's tip is approached. The scale of this deviation is characterized by δ, the distance between the true crack tip and the tip location predicted by LEFM. (x',y') are the coordinates in the laboratory (deformed) frame, whereas (x,y) are the coordinates in the reference (undeformed) frame. (**B**) (Left) Blowup of the near-tip region of a different crack ($v = 0.48c_S$) with a tracer field imprinted on the gel (*24*). The displacement field $\mathbf{u} = (u_x,u_y)$ about the moving crack is found by comparing the tracer locations to their reference (pre-crack) state. (Right) The strain field, $\varepsilon_{yy} = \partial_y u_y$, up to 200 μm from the crack tip, is found by differentiating the measured displacement field. ε_{yy} diverges as the tip (located at the origin) is approached. The extreme strains in this region give rise to thickness variations, manifested by the lensing observed in the white region at the crack's tip (left).

near-vicinity of a crack tip, where extreme stresses prevail and the constitutive law cannot be directly measured.

Were we to assume a linear elastic material response, we would not find G to be constant, as demonstrated in Fig. 2A. Under these conditions, G converges asymptotically to the neo-Hookean value at large scales but deviates strongly as we approach the crack tip. Thus, although results derived from LEFM are correct for scales far enough from the crack tip (where strains are roughly <0.1), Fig. 2A shows that nonlinear elasticity becomes important as the crack tip is approached.

Are the values of G provided by Eq. 1 correct? By incorporating quadratic contributions to the stress-strain relation (*5*, *30*), a weakly nonlinear theory was recently derived that extended LEFM to strains of approximately 0.1 to 0.2. Whereas LEFM predicts singular strains of the form $r^{-1/2}$ in the near-tip vicinity (where r is the distance from the crack tip), this weakly nonlinear theory predicts additional strain contributions proportional to r^{-1} and displacement contributions proportional to $\log(r)$. At relatively large values of r, but still in regions where the strains are large enough to invalidate LEFM, this theory shows that a crack's tip has the same parabolic form (demonstrated in Fig. 1A) that is predicted by LEFM (*1*, *5*). The curvature of these parabolas provides an independent way to measure G (*1*, *28*). The comparison of this result in Fig. 2B with the J integral calculation, using neo-Hookean elasticity, indeed shows that the measurements are practically identical over the wide velocity range studied. This agreement is wholly nontrivial, because it results from entirely different measured inputs.

Just as the linear elastic description gives way to the weakly nonlinear description of fracture dynamics, the latter theory must, itself, break down at the smaller scales where even larger strains occur. This is demonstrated in Fig. 1A, right, where the far-field crack-tip profile breaks down as the crack tip is approached, and large discrepancies from its parabolic form are revealed. This breakdown has been characterized (*28*) by a velocity-dependent scale $\delta(v)$, defined as the distance from the measured crack tip to the one predicted by LEFM (Fig. 1A, right). For $r < \delta(v)$, strong elastic nonlinearities become increasingly important. We denote this region, where higher–than–second-order corrections to the stress-strain relations are needed, as "strongly nonlinear." Within this region, where strains are ~0.2 to 1, a perturbative approach is of limited applicability. Moreover, direct measurements of bulk deformation are, in general, difficult. The crack-tip profile, however, can be measured to even smaller scales.

The theoretical study of large deformations of neo-Hookean materials very close to the crack tip has a rich history (*29*, *31*–*34*). This work has yielded a solution for the deformation field asymptotically near a rapidly moving crack tip of the form (*33*)

$$u_y(r,\theta) = a(v)\, m(\theta;v)\, r^{1/2},$$
$$u_x(r,\theta) = [b(v) - 1]\cos(\theta)\, r \qquad (2)$$

where the function $m(\theta;v)$ is provided in (*24*) and a and b are velocity-dependent coefficients.

Equation 2 predicts an $r^{-1/2}$ variation of the strain $\partial_y u_y$, similar to the linear elastic prediction, but at much smaller scales. Thus, the crack-tip profile is parabolic in this limit, with the velocity-dependent curvature $b(v)/a^2(v)$ presented in Fig. 3. Figure 3A demonstrates that this parabolic profile differs significantly from the one at large scales (see also Fig. 1A). Such parabolic profiles, at comparable scales, are also observed in finite element calculations for static cracks in neo-Hookean materials (*35*).

Although the parabolic crack-tip profile, which is observed within the highly nonlinear region, is consistent with the asymptotic solution given in Eq. 2, one can imagine that any crack-tip profile that closes smoothly (that is, without a cusp) can be reasonably described by a parabolic form. To substantiate the theory, we now consider the energy flux through a contour C_{nl}, taken well within the nonlinear zone, at a scale of a few tens of micrometers. In this region, the asymptotic solution in Eq. 2, when used in Eq. 1, yields an expression for the asymptotic neo-Hookean energy flux G_{nl}

$$G_{nl}(v) = \mu a^2(v) \int_{-\pi}^{\pi} I(\theta; v)\, d\theta \qquad (3)$$

where the function $I(\theta;v)$ is provided in (*24*).

At $r < 200$ μm, we are generally unable to measure particle displacements because of the extreme strains and lensing effects in this region. We therefore use extrapolated values of $b(v)$ to extract $a(v)$ from the data of Fig. 3B and calculate G_{nl} in Eq. 3. G_{nl} is compared with G measured at the outer-millimeter scales in Fig. 2B. The values of G_{nl} and G agree to well within our uncertainty in $b(v)$ and thereby provide direct validation of both the solution in Eq. 2 and our interpretation of the small-scale crack-tip profile. Furthermore, because no dissipation is observed within the nonlinear zone, we conclude that dissipation is

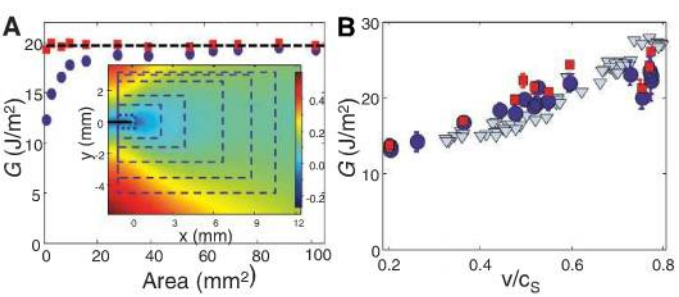

Fig. 2. (**A**) The energy flux G is computed over different contours using Eq. 1 for both the neo-Hookean (red squares) and linear elastic (blue circles) constitutive laws. (Inset) The measured displacement field u_x of the crack shown in Fig. 1B (color bar in millimeters). Dashed blue rectangles mark every second contour used for calculating G. The results are independent of the contour symmetry about the crack (denoted by the black line with its tip at the origin). (**B**) A comparison of G as a function of v, derived at different distinct regions using very different machineries: red squares, G derived using Eq. 1 for a neo-Hookean stress-strain relation; blue circles, G derived according to the weakly nonlinear theory (*5*) using the millimeter-scale parabolic crack-tip opening displacement [curvature data taken from (*28*)]; light blue triangles, G_{nl} derived from the small-scale curvature and estimated values of b (defined in Eq. 2) using the large deformation theory of Eq. 3.

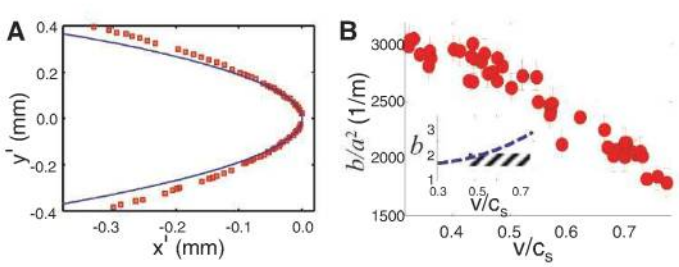

Fig. 3. The material deformation adjacent to the dissipative zone is quantitatively described by the large deformation theory. (**A**) Within ~40 μm from the crack tip (here, moving at $v = 0.43c_S$), the measured crack-tip profile (squares) corresponds to the parabolic form predicted by Eq. 2. The near-tip parabolic form of the crack-tip profile differs from that predicted by LEFM, which properly describes the measured profile at large scales. (**B**) The crack-tip curvature b/a^2 as a function of v. Independent measurements of a and b in the near-tip region, however, are hampered by lensing effects as seen in Fig. 1B (left). In the large-deformation region, $\partial_x u_x = (b - 1)$ along the crack propagation direction ($\theta = 0$). (Inset) An estimate of b (dashed blue curve) by extrapolating the $\partial_x u_x(v)$ measurements on this axis at $r = 200$ μm (typical measurement limit) by assuming a $1/r$ increase down to the typical outer scale, $r = 40$ μm, of the large-deformation region. This $1/r$ strain growth is predicted by the weakly nonlinear theory (*5*) and should become more dominant as the crack tip is approached. For comparison, the shaded region denotes values of b estimated from discrete $\partial_x u_x$ measurements at scales of $r = 120$ to 170 μm.

confined to a region that is smaller than our minimal observation scale (~20 μm).

These measurements provide experimental validation of both the existence of the asymptotic solution (Eq. 2) and the scales at which it is relevant. There is a long-standing conundrum in fracture mechanics that is solved by the existence of this solution. LEFM predicts that $\partial_x u_x$ is larger than $\partial_y u_y$ ahead of the crack tip. Because one would intuitively expect that the bonds that are most deformed would fail first, this implies that fracture should occur in the orthogonal direction (y) to the observed propagation direction (x). Equation 2 solves this problem [as first noted in (*31*)] if this asymptotic solution is indeed realized. Our measurements now demonstrate this explicitly under fully dynamic conditions; indeed, $\partial_y u_y$ is greater than $\partial_x u_x$ at the near-tip scales $r < 30$ to 40 μm. This example demonstrates how the structure of the highly nonlinear region near the crack tip may be critical in determining a crack's path.

With the validity of Eq. 2 established, we can combine this small-scale solution with the weakly nonlinear solution (*5*) to construct both the overall shape of the crack tip and $\delta(v)$. An estimate of the crack-tip location is obtained by extrapolating the weakly nonlinear solution (*5*, *30*) to the strongly nonlinear zone until it closes. Although it is beyond the theory's formal range of validity, this estimate yields values of $\delta(v)$ that agree well (see Fig. 4B) with measured values over the entire range of v. The scale of $\delta(v)$ is an intrinsic one and is determined by the ratio of the linear and quadratic terms in the stress-strain relation of a given material. For neo-Hookean materials, $\delta(v) \sim G/\mu$.

The crack-tip profile is then obtained from Eq. 2 by plotting the small-scale parabolic crack-tip profile [using measured values of either $b(v)/a^2(v)$ or G and $b(v)$] from the estimated crack-tip location until it intersects the weakly nonlinear solution. Concatenating these solutions yields profiles (for example, Fig. 4A) that are in excellent agreement with the measured ones. Surprisingly, even in the strongly nonlinear zone, the form of the divergences from a parabolic form of the crack-tip profile is reasonably captured by the logarithmic corrections to the displacement fields that are predicted by the weakly nonlinear theory (*5*, *30*), which justifies the only assumption made in this approach. The weakly nonlinear solution is uniquely defined once G and the constitutive law are known.

We have shown that linear elasticity, which provides a good description at large scales (Fig. 4C, left), must be supplemented by a fully nonlinear elastic description as the crack tip is approached (Fig. 4C, right). These nonlinear fields form the bridge to scales where irreversible deformation and fracture are really taking place ($r <$ 20 μm in our system).

This work describes a combined experimental and analytic description of the nonlinear elastic region that links LEFM to scales bordering dissipative scales. This quantitative description of the elastic fields surrounding a single straight crack has been demonstrated here for a specific class of materials. We expect, however, that the same qualitative picture holds true for any brittle material. In the near-tip vicinity where extreme strains prevail, linear elasticity cannot be expected to give a correct description of a material's elastic response. Addressing the nonlinear elastic response near the crack tip extends LEFM to the small scales where fracture takes place. Nonlinearity of elastic fields must occur in the region of high strains that is generated near a crack's tip in any material undergoing fracture, even in materials that macroscopically appear to be ideally brittle, although the complete separation of the nonlinear elastic region from the dissipative zone as shown here may not, necessarily, be general.

The existence of this nonlinear elastic region may hold the key to resolving many previously intractable puzzles in fracture mechanics. The correct description of the fields in this region has already presented concrete solutions to open problems related to dynamic crack path selection. Other open problems, such as LEFM's failure to predict how the straight single-crack states studied here become unstable at high velocities (*4*, *27*), may now be resolvable in this framework (*36*). Two possibilities exist: Either the instabilities are critically dependent on the dissipative mechanisms that were not considered here or they are due to the elastic fields surrounding the dissipative zone (*11*). Identical crack-tip instabilities have been observed in materials with wholly different dissipative mechanisms (*27*); therefore, we view the latter possibility as likely, although the former cannot be entirely ruled out.

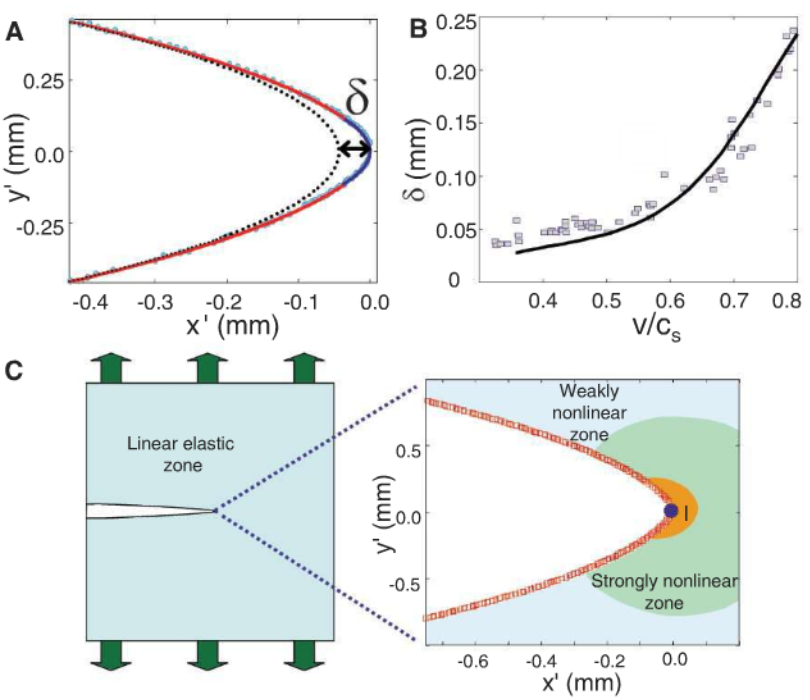

Fig. 4. Addressing the different elastic zones in the vicinity of a crack tip provides a full description of the material deformation down to the dissipation scales. (**A**) The circles indicate the measured crack-tip profile of Fig. 3A, compared to concatenation of the predicted profiles of the (red line) weakly nonlinear (*5*) and (blue line) asymptotic (see Eq. 2) theories. The dotted line is the LEFM solution. (**B**) Comparison of measured values (squares) of $\delta(v)$ with the estimated values (line) obtained by extrapolating the weakly nonlinear solution (*5*, *30*) to the strongly nonlinear zone until it closes. (**C**) A schematic sketch of the different elastic regions surrounding a crack. Energy and stresses are transmitted from the large scales, where material deformation is described by linear elasticity (left), through a hierarchy of nonlinear elastic regions (right) until dissipated by plastic deformation and fracture at the smallest scales (circle). The asymptotic region, denoted by *I*, is where strains become larger than unity and Eq. 2 is valid. Shown (squares) are measurements of the crack-tip profile extracted from Fig. 1A (right).

References and Notes

1. L. B. Freund, *Dynamic Fracture Mechanics* (Cambridge Univ. Press, New York, 1990).
2. E. Sharon, J. Fineberg, *Nature* **397**, 333 (1999).
3. J. Fineberg, M. Marder, *Phys. Rep.* **313**, 1 (1999).
4. A. Livne, O. Ben-David, J. Fineberg, *Phys. Rev. Lett.* **98**, 124301 (2007).
5. E. Bouchbinder, A. Livne, J. Fineberg, *Phys. Rev. Lett.* **101**, 264302 (2008).
6. T. Baumberger, O. Ronsin, *Eur. Phys. J. E*, **31**, 51 (2010).
7. F. F. Abraham, D. Brodbeck, R. A. Rafey, W. E. Rudge, *Phys. Rev. Lett.* **73**, 272 (1994).
8. D. Holland, M. Marder, *Phys. Rev. Lett.* **80**, 746 (1998).
9. P. Gumbsch, R. M. Cannon, *MRS Bull.* **25**, 15 (2000).
10. J. S. Langer, *Phys. Rev. E Stat. Phys. Plasmas Fluids Relat. Interdiscip. Topics* **62**, 1351 (2000).
11. M. J. Buehler, H. J. Gao, *Nature* **439**, 307 (2006).
12. E. Bouchbinder, A. Pomyalov, I. Procaccia, *Phys. Rev. Lett.* **97**, 134301 (2006).
13. M. L. Falk, A. Needleman, J. R. Rice, *J. Phys. IV* **11**, 43 (2001).
14. A. E. Lobkovsky, J. S. Langer, *Phys. Rev. E Stat. Phys. Plasmas Fluids Relat. Interdiscip. Topics* **58**, 1568 (1998).
15. O. Miller, L. B. Freund, A. Needleman, *Model. Simul. Mater. Sci. Eng.* **7**, 573 (1999).
16. M. J. Buehler, F. F. Abraham, H. J. Gao, *Nature* **426**, 141 (2003).

17. H. J. Gao, *J. Mech. Phys. Solids* **44**, 1453 (1996).
18. E. Bouchbinder, T. S. Lo, *Phys. Rev. E Stat. Nonlin. Soft Matter Phys.* **78**, 026119 (2008).
19. E. Bouchbinder, J. Mathiesen, I. Procaccia, *Phys. Rev. Lett.* **92**, 245505 (2004).
20. K. Ravi-Chandar, B. Yang, *J. Mech. Phys. Solids* **45**, 535 (1997).
21. T. Pardoen, J. W. Hutchinson, *J. Mech. Phys. Solids* **48**, 2467 (2000).
22. I. S. Aranson, V. A. Kalatsky, V. M. Vinokur, *Phys. Rev. Lett.* **85**, 118 (2000).
23. A. Karma, D. A. Kessler, H. Levine, *Phys. Rev. Lett.* **87**, 045501 (2001).
24. See supporting material on *Science* Online.
25. R. S. Rivlin, *Philos. Trans. R. Soc. Lond. Ser. A* **240**, 459 (1948).
26. L. R. G. Treloar, *The Physics of Rubber Elasticity* (Oxford Univ. Press, New York, 1975).
27. A. Livne, G. Cohen, J. Fineberg, *Phys. Rev. Lett.* **94**, 224301 (2005).
28. A. Livne, E. Bouchbinder, J. Fineberg, *Phys. Rev. Lett.* **101**, 264301 (2008).
29. J. K. Knowles, E. Sternberg, *J. Elast.* **13**, 257 (1983).
30. E. Bouchbinder, A. Livne, J. Fineberg, *J. Mech. Phys. Solids* **57**, 1568 (2009).
31. J. K. Knowles, E. Sternberg, *J. Elast.* **3**, 67 (1973).
32. J. K. Knowles, A. J. Rosakis, *J. Appl. Mech.* **53**, 545 (1986).
33. A. M. Tarantino, *J. Elast.* **57**, 85 (1999).
34. M. Marder, *J. Mech. Phys. Solids* **54**, 491 (2006).
35. V. R. Krishnan, C. Y. Hui, R. Long, *Langmuir* **24**, 14245 (2008).
36. E. Bouchbinder, *Phys. Rev. Lett.* **103**, 164301 (2009).
37. This research was supported by grant 57/07 of the Israel Science Foundation. J.F. acknowledges the support of the Max Born Chair for Natural Philosophy.

Supporting Online Material
www.sciencemag.org/cgi/content/full/327/5971/1359/DC1
Materials and Methods
References

12 August 2009; accepted 22 January 2010
10.1126/science.1180476

Imaging Local Electrochemical Current via Surface Plasmon Resonance

Xiaonan Shan,[1,2] Urmez Patel,[1] Shaopeng Wang,[1] Rodrigo Iglesias,[1] Nongjian Tao[1,2]*

We demonstrated an electrochemical microscopy technique based on the detection of variations in local electrochemical current from optical signals arising from surface plasmon resonance. It enables local electrochemical measurements (such as voltammetry and amperometry) with high spatial resolution and sensitivity, because the signal varies with current density rather than current. The imaging technique is noninvasive, scanning-free, and fast, and it constitutes a powerful tool for studying heterogeneous surface reactions and for analyzing trace chemicals.

Electrochemical detection is a powerful analytical method that has been used for a wide range of applications, including trace chemical analysis, glucose and neurotransmitter monitoring, DNA and protein detections, and electrocatalysis studies. Measurement of the total electrochemical current or other related electrical quantities of an electrode cannot directly provide local reaction information from the electrode surface, which is required for analyses of heterogeneous reactions, local activities of cells, and protein and DNA microarrays. Scanning electrochemical microscopy (SECM) (*1*), which probes local electrochemical current by scanning a microelectrode across the surface, can overcome this limitation and has found numerous applications (*2*). However, the sequential scanning of the microelectrode limits its speed, and the scanning probe may perturb the local electrochemical processes under study. The current measured by the microelectrode in SECM scales with the size of the microelectrode, making it increasingly difficult to improve the spatial resolution by shrinking the microelectrode.

Here, we report a method for imaging local electrochemical current without the use of a scanning probe or a microelectrode. Instead of measuring the current with an electrode, it determines the electrochemical current density from an optical signal of the electrode surface generated from a surface plasmon resonance (SPR) (*3*, *4*). Important benefits of this approach include fast and noninvasive electrochemical current imaging of the surface. In addition, the measured local current signal is proportional to the optical signal, which does not scale with the area of a region of interest. We imaged local electrochemical currents generated by heterogeneous surface reactions, and we could perform the traditional electrochemical detection methods—such as amperometry, cyclic voltammetry, and square-wave voltammetry—locally, interrogating areas as small as 0.2 μm by 3 μm with a current sensitivity of 0.3 pA. We also demonstrate sensitive and selective trace analysis with the technique.

An electrochemical reaction taking place on an electrode always involves electron transfer between the electrode and the reactant, which is measured as an electrochemical current or related electrical signal in the conventional electrochemical methods. The electron transfer process is always accompanied by a conversion of chemical species between oxidized and reduced states, so the electrochemical current can be determined by monitoring the conversion of the chemical species on the surface, which is the principle of the present imaging technique. Relative to other optical detection methods such as phase-measurement microscopy (*5*) that have been used to study local molecular binding events and electrochemical reactions on surfaces (*6*, *7*), SPR is extremely sensitive to the species generated (or consumed) on the electrode surface (Fig. 1A). We show that the concentration of the species is directly related to the electrochemical current via Fick's law of diffusion (*8*); more important, the electrochemical current density $i(t)$ can be easily calculated from the local SPR signal according to

$$i(t) = bnFL^{-1}[s^{1/2}\Delta\tilde{\theta}_{SPR}(s)] \quad (1)$$

(*9*), where $b = [B(\alpha_R D_R^{-1/2} - \alpha_O D_O^{-1/2})]$, n is the number of electrons involved in the redox reaction, F is the Faraday constant, L^{-1} is the inverse Laplace transform, and $\Delta\tilde{\theta}_{SPR}(s)$ is the Laplace transform of the SPR signal. In the expression for b, α_O and α_R are the changes in the local refractive indices per unit concentration for the oxidized and reduced molecules, D_O and D_R are the diffusion coefficients of the oxidized and reduced molecules, and B measures the sensitivity of the SPR signal to a change in the bulk index of refraction, which can be calibrated independently. According to Eq. 1, the measured signal, $i(t)$, does not scale with the image area, which is in contrast to the conventional electrochemical detection methods. Note that double layer charging current also contributes to the SPR signal (*10*), which is, however, small (*11*) relative to faradaic current.

We show below that (i) the electrochemical current determined using Eq. 1 is indeed equivalent to that obtained from the conventional electrochemical methods; (ii) the new electrochemical imaging technique provides local electrochemical current (e.g., cyclic voltammograms) associated with heterogeneous surface reactions; (iii) the advantages of this imaging technique allow for sensitive and selective trace analysis; and (iv) the technique offers high current sensitivity, a fast imaging rate, and good spatial resolution.

Two optical configurations were used in the experiments. In the first configuration, the working electrode was an Au-coated glass slide attached onto a prism via index-matching fluid. An electrochemical cell made from Teflon was mounted on top of the Au electrode. A Pt wire counterelectrode and an $Ag|AgCl|KCl_{(sat.)}$ reference electrode, together with a potentiostat, were used to control the potential of the working electrode. A light-emitting diode (LED) with a peak wavelength of 670 nm was used to excite the surface plasmons in the Au electrode, and a charge-coupled device (CCD) camera was used to record the image. Calculating the current at each pixel from the image by means of Eq. 1 creates an elec-

[1]Center for Bioelectronics and Biosensors, Biodesign Institute, Arizona State University, Tempe, AZ 85287, USA. [2]Department of Electrical Engineering, Arizona State University, Tempe, AZ 85287, USA.

*To whom correspondence should be addressed. E-mail: njtao@asu.edu

trochemical current image, and plots of the current image versus time or potential provide local amperometric and voltammetric measurements of the electrode. The second configuration (Fig. 1A) used an oil immersion objective with a high numerical aperture of 1.65 (*12*) to replace the prism and a HeNe laser to replace the LED. This second configuration provided higher spatial resolution than the first configuration.

To demonstrate the imaging principle, we studied the redox reaction of $Ru(NH_3)_6^{3+}$ complex with conventional cyclic voltammetry and electrochemical imaging simultaneously. The conventional method measures the total electrochemical current of the entire electrode surface, and the voltammogram shows the characteristic redox peaks corresponding to the reduction and oxidation of the ruthenium complex (Fig. 1B, red line). The electrochemical imaging technique probes the local electrochemical current, so the current averaged over the entire surface versus the potential (Fig. 1B, open circles) is compared with the conventional voltammetry. The cyclic voltammograms obtained by the two methods are in good agreement with each other (overall deviation = 5.75%). Note that the parameter b in Eq. 1 was calibrated independently from a separate experiment (*9*), so the agreement between the voltammograms obtained with the conventional and present imaging methods is quantitative and involves no adjustment of parameters.

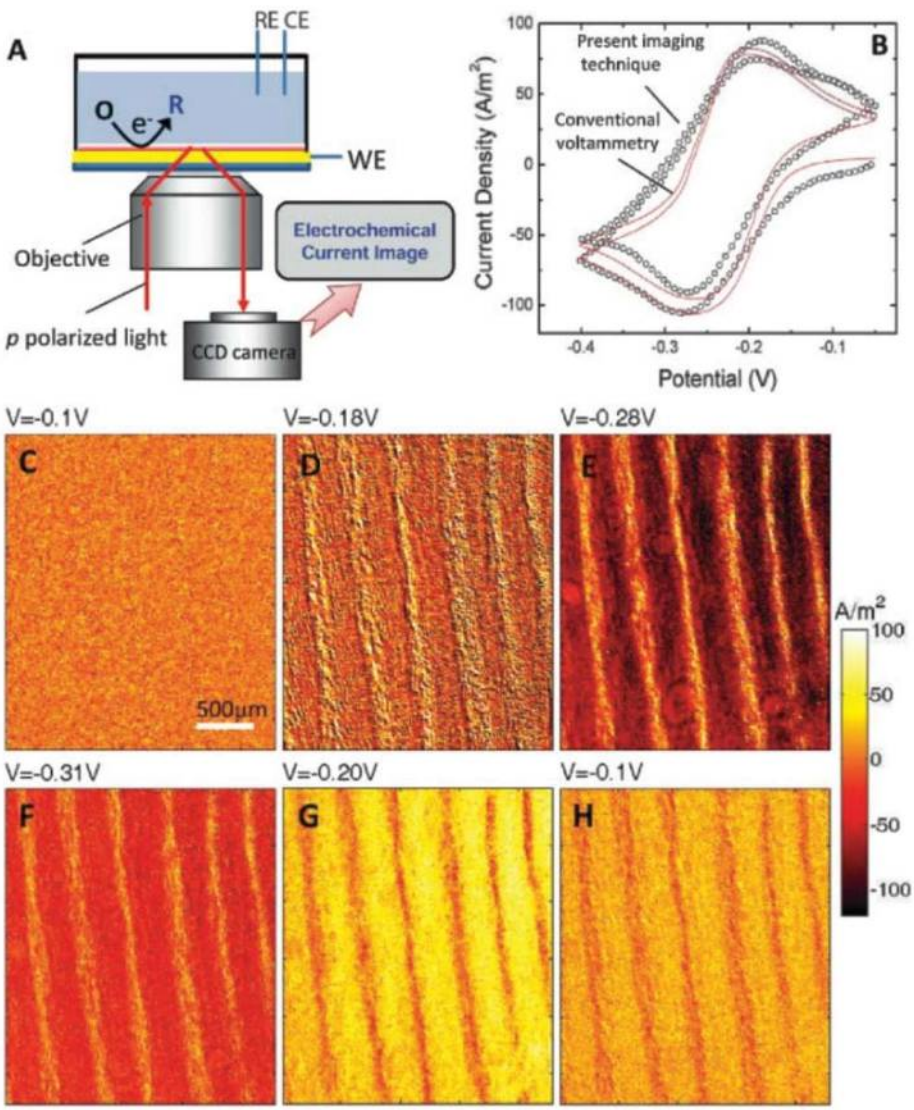

Fig. 1. (**A**) Schematic illustration of an electrochemical current imaging technique, where RE, CE, and WE are reference, counter, and working electrodes, respectively. (**B**) Cyclic voltammograms measured by the conventional electrochemical method (red line) and by the electrochemical current imaging technique (open circles) of a bare gold electrode. Note that for a close comparison between the two approaches, the cyclic voltammogram from the imaging technique is averaged over the entire electrode surface. The electrolyte is 0.25 M phosphate buffer containing 10 mM $Ru(NH_3)_6^{3+}$, and the potential sweep rate is 0.1 V/s. (**C** to **H**) Electrochemical current images of a fingerprint at different potentials recorded during continuous cycling of the electrode potential between −0.10 V and −0.35 V at a rate of 0.1 V/s (see movie S1). The electrolyte is 0.25 M phosphate buffer containing 10 mM $Ru(NH_3)_6^{3+}$.

One of the most important applications of the technique is imaging of the local electrochemical current associated with heterogeneous reactions. To demonstrate this capability, we created a fingerprint (*13*) on an Au electrode by touching it, which transferred the secretions from the skin ridges of the finger onto the electrode surface. We imaged the local electrochemical current of the surface by cycling the electrode potential in an electrolyte [0.25 M phosphate buffer containing 10 mM $Ru(NH_3)_6^{3+}$]. Figure 1, C to F, shows several snapshots of the electrochemical current video (movie S1) at different potentials. At –0.10 V, far away from the redox potential, almost no electrochemical reaction takes place and the image does not show any contrast (Fig. 1C). As the potential decreases, reduction of $Ru(NH_3)_6^{3+}$ takes place and the contrast of the fingerprint begins to show up (Fig. 1D). At –0.28 V, the contrast reaches maximum, corresponding to the maximum reduction current (Fig. 1E). As the potential cycles back toward positive values, the contrast is inverted (Fig. 1G), which reflects a sign change in the electrochemical current (from reduction to oxidation). Finally, when the potential cycles back to –0.10 V, the contrast disappears nearly completely; the small remaining contrast is the result of residual electrochemical reactions at the potential, in agreement with the cyclic voltammetry, which shows a finite current when the potential returns to the starting value (Fig. 1B). The entire process was repeated by continuously cycling the potential. Note that the imaging speed is solely determined by the CCD imager, which was ~2000 frames/s in the present setup, much faster than the SECM rate.

The contrast of the fingerprint revealed by the electrochemical current images arises from the blockade of the electrochemical reactions in the regions covered by the secretions from the finger. This interpretation is directly confirmed by the conventional SPR image acquired on the same electrode by switching off the potential (Fig. 2A). The regions covered with the secretions are shown as positive contrast in the SPR image, from which we estimated the average thickness of the fingerprint to be ~2.5 nm. This thin layer of molecules blocks the electrochemical reaction of the redox molecules. The fact that conventional SPR images can also be obtained using the same optics provides additional value to the present electrochemical current imaging technique.

The snapshots in Fig. 1, C to F, show only a small fraction of the information in the time and potential sequences of the electrochemical current image. At each point of the image, a local cyclic voltammogram can be readily obtained. Figure 2, B to E, shows a few examples of local cyclic voltammograms at different locations marked in Fig. 2A. First, the voltammogram from a bare gold region shows a large electrochemical current with well-defined redox peaks (Fig. 2B). In contrast, the voltammogram from a region covered with finger secretions shows only small background current with no obvious redox peaks (Fig. 2C).

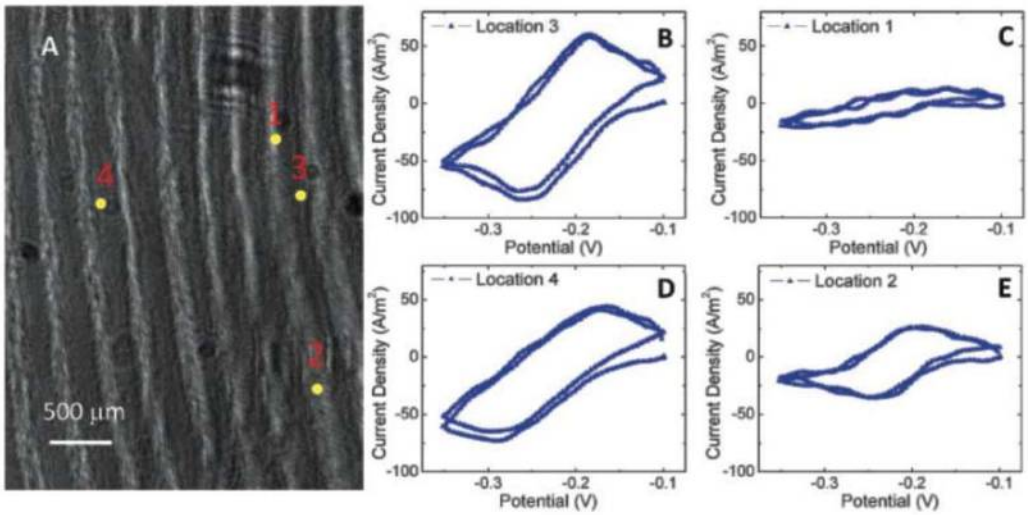

Fig. 2. (**A**) SPR image of a fingerprint. (**B** to **E**) Local cyclic voltammograms at different locations of the surface as numbered in (A). The electrolyte is 0.25 M phosphate buffer containing 10 mM $Ru(NH_3)_6^{3+}$, and the potential sweep rate is 0.1 V/s.

Second, the voltammograms obtained from different regions of a bare Au electrode also vary. For example, voltammograms from two different Au regions are shown in Fig. 2, B and D. Although both display the well-defined redox peaks, the separations of the redox peaks are quite different, which is likely a result of the variation in the coverage of the secretions transferred from the finger. Finally, the voltammograms from different regions of the fingerprint are also different (Fig. 2, C and E), reflecting changes in the coverage of the finger secretions.

The capability of imaging local electrochemical current has many applications, including trace analysis. As an example, we used the technique to detect traces of trinitrotoluene (TNT) (*14*). TNT has a very low vapor pressure and often appears in the form of particulates. A small TNT particle can be visualized with an optical microscope, but it is difficult to distinguish it from dusts or other airborne particulate matter. TNT is known to undergo electrochemical reductions at certain potentials, which has led to the detection of TNT by electrochemical methods (*15*). However, if the amount of TNT particulates is small, it is difficult to detect them using conventional electrochemical detection methods that measure the total current from the entire electrode. We prepared a sample including a fingerprint and TNT particulates on the electrode surface. Although the fingerprint is visible in the SPR image, the TNT particulates could not be resolved (Fig. 3A). We recorded the electrochemical current image of the surface while cycling the potential. Figure 3B shows five snapshots at different potentials. At 0 V, the electrochemical current image shows a uniform surface with no contrast for either the fingerprint or the TNT particulates because no electrochemical reactions take place at this potential (Fig. 3B, image 1). When we sweep the potential toward negative values, contrast of the fingerprint begins to show up (Fig. 3B, image 2) from the reduction of dissolved oxygen gas in the electrolyte, which results in different electrochemical currents in the regions with and without the fingerprint secretions. At this point, it is still difficult to resolve features attributable to the TNT particulates. When we lower the potential further toward the reduction potential of TNT, "spots" in the electrochemical current image associated with the reduction of the TNT particulates begin to appear (Fig. 3B, images 3 to 5), which allow us to detect and identify the individual TNT particulates.

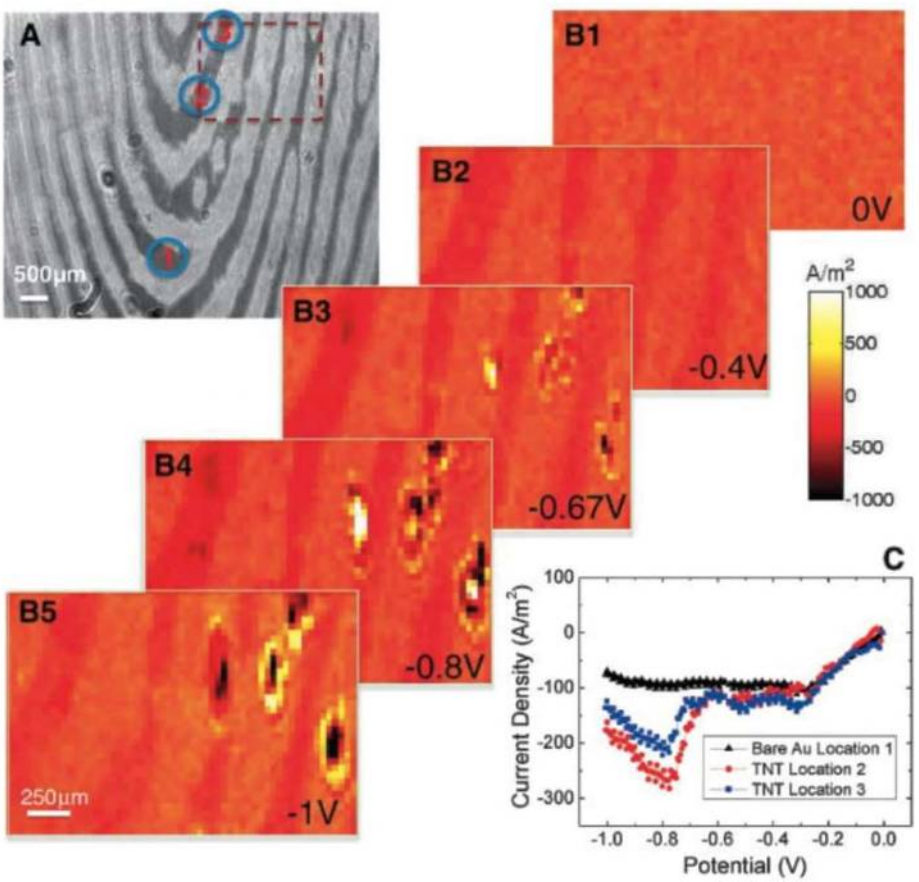

Fig. 3. Detection of TNT traces on a fingerprint using the electrochemical current imaging technique. (**A**) SPR image of a fingerprint. (**B**) Five snapshots recorded while sweeping the potential negatively from 0 to −1.0 V at a rate of 0.05 V/s. The appearance of the "spots" is due to the reduction of TNT particulates. (**C**) Local voltammograms of the regions with (blue and red dots) and without (black dots) TNT particulates. The electrolyte is 0.5 M KCl.

By selecting regions where "spots" appear, we obtained local voltammograms showing peaks from the reduction of TNT (Fig. 3C). For comparison, a local voltammogram from a region without TNT is also shown (black dots, Fig. 3C). We note that the TNT peak shapes and positions are not exactly the same as those in the cyclic

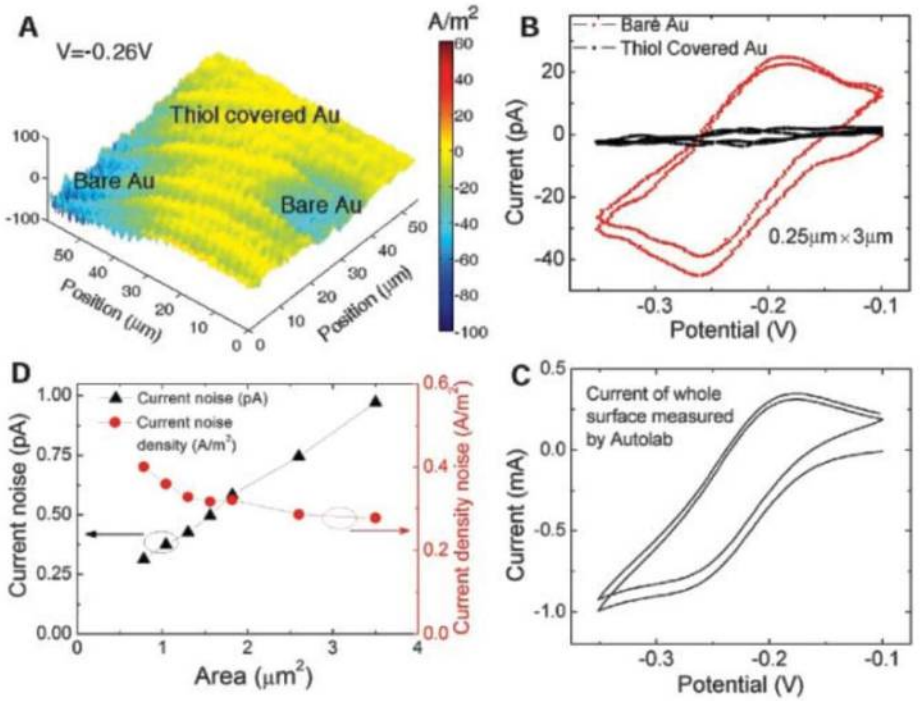

Fig. 4. Spatial resolution and current detection limit. (**A**) Electrochemical current image of 1-hexadecanethiol self-assembled on an Au electrode in 0.25 M phosphate buffer containing 10 mM $Ru(NH_3)_6^{3+}$, where the blue regions (negative current) are due to the reduction of $Ru(NH_3)_6^{3+}$. (**B**) Cyclic voltammograms of regions covered with densely packed (black lines) and exposed gold (red lines) regions. (**C**) Cyclic voltammogram obtained with the conventional electrochemical method (that measured the current over the entire electrode surface). (**D**) Dependence of current noise and current density noise on the area of detection.

voltammograms of TNT dissolved in an electrolyte as measured by the conventional electrochemical method (*16*). The difference may arise from differences in the mass transport between two experiments. From the integrated area of the reduction current peak at –0.8 V shown in the local voltammograms (Fig. 3C), we estimated the mass of the corresponding TNT particulate to be as small as ~0.5 ng (for an area of 50 μm by 50 μm). Because the current detection limit is ~0.3 pA (see below), the estimated detection limit is 0.3 fg.

We also used the conventional electrochemical method to record the voltammogram of the surface and did not observe the distinctive reduction peaks of TNT (fig. S1); the TNT signal was washed out by the large background current from areas without TNT. In contrast, the present electrochemical imaging technique obtains the local voltammograms of the particulate regions, which eliminates the background current contribution from other regions to the measured signal. The capability of performing local electrochemical analysis on the regions of interest (determined by the image) also reduces potential interference in electrochemical analysis. For instance, the large electrochemical reduction peak of the dissolved oxygen—a known source of interference taking place over the entire electrode surface—does not substantially affect the local voltammogram of a small particulate region.

Conventional optical imaging techniques, including SPR, can resolve small particles, but they usually cannot reveal the chemical identities of the particles. To further demonstrate the capability of trace chemical analysis with the imaging technique, we introduced other particulate matter, such as candle wax, onto the fingerprint in the presence of TNT particulates. The conventional SPR could image but could not distinguish the two types of particles (fig. S2). However, the electrochemical current image shows the distinct contrast changes in the regions of TNT particulates associated with the electrochemical reduction.

We now examine the spatial resolution and current detection limit of the electrochemical imaging technique. The spatial resolution along the surface plasmon propagation direction is limited by the propagation length, which depends on the wavelength of light. For a wavelength of 638 nm, the propagation length is ~3.1 μm; for a wavelength of 532 nm, the propagation length decreases to 0.2 μm (*12*). In the direction perpendicular to the surface plasmon propagation, the resolution is limited by the optical diffraction limit, which is about 0.19 μm using an objective with numerical aperture of 1.65. An electrochemical current imaging of a 1-hexadecanethiol–patterned electrode created by polydimethylsiloxane (PDMS) contact printing (*17*) is shown in Fig. 4A, where the current contrast arises from the variation in the coverage of the self-assembled monolayer. The local voltammogram from a gold surface region (0.25 μm by 3 μm) covered with densely packed 1-hexadecanethiol shows little current (Fig. 4B, black line). In contrast, the voltammogram from a region without covering of 1-hexadecanethiol (0.25 μm by 3 μm) shows well-defined redox peaks that are separated with ~60 mV, as expected for a reversible redox reaction (Fig. 4B, red line). In contrast, the simultaneously recorded voltammogram with the conventional electrochemical method shows distorted redox peaks caused by averaging of different reactions over the entire electrode (Fig. 4C).

This imaging technique measures light intensity, corresponding to current density, which does not decrease with the size of an imaged area, so high spatial resolution does not compromise the current detection limit. As shown in Fig. 4D, the noise level in the current density (red circles) does not change much with the area, so the noise in the current decreases with the area (black triangles). The smallest meaningful area is determined by the spatial resolution, which is ~0.2 μm by ~3 μm. The noise from such a small region in our present setup is ~0.3 pA. This level of current noise is excellent relative to other electrochemical detection methods, typically in the picoampere to nanoampere range (*18*), and could be further optimized by improving the light source and CCD detector. The electrode used here is gold, and other metal electrodes (e.g., Ag, Cu, and Pt) can also be used. Just like the current-based electrochemical detections, an electrochemical reaction is always accompanied by a change in the chemical species, so the electrochemical current imaging technique described here is universal.

References and Notes

1. A. J. Bard *et al.*, *Science* **254**, 68 (1991).
2. S. Amemiya, A. J. Bard, F. R. F. Fan, M. V. Mirkin, P. R. Unwin, *Annu. Rev. Anal. Chem.* **1**, 95 (2008).
3. B. Rothenhäusler, W. Knoll, *Nature* **332**, 615 (1988).
4. J. M. Brockman, B. P. Nelson, R. M. Corn, *Annu. Rev. Phys. Chem.* **51**, 41 (2000).
5. Q. G. Li, H. S. White, *Anal. Chem.* **67**, 561 (1995).
6. G. Flätgen *et al.*, *Science* **269**, 668 (1995).
7. O. Andersson, C. Ulrich, F. Bjorefors, B. Liedberg, *Sens. Actuators B Chem.* **134**, 545 (2008).
8. A. J. Bard, L. R. Faulkner, *Electrochemical Methods* (Wiley, New York, 1980).
9. See supporting material on *Science* Online.
10. D. G. Hanken, C. E. Jordan, B. L. Frey, R. M. Corn, *Electroanal. Chem.* **20**, 141 (1998).
11. K. J. Foley, X. Shan, N. J. Tao, *Anal. Chem.* **80**, 5146 (2008).
12. B. Huang, F. Yu, R. N. Zare, *Anal. Chem.* **79**, 2979 (2007).
13. M. Zhang, H. H. Girault, *Analyst* **134**, 25 (2009).
14. L. A. Pinnaduwage *et al.*, *Nature* **425**, 474 (2003).
15. J. Wang, *Electroanalysis* **19**, 415 (2007).
16. H. X. Zhang, A. M. Cao, J. S. Hu, L. J. Wan, S. T. Lee, *Anal. Chem.* **78**, 1967 (2006).
17. N. L. Abbott, J. P. Folkers, G. M. Whitesides, *Science* **257**, 1380 (1992).
18. The current noise value depends on bandwidth, instruments, and other experimental details.

19. We thank H. H. White, E. Forzani, and A. Cagan for discussions and L. Zhang for help in the lab. Supported by NSF grant CHM-0554786.

Supporting Online Material

www.sciencemag.org/cgi/content/full/327/5971/1363/DC1
Materials and Methods
SOM Text
Figs. S1 and S2
Movie S1
References

28 December 2009; accepted 3 February 2010
10.1126/science.1186476

Gravity Field, Shape, and Moment of Inertia of Titan

Luciano Iess,[1]* Nicole J. Rappaport,[2] Robert A. Jacobson,[2] Paolo Racioppa,[1] David J. Stevenson,[3] Paolo Tortora,[4] John W. Armstrong,[2] Sami W. Asmar[2]

Precise radio tracking of the spacecraft Cassini has provided a determination of Titan's mass and gravity harmonics to degree 3. The quadrupole field is consistent with a hydrostatically relaxed body shaped by tidal and rotational effects. The inferred moment of inertia factor is about 0.34, implying incomplete differentiation, either in the sense of imperfect separation of rock from ice or a core in which a large amount of water remains chemically bound in silicates. The equilibrium figure is a triaxial ellipsoid whose semi-axes a, b, and c differ by 410 meters ($a - c$) and 103 meters ($b - c$). The nonhydrostatic geoid height variations (up to 19 meters) are small compared to the observed topographic anomalies of hundreds of meters, suggesting a high degree of compensation appropriate to a body that has warm ice at depth.

Titan is Saturn's largest moon and is second in size only to Ganymede in the solar system. After being gravitationally captured by Saturn on 1 July 2004, the spacecraft Cassini has encountered Titan more than 50 times, carrying out science observations and using the moon's gravity field to change its orbit. Cassini's observations have unveiled a variety of features and phenomena not found on any other solar system satellite, such as hydrocarbon lakes, river channels, and dune fields (*1*). Although exogenic processes driven by the dense hydrocarbon-rich atmosphere play a crucial role in shaping the complex topography observed by Cassini's radar, contributions from endogenic processes are far less clear. Assessing the presence of active endogenic processes and understanding the origin of Titan's complex topography require knowledge of the moon's interior structure, which can be indirectly inferred from gravity and rotation data. Here we present results about Titan's gravity, shape, and moment of inertia (MoI) that constrain models of the deep interior structure and provide the appropriate reference to the large-scale topography.

Of the more than 50 Titan flybys completed so far by the Cassini spacecraft, only 4 were devoted to the determination of the gravity field. Titan's gravity field is estimated from the spacecraft's range rate, measured to an accuracy up to 7.5×10^{-5} m/s at 60-s integration times from the Doppler shift of the microwave carrier used in the radio link to the ground. A detailed description of the flyby characteristics, the observable quantities, and the estimation methods is given in the supporting online material (SOM). We processed the data using two different approaches. In the first one, radio tracking data acquired during each flyby were individually fitted for the spacecraft state vector (position and velocity) at a reference epoch, and for the degree 2 and 3 gravity coefficients. The four gravity field solutions and the associated covariances were then combined in a single multiarc solution (SOL1). In a second, more general approach (SOL2), all available radiometric tracking and optical navigation imaging data from the Cassini mission, as well as data from the Pioneer and Voyager Saturn encounters and astronomical observations of Saturn and its satellites, were combined in a global solution for the planet and satellite ephemerides and the gravitational parameters of the bodies in the Saturnian system (*2*).

In spite of the different approaches, the discrepancy between the two solutions is statistically insignificant (Table 1). Although neither solution was constrained a priori to the hydrostatic ratio $J_2/C_{22} = 10/3$ between the degree 2 harmonic coefficients the gravity field appears to be dominated by a nearly hydrostatic quadrupole. The remaining degree 2 and 3 coefficients are at least one order of magnitude smaller than J_2, an indication that nonhydrostatic features, although significant, do not play a major role in shaping the gravity body. The orientation of the principal axes of inertia, determined by diagonalizing the quadrupole tensor, is consistent (to a 2σ level) with the assumed rotation model (with the spin pole oriented along the normal to the orbital plane, synchronous rotation, and the prime meridian toward Saturn at pericenter). The formal accuracy in the principal axes orientation is about 0.5° for the long axis (pointing to Saturn) and 0.8° for the polar (short) axis.

The ratio J_2/C_{22} is 3.186 ± 0.042 for SOL1 and 3.339 ± 0.067 for SOL2, which are therefore indistinguishable from each other (to a 2σ level) and consistent with the value of 10/3 that is

Table 1. The 3 × 3 gravity field of Titan, estimated from combined solutions using different approaches (for unnormalized spherical harmonics, reference radius 2575 km). The value of Titan *GM* [estimated only in SOL2 and reported in SOM ref. (*S4*)] is 8978.1394 km^3/s^2, corresponding to a density of 1881 kg/m^3.

	Multi-arc (SOL1) [value ± 1σ (×10^{+06})]	Global (SOL2) [value ± 1σ (×10^{+06})]
J_2	31.808 ± 0.404	33.462 ± 0.632
C_{21}	0.338 ± 0.350	0.048 ± 0.115
S_{21}	−0.352 ± 0.438	−0.620 ± 0.496
C_{22}	9.983 ± 0.039	10.022 ± 0.071
S_{22}	0.217 ± 0.041	0.256 ± 0.072
J_3	−1.879 ± 1.019	−0.074 ± 1.051
C_{31}	1.058 ± 0.260	1.805 ± 0.297
S_{31}	0.509 ± 0.202	0.283 ± 0.354
C_{32}	0.364 ± 0.113	0.136 ± 0.158
S_{32}	0.347 ± 0.080	0.159 ± 0.105
C_{33}	−0.199 ± 0.009	−0.185 ± 0.012
S_{33}	−0.171 ± 0.015	−0.149 ± 0.016

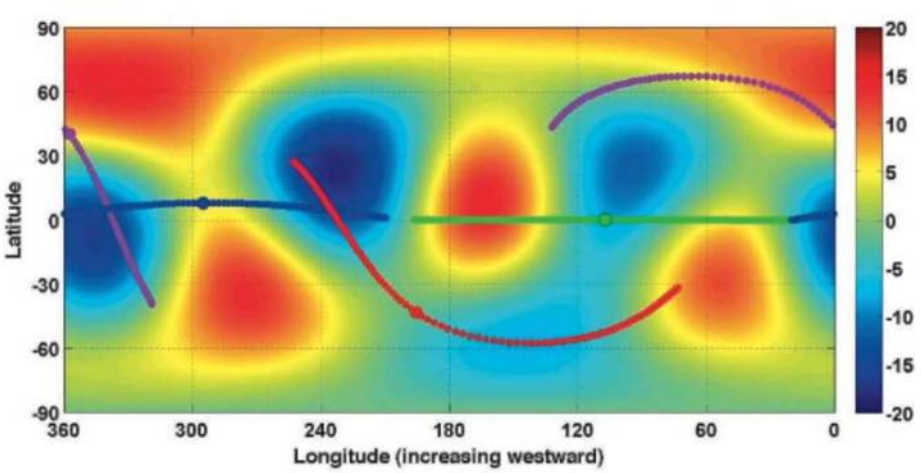

Fig. 1. Titan's geoid with respect to the reference ellipsoid, in meters. The lines represent the subspacecraft trajectory for ±2 hours for Cassini's flybys of Titan (T) T11 (green), T22 (magenta), T33 (blue), and T45 (red). The large solid circles represent the points at closest approach.

[1]Dipartimento di Ingegneria Aerospaziale ed Astronautica, Università La Sapienza, via Eudossiana 18, 00184 Rome, Italy. [2]Jet Propulsion Laboratory, 4800 Oak Grove Drive, Pasadena, CA 91109, USA. [3]California Institute of Technology, 150-21 Pasadena, CA 91125, USA. [4]DIEM-II Facolta' di Ingegneria, Universita' di Bologna, I-47100 Forli, Italy.

*To whom correspondence should be addressed. E-mail: luciano.iess@uniroma1.it

appropriate for a body responding only to the time-averaged tide raised by Saturn and synchronous rotation, assuming that the material properties have no substantial deviation from spherical symmetry (*3*). This is consistent with hydrostatic equilibrium but does not by itself require hydrostatic equilibrium. For that additional step, we consider the smallness of the other harmonics and the billion-year time scales in which the tidal and rotational bulges have had time to adjust. If Titan is in hydrostatic equilibrium (an assumption well supported from the orbital solutions), the static part of the gravity field depends on a single parameter, the fluid Love number k_f. The value of C_{22} obtained from SOL1 and SOL2 implies $k_f = 1.0097 \pm 0.0039$ and 1.0136 ± 0.0072, respectively (*4*); k_f would be equal to 1.5 for a fluid body of uniform density.

Traditionally, there are two ways to represent the gravity field: by the geoid and by the gravity disturbances. Both require defining a reference ellipsoid. We define the reference ellipsoid as the equipotential surface around the sphere of radius equal to the mean radius of Titan, whose potential is composed of the sum of (i) the gravitational potential produced by the monopole potential, $J_2^H = (10/3)\, C_{22}$, and C_{22}; (ii) the tidal potential due to Saturn; and (iii) the rotational potential (*4*). Analytically, we derived the equations for the semi-axes of the reference ellipsoid from SOL1 as (*5*)

$$a = R_t\left[1 + \tfrac{14}{3} C_{22} + \tfrac{7}{6} q_r\right] = 2575.239 \text{ km},$$
$$b = R_t\left[1 - \tfrac{4}{3} C_{22} - \tfrac{1}{3} q_r\right] = 2574.932 \text{ km},$$
$$c = R_t\left[1 - \tfrac{10}{3} C_{22} - \tfrac{5}{6} q_r\right] = 2574.829 \text{ km}$$

for a reference radius $R_t = 2575$ km. The formal errors are less than 1 m. These values change by about the same amount if SOL2 is adopted. A nonhydrostatic reference ellipsoid, constructed from the measured values of J_2 and C_{22}, would differ from the hydrostatic one by at most –9 m for SOL1 and only +0.2 m for SOL2. In both solutions, $(a - c)/(b - c) \simeq 4$, as expected for a synchronously rotating satellite in hydrostatic equilibrium subjected to the rotational and tidal deformation (*6*).

The axes of the reference ellipsoid are larger than the radii found from radar altimetry (*7*) ($a = 2575.15 \pm 0.02$ km, $b = 2574.78 \pm 0.06$ km, $c = 2574.47 \pm 0.06$ km). In (*7*), the mean planetary radius (2574.73 ± 0.09 km), is smaller by 3σ than the value of 2575 km adopted here. If this smaller value is used, the axes of the reference ellipsoid become 2574.969, 2574.662, and 2574.559 km (the rescaling of the gravity coefficients, being a second-order effect, can be neglected). These values differ respectively by –181, –118, and +89 m from those determined from radar altimetry, a statistically significant difference for the long axis (a).

We computed Titan's geoid heights and gravity disturbances following (*8*) (Fig. 1 and 2). The geoid heights vary from –19 to 14 m (root mean square value, 6.9 m), well below the hundreds of meters of large-scale topography (*7*). The gravity disturbances vary from –3.73 to 3.05 mGal (10^{-3} galileo). A negative disturbance of –0.2 to –0.1 mGal appears under Xanadu. For this prominent feature, the geoid height variations and gravity disturbances correlate well with the altimetric data (*7*); such a correlation does not exist for the reference ellipsoid defined by gravity and the ellipsoid fitted to altimetric data.

Using the Radau-Darwin equation (*6*), the average normalized MoI is $\tilde{C} = 0.3414 \pm 0.0005$ ($\tilde{C} = 0.3419 \pm 0.0010$ for SOL2) (*9*). The MoI factor $\tilde{C}$ is a crucial parameter to study a satellite interior. Titan's MoI factor is clearly different from and intermediate to those inferred for Ganymede (about 0.31) and Callisto (about 0.36) (*10,11*). The value for Ganymede admits a simple interpretation: a fully differentiated structure, consistent with the presence of an iron core (needed to explain the existence of a dynamo). The difference between Ganymede and Titan cannot be explained merely by assuming that Titan lacks an iron core. Like Callisto, the larger value of 0.34 can be accomplished by a range of models (*12*). If we assume that Titan consists of two layers, an outermost pure water-ice shell (allowing for the different densities of the various ice phases) and an inner constant-density core, then the mean density and MoI determine the radius of the core to be 2050 to 2100 km and the density of the core to be 2550 to 2600 kg/m^3. Because this core is necessarily rock-rich and therefore less compressible than ice, it is a reasonable approximation to treat it as having uniform density. The uncertainty in core size and mean density arises from the small thermal contributions to the density of ice and the location of the phase boundaries, and also encompasses the small changes that come from assuming an ocean (with or without dissolved ammonia). The core in this two-layer model would most reasonably be interpreted as a mixture of ice and rock. In many accretional models, the outermost regions are heated most severely and therefore are most susceptible to melting of the ice component. The rock would then settle to mix with the deeper regions, assuming it is in the form of particles that are sufficiently small that they cannot settle of their own accord by Stokes flow through the viscous ice. However, models that have three or more layers cannot be excluded; for example, a pure rock core surrounded by a mixture of ice and rock, surrounded in turn by pure ice. The extent of separation of ice from rock is most likely a consequence of the details of the timing and duration of Titan's accretion process (*13*). It may also be affected by later radiogenic heating and partial melting of the ice-rock mixture. The MoI factor might also be accomplished by fully separating ice from rock but demanding a low rock density appropriate to hydrated silicates (*14*, *15*). A problem with these models is the low core density required and the likelihood that radiogenic heating would cause partial dehydration. There is no straightforward way of resolving this issue observationally, but through detailed modeling it is possible to assess which models are most plausible.

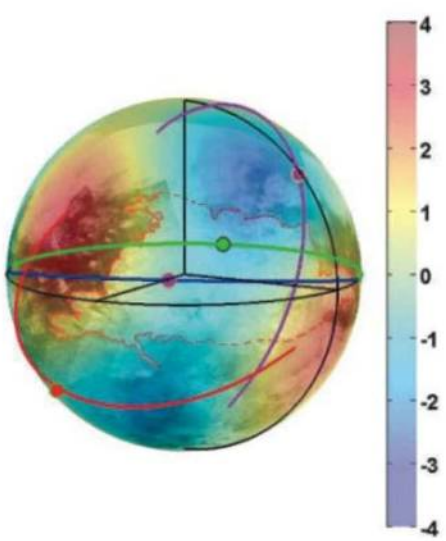

Fig. 2. Titan's gravity disturbances with respect to the reference ellipsoid, in mGal, plotted over Titan's albedo. The region delimited by the red dashed line is Xanadu. South of Xanadu is an area of negative gravity anomaly. The coordinate axes, the equator, and the prime meridian are shown in black.

Zebker *et al.* (*7*) suggested that the shape and therefore by implication much of the gravity of Titan are those of a body that froze during a previous spin and tidal state corresponding to a smaller distance from Saturn. This hypothesis cannot be assessed by looking at degree 2 gravity and topography alone, because there is no way to separate hydrostatic and nonhydrostatic parts, and their hypothesis would also satisfy $J_2/C_{22} = 10/3$. However, the smallness of the degree 3 terms is not consistent with this interpretation. It is unreasonable to suppose that a body is able to maintain hundreds of meters of frozen topography when its gravity is close to that expected for a fluid body (SOM). To quantify this, we considered the geoid anomalies expected for a given topography anomaly. For completely uncompensated topography, the geoid-to-topography ratio (GTR) is given by (*16*) $\mathrm{GTR} = \frac{3\rho_c}{\bar{\rho}(2l+1)}$, where ρ_c is the near-surface ("crustal") material ($\sim 1 \times 10^3$ kg/m^3), $\bar{\rho}$ is the mean density of the body ($\sim 1.9 \times 10^3$ kg/m^3), and l is the harmonic degree. For $l = 2$, this is about 0.3, implying that a topographic feature of 300 m would be expected to give a geoid anomaly of 100 m, but with a large uncertainty. The observed geoid anomalies are at least one order of magnitude smaller. The orientation of the shape with that of the current tidal and rotational effects is therefore best interpreted as

telling us nothing about the physical origin of the excess topography but confirming the view that the body should reorient to the lowest energy state. This makes sense if the topography is positively correlated with the geoid. One way of producing the small GTR suggested here is to have a compensation at depth D that nearly cancels the gravity of the surface mass anomaly. The predicted GTR is then reduced from that given above by a factor $f = 1 - (1 - D/R)^3$. The data suggest $f \sim 0.1$ and this requires $D \sim 100$ km, but with a large uncertainty. There are many possible interpretations of this result. It might correspond to the base of the cold ice lithosphere. It could be a thermal anomaly on the order of 10 K, corresponding to a density anomaly of one part in a thousand extending over a depth range of 100 km (because this would be equivalent to the mass of 100 m of ice). If this arose from convection, it would argue against a thin outer convective shell. However, the geoid anomalies arising from convection do not necessarily correspond to a simple estimate of density anomalies alone (i.e., thermal isostasy) and depend on the viscosity structure. The compensation could correspond to a density anomaly in the deeper region (the mixture of ice and rock), but this seems less likely given the depth of ~500 km to the core. The compensation could be a structure that develops at depth because of a physical process that creates topography at the surface, or it could be a structure that forms at depth, causing the surface to deform. The only firm conclusion that seems possible at present is that the extent of compensation is not consistent with a cold interior that supports loads over geologic time scales.

As has been suggested for Callisto, the proposed incomplete differentiation of Titan may have arisen because of a long accretion time (on the order of 1 million years), perhaps because both bodies are at a large distance from the parent planet, as measured in units of planet radii.

References and Notes

1. J. I. Lunine, R. D. Lorenz, *Annu. Rev. Earth Planet. Sci.* **37**, 299 (2009).
2. R. A. Jacobson *et al.*, *Astron. J.* **132**, 2520 (2006).
3. N. Rappaport *et al.*, *Icarus* **126**, 313 (1997).
4. We use the rotational parameter $q_t = \omega^2 R_t^3 / GM_t = 3.9555 \times 10^{-5}$, where ω, R_t, and M_t are Titan's spin rate, radius, and mass.
5. The shape of the ellipsoid is given by $r_{ell}(\lambda,\varphi) = \frac{abc}{\sqrt{(bc\cos(\varphi)\cos(\lambda))^2 + (ca\cos(\varphi)\sin(\lambda))^2 + (ab\sin(\varphi))^2}}$, where φ is the latitude and λ is the longitude.
6. C. D. Murray, S. F. Dermott, *Solar System Dynamics* (Cambridge Univ. Press, Cambridge, 1999).
7. H. Zebker *et al.*, *Science* **324**, 921 (2009).
8. W. A. Heiskanen, H. Moritz, *Physical Geodesy* (Institute of Physical Geodesy, Technical University, Graz, Austria, 1979).
9. The associated uncertainties do not account for the limitations of the Radau-Darwin model or for the small nonhydrostatic contributions to J_2 and C_{22} and have to be regarded as purely formal. See SOM for additional discussion.
10. A. P. Showman, R. Malhotra, *Science* **286**, 77 (1999).
11. The MoI factors for Ganymede and Callisto were also obtained from the Radau-Darwin equation, from a gravity field forced to the hydrostatic ratio.
12. C. Sotin *et al.*, in *Titan from Cassini-Huygens*, R. H. Brown, J.-P. Lebreton, J. Hunter Waite, Eds. (Springer, New York, 2009), pp. 61–73.
13. A. C. Barr, R. M. Canup, *Icarus* **198**, 163 (2008).
14. A. D. Fortes, P. M. Grindrod, S. K. Trickett, L. Vočadlo, *Icarus* **188**, 139 (2007).
15. P. M. Grindrod *et al.*, *Icarus* **197**, 137 (2008).
16. W. M. Kaula, *Theory of Satellite Geodesy* (Blaisdell, Waltham, MA, 1966).

17. The work of L.I., P.R., and P.T. was funded in part by the Italian Space Agency. The work of N.J.R., R.A.J., J.W.A., and S.W.A. was carried out at the Jet Propulsion Laboratory, California Institute of Technology, under a contract with NASA. D.J.S. acknowledges support from NASA's planetary geology and geophysics program.

Supporting Online Material

www.sciencemag.org/cgi/content/full/327/5971/1367/DC1
Materials and Methods
Figs. S1 to S3
Table S1
References and Notes

28 September 2009; accepted 5 January 2010
10.1126/science.1182583

Plumage Color Patterns of an Extinct Dinosaur

Quanguo Li,[1] Ke-Qin Gao,[2] Jakob Vinther,[3,4]* Matthew D. Shawkey,[5] Julia A. Clarke,[6] Liliana D'Alba,[5] Qingjin Meng,[1] Derek E. G. Briggs,[3,4] Richard O. Prum[4,7]

For as long as dinosaurs have been known to exist, there has been speculation about their appearance. Fossil feathers can preserve the morphology of color-imparting melanosomes, which allow color patterns in feathered dinosaurs to be reconstructed. Here, we have mapped feather color patterns in a Late Jurassic basal paravian theropod dinosaur. Quantitative comparisons with melanosome shape and density in extant feathers indicate that the body was gray and dark and the face had rufous speckles. The crown was rufous, and the long limb feathers were white with distal black spangles. The evolution of melanin-based within-feather pigmentation patterns may coincide with that of elongate pennaceous feathers in the common ancestor of Maniraptora, before active powered flight. Feathers may thus have played a role in sexual selection or other communication.

Exceptionally preserved specimens from the Lower Cretaceous of China have shown that simple body contour feathers and elongate pennaceous forelimb and tail feathers, bearing both barbs and barbules, were present in basal maniraptoran dinosaurs before powered flight evolved (*1*–*3*). Discoveries of elongate leg and foot feathering in Paraves (*4*–*6*) have raised new questions about the evolutionary origin of aerodynamic feather function (*2*, *3*). Preserved color patterns have also been noted, such as the light and dark regions in the tail of *Caudipteryx* (*1*), but there has been no evidence to indicate how such patterns, or color more generally, evolved.

Fossil avian feathers preserve the morphologies of melanosomes, the melanin-containing organelles that determine key aspects of color (*7*, *8*). A recent study (*9*) reported melanosome impressions in Cretaceous feathers, but the limited sample of small regions of distinct animals and comparison on the basis of gross melanosome shape prevented the interpretation of overall plumage color patterns. Here, we analyze melanosome size, shape, density, and distribution in order to reconstruct the plumage color patterns of a new specimen of a feathered dinosaur. The specimen, BMNHC PH828 (*10*) (Figs. 1 and 2 and figs. S3 and S4), comprises part and counterpart of a partial skeleton in three shale blocks, with elements of the forelimbs and distal hindlimbs in near-complete articulation. Preparation was minimal, and most feathers are well preserved even to their insertions (fig. S4). Elongate pennaceous forelimb (primaries, secondaries, and coverts) and hindlimb feathers are present, as are contour feathers associated with the skull and body (Figs. 1 and 2 and figs. S3 and S4). The new specimen is referred to *Anchiornis huxleyi* Xu *et al.* (*11*) and preserves morphologies that are consistent with the recovered placement of this species within Paraves as a part of Troodontidae [supporting online material (SOM) text] (*6*). It was found in strata estimated to be Late Jurassic in age from the Daxishan site (Jianchang County, Liaoning Province), which

[1]Beijing Museum of Natural History, 126 Tianqiao South Street, Beijing 100050, People's Republic of China. [2]School of Earth and Space Sciences, Peking University, Beijing 100871, People's Republic of China. [3]Department of Geology and Geophysics, Yale University, New Haven, CT 06511, USA. [4]Peabody Museum of Natural History, Yale University, New Haven, CT 06511, USA. [5]Department of Biology and Integrated Bioscience Program, University of Akron, Akron OH 44325-3908, USA. [6]Department of Geological Sciences, University of Texas at Austin, 1 University Station C1100, Austin, TX 78712, USA. [7]Department of Ecology and Evolutionary Biology, Yale University, New Haven, CT 06511, USA.

*To whom correspondence should be addressed. E-mail: jakob.vinther@yale.edu

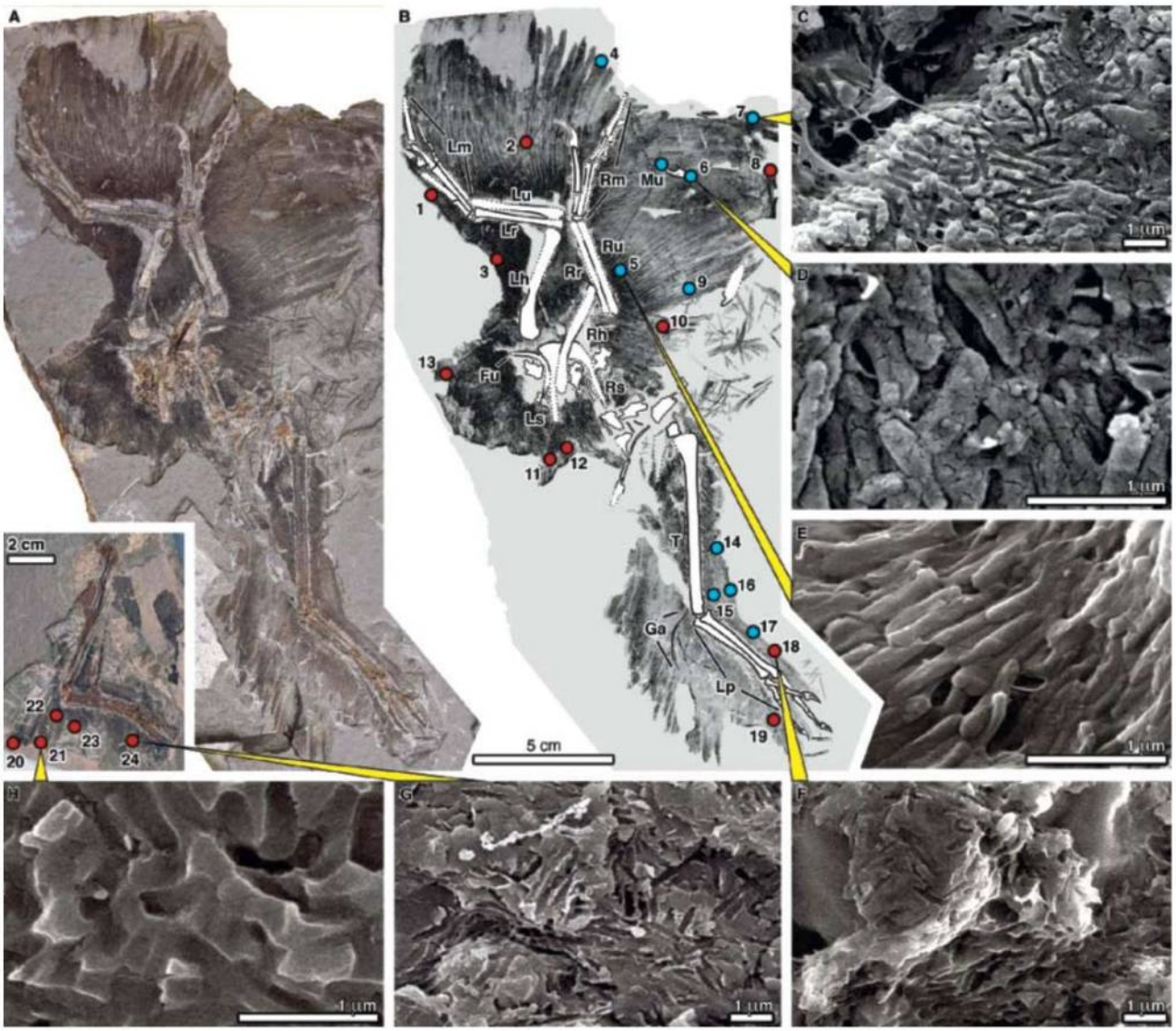

Fig. 1. *A. huxleyi* (BMNHC PH828) with SEMs of samples from the feathers. (**A**) Part, with inset of isolated right hindlimb. The left forelimb is seen in ventral view, and the right is seen in dorsal view. (**B**) Explanatory illustration. Numbered dots indicate samples from the part (red) and counterpart (blue) (table S4 and fig. S5). (**C** to **H**) SEMs of melanosomes and melanosome impressions taken from samples 7 (C), 6 (D), 5 (E), 18 (F), 24 (G), and 21 (H). Ga, gastralia; Fu, furcula; Lh, left humerus; Lm, left manus; Lp, left pes; Lr, left radius; Ls, left scapula; Lu, left ulna; Mu, manual ungual; Rh, right humerus; Rm, right manus; Rr, right radius; Ru, right ulna; Rs, right scapula.

is the same locality as a specimen recently referred to this taxon (LPM-B00169) (*6*).

We sampled proximal and distal parts of all feather types and all body regions preserved in BMNHC PH828 (Figs. 1 and 2 and table S4). Scanning electron micrographs (SEMs) of all 29 samples revealed impressions of spherical to oblate carbonaceous bodies or impressions 100 to 1908 nm in length (Figs. 1 and 2 and fig. S2) identified as melanosomes (*8*). Most samples revealed elongate eumelanosomes that varied slightly in morphology and distribution in different regions of the body. The distal crown feathers contained distinct subspherical phaeomelanosomes ~500 nm in length (Fig. 2B). A posteroventral sample from the skull showed distinct regions of spherical and elongate melanosomes.

For comparison, we assembled a data set on melanosomes from a phylogenetically diverse sample of extant bird feathers with black, gray, and brown melanin pigmentation but lacking structural coloration (*12*). Other molecular pigments, such as carotenoids and porphyrins, also produce plumage colors but are not preserved morphologically; thus, we cannot address their possible effects here. Four properties of melanosome morphology and distribution—long axis variation, short axis skew, aspect ratio, and density—were used as variables in a canonical discriminant analysis (table S1) (*12*). In general, eumelanosomes that produce black and gray colors are long and narrow, whereas those that produce rufous red and brown colors are short and wide (SOM text). We assigned colors to the fossil samples on the basis of the discriminant analysis of modern feather colors (Fig. 3 and fig. S1). All the melanosome morphologies in the fossil fell within the range of those observed in extant birds (fig. S2). Twenty-four samples were assigned a color with >0.9 probability (table S4). Three samples were ambiguous, with probabilities between 0.56 and 0.74, and three samples lacked significant numbers of melanosomes and were interpreted as unpigmented (table S4) (*8*). Sample 14 is a distinct outlier in the analysis, probably because of its high aspect ratio and long axis variation, and was predicted as gray.

Although melanosome morphologies for black and brown are strongly diagnostic, a variety of melanosome morphologies and densities generate gray colors (SOM text, tables S2

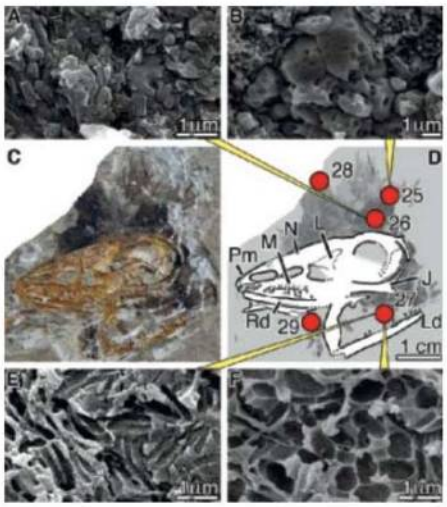

Fig. 2. *A. huxleyi* (BMNHC PH828) isolated skull with SEMs of samples from the feathers. (**C**) Skull. (**D**) Explanatory illustration. Numbered dots indicate samples. J, jugal; L, lacrimal; Ld, left dentary; M, maxillare; N, nasale; Pm, premaxillare; Rd, right dentary. (**A**, **B**, **E**, and **F**) SEMs of samples 26 (A), 25 (B), and 27 (E) and (F).

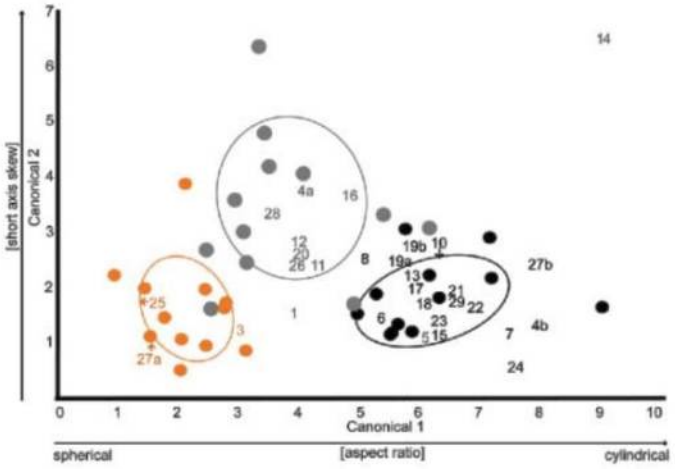

Fig. 3. Quadratic discriminant analysis of color (black, brown, or gray) in extant birds (dots) and in samples from BMNHC PH828 (numbers). The analysis identified properties of melanosome morphology and distribution that predicted color in extant birds and then used these data to predict colors in the fossil sample (fig. S1, and tables S1 to S4) (*12*). Canonical axis 1 is strongly positively associated with melanosome aspect ratio, and axis 2 is strongly positively associated with melanosome density skew. When present, arrows point to the locations of the samples in canonical space; this was done to avoid overlap of sample names.

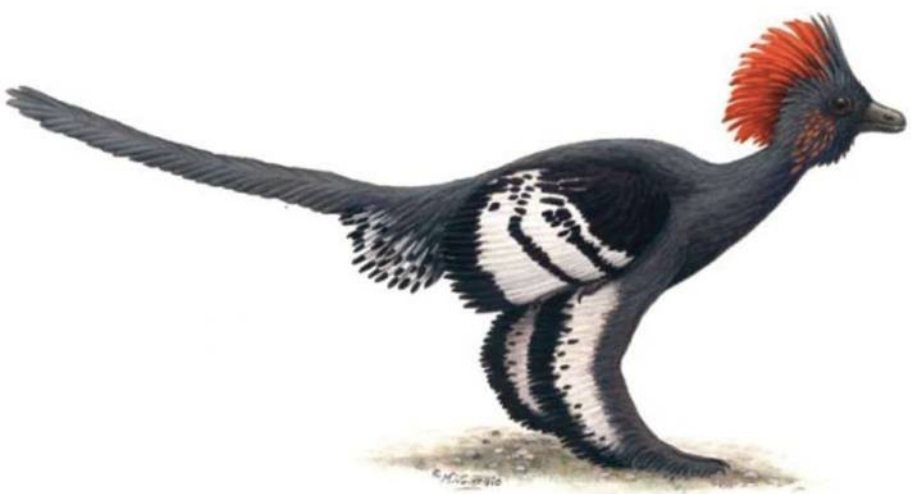

Fig. 4. Reconstruction of the plumage color of the Jurassic troodontid *A. huxleyi*. The tail is unknown in specimen BMNHC PH828 and reconstructed according to the complete specimen previously described (*6*). Color plate is by M. A. DiGiorgio.

and S3, and fig. S1). Samples from body contour feathers (samples 10 to 13) indicate a black or gray color (Fig. 3 and table S4). Samples from the marginal forelimb coverts (samples 1 and 5) and the front and dorsal surface of the legs (samples 14 to 16 and 18) were also black or gray. The undercoverts in the propatagial region were predicted as brown (table S4), albeit with low probability (0.7). Samples from the distal tips of the elongate primary and secondary feathers of the forelimb (samples 4 and 6 to 8), the toes (sample 19), and the elongate pennaceous feathers of the pedal surface of the shank (tibia) and foot (samples 20 to 24) were reconstructed as black. Melanosomes in sample 17 are poorly preserved, preventing the interpretation of color. A heterogeneous sample from the contour feathers on the side of the face (sample 27) showed separate regions of distinct melanosomes and was reconstructed as containing distinct, adjacent black and rufous feathers or parts of feathers. Samples from the long forecrown feathers and the shorter feathers from the sides of the crest (samples 28 and 26) indicate gray, whereas the longest feathers from the center of the crest (sample 25) indicate a brown in close proximity to rufous. The discriminant analysis clustered sample 25 with rufous feathers of living birds. Melanosomes were sparse in basal portions of the elongate pennaceous feathers of the forelimb and the hindlimb (samples 2, 9, and 15), indicating that these areas were lightly pigmented and whitish in color (*8*). The correlation between the colors reconstructed on the basis of melanosome morphology and density and the preserved appearance of the fossil (*8*) supports extrapolation of at least dark and light color patterning (SOM text); for example, part and counterpart of the *Anchiornis* specimen exhibit dark tips on many of the upper covert feathers of the forelimb and the hindlimb that are consistent with eumelanin pigmention (fig. S4, A and D).

A. huxleyi was darkly colored with gray and black body plumage (Fig. 4). The head was gray and mottled with rufous and black. Elongate gray feathers on the front and sides of the crest appear to frame a longer rufous hindcrown. Gray marginal wing coverts formed a dark epaulet that contrasted strongly with the black- and gray-spangled light primaries, secondaries, and greater coverts of the forelimb. The large black spangles of the primaries and secondaries created a dark outline to the trailing edge of the forelimb plumage. The spangles of the outermost primaries were black. The greater coverts of the upper wing were spangled with gray or black, creating an array (secondary coverts) or rows (primary coverts) of conspicuous dots. The contour feathers of the legs were gray on the shank and black on the foot. Like the forelimb, the elongate feathers of the lateroplantar surface of the hindlimb were white at their bases with broad black distal spangles. The tail is unknown in BMNHC PH828.

The plumage color pattern elements of the Late Jurassic *A. huxleyi* are strikingly similar to various living birds, including domesticated fowl, providing insights into the evolution of feather-pigment pattern development (SOM text). The identification of melanin-based within- and among-feather plumage coloration patterns in *Anchiornis* helps reveal the evolution of color pigmentation patterning mechanisms in dinosaurs. For example, the pattern observed in the simple tail integumentary structures of the basal coelurosaur *Sinosauropteryx prima* (*13*) has been interpreted as representing spaced light and dark patches among feathers. Our results confirm that

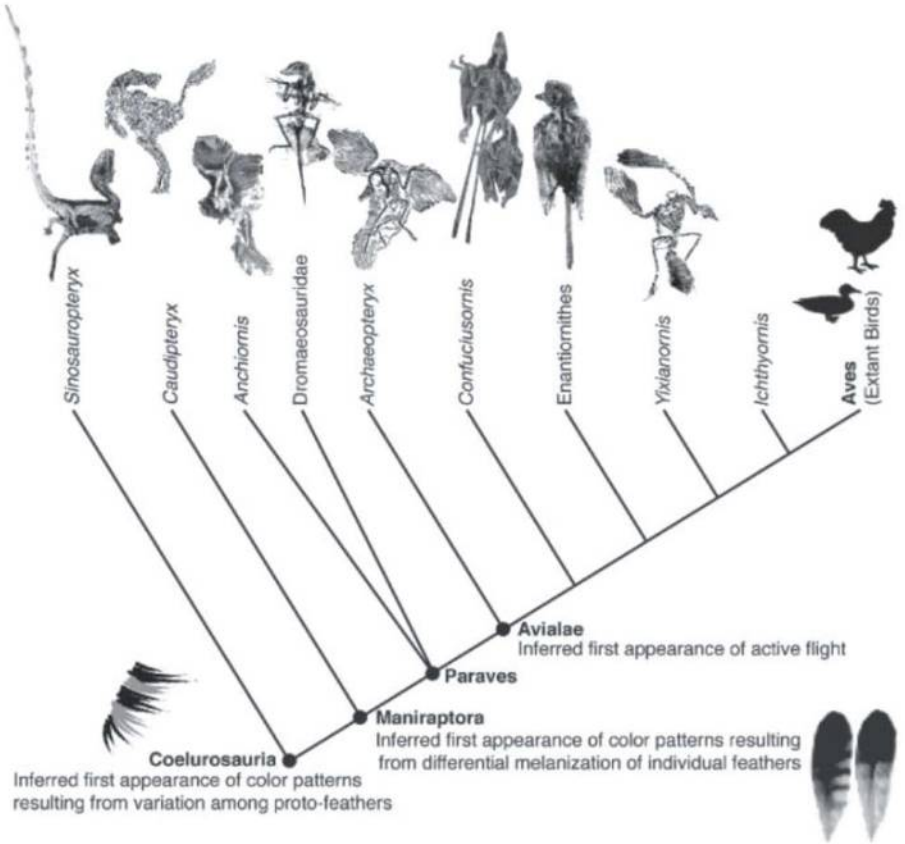

Fig. 5. The distribution of integumentary types in coelurosaurian theropod dinosaurs and inferred distribution of plumage patterning (*2*, *3*, *6*). Protofeather-like appendages appeared at the base of Coelurosauria, if not earlier (*3*). Color patterns reported in the tail of the compsognathid *Sinosauropteryx* (*9*) indicate that among-feather color patterns may have also appeared at this stage. Pinnate feathers and within-feather color patterns first appear in Maniraptora, as observed in the striped pinnate tail feathers of the oviraptorosaur *Caudipteryx* (*1*, *20*, *21*) and the troodontid *A. huxleyi*.

melanin-based patterning is a mechanism for within- and among-feather variation, producing lighter and darker regions. According to our data from *Anchiornis* and its phylogenetic placement (*6*), these two common mechanisms of plumage patterning in crown group Aves are supported as minimally having a first appearance in the most recent common ancestor of Troodontidae + crown Aves. Further, although paravian relationships remain controversial, recent analyses recover a monophyletic Deinonychosauria (*6*, *14*), indicating support for within- and among-feather variation as ancestral to at least Paraves (Fig. 5).

Complex within- and among-feather plumage coloration, such as that in *A. huxleyi*, is used in display and communication in living birds. Such communication, however, may function in different ways: commonly in intersexual communication (*15*), and less so in interspecific and intraspecific competition for restricted foraging [for example, multiple species of antbirds forage on army ant swarms (*16*)]. Alternatively, bold plumage color patterns can function in interspecific threat and defense postures [such as in some owls or the sunbittern (*Eurypygia helias*)], in startling predators or warning conspecifics within a flock (*17*), or in startling invertebrate prey that are seized as they attempt to flee (such as with North American *Setophaga* redstarts, Neotropical *Myioborus* whitestarts, and Australian *Rhipidura* fantails) (*18*, *19*). Melanin deposition in the distal portion of primaries in birds such as gulls (Laridae) may offer added resistance to wear (*20*).

The plumage of *Anchiornis* is composed of a variety of differently sized pennaceous (closed-vaned and rachidial) feathers that vary little in feather shape (Fig. 1 and figs. S3 and S4). The body contour feathers, the primary and secondary forelimb feathers, and the forelimb and hindlimb coverts all share a similar aspect ratio (length to width). Thus, mechanisms producing varieties of feather shape may postdate the evolutionary first appearance of plumage color variation (SOM text).

The most recent common ancestor of *Anchiornis* and Aves must have had the capacity to develop white, gray, black, and rufous plumage color patterns both within and among feathers. Both mechanisms of melanin-based plumage patterning evolved before the derived form of active powered flight minimally inferred as ancestral to Avialae (Fig. 5). The observed color pattern in *Sinosauropteryx* is consistent with only among-feather variation in melanin pigment deposition. Such variation occurs in Aves and would be optimized as ancestral to at least Coelurosauria (Fig. 5). However, the evolutionary origin of within-feather pigmentation patterning, including stripes, feather spots, and spangles, appears phylogenetically later. Its origin is presently coincident with the origin of elongate pennaceous feather structure in the most recent common ancestor of Maniraptora when data from *Caudipteryx* (*1*, *10*, *20*) are considered (Fig. 5). Thus, the first evidence for plumage color patterns in a feathered nonavian dinosaur suggests that selection for signaling function may be important in the early evolution of feathers.

References and Notes

1. Q. Ji, P. J. Currie, M. A. Norell, S.-A. Ji, *Nature* **393**, 753 (1998).
2. M. A. Norell, X. Xu, *Annu. Rev. Earth Planet. Sci.* **33**, 277 (2005).
3. X. Xu, Y. Guo, *Vertebrata PalAsiatica* **47**, 311 (2009).
4. F. Zhang, Z. Zhou, *Nature* **431**, 925 (2004).
5. X. Xu *et al.*, *Nature* **421**, 335 (2003).
6. D. Hu, L. Hou, L. Zhang, X. Xu, *Nature* **461**, 640 (2009).
7. J. Vinther, D. E. G. Briggs, J. Clarke, G. Mayr, R. O. Prum, *Biol. Lett.* **6**, 128 (2010).
8. J. Vinther, D. E. G. Briggs, R. O. Prum, V. Saranathan, *Biol. Lett.* **4**, 522 (2008).
9. F. Zhang *et al.*, *Nature*; published online 27 January 2010 (10.1038/nature08740).
10. Z. Zhou, X. Wang, *Vertebrata PalAsiatica* **38**, 113 (2000).
11. X. Xu *et al.*, *Chin. Sci. Bull.* **54**, 430 (2009).
12. Materials and methods are available as supporting material on *Science* Online.
13. Q. Ji, S. Ji, *Chin. Geol.* **23**, 30 (1996).
14. A. H. Turner, D. Pol, J. A. Clarke, G. M. Erickson, M. A. Norell, *Science* **317**, 1378 (2007).
15. G. E. Hill, K. J. McGraw, Eds., *Bird Coloration*, vol. 2, *Function and Evolution* (Harvard Univ. Press, Cambridge, MA, 2006).
16. S. K. Willson, *Ornithol. Monogr.* **55**, 1 (2004).
17. G. R. Bortolotti, in *Bird Coloration*, vol. 2, *Function and Evolution*, G. E. Hill, K. J. McGraw, Eds. (Harvard Univ. Press, Cambridge, 2006), pp. 3–35.
18. P. G. Jablonski, *Behav. Ecol.* **10**, 7 (1999).
19. R. L. Mumme, *Auk* **119**, 1024 (2002).
20. E. H. Burtt Jr., in *The Behavioral Significance of Color*, E. H. Burtt Jr., Ed. (Garland STPM Press, New York, 1979) pp. 75–110.
21. Z. Zhou, X. Wang, F. Zhang, X. Xu, *Vertebrata PalAsiatica* **38**, 241 (2000).

22. E. Champion and S. Nesbitt helped produce the figures. N. Vitek, J. A. Cundiff, and C. L. Canter made initial investigations of modern feathers. The research was funded by NSF (EAR-0720062 and EAR-0719758), the Air Force Office of Scientific Research (FA9550-09-1-0159), University of Akron startup funds, the National Geographic Society, and the Yale University W. R. Coe Fund. K. J. McGraw and R. J. Safran provided modern feather samples. The studied specimen is accessioned at Beijing Museum of Natural History (BMNHC). The color plate in Fig. 4 was painted by M. D. DiGiorgio.

Supporting Online Material

www.sciencemag.org/cgi/content/full/science.1186290/DC1
Materials and Methods
SOM Text
Tables S1 to S5
Figs. S1 to S5
References

22 December 2009; accepted 25 January 2010
Published online 28 January 2010;
10.1126/science.1186290
Include this information when citing this paper.

Parent-Offspring Conflict and Coadaptation

Camilla A. Hinde, Rufus A. Johnstone, Rebecca M. Kilner

The evolution of family life has traditionally been studied in parallel by behavioral ecologists and quantitative geneticists. The former focus on parent-offspring conflict and whether parents or offspring control provisioning, whereas the latter concentrate on the coadaptation of parental supply and offspring demand. Here we show how prenatal effects on offspring begging can link the two different approaches. Using theoretical and experimental analyses, we show that when offspring control provisioning, prenatal effects primarily serve the parent's interests: Selection on parents drives coadaptation of parent and offspring traits. In contrast, when parents control provisioning, prenatal effects primarily serve the offspring's interests: Selection on the offspring drives coadaptation of parent and offspring traits. Parent-offspring conflict may thus be responsible for the selective forces that generate parent-offspring coadaptation.

The complex social interactions that underpin family life are of considerable interest to both behavioral ecologists (*1*–*4*) and quantitative geneticists (*5*–*7*). Yet researchers in each field have largely ignored the questions raised by the other (*8*). Behavioral ecologists have focused on the evolutionary conflict of interests between parents and their young (*1*, *2*) and how it is resolved (*9*): Is it offspring who control provisioning or parents? Quantitative geneticists, in contrast, have focused on parent-offspring coadaptation: How is parental supply correlated with offspring demand, and is this correlation attributable chiefly to selection on parents or selection on offspring? We show here that both sets of questions are, in reality, tightly linked.

The empirical connection between the two approaches lies in the recent discovery that maternal substances in the developmental environment, such as testosterone, antibodies, and carotenoids, modulate later expression of offspring solicitation behaviors (*10*–*12*). In some cases, these maternal effects match offspring begging to parental capacity by providing a prenatal cue of parental generosity (*13*, *14*), thus facilitating the coadaptation of offspring and parental behaviors (*7*, *8*, *14*). However, although it is commonly assumed that this arrangement favors the mother (*10*, *11*, *15*), it is in fact unclear whether maternal effects serve the evolutionary interests of parents or offspring (*4*, *13*, *14*). Here we show how understanding the role of maternal effects in resolving parent-offspring conflict can help to explain how and why a correlation arises between parental supply and offspring demand.

We begin with a theoretical analysis, in which we extend existing models of parent-offspring conflict resolution to incorporate variation in parental supply (attributable to variation in the cost of provisioning) and allow offspring to adjust their demand in response to prenatal cues of parental generosity. We then explore the predicted consequences of disrupting the correlation between parental supply and offspring demand by exchanging young between parents. We show that when offspring control provisioning, it is parents who are predicted to suffer most when young are exchanged; under these circumstances, maternal effects primarily serve the parent's interests, and it is selection on the parents that is responsible for the coadaptation of parent and offspring traits. In contrast, when parents control provisioning, it is offspring who are predicted to suffer most when young are exchanged; under these circumstances, maternal effects primarily serve the offspring's interests, and it is selection on the offspring that drives coadaptation of parent and offspring traits.

We focus on provision of food by a parent to a brood (treating the brood as a single unit). The fitness benefit of provisioning to the offspring depends on the amount of food provided, y, and upon offspring need, n, and is denoted $b(n,y)$ [where $b(n,0) = 0$]. We assume that $\partial b/\partial y > 0$, $\partial^2 b/\partial y^2 < 0$, and $\partial^2 b/\partial y \partial n > 0$, implying that greater quantities of food yield greater benefits and that the marginal benefits of provisioning increase with need but decrease with quantity provided. Provisioning also entails a cost to the parent (it reduces future reproductive success), which depends on the amount of food provided and on parental quality, q, and is denoted $c(q,y)$ [where $c(q,0) = 0$]. We assume that $\partial c/\partial y > 0$, $\partial^2 c/\partial y^2 \geq 0$, and $\partial^2 c/\partial y \partial q < 0$, implying that provision of more food entails greater costs and that the marginal cost of provisioning is nondecreasing with quantity provided but decreases with the quality of the parent (we assume that $\partial b/\partial y > \partial c/\partial y$ for $y = 0$ and $n > n_{min}$, implying that parents stand to gain by supplying at least some food to offspring of greater than the lowest possible level of need n_{min}). For simplicity, we shall also assume that costs incurred by the parent do not affect the fitness of its mate.

Suppose that offspring are related to their parent's future progeny by a coefficient r (>0). Provided that $r < 1$, there exists a conflict of interest between parent and young over resource

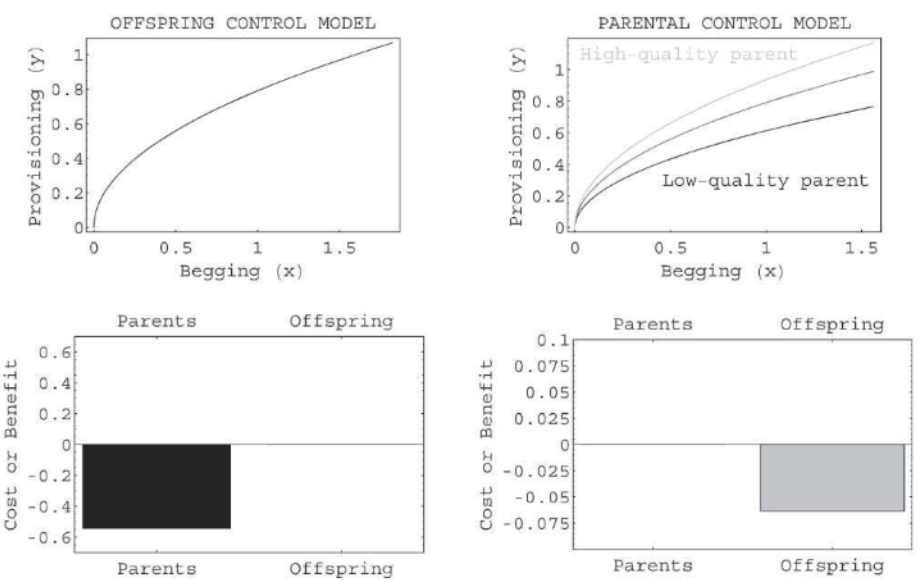

Fig. 1. Provisioning behavior and predicted consequences of exchanging young, under the offspring control and parental control models. All results are for the specific illustrative case in which $b(n,y) = ny - y^2/2$, $c(q,y) = 16y^2/(1 + 8q)$, $Y(x) = \sqrt{5x/8}$, parental quality is evenly distributed between 0 and 1, and offspring need is drawn from a scaled beta distribution ranging from 0 to 5. Upper graphs show provisioning as a function of offspring begging intensity under the offspring control and parental control models; in the latter case, successively lower curves correspond to parents of high, medium, and low quality (q = 1/4, 1/2, and 3/4). Lower graphs show the expected direct fitness impact of exchanging eggs on parents (black bars) and on offspring (gray bars) under both models; values are scaled relative to the standard deviation in expected direct fitness across parents of different qualities under normal conditions. There are different scales on the two lower graphs: The impact of egg exchange is much larger under the offspring control model.

Department of Zoology, University of Cambridge, Downing Street, Cambridge CB2 3EJ, UK.

allocation. Now let us contrast two models of conflict resolution. Under the offspring control model, offspring invest some level of effort x in costly begging in order to extract food from the parent. The parental response in this case is externally specified and cannot be adjusted optimally in relation to parental quality. Under the parental control model, parents may actively choose how much food to supply but benefit by attending to costly begging on the part of the offspring because this serves as a signal of condition.

In both models, offspring should be expected to adjust their begging effort in response to cues of maternal quality present in the egg (*16*). But what is the effect of swapping eggs between parents and thereby scrambling the cues of parental quality available to the offspring? The answer depends on whether the parents or offspring control resource allocation.

Consider two parents of quality q_1 and q_2 (we assume without loss of generality that $q_1 > q_2$), who produce offspring of need n_1 and n_2, independently drawn from a distribution with probability density $f(n)$. We wish to determine both the expected direct fitness costs incurred by these parents and the expected direct fitness benefits obtained by their offspring, under normal circumstances and when the offspring are exchanged (as eggs) between the parents. In the latter case, we assume that the offspring receive cues of parental quality corresponding to their original parent rather than the parent with whom they actually interact [i.e., experimental results described in (*14*)].

Under the offspring control model (regardless of the precise form of the various cost and benefit functions), exchanging young is predicted to have no net effect on the expected direct fitness of offspring, but a negative effect on the expected direct fitness of parents (Fig. 1). It is thus parents who normally benefit directly from the modulation of offspring behavior in response to cues in the egg. In contrast, under the parental control model (again regardless of the precise form of the various cost and benefit functions), exchanging young is predicted to have no net effect on the expected direct fitness of parents, but a negative effect on the expected direct fitness of offspring. Under normal circumstances, it is the offspring who benefit directly from the information provided by cues in the egg. In Fig. 1 we show these predicted results graphically for a specific illustrative case.

We tested these two contrasting predictions, using the domesticated canary *Serinus canaria* (*16*). Canaries are ideal for such work because we know from previous work that canary parents provide more food when nestlings beg more intensely (*17*, *18*) but that unrewarded begging is costly because it can retard nestling growth (*19*). In addition, a prenatal cue that influences offspring begging behavior has been well characterized (*14*, *20*–*22*). Mothers deposit small quantities of maternal androgens [and possibly other substances (*11*, *12*)] in the egg (*20*), and the precise dose varies among clutches according to maternal and environmental conditions (*23*), with downstream effects on nestling begging intensity (*14*, *22*). Because canaries have been inbred for many generations to produce distinct types (*24*), any genetic variation in begging behavior within each type is likely to be relatively small (*25*). We therefore assume that much of the variation among canary

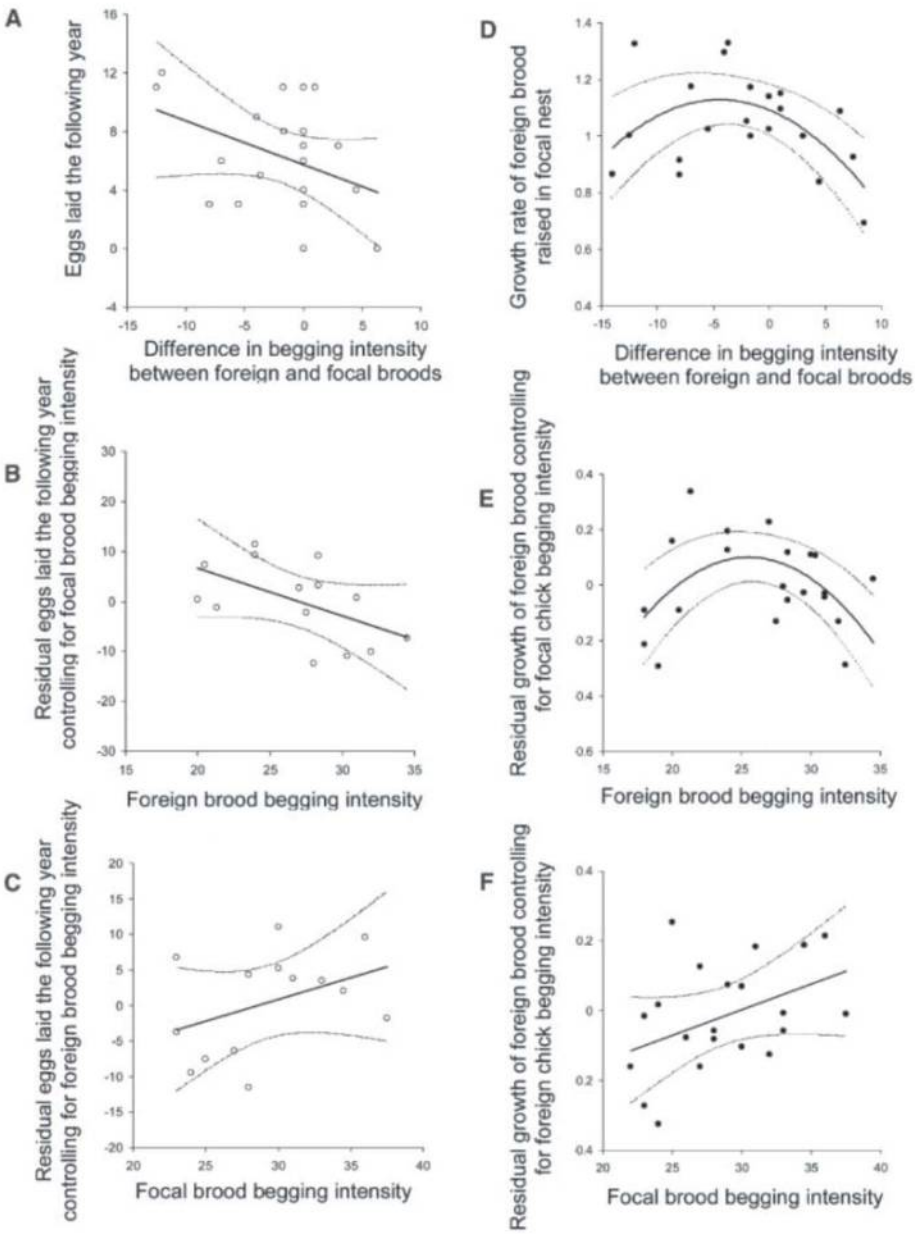

Fig. 2. Regression plots showing (**A**) the effect of a change in brood demand at the focal nest on maternal fecundity the following year. Each data point represents one mother (n = 21 females that reared one brood of their own and one foreign brood; n = 8 control females that reared two broods of their own). The least-squares regression line is shown with 95% confidence intervals (CIs). (**B**) The correlation between the mean begging intensity of the foreign young in the focal nest and the residuals of maternal fecundity the following year after controlling for focal chick begging intensity. (**C**) The correlation between the mean begging intensity of the focal young and the residuals of maternal fecundity the following year after controlling for foreign chick begging intensity. In (B) and (C), lines of fit with 95% CIs are shown. (**D**) The effect of a change in brood demands at the focal nest on the growth rate of the foreign brood. Each data point is collected from one pair (n = 21 pairs with begging data that reared one foreign brood and one brood of their own). (**E**) The correlation between the mean begging intensity of the foreign young in the focal nest and the residuals of the growth rate of the foreign brood after controlling for focal chick begging intensity. (**F**) The correlation between the mean begging intensity of the focal young and the residuals of the growth rate of the foreign brood after controlling for foreign chick begging intensity. In (E) and (F), the least-squares regression lines are shown with 95% CIs.

broods in nestling begging intensity (*22*) is attributable to maternal factors in the egg, an assumption further justified by the fact that our breeding females exhibited considerable variation in other aspects of prenatal investment such as egg mass and clutch size (*16*).

We began by determining whether parents or offspring control provisioning. To do this, we exploited our recent discovery that canary nestling begging intensity is strongly influenced by prenatal factors in the egg and is relatively unperturbed by a changed rearing environment (*14*). Cross-fostering broods between parents thus generates a long-term manipulation of brood begging intensity, and parents exposed to intensely begging broods should pay a fitness cost for supplying food at a greater rate. If offspring alone control the supply of food, then broods that beg most intensely should routinely receive the most food and exhibit the fastest growth rates. If parents have some control over provisioning, then parental quality, in conjunction with brood begging intensity, should influence how begging is rewarded. Highly demanding broods reared by low-quality parents should then suffer reduced growth rates when their costly begging is unrewarded.

In our experiment, parents were allowed to raise two broods per year: one of their own and one fostered from a different pair (*16*). For each breeding attempt, we measured brood begging intensity and the future fitness consequences of our manipulation for mothers and young (*16*). We quantified offspring fitness in our experiments by measuring their growth rate. Just as has been found in free-living passerines (*26*), the chance that our canary offspring survive until they are independent of their parents is strongly related to their rate of growth during the nestling period (Generalized Linear Mixed Effects Model: $F_{1,325.6} = 134.19$, $P < 0.001$, $n = 346$ chicks from 107 different pairs). Maternal future fitness was quantified by comparing the number of eggs that females laid the following year.

We found that provisioning was costly. Mothers that were exposed to a less demanding brood than their own laid more eggs the following year, whereas females that cared for a more demanding foster brood produced fewer eggs (simple linear regression: $R^2 = 0.25$, $F_{1,21} = 5.63$, $P = 0.019$; Fig. 2A). Using a multiple regression, we found that the negative slope of this relationship was attributable to the demands of the fostered offspring ($R^2 = 0.33$, $t_{14} = -2.20$, $P = 0.048$; Fig. 2B) rather than to those of the mother's own brood ($t_{14} = 1.59$, $P = 0.14$; Fig. 2C).

We also found that parents mitigate the costs of provisioning by exerting a high level of control over the rate at which they provide food, as assumed by the parental control model. Although canary broods were able to use their begging behavior to enhance their growth rate, and hence gain fitness benefits, this was only possible within limits of generosity prescribed by parents (Fig. 2D). Foreign young raised in the focal nest grew at a faster rate if they begged more intensely, until their begging levels more or less matched the demands made by the focal brood (measured in a separate breeding attempt). Beyond this point, parents continued to feed begging young but presumably not sufficiently well to compensate for the high levels of energy expended during excessive begging (*19*), and so growth rates then fell (second-order polynomial regression: $R^2 = 0.30$, $F_{2,20} = 3.91$, $P = 0.022$; Fig. 2D). A multiple regression reveals the separate contribution of begging by foreign and focal broods to this curvilinear relationship. The begging of the foreign brood, mismatched with their foster parent's generosity (*14*), caused the curvilinear relationship shown in Fig. 2D [$R^2 = 0.33$, foreign brood begging $t_{20} = 2.40$, $P = 0.028$; (foreign brood begging)^2 $t_{20} = -2.43$, $P = 0.026$ (Fig. 2E)], whereas the begging of the focal brood was positively and linearly correlated with growth [focal brood begging $t_{20} = 2.26$, $P = 0.037$; (focal brood begging)^2 = NS, term dropped from minimal model (Fig. 2F)].

Having established that parents control provisioning in canaries, we next tested the parental control model's prediction that offspring should sustain the greater loss in fitness when exchanged between nests. Our second experiment mimicked our model by investigating how exchanging offspring between parents affected the mean fitness of parents versus offspring. Once again, parents were allowed to raise two broods per year: a brood of their own young and a brood of foster young from a different pair, each swapped before hatching (*16*).

Overall, we found that cross-fostered young grew at a slower rate on average than those that were raised by their own parents [$F_{1,143} = 16.42$, $P < 0.001$; Fig. 3 (*16*)]. In contrast, mothers that had raised a foreign brood had similar mean fecundity the following year to that of mothers that had reared only their own offspring ($F_{1,36} = 0.014$, $P = 0.91$; Fig. 3). Just as predicted by the parental control model, offspring suffered a greater loss in direct fitness as a result of the disruption in prenatal signaling than did their mothers (General Linear Model: cross-fostering treatment × brood/mother, $F_{1,180} = 4.98$, $P = 0.027$) (*16*). Contrary to a widely held assumption (*11*), our data therefore show that the prenatal matching of offspring begging to parental capacity serves the offspring's evolutionary interests. Their mothers benefit only indirectly, through the effect on the young.

Our results also imply, as shown in Fig. 2D, that parental control of provisioning imposes stabilizing selection on the begging intensity of the brood (*7*). Within each family, nestlings optimally balance the costs and benefits of begging by matching their demands to parental quality (Fig. 2C, 2F) (*14*). This gives rise to the positive correlation between parental provisioning and nestling begging (*6*, *14*, *27*) predicted by quantitative genetic models when selection acts on offspring (*7*). However, it is probable that in some other species, provisioning at the nest is under the control of offspring rather than parents (*3*). Our theoretical analysis predicts that such offspring control would lead to selection on parents which, quantitative genetic models suggest, should give rise to a negative correlation between parental supply and offspring demand (*7*). In short, understanding who controls provisioning in the evolutionary conflict between parents and their young is key to understanding the selective pressures responsible for parent-offspring coadaptation. The challenge for future work is to identify the ecological factors that predict who controls the supply of parental investment and to determine their effect on the genes involved in parent-offspring interactions.

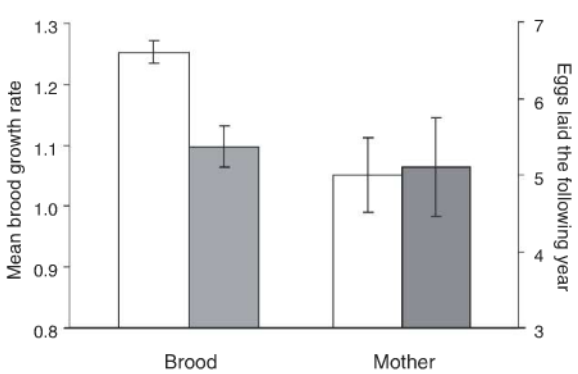

Fig. 3. The average effect of cross-fostering on correlates of nestling and maternal fitness. White bars show the fitness correlates of the brood and the mother when the brood is reared by the natal mother; gray bars show the fitness correlates when it is cross-fostered. Means with standard error bars are shown.

References and Notes

1. R. L. Trivers, *Am. Zool.* **14**, 249 (1974).
2. D. W. Mock, G. A. Parker, *The Evolution of Sibling Rivalry* (Oxford Univ. Press, Oxford, 1997).
3. N. J. Royle, I. R. Hartley, G. A. Parker, *Trends Ecol. Evol.* **17**, 434 (2002).
4. R. M. Kilner, C. A. Hinde, *Adv. Stud. Behav.* **38**, 283 (2008).
5. J. B. Wolf, E. D. Brodie, *Evolution* **52**, 299 (1998).
6. J. E. Lock, P. T. Smiseth, A. J. Moore, *Am. Nat.* **164**, 13 (2004).
7. M. Kölliker, E. D. Brodie III, A. J. Moore, *Am. Nat.* **166**, 506 (2005).
8. P. T. Smiseth, J. Wright, M. Kölliker, *Proc. R. Soc. London Ser. B* **275**, 1823 (2008).
9. H. C. J. Godfray, *Nature* **376**, 133 (1995).
10. H. Schwabl, D. W. Mock, J. A. Gieg, *Nature* **386**, 231 (1997).
11. T. G. G. Groothuis, W. Müller, N. von Engelhardt, C. Carere, C. Eising, *Neurosci. Biobehav. Rev.* **29**, 329 (2005).
12. D. Gil, *Adv. Stud. Behav.* **38**, 337 (2008).
13. W. Müller, C. M. Lessells, P. Korsten, N. von Engelhardt, *Am. Nat.* **169**, E84 (2007).
14. C. A. Hinde, K. L. Buchanan, R. M. Kilner, *Proc. R. Soc. London Ser. B* **276**, 2787 (2009).

15. H. Drummond, C. Rodriguez, H. Schwabl, *J. Avian Biol.* **39**, 139 (2008).
16. Supporting material is available on *Science* Online.
17. R. Kilner, *Proc. R. Soc. London Ser. B* **260**, 343 (1995).
18. R. M. Kilner, in *The Evolution of Begging: Competition, Cooperation and Communication*, J. Wright, M. L. Leonard, Eds. (Kluwer Academic, Dordrecht, Netherlands, 2002), pp. 87–107.
19. R. M. Kilner, *Proc. Natl. Acad. Sci. U.S.A.* **98**, 11394 (2001).
20. H. Schwabl, *Proc. Natl. Acad. Sci. U.S.A.* **90**, 11446 (1993).
21. H. Schwabl, *Comp. Biochem. Physiol. A* **114**, 271 (1996).
22. K. L. Buchanan, A. R. Goldsmith, C. A. Hinde, S. C. Griffith, R. M. Kilner, *Horm. Behav.* **52**, 664 (2007).
23. H. Schwabl, *J. Exp. Zool.* **276**, 157 (1996).
24. T. Price, *Speciation in Birds* (Roberts & Co, Greenwood Village, CO, 2007).
25. D. S. Falconer, T. F. C. Mackay, *Introduction to Quantitative Genetics* (Longman, Harlow, UK, ed. 4, 1996).
26. S. G. Gebhardt-Henrich, H. Richner, in *Avian Growth and Development*, J. M. Starck, R. E. Ricklefs, Eds. (Oxford Univ. Press, Oxford, 1998), pp. 324–339.
27. J. E. Lock, P. T. Smiseth, P. J. Moore, A. J. Moore, *Am. Nat.* **170**, 709 (2007).
28. R.M.K. was supported by a Natural Environment Research Council (NERC) studentship, then a Junior Research Fellowship at Magdalene College Cambridge, a Royal Society Dorothy Hodgkin Research Fellowship (sponsored by the Wolfson Foundation), and finally a Royal Society University Research Fellowship. The experiments were funded by three NERC grants (GR9/02650, GR9/04621, and NER/A/S/2002/00776), which also supported C.A.H., and a Royal Society Equipment Grant. Additional funding for C.A.H. was provided by the Isaac Newton Trust, Cambridge, and a Junior Research Fellowship at Newnham College, Cambridge. We thank L. Barden, N. Bates, C. Donovan, P. Heavens, P. Hynes, I. Millar, J. Nightingale, and S. Shelton for their help in maintaining the birds and constructing equipment; T. Roberts, M. Wade, and J. Theaker for supplying the birds; and N. Davies, M.Clinchy, L. Zanette, and especially M. Kölliker for comments on early drafts of the manuscript. R.M.K. conceived and designed the experiments, collected data, and wrote the paper. C.A.H. analyzed data and co-wrote the paper. R.A.J. contributed the theoretical analysis and co-wrote the paper.

Supporting Online Material

www.sciencemag.org/cgi/content/full/327/5971/1373/DC1
Methods
SOM Text
References

16 December 2009; accepted 12 February 2010
10.1126/science.1186056

Toward Extracting All Phylogenetic Information from Matrices of Evolutionary Distances

Sebastien Roch

The matrix of evolutionary distances is a model-based statistic, derived from molecular sequences, summarizing the pairwise phylogenetic relations between a collection of species. Phylogenetic tree reconstruction methods relying on this matrix are relatively fast and thus widely used in molecular systematics. However, because of their intrinsic reliance on summary statistics, distance-matrix methods are assumed to be less accurate than likelihood-based approaches. In this paper, pairwise sequence comparisons are shown to be more powerful than previously hypothesized. A statistical analysis of certain distance-based techniques indicates that their data requirement for large evolutionary trees essentially matches the conjectured performance of maximum likelihood methods—challenging the idea that summary statistics lead to suboptimal analyses. On the basis of a connection between ancestral state reconstruction and distance averaging, the critical role played by the covariances of the distance matrix is identified.

Information about evolutionary trees can be inferred from the fact that species that are close in the tree of life tend to have similar molecular sequences. In its most basic form, the evolutionary distance between two DNA sequences is estimated from the proportion of homologous sites differing between them, typically corrected for back-mutations under common modeling assumptions (*1*). For a collection of sequences, the pairwise evolutionary distances form a matrix—the distance matrix—which underlies a popular class of tree reconstruction methods. Technically, distance-matrix methods include all phylogenetic inference techniques relying solely on pairwise sequence comparisons, including neighbor-joining (NJ), BIONJ, WEIGHBOR, and FastME (*2*–*5*). Because of their simplicity, such methods are often considerably faster than parsimony- and likelihood-based approaches (*6*, *7*), and distance-matrix methods are used for large-scale phylogenetic reconstruction and bootstrap analysis or to produce starting trees for maximum likelihood (ML) heuristics. However, it is unknown if this advantage in speed affects accuracy adversely.

The use of distance-matrix information has been criticized for seemingly ignoring higher-order information, that is, data patterns involving more than two sequences (*1*). Moreover, it has been observed through combinatorial arguments that the conversion from molecular sequences to the distance matrix is far from invertible (*8*). However, this hypothesized information loss has not been quantified in a model-based framework. In reality, the comparison of distances between different pairs of sequences does involve higher-order signals, albeit in a highly summarized form. But it is unclear how to use such information. In particular, the correlation between the entries of the distance matrix has largely been ignored in the design and analysis of distance-matrix methods with a few notable exceptions (*3*, *9*, *10*).

Formally, phylogenetic data consist of n aligned DNA sequences of length k (without gaps): $s_1^a,\ldots,s_k^a$, where a ranges over the n terminal taxa (Fig. 1). The evolutionary distance between the sequences at a and b is denoted by $\hat{\delta}(a,b)$. In the Jukes-Cantor model, a classical substitution model which treats all nucleotides symmetrically, the standard distance formula takes the form

$$\hat{\delta}(a,b) = -\frac{3}{4}\log\left(1-\frac{4}{3}\,\hat{p}_{a,b}\right) \qquad (1)$$

where $\hat{p}_{a,b}$ is the proportion of homologous sites differing between sequences a and b.

A variety of distance-matrix methodologies have been proposed, of which this study focuses on agglomerative methods, including unweighted pair-group method using arithmetic averages (UPGMA) and NJ (*2*, *11*, *12*). Such methods proceed in two steps that are repeated until termination: (i) a selection step, where a pair of operational taxonomic units (OTUs) is selected for agglomeration, and (ii) a reduction step, where a reduced distance matrix is computed on the remaining OTUs. As an example, in the case of a molecular clock (that is, under the assumption that substitutions occur at the same rate in all branches of the tree), one can simply select the two closest

```
                 1 23 45 67 8910
Homo sapiens     A-CAATGGAG-AAA
Pan              A-TAATA-AGCAAA
Gorilla          ATCA-CA-AGCGGA
```

Fig. 1. Example of a DNA sequence data set. The alignment is typically obtained by using a multiple sequence alignment heuristic applied to the collected sequences. The dash is a gap. The columns are homologous sites; that is, they are derived from a common ancestor through substitutions. Those columns that include gaps are ignored. For instance, using the notation introduced in the text, we have k = 10, and the sequences at a = *Homo sapiens* and b = *Pan* are $s_i^a,\ldots,s_{10}^a$ = ACATGAGAAA and $s_i^b,\ldots,s_{10}^b$ = ATATAAGAAA, respectively. In particular, the preceding sequences agree on 8 out of 10 sites, so that $\hat{p}_{a,b} = 0.2$ and $\hat{\delta}(a,b) = 0.457$, using the Jukes-Cantor formula.

Department of Mathematics, University of California at Los Angeles, 520 Portola Plaza, Los Angeles, CA 90095, USA. E-mail: roch@math.ucla.edu

OTUs A' and A'' to form a new composite OTU A, and the matrix is reduced with the rule

$$\bar{\delta}(A,B) = \mu\bar{\delta}(A',B) + (1-\mu)\bar{\delta}(A'',B) \quad (2)$$

where $\bar{\delta}$ was used to indicate the reduced distance matrix, with the convention $\bar{\delta}(\{a\},\{b\}) = \hat{\delta}(a,b)$. The choice of the reduction coefficient, μ, is critical, and the appropriate value has been debated (*3*, *4*, *13*). Standard choices are $\mu = |A'|/|A|$ where $|A|$ denotes the number of terminal taxa in A, which leads in the clock case to UPGMA, and $\mu = 1/2$, which leads in the clock case to the less common weighted version of UPGMA known as weighted pair-group method using arithmetic averages (WPGMA) (*11*, *12*).

An important criterion in designing the selection and reduction steps above is the statistical consistency of the resulting method: As sequence length increases, the reconstructed tree should converge on the true phylogeny. However, because consistency is a coarse statistical property, it is of limited use in comparing different methods (*14*). A case in point is that both reduction coefficients above produce a consistent estimation under a molecular clock. A finer contrast is obtained with the sample complexity (SC), that is, the sequence length required to guarantee that the reconstruction is correct with a given confidence when the data are generated according to a standard substitution model on the true tree.

Because the sample complexity of a method depends in an intricate manner on the parameters of the generating model, it is more feasible to evaluate its asymptotic behavior as a designated parameter of interest converges to a limit. For instance, any inference method requires at least an SC proportional to $1/f^2$ as the shortest branch length $f \to 0$ (*15*). In statistical theory, sample complexities are often compared between two inference methods in the form of a ratio called the asymptotic relative efficiency (*16*).

In this study, the regime of interest is large phylogenies, and the structural parameters considered are the number of terminal taxa n; the shortest branch length f; and the depth of the tree, which we denote by Δ. (All branch and path lengths are expressed in number of substitutions per site.) The depth measures how far the edges are from the terminal taxa (leaves). Precisely, the depth of an edge e is defined to be the length of the shortest path between two leaves that crosses e, and the depth of the tree is the largest such quantity over all its edges (*17*). The length of the longest branch, g, also plays a nonasymptotic role. Here it is claimed that the following sample complexity can be achieved with only distance-matrix information under the Jukes-Cantor model (more general models as well as random trees are discussed below):

$$\mathrm{SC} = \begin{cases} C_0 \cdot 1/f^2 \cdot \log n \text{ if } g < g^*_{\mathrm{JC}} \approx 0.26 \\ C_1 \cdot 1/f^2 \cdot e^{C_2\Delta} \cdot \log n \text{ if } g \geq g^*_{\mathrm{JC}} \end{cases} \quad (3)$$

where C_0, C_1, and C_2 are positive constants independent of f, Δ, and n, but C_0 may depend on g. (To simplify the formula above, it was assumed that f is small; precisely, $f \leq 1$. In general, the factor $1/f^2$ should be replaced with $\max\{1/f^2, 1\}$.) Table 1 shows a comparison with previous results.

The significance of Eq. (3) is that its functional dependence in f, Δ, and n is the best possible among all phylogenetic reconstruction methods, except possibly for the values of the constants C_0, C_1, and C_2 (*18*). In particular, it is natural to conjecture that the SC of maximum likelihood estimation, currently unknown (*15*), is also given by the same expression. In comparison, the performance of NJ scales exponentially in the diameter (that is, the length of the longest path) for all values of g (*19*, *20*). Note that the diameter is larger than the depth, often much larger (think of a tree with a toplogy like that of a caterpillar). Therefore, not all distance-matrix methods achieve the SC in Eq. (3). In fact, the current study produces explicit prescriptions in designing accurate distance-based techniques.

In Eq. (3) the constants C_0, C_1, and C_2 may be evaluated through simulations or approximations on special cases (Fig. 2). The scaling in $1/f^2$ is necessary and sufficient for all phylogenetic methods, whether distance- or likelihood-based (*15*). Likewise, by information-theoretic arguments the factor of $\log n$ is necessary (*18*). Here it arises as a Bonferroni correction, that is, it accounts for the high number of evolutionary distances that must be estimated simultaneously in order to infer a large phylogeny. In particular, to reconstruct a single deep branching in an otherwise known tree, the factor of $\log n$ can be dropped.

The depth, on the other hand, displays an unexpected behavior. The thresholding effect at $g^*_{\mathrm{JC}} = 3\ln 2/8$ mirrors a similar phenomenon in ancestral state reconstruction. Because of the treelike nature of phylogenies, there exists a fundamental tradeoff between how fast information is lost through mutations along each path connecting the root to the leaves and, on the other hand, how fast information is replicated through the exponential growth of the tree. Under the Jukes-Cantor model, the critical threshold at which these two effects balance each other out on a bifurcating tree is $g = g^*_{\mathrm{JC}}$, which corresponds roughly to an average of 22 substitutions per 100 sites per branch. When $g < g^*_{\mathrm{JC}}$ (which I refer to as the lower phase of the parameter space), good estimates of ancestral sequences can be obtained, no matter how deep the tree is, whereas if $g \geq g^*_{\mathrm{JC}}$ (the upper phase), even the best ancestral estimation methods exhibit a quickly deteriorating accuracy as deeper parts of the tree are analyzed. This phase transition has been studied in statistical physics (*21*).

In addition, this information-theoretic limitation affects the accuracy of phylogenetic tree reconstruction: The functional dependence in Δ in Eq. (3) is necessary and sufficient for general phylogenetic reconstruction methods, except possibly for the values of the constants C_0, C_1, and C_2 (*18*). In particular, in the lower phase, the sequence length required to infer a deep branching does not grow with the depth.

Regarding distance-matrix methods, however, the best previous results had an SC exponential in Δ for any value of g, using so-called short quartet methods (SQM) (*17*)—which was expected to be best for distance-based techniques (*22*). This study concludes that distance-matrix methods are capable of achieving the asymptotically optimal SC in Eq. (3). This is surprising in that it is not immediately clear how to exploit ancestral state reconstruction through the use of summary statistics alone. This hidden relation between ancestral states and the distance matrix (*22*) forms the basis of the analysis.

The assumption that the largest branch length is bounded, even for large trees, may seem unrealistic. After all, standard random tree models do not satisfy this kind of condition. However, classical results on ancestral state reconstruction (*21*) naturally lead to the conjecture that the results discussed here—at least for the reconstruction of a single deep branching—are still true under the relaxed assumptions that an appropriately defined average branch length $\bar{g}$ is bounded above by g^*_{JC}. The sample complexity for full reconstruction may require an extra factor depending on g, but that is likely for any method. This is only conjecture, as a rigorous analysis of the random tree case is still needed.

Although the molecular clock case is less relevant in practice, it is illustrative of the techniques used. Analysis of the Jukes-Cantor model under a molecular clock was performed abandoning the standard Jukes-Cantor distance of Eq. (1) and, instead, with the following transformation: For each species a we define a new sequence $\sigma^a_1,\ldots,\sigma^a_k$ with $\sigma^a_i = 1$ if $s^a_i = A$ or G (purines) and $\sigma^a_i = -1$ if $s^a_i = $ C or T (pyrimidines), letting the evolu-

Table 1. Summary of previous results on the SC of distance-matrix methods with constants omitted for clarity. MC stands for the molecular clock case. The last row of the table gives the conjectured SC of ML for comparison.

Method	$g < g^*_{\mathrm{JC}}$	$g \geq g^*_{\mathrm{JC}}$
NJ (*19*)	$1/f^2 \cdot e^{\mathrm{Diam}} \cdot \log n$	$1/f^2 \cdot e^{\mathrm{Diam}} \cdot \log n$
SQM (*17*) (+ UPGMA in MC)	$1/f^2 \cdot e^{\Delta} \cdot \log n$	$1/f^2 \cdot e^{\Delta} \cdot \log n$
Here (+ WPGMA in MC)	$1/f^2 \cdot \log n$	$1/f^2 \cdot e^{\Delta} \cdot \log n$
Conjecture for ML (best possible)	$1/f^2 \cdot \log n$	$1/f^2 \cdot e^{\Delta} \cdot \log n$

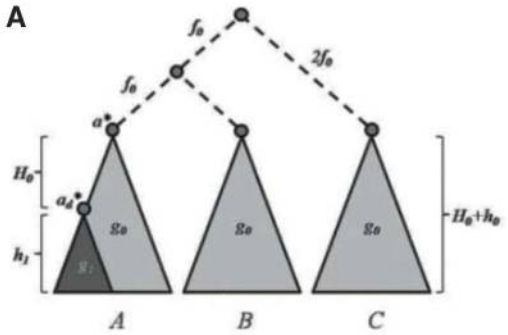

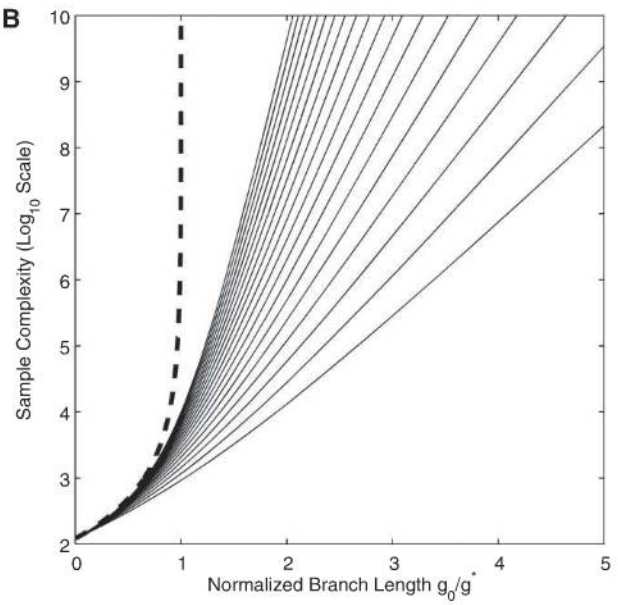

Fig. 2. **(A)** Illustrative example (not to scale) where f_0, g_0, and g_1 values are branch lengths. The H_0, h_0, and h_1 values indicate numbers of levels. The subtrees B and C are complete binary trees. The subtree A is a complete binary tree with one subtree at height H_0 replaced by a complete binary tree with h_1 levels. The top dashed subtree is referred to as the deep triplet in the text. The dark subtree is denser, that is, $g_1 < g_0$. To satisfy the molecular clock assumption, $h_1\, g_1 = h_0\, g_0$. **(B)** Sample complexity for correct reconstruction of the deep triplet in A with $h_0 = h_1 = 0$ (no dense subtree) with WPGMA at 99% confidence level. Results are shown for various tree depths H_0: from 5 (lowest curve; corresponding to $n = 3 \cdot 2^5 = 96$ terminal taxa) to 23 (highest curve; corresponding to $n = 3 \cdot 2^{23} \approx 25 \cdot 10^6$). Although f_0 and g_0 may not be the shortest and longest branch lengths, they play the roles of f and g in the analysis (*24*). A normalized branch length of 1 corresponds to $g_0 = g^*$. The effect of f is factored out by by fixing the value of f_0 to 2 (which explains the absence of the standard U-shaped form that is typical for such curves). The bold dashed line indicates the predicted sample complexity for an infinitely deep tree. The results were obtained from a Gaussian approximation with full variance-covariance matrix (*24*).

tionary distance between species a and b be given by $\hat{\delta}_u(a,b) = [1 - \hat{\Theta}(a,b)]/2$ where

$$\hat{\Theta}(a,b) = \frac{1}{k}\sum_{i=1}^{k} \sigma_i^a \sigma_i^b \qquad (4)$$

is a similarity score between sequences at a and b. A simple calculation shows that $\hat{\delta}_u$ is in fact the standard uncorrected Cavender-Farris-Neyman distance, although an extension to general time-reversible (GTR) models reveals some differences with standard distance definitions. Note that, under the molecular clock assumption, correction for back-mutations is not needed (*23*).

The choice of a reduction coefficient in Eq. (2) can be cast in a more general context by using positive weights $w(a)$, $a \in A$, and $w(b)$, $b \in B$, which sum to 1 on each OTU, and letting $\overline{\delta}_u(A,B) = [1 - \overline{\Theta}_u(A,B)]/2$ where

$$\overline{\Theta}_u(A,B) = \sum_{a\in A}\sum_{b\in B} w(a)w(b)\hat{\Theta}(a,b) \qquad (5)$$

For instance, the μ's corresponding to UPGMA and WPGMA coincide respectively with $w(a) = 1/|A|$ and $w(a) = 2^{-|a|_{a^*}}$, where $|a|_{a^*}$ is the number of branches between a and the most recent common ancestor (MRCA) a^* of A.

It is natural to choose those $w(a)$s that minimize the variance of Eq. (5). If one were to ignore the correlations between the $\hat{\Theta}(a,b)$s and use the fact that the variances of the $\hat{\Theta}(a,b)$s are identical under a molecular clock (assuming that A and B correspond to true clades), then the solution is given by the minimizer of $\sum_{a\in A} w(a)^2 \sum_{b\in B} w(b)^2$, which is simply $w(a) = 1/|A|$ and $w(b) = 1/|B|$, which shows that UPGMA would be the best choice. However, the $\hat{\Theta}(a,b)$s are, in fact, correlated, which complicates the variance minimization. To solve the problem, Eqs. (4) and (5) were combined into

$$\overline{\delta}_u(A,B) = \frac{1}{2}\left(1 - \frac{1}{k}\sum_{i=1}^{k}\left[\sum_{a\in A} w(a)^2\sigma_i^a\right]\left[\sum_{b\in B} w(b)^2\sigma_i^b\right]\right) \qquad (6)$$

The expressions in square brackets can be interpreted as linear ancestral state estimators: The value of $\sum_{a\in A} w(a)\sigma_i^a$ is a form of weighted majority vote that tends to be positive if the MRCA of A has a purine at site i and negative in the case of a pyrimidine. In other words, the distance average in the reduction step is equivalent to an implicit ancestral sequence estimation. As a result, the task of minimizing the variance of $\overline{\delta}_u(A,B)$ requires the identification of good linear ancestral estimators. Such estimators have been investigated in statistical physics, and a formula for the variance of $\sum_{a\in A} w(a)\sigma_i^a$ has been derived (*21*, *24*).

With this interpretation of the reduction step, insights about ancestral estimation were used to derive new results about distance-matrix methods. When $g < g^*_{JC}$, a particularly good choice of weights is $w(a) = 2^{-|a|_{a^*}}$—the WPGMA choice. Although these weights are not, strictly speaking,

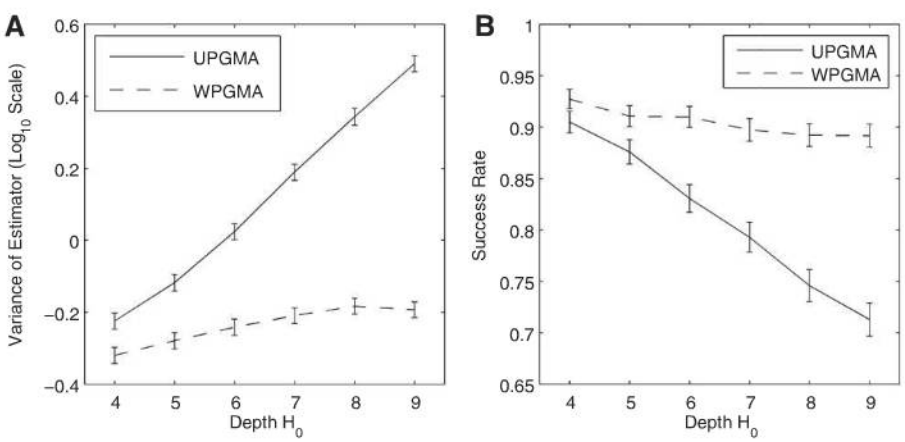

Fig. 3. On the example of Fig. 2A, a correct reconstruction of the deep triplet using UPGMA or WPGMA requires that the estimated distance between the clades A and C exceeds the estimated distance between the clades A and B, or equivalently, that $\beta = \overline{\delta}_u(A,C) - \overline{\delta}_u(A,B) > 0$. Shown is the performance of the test $\{\overline{\delta}_u(A,C) - \overline{\delta}_u(A,B) > 0?\}$ over 3000 Jukes-Cantor simulations with $h_1 = H_0$, $h_0 = 1$, $g_0 = 0.7$, $f_0 = 2$, and sequence length $k = 500$ (where the subtrees corresponding to A, B, and C are known). **(A)** The variance of the estimator β. **(B)** The success rate. Confidence intervals at 95% are shown (using an approximation by the central limit theorem).

variance minimizers, they produce a linear ancestral estimator with a relatively small (bounded) variance, no matter how deep the tree. A rigorous analysis of WPGMA on the basis of this observation showed that the asymptotically optimal SC in Eq. (3) is achieved (*24*).

In contrast, although UPGMA is expected to behave similarly to WPGMA on balanced trees, it may perform more poorly on unbalanced ones, for instance, under uneven taxon sampling (*25*). In fact, the performance of UPGMA deteriorates drastically under unbalanced conditions. Consider the idealized example of Fig. 2, where one seeks to infer a deep branching in a phylogeny containing a dense subtree. In this case, a uniform weighting of the terminal taxa disproportionately favors the dense subtree and produces, in the lower phase, an ancestral estimator of the MRCA a^*_{d} of the dense subtree rather than of the MRCA a^* of the full clade (i.e., clade A) (*26*). As a result, the long path between a^*_{d} and a^* leads to a sample complexity that scales exponentially with the depth (*24*) (Fig. 3). In comparison, WPGMA achieves the lower SC in Eq. (3) for any tree topology. In particular, the asymptotic efficiency of UPGMA relative to WPGMA tends to 0 as $\Delta \rightarrow +\infty$ (Fig. 3). In other words, ignoring the correlation structure of the distance matrix may lead to significantly poorer performance in such cases.

To extend the analysis to GTR models, a generalized sequence transformation was applied (*22*, *24*). A GTR model is specified by a reversible 4×4 substitution rate matrix Q with stationary distribution π. The rate matrix is by convention normalized so that the total rate of change per unit time at stationarity is 1, that is, $\sum_i \pi_i Q_{ii} = -1$. Let v be an eigenvector of Q corresponding to the largest negative eigenvalue $-\lambda_Q$ (normalized so that $\sum_i \pi_i v_i^2 = 1$). For each species a, define a new sequence $\sigma_1^a, \ldots, \sigma_k^a$ with $\sigma_i^a = v_{\mathrm{A}}$ (respectively, v_{G}, v_{C}, and v_{T}) if $s_i^a = \mathrm{A}$ (respectively, G, C, and T), and let the evolutionary distance between species a and b be given by Eq. (4). This transformation is justified by the fact that, in an asymptotic sense, the best linear ancestral state estimator is a function of v (*27*, *28*). In particular, the critical threshold g^*_Q can be expressed as $g^*_Q = \lambda_Q^{-1} \ln\sqrt{2}$. For instance, in the Tamura-Nei model (*29*), the critical branch length is $g^*_Q = \pi_{\mathrm{R}}\pi_{\mathrm{Y}}(1+R)\ln 2$, where $\pi_{\mathrm{R}} = \pi_{\mathrm{A}} + \pi_{\mathrm{G}}$, $\pi_{\mathrm{Y}} = \pi_{\mathrm{C}} + \pi_{\mathrm{T}}$, and R is the transition to transversion ratio (*24*). For reference, under a uniform stationary distribution with ratios $R = 2$ and $R = 10$ [ratios typical of mammalian nuclear DNA and mitochondrial DNA, respectively (*1*)], the critical branch lengths are 0.520 and 1.906.

To remove the molecular clock assumption, the corrected reduced distance matrix

$$\bar{\delta}_{\mathrm{c}}(a^*,b^*) = -\ln\left[\sum_{a\in A}\sum_{b\in B} w(a)w(b)e^{\delta(a^*,a)}e^{\delta(b^*,b)}\hat{\Theta}(a,b)\right] \quad (7)$$

was used, where a^* and b^* are respectively the roots of clusters A and B. The quantity $\delta(a^*,a)$ is the expected number of changes per site between a^* and a. It is estimated by summing the corresponding branch lengths, which are themselves estimated from previously computed $\bar{\delta}_{\mathrm{c}}$ values progressively as the tree is built (*24*). If the parenthesis above is negative [known as the saturation problem (*30*)], the logarithm is not defined. For the analysis, $\bar{\delta}_{\mathrm{c}}(a^*,b^*)$ was set to $+\infty$ in that case. Equation (7) can be interpreted as a correction-uncorrection scheme, where the reduction step is performed (inside the logarithm) with uncorrected similarity scores, as in Eq. (5); the estimate is then corrected (by taking the logarithm) for the selection step. Beyond guaranteeing consistency, this scheme presents two advantages. By averaging uncorrected distances only, exact formulas can be applied for the variances and covariances needed in designing the reduction step. Second, because the reduced distance $\bar{\delta}_{\mathrm{c}}(a^*,b^*)$ is more tightly concentrated (thanks to the variance minimization), the saturation problem is minimized. Similarly to the molecular clock case, a particularly good choice of averaging weight is $w(a) = 2^{-|a|_{a^*}}$. A further issue in removing the molecular clock assumption is that standard agglomerative schemes such as NJ suffer from a basic flaw (*20*): Typical selection criteria involve large distances—which tend to be noisy. Generalized, computationally efficient agglomerative methods were recently devised that avoid this problem with a local selection criterion, although occasionally backtracking is necessary (*31*). Alternatively, OTUs are merged at internal branches (*32*). By combining a correction-uncorrection scheme with a local agglomerative method, it was established that pairwise sequence comparisons alone achieve the SC in Eq. (3) in this more general setting as well (*24*). [For technical reasons, in the analysis of the non-clocklike case, it was assumed that the branch lengths are, roughly speaking, multiples of f (*33*).]

The SC in Eq. (3) indicates that the difference between distance- and likelihood-based methods is more subtle than a cursory analysis would suggest. Note, however, that, because the bounds examined here are asymptotic, they are mostly relevant for large-scale phylogenies. Moreover, the constants C_0, C_1, and C_2 are possibly smaller in the case of likelihood-based methods, although proof is still needed. On the other hand, because the maximum likelihood problem is rarely, if ever, solved to optimality, its actual sample complexity may be affected. Another potential advantage of maximum likelihood is that, for some substitution models, good likelihood-based ancestral estimators exist beyond g^* [up to a slightly higher threshold (*34*)], which may translate into a better SC for maximum likelihood. In the presence of noise, however, that advantage disappears (*28*). Finally, under rates-across-sites models, it is possible for topologically different trees to generate identical distributions of pairwise sequence comparisons, making them indistinguishable through distance-matrix computations (*35*); more general summary statistics are needed. Last, practical reconstruction algorithms are needed, a nontrivial task, in order to apply the theoretical insights discussed here.

References and Notes

1. J. Felsenstein, *Inferring Phylogenies* (Sinauer, Sunderland, MA, 2004).
2. N. Saitou, M. Nei, *Mol. Biol. Evol.* **4**, 406 (1987).
3. O. Gascuel, *Mol. Biol. Evol.* **14**, 685 (1997).
4. W. J. Bruno, N. D. Socci, A. L. Halpern, *Mol. Biol. Evol.* **17**, 189 (2000).
5. R. Desper, O. Gascuel, *J. Comput. Biol.* **9**, 687 (2002).
6. R. L. Graham, L. R. Foulds, *Math. Biosci.* **60**, 133 (1982).
7. B. Chor, T. Tuller, *J. ACM* **53**, 722 (2006).
8. M. A. Steel, M. D. Hendy, D. Penny, *Nature* **336**, 118 (1988).
9. M. Bulmer, *Mol. Biol. Evol.* **8**, 868 (1991).
10. E. Susko, *Mol. Biol. Evol.* **20**, 862 (2003).
11. R. Sokal, C. Michener, *Univ. Kans. Sci. Bull.* **38**, 1409 (1958).
12. P. H. A. Sneath, R. R. Sokal, *Numerical Taxonomy* (W. H. Freeman and Co., San Francisco, CA, 1973).
13. R. Mihaescu, L. Pachter, *Proc. Natl. Acad. Sci. U.S.A.* **105**, 13206 (2008).
14. J. Kim, *Syst. Biol.* **47**, 43 (1998).
15. M. A. Steel, L. A. Székely, *SIAM J. Discrete Math.* **15**, 562 (2002).
16. M. J. Schervish, *Theory of Statistics* (Springer-Verlag, New York, 1995).
17. P. L. Erdös, M. A. Steel, L. A. Székely, T. A. Warnow, *Random Struct. Algor.* **14**, 153 (1999).
18. E. Mossel, *Trans. Am. Math. Soc.* **356**, 2379 (2004).
19. K. Atteson, *Algorithmica* **25**, 251 (1999).
20. M. R. Lacey, J. T. Chang, *Math. Biosci.* **199**, 188 (2006).
21. W. S. Evans, C. Kenyon, Y. Peres, L. J. Schulman, *Ann. Appl. Probab.* **10**, 410 (2000).
22. S. Roch, *FOCS'08: Annual IEEE Symposium on Foundations of Computer Science* (IEEE Computer Society, Los Alamitos, CA, 2008), pp. 729–738.
23. A. Rzhetsky, T. Sitnikova, *Mol. Biol. Evol.* **13**, 1255 (1996).
24. Details appear in the supporting materials available on *Science* Online.
25. R. R. Sokal, P. H. A. Sneath, *Principles of Numerical Taxonomy* (W. H. Freeman and Co., San Francisco, CA, 1963).
26. E. Mossel, personal communication.
27. E. Mossel, Y. Peres, *Ann. Appl. Probab.* **13**, 817 (2003).
28. S. Janson, E. Mossel, *Ann. Probab.* **32**, (3B), 2630 (2004).
29. K. Tamura, M. Nei, *Mol. Biol. Evol.* **10**, 512 (1993).
30. D. H. Huson, K. A. Smith, T. Warnow, *WAE '99: Proceedings of the 3rd International Workshop on Algorithm Engineering* (Springer-Verlag, London, 1999), pp. 271–285.
31. C. Daskalakis, E. Mossel, S. Roch, *STOC'06: Proceedings of the 38th Annual ACM Symposium on Theory of Computing* (ACM, New York, 2006), pp. 159–168.
32. R. Mihaescu, Ph.D. thesis, University of California, Berkeley (2008).
33. C. Daskalakis, E. Mossel, S. Roch, *Probab. Theory Relat. Fields*, published online 1 October 2009 (10.1007/s00440-009-0246-2).
34. E. Mossel, *Ann. Appl. Probab.* **11**, 285 (2001).
35. M. Steel, *J. Theor. Biol.* **256**, 467 (2009).
36. This work was triggered by a discussion with E. Mossel about lower bounds for distance methods in which he pointed out that the distance matrix has a potentially useful correlation structure. I am also indebted to Y. Peres for his assistance with technical work that made the results presented here possible. I thank J. Chayes and C. Borgs from Microsoft Research, where part of this work was performed.

Supporting Online Material

www.sciencemag.org/cgi/content/full/327/5971/1376/DC1
Materials and Methods
SOM Text
Figs. S1 to S14
References

22 September 2009; accepted 21 January 2010
10.1126/science.1182300

Restriction of Receptor Movement Alters Cellular Response: Physical Force Sensing by EphA2

Khalid Salaita,[1,2,3]*† Pradeep M. Nair,[1,2,3]* Rebecca S. Petit,[1,2,3] Richard M. Neve,[4]‡ Debopriya Das,[4] Joe W. Gray,[4,5] Jay T. Groves[1,2,3,6]§

Activation of the EphA2 receptor tyrosine kinase by ephrin-A1 ligands presented on apposed cell surfaces plays important roles in development and exhibits poorly understood functional alterations in cancer. We reconstituted this intermembrane signaling geometry between live EphA2-expressing human breast cancer cells and supported membranes displaying laterally mobile ephrin-A1. Receptor-ligand binding, clustering, and subsequent lateral transport within this junction were observed. EphA2 transport can be blocked by physical barriers nanofabricated onto the underlying substrate. This physical reorganization of EphA2 alters the cellular response to ephrin-A1, as observed by changes in cytoskeleton morphology and recruitment of a disintegrin and metalloprotease 10. Quantitative analysis of receptor-ligand spatial organization across a library of 26 mammary epithelial cell lines reveals characteristic differences that strongly correlate with invasion potential. These observations reveal a mechanism for spatio-mechanical regulation of EphA2 signaling pathways.

Mammalian cells exhibit marked sensitivity to physical aspects of their environment, such as compliance (*1*), texture (*2*), and geometry (*3*). Tensional homeostasis between and within cells contributes to proper cell differentiation, development, and, ultimately, survival (*4*). Because most cellular decision making occurs via chemical processes, understanding the coupling between physical forces and chemical signaling networks is of fundamental importance. Focal adhesions, which consist of protein assemblies organized at sites where cell-surface integrin receptors bind extracellular matrix ligands, are the most widely studied interface for tensile force transduction (*5*). However, the majority of membrane receptors are not associated with focal adhesions. The mechanisms (and even existence) of chemomechanical regulatory coupling in these systems remain largely unknown.

It is becoming clear that spatial organization of cell surface receptors can regulate associated signal transduction pathways (*6*–*9*). An important corollary is that mechanical forces acting on ligands can influence receptor spatial organization and, correspondingly, signaling (*10*–*12*). Juxtacrine signaling, in which receptor and ligand reside in apposed cell membranes, represents an important class of intercellular communication where physical restriction of ligand spatial organization and movement is evident (*6*, *13*). Here, we reconstitute the juxtacrine signaling geometry between live cells expressing the EphA2 receptor tyrosine kinase and supported membranes displaying laterally mobile ephrin-A1 ligand.

EphA2 is implicated and functionally altered in a number of cancers. In particular, 40% of human breast cancers overexpress the receptor (*14*). Upon binding to natively membrane-anchored ephrin-A1, EphA2 undergoes dimerization, transphosphorylation of the cytoplasmic domains, recruitment of a molecular complex with SHC and GRB2 adaptor proteins, and subsequent activation (*15*). EphA2 activation stimulates the mitogen-activated protein kinase (MAPK) and the phosphoinositide 3-kinase pathways and recruits the c-Cbl adaptor protein and a disintegrin and metalloprotease 10 (ADAM10), both of which regulate receptor degradation (*16*, *17*). Freely soluble ephrin-A1 ligand binds to EphA2 but fails to trigger activation unless the ligand is chemically cross-linked (*18*). Despite this observation, most biological and biochemical studies of EphA2 stimulation rely on soluble variants of the ligand (*14*). We employ a supported-membrane presentation of ephrin-A1 (Fig. 1) that reveals effects of the intrinsic intermembrane physiology on the EphA2 signaling system. This presentation system allows for precise control of membrane chemical composition and lateral organization. Molecules within the supported membrane can be confined within nanoscale corrals by physical barriers to lateral mobility that are prefabricated onto the underlying substrate (*7*). In the present study, the barriers restrict ephrin-A1 transport (and, thus, EphA2 transport in the live cell) in precisely defined ways. We refer to this type of manipulation as a spatial mutation (*7*, *19*); it generates chemically identical cells that differ only by the spatial configuration of molecules within the specific signal transduction pathway under study.

A fluid supported membrane doped with 0.1% biotin-functionalized lipid was used to generate synthetic cell surfaces presenting laterally mobile ephrin-A1 (Fig. 1 and fig. S1) (*20*–*22*).

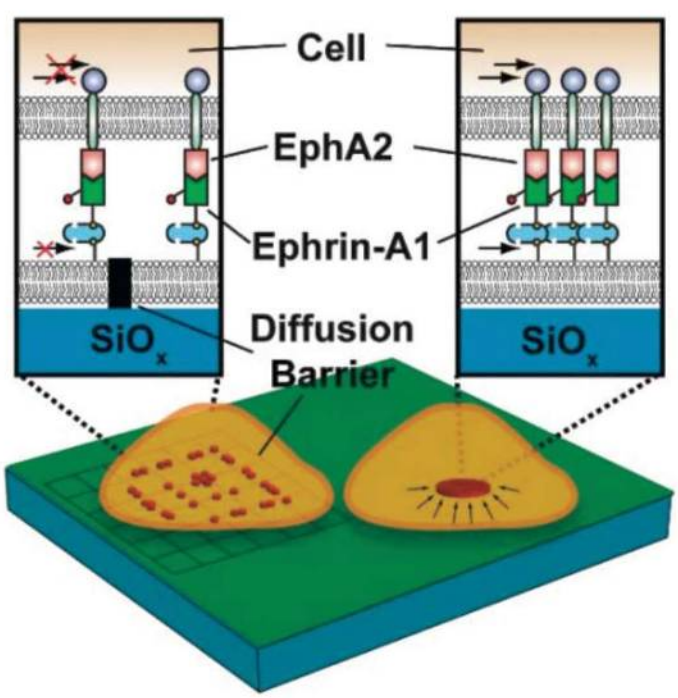

Fig. 1. Scheme of the experimental platform used to trigger and manipulate the EphA2 receptor on the surface of living cells. EphA2-expressing mammary epithelial cells are cultured onto a supported membrane displaying laterally mobile, fluorescently labeled ephrin-A1 ligand. Receptors engage ligands, form clusters that coalesce, and are transported to the center of the cell–supported membrane junction. Nanofabricated chromium metal lines 10 nm in height and 100 nm in linewidth (left cell) act as diffusion barriers and impede the transport of receptor-ligand complexes, leading to an accumulation of Eph-ephrin clusters at boundaries.

[1]Howard Hughes Medical Institute, Department of Chemistry, University of California, Berkeley, CA 94720, USA. [2]Physical Biosciences Division, Lawrence Berkeley National Laboratory, Berkeley, CA 94720, USA. [3]Materials Sciences Division, Lawrence Berkeley National Laboratory, Berkeley, CA 94720, USA. [4]Life Sciences Division, Lawrence Berkeley National Laboratory, Berkeley, CA 94720, USA. [5]Department of Laboratory Medicine and Radiation Oncology, University of California, San Francisco, CA 94143, USA. [6]Research Center of Excellence in Mechanobiology, National University of Singapore, Singapore 117543.

*These authors contributed equally to this work.
†Present address: Department of Chemistry, Emory University, 1515 Dickey Drive, Atlanta, GA 30322, USA.
‡Present address: Genentech, 1 DNA Way, South San Francisco, CA 94080, USA.
§To whom correspondence should be addressed. E-mail: jtgroves@lbl.gov

The ligand density on the membrane surface was adjusted to 800 ± 200 molecules/μm^2 (fig. S2) (*23*), which is comparable to the density of EphA2 receptors on the surface of a representative invasive breast cancer cell line, MDA-MB-231 (fig. S3). When these cells contact functionalized supported membranes, ephrin-A1 becomes organized into microclusters over the course of 15 min (Fig. 2, A and B). Dimerization and oligomerization of Eph receptors upon ligand stimulation is well-documented (*24*, *25*), and higher-order clusters, such as those we observe, have been proposed to exist on the basis of crystallographic studies of the molecular interface in Eph-ephrin complexes (*25*, *26*).

We additionally observe the microclusters to undergo inward radial transport while still bound to the supported membrane, as confirmed by live-cell fluorescence imaging and reflection interference contrast microscopy (RICM), which reveals cell-substrate contact distances (fig. S4 and movie S1) (*27*). Radial transport characteristics can be quantified for a population of cells by averaging the radial distribution of ligand underneath each cell at defined time points (Fig. 2B and fig. S5). Two-color total internal reflection fluorescence microscopy (TIRFM) tracking of ephrin-A1 and enhanced green fluorescent protein (EGFP) β-actin reveals substantial comovement between image pairs, suggesting association of the actin cytoskeleton with EphA2 clusters (fig. S6) (*22*). Further experiments with a Rho kinase inhibitor (detailed below) confirm that EphA2 transport is driven by actomyosin contractility.

The eight different EphA receptors and the five ephrin-A ligands are known to display some promiscuous interactions, but control experiments indicate that ephrin-A1 specifically binds EphA2 (*15*). First, the EphA2 receptor was highly colocalized with ephrin-A1 (fig. S7A). Additionally, when cells were pretreated with EphA2 antibodies that block the binding site for ephrin-A1, no ligand clustering or cell-surface adhesion was observed (fig. S7B). Large-scale clustering of EphA2 in live cell junctions was also observed when cells that express ephrin-A1 (ZR-75-1) and cells that express EphA2 (MDA-MB-231) were brought into contact for 30 minutes. Immunostaining of cellular junctions with antibodies specific to either ephrin-A1 or EphA2 indicated accumulation at the contact zone between cells displaying cognate receptor-ligand pairs. Such accumulations resemble those observed in cell–supported membrane experiments (Fig. 2A and fig. S8). Radial transport of receptor-ligand complex was not observed when ephrin-A1–expressing cells contacted EphA2-functionalized supported membranes (fig. S9); thus, receptor translocation is ligand-induced and driven only by the EphA2-expressing cells.

In the preceding experiments, Eph-ephrin binding provided the only physical link between the cell and the supported membrane. RICM confirmed that EphA2–ephrin-A1 clusters colocalize with the regions of closest intermembrane contact (Fig. 2C). To determine if the observed inward radial transport may be an indirect consequence of intermembrane anchoring, a cyclic RGD (Arg-Gly-Asp) peptide-lipid conjugate was included in the supported membrane (*22*). This peptide serves as a binding partner for integrins on the cell surface (*28*) and was presented as a binary mixture with ephrin-A1 on the supported membrane in varying densities. RICM images

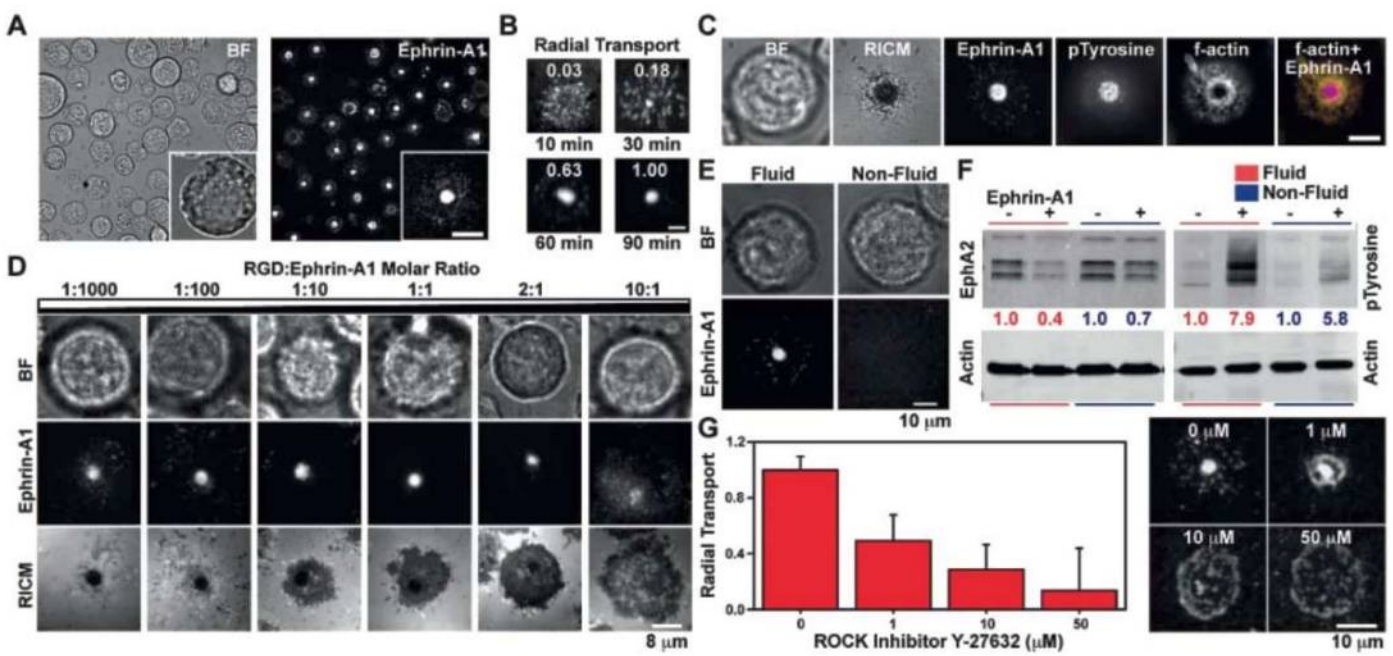

Fig. 2. Mechanical reorganization of ligand-stimulated EphA2. (**A**) Representative bright field and epifluorescence images of MDA-MB-231 cells within 1 hour of interaction with an Alexa Fluor 647–tagged ephrin-A1–functionalized supported membrane. (**B**) Dynamics of receptor-ligand reorganization as a function of time. The radial distribution of ephrin-A1 was measured under each cell, and the population average value (n = 77 cells) is indicated above the fluorescence image for each time point. (**C**) The central EphA2 cluster is the region of highest ephrin-A1 concentration, greatest tyrosine phosphorylation, and tightest cell adhesion to the substrate and results in reorganization of the actin cytoskeleton to form a peripheral annulus. Scale bar is 5 μm in (A) to (C). (**D**) Representative bright field, epifluorescence, and RICM images of cells 1 hour after plating on a supported membrane functionalized with binary mixtures of ephrin-A1 and cyclic RGD peptide. Ephrin-A1 and RGD were incubated in the molar ratios indicated above each panel and show EphA2 translocation regardless of the area of the cell–supported membrane contact. (**E**) Mechanical reorganization of EphA2 requires a fluid membrane. Bilayers composed of 99.9% DPPC and 0.1% biotin-DPPE are not fluid during cell engagement at 37°C; as a result, no long-range EphA2 reorganization is observed on DPPC bilayers. (**F**) Western blots of lysates collected from 1×10^5 cells cultured onto fluid and nonfluid membranes. Presentation of fluid ephrin-A1 results in more rapid and complete EphA2 activation than presentation of nonfluid ephrin-A1, as measured by EphA2 degradation and total phosphorylated tyrosine intensities. EphA2 bands are at a mass of ~100 kD. (**G**) When cells were treated with the Rho kinase inhibitor Y-27632, a dosage-dependent decrease in Eph-ephrin radial transport was observed (n = 627 cells), demonstrating that the cytoskeleton drives radial transport. Experiments were performed in duplicate, and radial transport was independently normalized to untreated samples from each replicate. Error bars indicate SE for at least 139 cells at each dosage.

revealed progressively larger cell–supported membrane contact areas with increasing RGD peptide density, but with no change in EphA2 organization (Fig. 2D). Immunostaining for β_1, $\alpha_V\beta_3$, and $\alpha_V\beta_5$ integrins, known markers of focal adhesions, did not show colocalization with EphA2 (fig. S10). Thus, we conclude that the radial transport of EphA2 is selective and independent of integrin-mediated adhesion and signaling.

Importantly, radial transport of ligand-stimulated EphA2 is dependent on the lateral mobility of ephrin-A1 in the supported membrane. Fully saturated 1,2-dipalmitoyl-*sn*-glycero-3 phosphocholine (DPPC) lipids form a nonfluid bilayer in the gel phase at 37°C, and ephrin-A1 displayed on these membranes (*22*) failed to exhibit microcluster formation or inward transport upon interaction with cells (Fig. 2E). This correlated with differences in EphA2 signaling as measured by receptor phosphorylation and degradation, which are hallmarks of ligand-induced activation (*16*). When identical numbers of cells (~1×10^5) were plated onto fluid and nonfluid supported membranes doped with an identical density of ephrin-A1 binding sites (1:1000 biotin-DPPE), the ephrin-A1 tethered to nonfluid DPPC membranes induced ~50% less EphA2 degradation and ~40% less tyrosine phosphorylation than did ephrin-A1 tethered to control fluid membranes (Fig. 2F). Furthermore, on fluid membranes, ephrin-A1 clusters colocalized with the areas of highest tyrosine phosphorylation, and radial transport of Eph-ephrin complexes coincided with substantial f-actin reorganization (Fig. 2C and fig. S11).

Cytoskeleton reorganization is known to result from ligand-dependent tyrosine phosphorylation of EphA2 and subsequent downstream signaling processes (*29*). This ultimately contributes to cell contact–dependent repulsion and tissue patterning (*15*). EphA2 can remodel the cytoskeleton through activation of the small guanosine triphosphatase RhoA (*30*), a process implicated in the high motility and invasive ability of malignant tumor cells (*31*). To explore the effects of this process on EphA2 transport, we used the selective Rho-associated kinase inhibitor Y-27632 to block actomyosin contractility (*32*). MDA-MB-231 cells treated with inhibitor concentrations ranging from 1 to 50 μM exhibited a dose-dependent decrease in their capacity to transport EphA2-ephrin-A1 complexes to the center of the cell–supported membrane contact junction (Fig. 2G). This observation indicates that EphA2 transport is actively driven by actomyosin contractile forces.

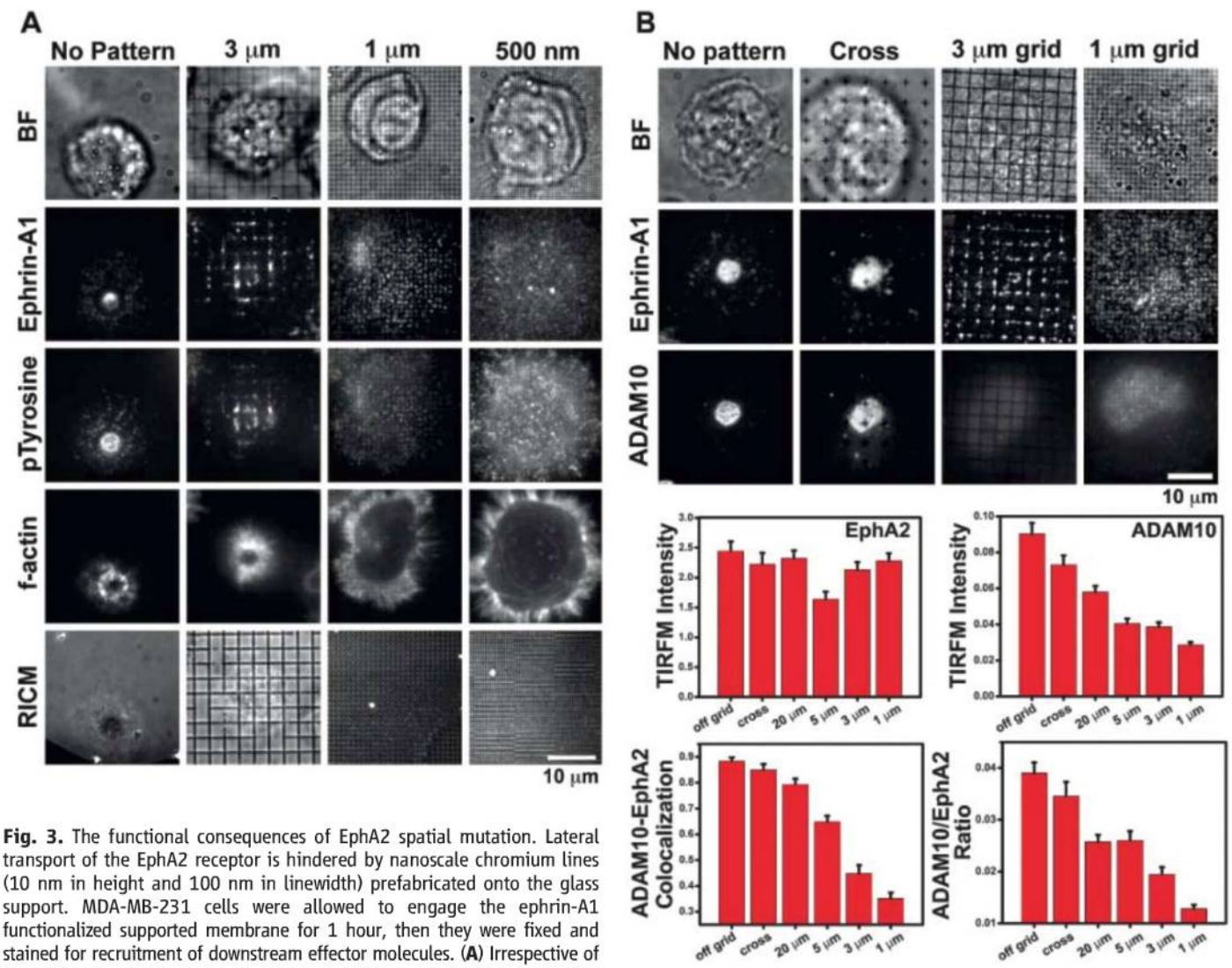

Fig. 3. The functional consequences of EphA2 spatial mutation. Lateral transport of the EphA2 receptor is hindered by nanoscale chromium lines (10 nm in height and 100 nm in linewidth) prefabricated onto the glass support. MDA-MB-231 cells were allowed to engage the ephrin-A1 functionalized supported membrane for 1 hour, then they were fixed and stained for recruitment of downstream effector molecules. (**A**) Irrespective of the presence or the scale of spatial mutations, phoshorylated tyrosine colocalized with ephrin-A1. F-actin adopted an annulus peripheral to the receptor-ligand assembly when EphA2 transport was unrestricted. However, when EphA2 organization was altered, the cytoskeleton assumed a spread morphology with f-actin primarily present in peripheral lamellipodia. The spread actin morphology switched to an annulus surrounding the EphA2-ephrin-A1 assembly when cells were exposed to 3-μm–pitch barriers. (**B**) ADAM10 colocalized with the EphA2-ephrin-A1 assembly on unrestricted supported membranes. However, when EphA2 transport was restricted by metal lines on the silica substrate, the measured colocalization decreased, and the ratio of ADAM10 to EphA2 also decreased (n = 477 cells). This indicates that mechanical restriction of EphA2 modulates ADAM10 recruitment.

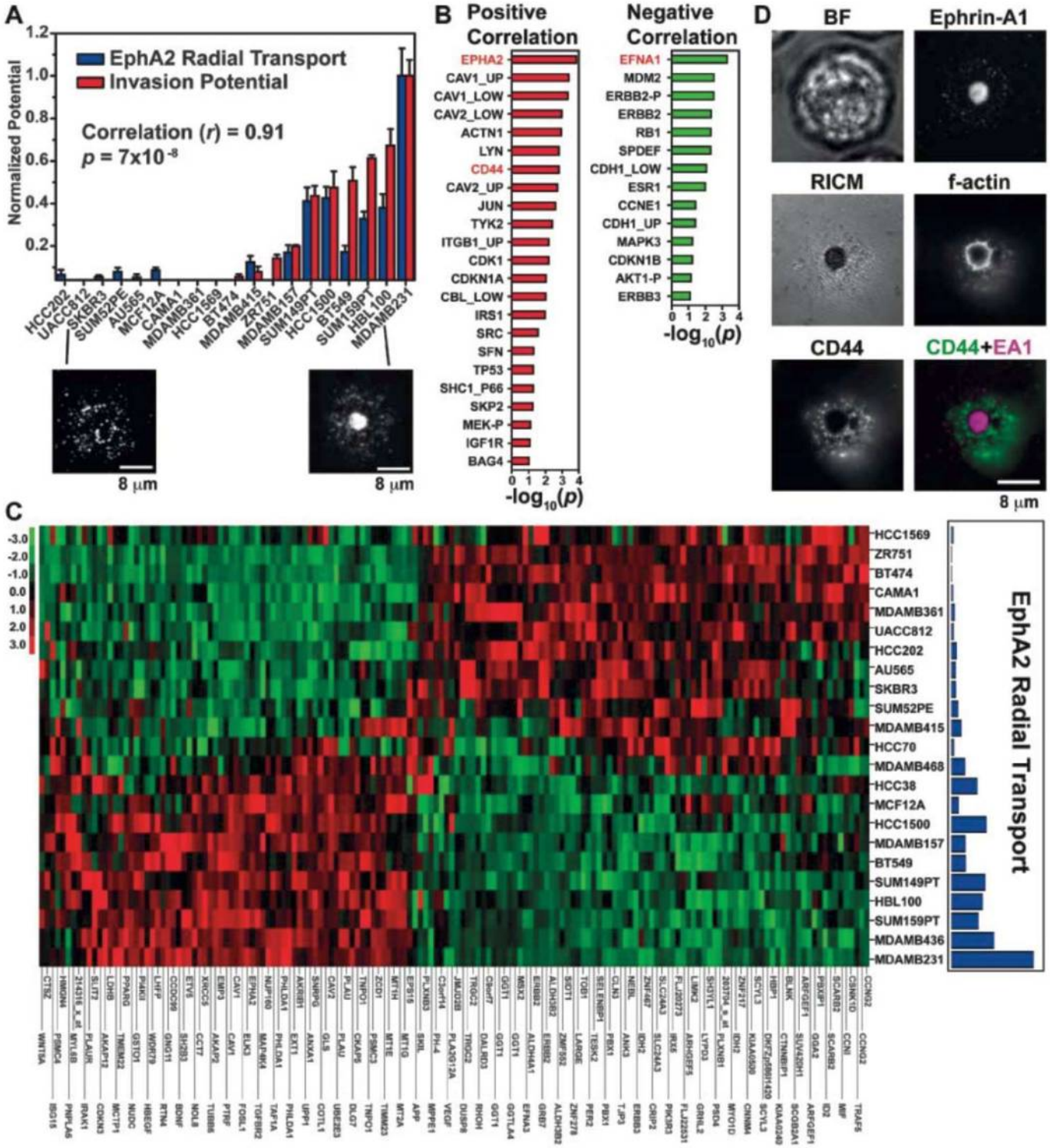

Fig. 4. Correlation of EphA2 radial transport to molecular and behavior properties in breast cancer. The average ephrin-A1 ligand radial distribution functions for 26 cell lines are quantified, parameterized, and then used as a spatial biomarker that is directly correlated to known biological characteristics and proteomic and genomic expression levels. (**A**) The average radial distribution function was found to exhibit a strong correlation ($r = 0.91$, $p = 7 \times 10^{-8}$) to invasion potentials that were determined with modified Boyden chamber analysis. (**B**) The proteomic correlates ($p < 0.1$) of EphA2 radial transport are shown in the table with their associated p values and are grouped based on the type of association (positive or negative). Proteins highlighted in red are those whose role in EphA2 reorganization has been experimentally observed. (**C**) Transcriptomic correlates ($p < 1 \times 10^{-4}$, false discovery rate $< 5 \times 10^{-3}$) of EphA2 radial transport are illustrated in a heat map. Unsupervised hierarchical clustering of expression profiles of mRNAs that are predicted to be surrogates of EphA2 radial transport shows two distinct clusters of cell lines associated with the phenotype. Red indicates up-regulated expression, whereas green indicates down-regulated expression. (**D**) Representative bright field, epifluorescence immunostaining, and RICM images of a cell 1 hour after plating on a supported membrane functionalized with ephrin-A1. The cell adhesion molecule CD44 was found to be substantially up-regulated in protein expression in cells that underwent EphA2 radial transport. This signaling molecule was also found to be antilocalized with EphA2 upon ligand-induced activation.

To examine the functional consequences of EphA2 transport, we physically manipulated EphA2 spatial organization. Supported membranes were formed on glass substrates with various patterns of metal lines (100-nm linewidth and 10-nm height) prefabricated by electron beam lithography (*22*). These create barriers to lateral transport within the supported membrane without otherwise influencing mobility or altering topography (fig. S12). Lipids and membrane-tethered proteins diffuse freely but cannot cross barriers (fig. S13) (*7*, *10*, *33*). Upon binding its supported membrane–bound ephrin-A1 ligand, the EphA2 receptor and other physically associated signaling molecules become subject to the same geometrical constraints to mobility. The approach applies physical perturbations to the living cell exclusively through specific receptor-ligand couplings, and the entire ensemble of receptors is uniformly affected. A variety of non-native EphA2 spatial configurations were generated by engaging cells with patterned membranes whose grid pitches ranged from 0.5 to 20 μm (Fig. 3). Immunofluorescence imaging of cells on grid-patterned constraints reveals that the confined EphA2 clusters remain heavily phosphorylated in all cases (unrestricted, 3-, 1-, and 0.5-μm–pitch barriers). EphA2 is locally triggered irrespective of geometrical constraint (Fig. 3A).

In contrast, the morphology of the f-actin exhibited two discrete states as a function of the degree of physical partitioning forced onto the EphA2 receptor pattern. Cells engaging membranes with 500-nm–pitch barriers displayed a spreading morphology, with f-actin primarily in peripheral lamellipodia. This behavior is similar to that observed in cells cultured on standard glass slides or on RGD-functionalized surfaces without ephrin (fig. S14). The actin morphology dramatically changed into an annulus immediately surrounding the EphA2-ephrin-A1 assembly when cells were exposed to substrates with grid barrier pitches of 3 μm or larger (Fig. 3A). These observed differences in f-actin morphology at identical ephrin-A1 densities indicate that physical resistance to EphA2 receptor transport can change the threshold for ephrin-A1–triggered cytoskeleton reorganization.

The recruitment of effector molecules such as phosphatases or proteases is one mechanism used to dampen EphA2 signaling levels. In particular, ADAM10, a zinc-dependent transmembrane protease, is implicated in the ectodomain transshedding of ephrin-As as a consequence of Eph receptor binding (*17*). ADAM10 has been shown to weakly associate with Eph receptors at the plasma membrane and to preferentially bind receptor-ligand complexes. Proteolytic cleavage by ADAM10 occurs at the extracellular domain of ephrin-As and is hypothesized to initiate release and endocytosis of the receptor-ligand complex (*17*). Disengagement of the physical tether between apposed cells is thought to play a role in the observed Eph-driven cell repulsion, rather than the cell adhesion that might be anticipated due to strong receptor-ligand binding (*14*, *17*). When cells were triggered with fluid ephrin-A1 for 1 hour and stained for ADAM10, we observed that ADAM10 was selectively recruited to the cell–supported membrane interface (Fig. 3B and figs. S5 and S15). However, when the EphA2 radial transport was mechanically hindered with metal grid patterns, ADAM10 recruitment was substantially reduced, and selective colocalization with EphA2 was abrogated at the 60-min time point (Fig. 3B). Cross-shaped metal patterns with a similar coverage area to that of the grids (4% of surface area) still allow ephrin-A1 radial transport and do not drastically affect ADAM10 recruitment. This confirms that ADAM10 recruitment can be regulated by physically interfering with EphA2 transport and is not simply diminished by the presence of metal patterns in the supported membrane.

To quantify ADAM10 recruitment to receptor-ligand complexes, TIRFM was used to measure cell surface EphA2 and ADAM10 levels of an identical set of cells ($n = 477$ cells) that displayed a range of receptor spatial mutations. Whereas the amount of EphA2 remained constant, the amount of recruited ADAM10 decreased with the size of the observed EphA2-ephrin-A1 clusters (Fig. 3B). In addition, the colocalization of ADAM10 with EphA2 (as measured by Pearson correlation coefficient r) also decreased. Control experiments with cross-shaped metal lines and 20-μm–pitch grids all confirm that these results are a consequence of receptor spatial organization and physical constraint. Cells cultured on two-component membranes displaying the cyclic RGD peptide along with ephrin-A1 displayed the same response to spatial mutations, confirming that this phenomenon is independent from RGD-mediated integrin adhesion and signaling (fig. S16).

These spatial mutation experiments demonstrate that physical manipulation of EphA2–ephrin-A1 microcluster organization alters the cellular response to ephrin-A1. There are both spatial and mechanical aspects to these results. The cell applies force, via actomyosin contractility, to ligand-engaged EphA2 receptors. According to Newton's third law, grid barriers that block EphA2 transport in the spatial mutation must necessarily exert opposing forces on the receptor clusters. Spatial organization and mechanical forces are thus interconnected, resulting in an overall sensitivity of the EphA2 signaling pathway to spatio-mechanical aspects of the cellular microenvironment in which ephrin-A1 is displayed.

To investigate the generality of ligand-induced EphA2 transport beyond the MDA-MB-231 cell line, we examined a library of breast cancer cell lines. Such cell lines derived from primary tumors have been the most widely used models to elucidate how genes and signaling pathways regulate disease progression (*34*). When a panel of cell lines is used as a system, rather than individually, it can serve as a powerful tool to identify and investigate recurrent markers for disease progression (*35*). Therefore, the propensity to radially transport the EphA2 receptor was characterized in 26 cell lines (*22*, *34*). An aliquot of ~50×10^3 cells was plated onto ephrin-A1–functionalized supported membranes for 1 hour for each cell line. Live-cell fluorescence microscopy was used to image the resulting distribution of ligand under individual cells, and a signature radial distribution function was determined for each cell line type. Radial transport was not unique to MDA-MB-231; rather, each cell line tested displayed a distinct and characteristic degree of ligand-induced receptor reorganization (fig. S17). The diversity observed in EphA2 transport between different cell lines may result from the wide range of deregulations inherent to this library, as well as variance in EphA2 expression levels. To quantify the EphA2 radial transport phenotype, we parameterized the radial distribution functions for each cell line using linear regression, integration of area under the curve, and the ratio of peak-height to peak-width at half-maximum at time $t = 60$ min (fig. S18). These different scoring methods were robust and led to very similar values across the cell-line library.

To identify the molecular signature of this spatial organization phenotype, we next performed large-scale analyses using the wealth of available data for the panel of cell lines (*22*). In these analyses, the measured radial transport scores serve as an unconventional spatial biomarker unique to each cell line and potentially associated with genomic, proteomic, or phenotypic signatures in neoplasia. Invasion potentials, as measured using a modified Boyden chamber assay (*34*), were strongly linked (Pearson correlation $r = 0.91$, $p = 7 \times 10^{-8}$) to the receptor radial transport phenotype across the library (Fig. 4A). In contrast, EphA2 mRNA and protein expression levels did not correlate as strongly with invasion potentials, and the correlation values (r) were 0.64 and 0.53, respectively, in agreement with previous reports (*34*, *36*). EphA2 translocation is distinct from expression, and a stronger degree of association is found between the scored receptor radial transport phenotype and invasion potentials across the breast cancer model, suggesting a link between EphA2 radial transport and tissue invasion. Additionally, a system-wide correlation of the spatial organization scores to protein and mRNA expression levels revealed 37 proteins ($p < 0.1$) and 141 mRNA transcripts ($p < 1 \times 10^{-4}$, 158 probe sets) that are associated with this phenotype (Fig. 4, B and C, and tables S1 and S2). Searches of the Kyoto Encyclopedia of Genes and Genomes and BioCarta pathway analysis databases (*37*) revealed that radial transport was associated with the ErbB, p53, integrin, and MAPK signaling pathways (tables S3 and S4). Notably, all of these pathways have been previously reported to associate with invasiveness and EphA2 signaling; we now show that they also associate with EphA2 spatial organization (*36*).

One of the proteins identified through this screen was CD44, a cell membrane-bound glycoprotein involved in cell adhesion and migration (*38*). The spatial organization of CD44 upon ephrin-A1 stimulation was found to antilocalize with the assembly of EphA2 (Fig. 4D), validating the involvement of CD44 in cell-driven EphA2 receptor reorganization. The system-wide correlation analysis does not necessarily provide the mechanistic details leading to EphA2 sorting; instead, it identifies proteins and genes that may serve as surrogate markers to centripetal transport.

In conclusion, we report a spatio-mechanical regulation of the EphA2 signaling pathway. Upon membrane-bound ligand stimulation, EphA2 is transported radially inwards by an actomyosin contractile process. Physical interference with this transport, which necessarily involves the imposition of opposing forces on EphA2, alters ligand-induced EphA2 activation as observed by the recruitment of the protease ADAM10 and cytoskeleton morphology. Quantitative measurement of centripetal receptor transport across a library of mammary epithelial cell lines reveals a high correlation with invasion potential and with specific gene and protein expression. These observations suggest that spatio-mechanical aspects of ephrin-A1 expressing cells and their surrounding tissue environment may functionally alter the response of EphA2 signaling systems and could play a contributing role in the onset and progression of cancer.

References and Notes

1. D. E. Discher, P. Janmey, Y.-l. Wang, *Science* **310**, 1139 (2005).
2. M. J. Dalby *et al.*, *Nat. Mater.* **6**, 997 (2007).
3. C. M. Nelson, M. M. VanDuijn, J. L. Inman, D. A. Fletcher, M. J. Bissell, *Science* **314**, 298 (2006).
4. D. T. Butcher, T. Alliston, V. M. Weaver, *Nat. Rev. Cancer* **9**, 108 (2009).
5. C. S. Chen, *J. Cell Sci.* **121**, 3285 (2008).
6. S. Y. Qi, J. T. Groves, A. K. Chakraborty, *Proc. Natl. Acad. Sci. U.S.A.* **98**, 6548 (2001).
7. K. D. Mossman, G. Campi, J. T. Groves, M. L. Dustin, *Science* **310**, 1191 (2005).
8. N. L. Andrews *et al.*, *Nat. Cell Biol.* **10**, 955 (2008).
9. S. Hurtley, *Science* **326**, 1205 (2009).
10. N. C. Hartman, J. A. Nye, J. T. Groves, *Proc. Natl. Acad. Sci. U.S.A.* **106**, 12729 (2009).
11. J. D. Scott, T. Pawson, *Science* **326**, 1220 (2009).
12. R. O. Hynes, *Science* **326**, 1216 (2009).
13. T. Marquardt *et al.*, *Cell* **121**, 127 (2005).
14. M. Lackmann, A. W. Boyd, *Sci. Signal.* **1**, re2 (2008).
15. K. Kullander, R. Klein, *Nat. Rev. Mol. Cell Biol.* **3**, 475 (2002).
16. J. Walker-Daniels, D. J. Riese II, M. S. Kinch, *Mol. Cancer Res.* **1**, 79 (2002).
17. P. W. Janes *et al.*, *Cell* **123**, 291 (2005).
18. S. Davis *et al.*, *Science* **266**, 816 (1994).
19. J. T. Groves, *Curr. Opin. Chem. Biol.* **10**, 544 (2006).
20. J. T. Groves, N. Ulman, S. G. Boxer, *Science* **275**, 651 (1997).
21. J. M. Nam, P. M. Nair, R. M. Neve, J. W. Gray, J. T. Groves, *ChemBioChem* **7**, 436 (2006).
22. Materials and methods are available as supporting material on *Science* Online.
23. W. J. Galush, J. A. Nye, J. T. Groves, *Biophys. J.* **95**, 2512 (2008).
24. J.-P. Himanen *et al.*, *Nature* **414**, 933 (2001).
25. B. Day *et al.*, *J. Biol. Chem.* **280**, 26526 (2005).
26. J. P. Himanen *et al.*, *Nat. Neurosci.* **7**, 501 (2004).
27. H. Verschueren, *J. Cell Sci.* **75**, 279 (1985).
28. J. D. Humphries, A. Byron, M. J. Humphries, *J. Cell Sci.* **119**, 3901 (2006).
29. N. Carter, T. Nakamoto, H. Hirai, T. Hunter, *Nat. Cell Biol.* **4**, 565 (2002).
30. M. L. Taddei *et al.*, *Am. J. Pathol.* **174**, 1492 (2009).
31. P. Friedl, K. Wolf, *Nat. Rev. Cancer* **3**, 362 (2003).
32. P. P. Provenzano, D. R. Inman, K. W. Eliceiri, S. M. Trier, P. J. Keely, *Biophys. J.* **95**, 5374 (2008).
33. J. T. Groves, S. G. Boxer, *Acc. Chem. Res.* **35**, 149 (2002).
34. R. M. Neve *et al.*, *Cancer Cell* **10**, 515 (2006).
35. T. Vargo-Gogola, J. M. Rosen, *Nat. Rev. Cancer* **7**, 659 (2007).
36. M. Macrae *et al.*, *Cancer Cell* **8**, 111 (2005).
37. G. Dennis Jr. *et al.*, *Genome Biol.* **4**, P3 (2003).
38. H. Ponta, L. Sherman, P. A. Herrlich, *Nat. Rev. Mol. Cell Biol.* **4**, 33 (2003).

39. We thank N. Bayani for assistance in performing Western blotting, A. Smoligovets and C.-H. Yu for performing transfection and imaging with EGFP-actin–expressing MDA-MB-231 cells, and A. Bershadsky for helpful discussions. This work was supported by the Director, Office of Science, Office of Basic Energy Sciences, Chemical Sciences, Geosciences, and Biosciences Division (K.S., P.M.N.; hybrid synthetic-live cell interfaces) and the Materials Sciences and Engineering Division (R.S.P.; supported membrane substrates) of the U.S. Department of Energy (DOE) under contract no. DE-AC02-05CH11231. Patterned substrate fabrication was performed, in part, at the Molecular Foundry, Lawrence Berkeley National Laboratory (LBNL), and was supported by the Office of Science, Office of Basic Energy Sciences, Scientific User Facilities Division, of the U.S. DOE under contract no. DE-AC02-05CH11231. This work was also supported by the Laboratory Directed Research and Development Program of LBNL under U.S. DOE contract no. DE-AC02-05CH11231. Seed support for biomedical aspects of this work was provided by the U.S. Department of Defense Breast Cancer Research Program Concept Award BC076701 under U.S. Army Medical Research Acquisition Activity no. W81XWH-08-1-0677, with follow-on support provided by Award U54 CA143836 from the National Cancer Institute (NCI) beginning in 2009. The content is solely the responsibility of the authors and does not necessarily represent the official views of the NCI or the NIH. J.W.G. acknowledges support from the Director, Office of Science, Office of Biological and Environmental Research, of the DOE under conract no. DE-AC02-05CH11231; the NIH; NCI grant P50 CA 58207; and the NIH NCI Integrative Cancer Biology Program grant number U54 CA 112970 to J.W.G. (bioinformatics and cell lines). The Regents of the University of California have filed a related patent application through LBNL.

Supporting Online Material

www.sciencemag.org/cgi/content/full/327/5971/1380/DC1
Materials and Methods
Figs. S1 to S18
Tables S1 to S4
References
Movie S1

9 September 2009; accepted 13 January 2010
10.1126/science.1181729

Lgr6 Marks Stem Cells in the Hair Follicle That Generate All Cell Lineages of the Skin

Hugo J. Snippert,[1]* Andrea Haegebarth,[1]* Maria Kasper,[2] Viljar Jaks,[2] Johan H. van Es,[1] Nick Barker,[1] Marc van de Wetering,[1] Maaike van den Born,[1] Harry Begthel,[1] Robert G. Vries,[1] Daniel E. Stange,[1] Rune Toftgård,[2] Hans Clevers[1]†

Mammalian epidermis consists of three self-renewing compartments: the hair follicle, the sebaceous gland, and the interfollicular epidermis. We generated knock-in alleles of murine *Lgr6*, a close relative of the *Lgr5* stem cell gene. *Lgr6* was expressed in the earliest embryonic hair placodes. In adult hair follicles, Lgr6+ cells resided in a previously uncharacterized region directly above the follicle bulge. They expressed none of the known bulge stem cell markers. Prenatal Lgr6+ cells established the hair follicle, sebaceous gland, and interfollicular epidermis. Postnatally, Lgr6+ cells generated sebaceous gland and interfollicular epidermis, whereas contribution to hair lineages gradually diminished with age. Adult Lgr6+ cells executed long-term wound repair, including the formation of new hair follicles. We conclude that Lgr6 marks the most primitive epidermal stem cell.

In the adult skin, interfollicular epidermis (IFE) and sebaceous glands (SGs) are subject to constant self-renewal, whereas hair follicles (HFs) cycle between growth, involution, and resting phases (fig. S1) (*1*). Under normal conditions, these three skin cell populations are each believed to be maintained by their own discrete stem cells (*2*). When tissue homeostasis is disrupted, however, any of the three stem cell populations is capable of producing all three structures (*2*, *3*). The IFE can be maintained without the recruitment of stem cells from the HF bulge (*4*–*8*), yet the exact identification of IFE stem cells has remained elusive. Within the SG, progenitors reportedly maintain this structure independent of the HF (*5*, *9*). HF stem cells

[1]Hubrecht Institute–KNAW (Royal Netherlands Academy of Arts and Sciences) and University Medical Center Utrecht, Uppsalalaan 8, 3584 CT Utrecht, Netherlands. [2]Karolinska Institutet, Center for Biosciences and Department of Biosciences and Nutrition, Novum, SE-141 57 Huddinge, Sweden.

*These authors contributed equally to this work.
†To whom correspondence should be addressed. E-mail: h.clevers@hubrecht.eu

reside in the bulge, express CD34 and cytokeratin 15 (*10*–*12*), and retain DNA or histone labels (*13*–*15*). However, stem cells may reside in other areas of the HF as well (*16*–*19*).

We recently identified *Lgr5* [leucine-rich repeat–containing G protein (heterotrimeric guanine nucleotide–binding protein)–coupled receptor 5] as a marker of cycling stem cells in the intestine (*20*). Subsequently, we demonstrated that *Lgr5* marks HF stem cells, which over very long periods of time contribute to all hair lineages but not to the SG or IFE (*21*). A closely related gene exists in the mammalian genome, *Lgr6* (*22*). To evaluate a potential involvement of *Lgr6* in stem cell biology, we obtained *LacZ*- and *EGFP-Ires-CreERT2* (where EGFP is enhanced green fluorescent protein and Ires is internal ribosomal entry site) knock-in alleles (*23*) (figs. S1 and S2). Both integrations create null alleles. Homozygous mice of both strains were healthy and fertile. In adult *Lgr6LacZ* and *EGFP-Ires-CreERT2* knock-in mice, we noticed prominent expression in rare cells in brain, mammary gland, lung, and skin. In the latter tissue, in situ hybridization confirmed the pattern observed with the knock-in alleles (Fig. 1 and figs. S1 to S3). *Lgr6* was first observed around embryonic day 14.5 (E14.5) (Fig. 1A). Expression was evident throughout the epithelial compartment of placodes, whereas the epidermis was entirely negative (Fig. 1B). Lgr6 is thus one of the earliest placode markers, resembling *Sonic Hedgehog* (*24*) and *Sox9* (*25*). *Lgr6* expression persisted during hair peg development (Fig. 1C and fig. S2C). The resulting hair breaks through the overlying epidermis postnatally. Lgr6+ cells appeared in the IFE coincident with the emergence of hair (Fig. 1D and fig. S2D), suggesting an origin in the developing follicles. Epidermal *Lgr6* expression peaked around postnatal day 7 to 15 (P7 to P15) and then became gradually more restricted, with expression persisting within adult HFs on the back and tail throughout life (Fig. 1, E and F, and fig. S2, E to I).

Detailed analysis in the first (P20) and second (P56) resting states (telogen) revealed that *Lgr6* marked a unique population, located directly above the CD34 and keratin 15–positive bulge (Figs. 1G and 2A and fig. S1). Lgr6 cells did not retain the DNA label 5-bromo-2′-deoxyuridine (BrdU) (fig. S4). MTS24 and Lrig1 (upper-isthmus markers) (*17*, *19*) and Blimp1 (SG) (*9*) showed limited overlap with the tight Lgr6 cell cluster (Figs. 1, H and I, and 2A and fig. S1). Analysis of LacZ staining in telogen follicles of *Lgr4* (*26*), *Lgr5* (*20*), and *Lgr6* LacZ knock-in mice confirmed that *Lgr6* marked the central isthmus directly above the bulge, whereas *Lgr4* expression was present in both the Lgr5+ and the Lgr6+ domains (Fig. 2B).

In agreement with our findings, gene expression profiles of late embryonic (E17.5) HF stem cells revealed *Lgr5* and *Lgr6* at the top of the enriched-gene list (*27*). We directly compared gene expression profiles of sorted $Lgr5^{high}$ and $Lgr6^{high}$ cells isolated from P20 dorsal skin. As expected, the Lgr5 population was strongly enriched for bulge markers such as CD34 (Fig. 2C). The only gene in the Lgr6 profile implicated in stem cell biology and HF development was *Tnfrsf19/Troy* (*28*, *29*). Another gene, *Il1r2*, marks cells at a corresponding position below the SGs in human HFs (*30*). Thus, Lgr6 marked a unique, tight cell cluster at the central isthmus of the HF (Fig. 2B). Of note, although embryonic expression in nascent whiskers resembled that of other hair follicle types, no Lgr6+ zone was established postnatally at the equivalent location (fig. S9).

To study lineage relationships of Lgr6+ cells, we intercrossed *Lgr6-EGFP-Ires-CreERT2* with the Cre reporter *R26R-LacZ* mice. Without tamoxifen, we essentially noted no leakiness of *Cre* activity. Single tamoxifen injections facilitated genetic tracing of Lgr6+ cells and their offspring. We first genetically marked Lgr6+ cells at E17.5, when Lgr6 expression is restricted to hair pegs (fig. S5A). Subsequent postnatal LacZ stainings were performed at various phases of the hair cycle. In all cases, widespread labeling of all three skin compartments was observed (Fig. 3B and fig. S5).

When lineage tracing was induced at P20, sporadic single LacZ-labeled cells first became visible at P23 (Fig. 3A). The overwhelming majority of labeled cells still appeared at the isthmus,

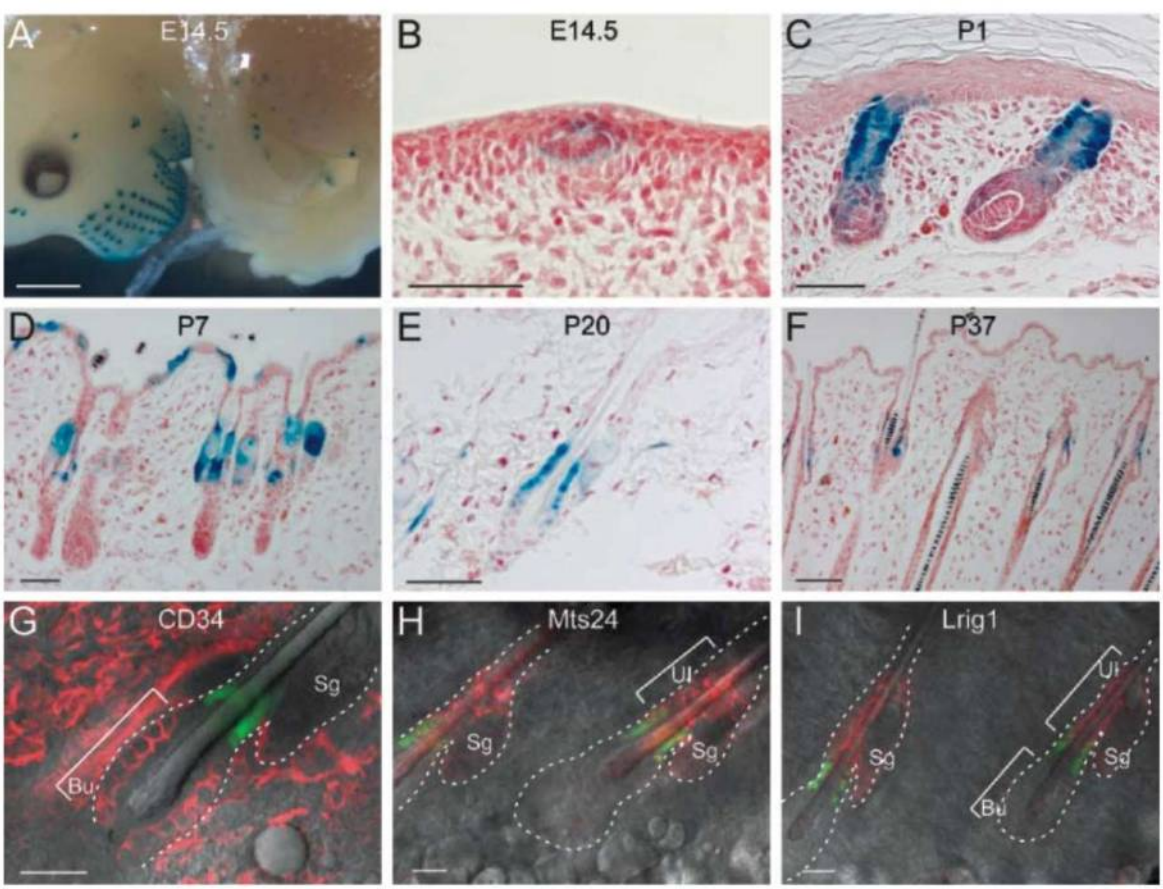

Fig. 1. Lgr6 is expressed in early hair progenitor cells and becomes restricted to a limited number of cells at the central isthmus. (**A**) Whole-mount picture of a *Lgr6-LacZ* embryo at E14.5. Scale bar indicates 500 μm. (**B** to **F**) Cross sections of dorsal skin from *Lgr6-LacZ* knock-in mice obtained at various developmental stages (E14.5, P1, P7, P20, and P37, respectively) reveal restricted *Lgr6* expression (blue) above the bulge. Scale bars, 50 μm. Confocal microscopy reveals limited overlap with known hair follicle stem cell markers (in red) CD34 (**G**), Mts24 (**H**), and Lrig1 (**I**) in *Lgr6-EGFP-Ires-CreERT2* mice analyzed at telogen stages. Scale bars, 25 μm. Bu, bulge; Sg, sebaceous gland; and UI, upper isthmus.

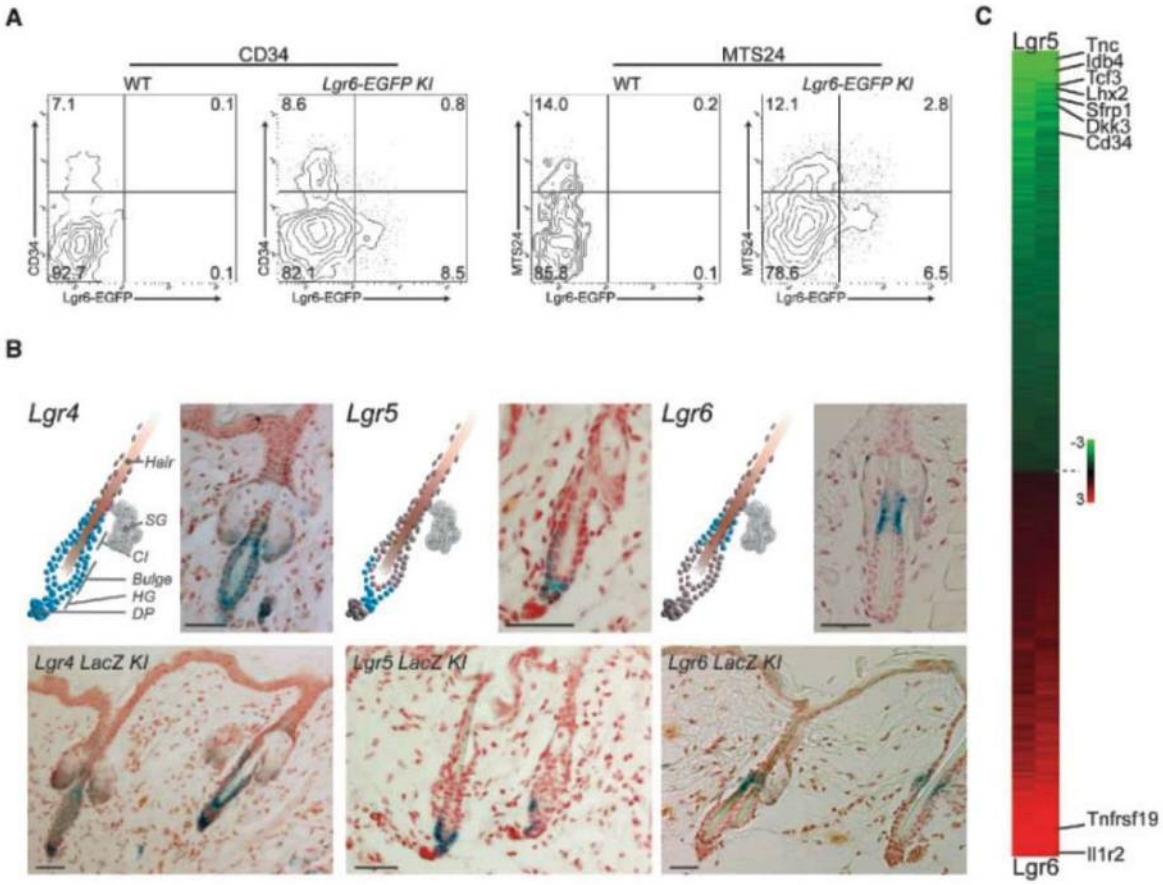

Fig. 2. Lgr6 marks a different stem cell population than Lgr5/CD34+ HF stem cells. (**A**) Fluorescence-activated cell sorting (FACS) analysis at first telogen reveals that Lgr6+ cells are largely distinct from CD34+ cells and MTS24+ cells. WT, wild type. (**B**) Expression analysis of *Lgr* family members illustrates that Lgr5 HF stem cells are located at the bulge (*21*), whereas *Lgr4* has a wider expression pattern, including the tight cluster of Lgr6+ stem cells at the central isthmus. Scale bar, 50 μm. CI, central isthmus; HG, hair germ; and DP, dermal papilla. (**C**) Gene expression analysis of Lgr5+ HF stem cells and Lgr6+ stem cells further indicates that Lgr6 marks a separate population with no overlap of bulge HF stem cells. Color scale bar represents $\log_2$ differences.

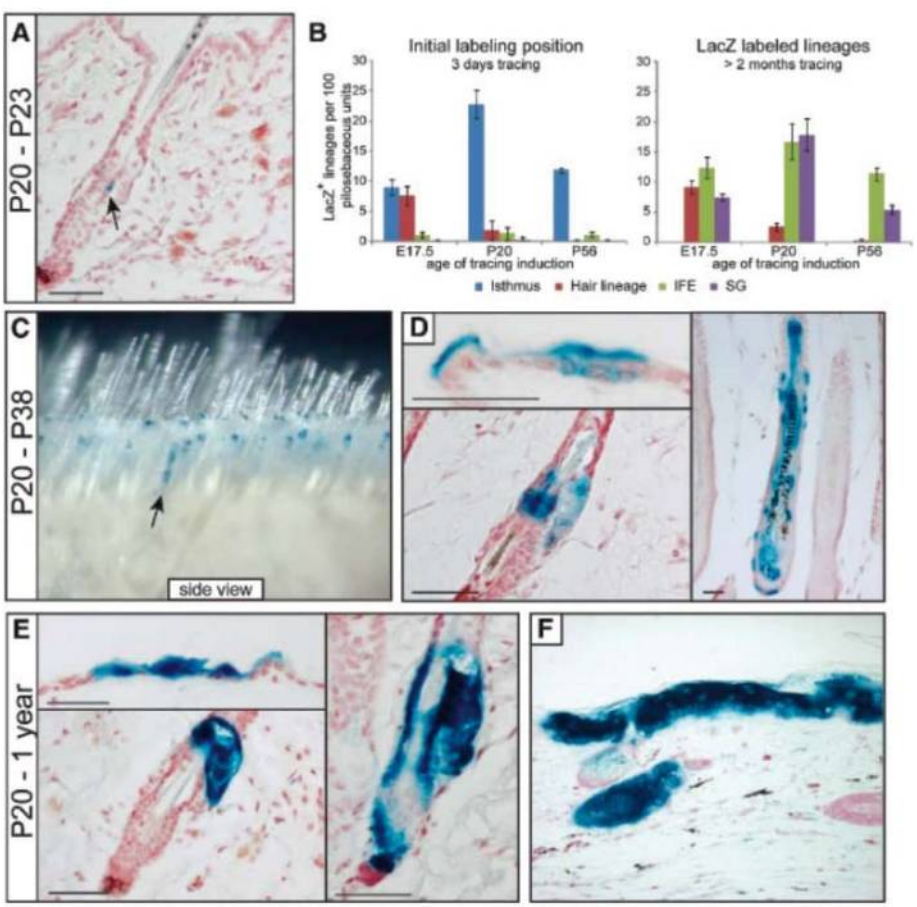

Fig. 3. After hair morphogenesis, Lgr6+ stem cells predominantly generate SGs and epidermis. Scale bars histochemistry (HC), 50 μm. (**A**) LacZ staining (arrow) in dorsal skin, first visible after 3 days of tracing. (**B**) Quantification of lineage tracing from Lgr6 stem cells initiated at E17.5, P20, and P56, respectively. (Left) In postnatal mice, the vast majority of lineage tracings (~90%) originate in the isthmus. (Right) Tracing events remain constant over time and Lgr6 stem cells persistently generate IFE and SG, whereas HF potential diminishes with age of the mice. Error bars indicate standard deviation. (**C** to **E**) LacZ analysis of dorsal skin from *Lgr6-EGFP-Ires-CreERT2/R26R-LacZ* mice after CreERT2 induction at P20. Analysis during anagen at P38 [(C) and (D)] or after >1 year (E) with whole-mount microscopy or HC, respectively. Lgr6+ stem cells persistently trace toward epidermal [(D) and (E), upper left images], SG lineages [(D) and (E), lower left images], and occasional HF [(D) and (E), right images]. (**F**) HC analysis of transplanted Lgr6+/LacZ+ stem cells onto backs of nude mice confirmed multipotency.

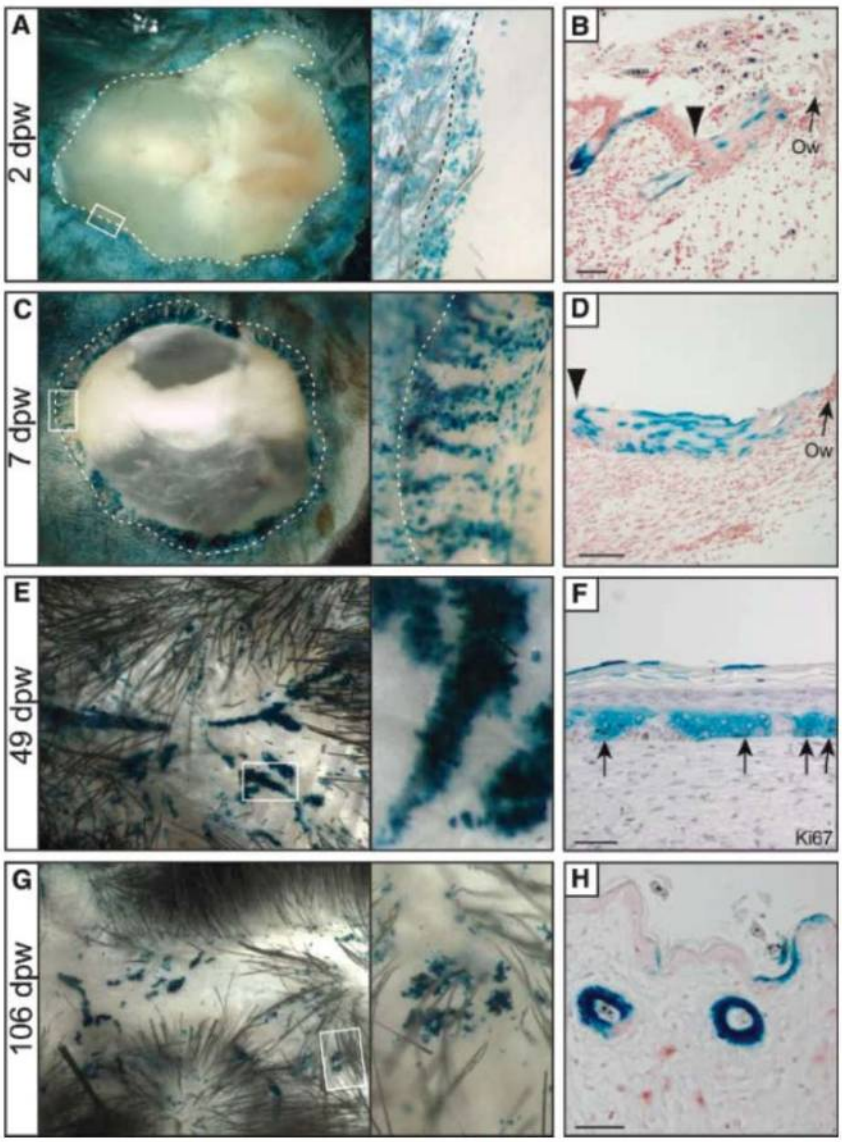

Fig. 4. Lgr6+ stem cells permanently contribute to wound healing, including hair neogenesis. (**A**) Top view of a wound in dorsal skin 2 days postwounding (dpw). White dashed line marks edge of the wound. Incision was made at day P25, 5 days after tracing initiation. Right image is magnification of the area marked by the white box. (**B**) Cross section of the wound reveals marked progeny migrating into the wound. Black arrowhead points to the edge of the wound. Scale bars IHC, 50 μm; Ow, open wound. (**C** and **D**) As in (A) and (B), dorsal wound 7 dpw. (**E** and **F**) As in (A) and (B), 49 dpw Lgr6+ stem cells made persistent contributions. Ki67+ basal layer of scar tissue is Lgr6-derived (black arrows). (**G** and **H**) As in (A) and (B). After >100 dpw, Lgr6 progeny is still present within the wound. Moreover, newly formed hairs within the wound are occasionally LacZ positive.

implying limited mobility in the intervening 3-day period (Fig. 3B). When analyzed 18 days after induction, blue clones were observed in SGs, the IFE, and, to a lesser extent, in the hair (Fig. 3, C and D). Even after >1 year, extensive lineage tracing was readily observed (Fig. 3E and fig. S6). Tracing induced at P56, the second telogen phase, yielded identical observations, albeit HF potential was further diminished (Fig. 3B and fig. S7). Quantification of lineage tracing initiated at E17.5, P20, or P56 underscored that, in virtually all cases, labeling was restricted to single cells in the isthmus 3 days after induction (Fig. 3B). Contribution to SG and IFE was relatively constant between E17.5, P20, and P56, whereas the contribution to the hair decreased with age (Fig. 3B).

In order to further document the stemness potential, we transplanted Lgr6+ stem cells, isolated at first telogen, onto the backs of nude mice. As expected, Lgr6+ cells reconstituted fully formed HFs. Multipotency of donor stem cells was confirmed by activating the *R26R-LacZ* locus in vivo 4 days before isolation. A small subset of Lgr6+ stem cells became LacZ-positive and contributed, once transplanted, to all skin lineages (Fig. 3F and fig. S6F).

The contribution of Lgr6+ cells to wound repair was assessed by inducing lineage tracing at first telogen (P20), followed by excision of 1 cm^2 of full-thickness back skin 5 days later. Lgr6 progeny was traced over >3 months after wounding. As observed previously when bulge stem cells were LacZ-labeled (*6*), convergent bands of blue cells emanated from the border of the wound and migrated toward its center (Fig. 4, A to D). Such bands originating from HF bulge stem cells disappear by 20 days postwounding (*6*). The blue clones derived from Lgr6+ cells involved cells in the basal layer of the wound epithelium (Fig. 4, E and F), whereas the clones persisted for >3 months within the newly formed epidermis. As reported by Cotsarelis and colleagues (*31*), HF growth occurred de novo within the wound epithelium. When scored in a 60- and 100-days postwounding mouse, about 10% of these new HFs were derived from LacZ-marked Lgr6+ stem cells (3 in 34 and 4 in 31, respectively), comparable to the estimated percentage of surface area comprising LacZ-marked keratinocytes in the same wounds (7% and 11%, respectively) (Fig. 4, G and H, and fig. S8).

Our study identifies Lgr6 as a marker for a distinct population of stem cells giving rise to all lineages of the skin. Unlike the *Lgr5* gene, we found no evidence that *Lgr6* is controlled by Wnt signaling. This is in agreement with the notion that the active hair lineage in the lower bulge requires Wnt signaling, whereas the sebaceous and epidermal lineages are Wnt-independent (*2*). A picture thus emerges in which a Wnt-independent Lgr6 stem cell pool can renew sebaceous cells and seed the epidermis throughout life, whereas a Wnt-dependent Lgr5 stem cell pool derives from the Lgr6 pool early in life but then becomes relatively independent.

References and Notes

1. L. Alonso, E. Fuchs, *J. Cell Sci.* **119**, 391 (2006).
2. E. Fuchs, V. Horsley, *Genes Dev.* **22**, 976 (2008).
3. V. Levy, C. Lindon, Y. Zheng, B. D. Harfe, B. A. Morgan, *FASEB J.* **21**, 1358 (2007).
4. S. Claudinot, M. Nicolas, H. Oshima, A. Rochat, Y. Barrandon, *Proc. Natl. Acad. Sci. U.S.A.* **102**, 14677 (2005).
5. S. Ghazizadeh, L. B. Taichman, *EMBO J.* **20**, 1215 (2001).
6. M. Ito *et al.*, *Nat. Med.* **11**, 1351 (2005).
7. V. Levy, C. Lindon, B. D. Harfe, B. A. Morgan, *Dev. Cell* **9**, 855 (2005).
8. E. Clayton *et al.*, *Nature* **446**, 185 (2007).
9. V. Horsley *et al.*, *Cell* **126**, 597 (2006).
10. C. S. Trempus *et al.*, *J. Invest. Dermatol.* **120**, 501 (2003).
11. C. Blanpain, W. E. Lowry, A. Geoghegan, L. Polak, E. Fuchs, *Cell* **118**, 635 (2004).
12. R. J. Morris *et al.*, *Nat. Biotechnol.* **22**, 411 (2004).
13. G. Cotsarelis, T. T. Sun, R. M. Lavker, *Cell* **61**, 1329 (1990).
14. K. M. Braun *et al.*, *Development* **130**, 5241 (2003).
15. T. Tumbar *et al.*, *Science* **303**, 359 (2004); published online 11 December 2003 (10.1126/science.1092436).
16. M. Ito, K. Kizawa, K. Hamada, G. Cotsarelis, *Differentiation* **72**, 548 (2004).
17. J. G. Nijhof *et al.*, *Development* **133**, 3027 (2006).
18. U. B. Jensen *et al.*, *J. Cell Sci.* **121**, 609 (2008).
19. K. B. Jensen *et al.*, *Cell Stem Cell* **4**, 427 (2009).
20. N. Barker *et al.*, *Nature* **449**, 1003 (2007).
21. V. Jaks *et al.*, *Nat. Genet.* **40**, 1291 (2008).
22. T. Van Loy *et al.*, *Gen. Comp. Endocrinol.* **155**, 14 (2008).
23. Materials and methods are available as supporting material on *Science* Online.
24. S. Iseki *et al.*, *Biochem. Biophys. Res. Commun.* **218**, 688 (1996).
25. V. P. Vidal *et al.*, *Curr. Biol.* **15**, 1340 (2005).
26. G. Van Schoore, F. Mendive, R. Pochet, G. Vassart, *Histochem. Cell Biol.* **124**, 35 (2005).
27. H. Rhee, L. Polak, E. Fuchs, *Science* **312**, 1946 (2006).
28. L. G. van der Flier *et al.*, *Cell* **136**, 903 (2009).
29. J. Pispa, M. Pummila, P. A. Barker, I. Thesleff, M. L. Mikkola, *Hum. Mol. Genet.* **17**, 3380 (2008).
30. M. Kasper *et al.*, *Mol. Cell. Biol.* **26**, 6283 (2006).
31. M. Ito *et al.*, *Nature* **447**, 316 (2007).

32. We acknowledge M. Cozijnsen, J. Korving, Å. Bergström, Å. Dackland, and Hubrecht Imaging Centre for technical help and support. This work was supported by the Koningin Wilhelmina Fonds and a European Research Council grant to H.C., a European Molecular Biology Organization Long-Term Fellowship to A.H., and by grants from the Swedish Cancer Society and the Swedish Research Council to R.T. A patent is pending on work with Lgr5 and Lgr6 (A.H., N.B., and H.C.). GEO microarray accession number is GSE20269.

Supporting Online Material

www.sciencemag.org/cgi/content/full/327/5971/1385/DC1
Materials and Methods
Figs. S1 to S9
References

16 November 2009; accepted 10 February 2010
10.1126/science.1184733

Structural Sources of Robustness in Biochemical Reaction Networks

Guy Shinar[1] and Martin Feinberg[2]*

In vivo variations in the concentrations of biomolecular species are inevitable. These variations in turn propagate along networks of chemical reactions and modify the concentrations of still other species, which influence biological activity. Because excessive variations in the amounts of certain active species might hamper cell function, regulation systems have evolved that act to maintain concentrations within tight bounds. We identify simple yet subtle structural attributes that impart concentration robustness to any mass-action network possessing them. We thereby describe a large class of robustness-inducing networks that already embraces two quite different biochemical modules for which concentration robustness has been observed experimentally: the *Escherichia coli* osmoregulation system EnvZ-OmpR and the glyoxylate bypass control system isocitrate dehydrogenase kinase-phosphatase–isocitrate dehydrogenase. The structural attributes identified here might confer robustness far more broadly.

Biological systems require robustness, that is, the capacity for sustained and precise function even in the presence of structural or environmental disruption (*1*–*11*). Examples of robustness exist over multiple scales of biological organization, from the biochemical circuit level [robust exact adaptation in bacterial chemotaxis (*2*–*4*)] to the cellular level [robustness of metabolic functions to changes caused by mutations (*12*)].

A biological system shows absolute concentration robustness (ACR) for an active molecular species if the concentration of that species is identical in every positive steady state the system might admit. The function of an ACR-possessing system is thereby protected even against large changes in the overall supply of the system's components.

[1]Department of Molecular Cell Biology, Weizmann Institute of Science, Rehovot 76100, Israel. [2]William G. Lowrie Department of Chemical and Biomolecular Engineering and Department of Mathematics, Ohio State University, 125 Koffolt Laboratories, 140 West 19th Avenue, Columbus, OH 43210, USA.

*To whom correspondence should be addressed. E-mail: feinberg@chbmeng.ohio-state.edu

We identify simple yet subtle structural attributes that will impart ACR to any mass-action network that includes them. We provide a mathematical theorem that precisely delineates a very large class of ACR-possessing systems, a class that embraces networks that differ in size, detail, and complexity. This class contains different ACR-possessing models (*9*, *11*) of known examples for which approximate concentration robustness has been verified experimentally. We thus uncover an underlying mathematical unity found at the heart of robustness-producing mechanisms that are biochemically quite different.

To elucidate the concept of ACR, we first consider the toy two-species mass-action system

$$\begin{aligned} A + B &\xrightarrow{\alpha} 2B \\ B &\xrightarrow{\beta} A \end{aligned} \qquad (1)$$

where A is the active form of a protein, B is the inactive form, and α and β are rate constants. Suppose the protein is synthesized and degraded over long time scales, so that the total protein concentration can be regarded as constant over the system's equilibration time scale. Under this assumption, the differential equations governing the time evolution of the molar concentrations of A and B, denoted c_A and c_B, are

$$\begin{aligned} \dot{c}_A &= -\alpha c_A c_B + \beta c_B \\ \dot{c}_B &= \alpha c_A c_B - \beta c_B \end{aligned} \qquad (2)$$

The positive steady states of Eq. 2 are given by

$$\begin{aligned} c_A &= \frac{\beta}{\alpha} \\ c_B &= \Theta - \frac{\beta}{\alpha} \end{aligned} \qquad (3)$$

where Θ is the conserved total protein concentration: $\Theta = c_A + c_B = c_A(0) + c_B(0)$. Eq. 3 shows that system (1) has ACR: There is a positive steady state for each value of Θ exceeding β/α, and in each of these steady states c_A has precisely the same value.

In contrast, consider the simple module

$$A \underset{\beta}{\overset{\alpha}{\rightleftarrows}} B \qquad (4)$$

Here, the positive steady states are given by

$$\begin{aligned} c_A &= \frac{\beta\Theta}{\alpha+\beta} \\ c_B &= \frac{\alpha\Theta}{\alpha+\beta} \end{aligned} \qquad (5)$$

The steady state values of both c_A and c_B are proportional to the conserved total concentration $\Theta = c_A + c_B$. Thus, as Θ varies, both c_A and c_B vary in step. The system does not have ACR.

To state our main result, we require some terminology from chemical reaction network theory (*13*–*16*). The display in Fig. 1A is an example of a standard reaction diagram, that is, a directed graph whose nodes (*17*) are the distinct linear combinations of chemical species that sit at the heads and tails of the reaction arrows. In Fig. 1A, the chemical species are A, B, C, D, E, and F,

and the nodes are 2A, B, C, B + C, D, 2B, A + E, and F. Note that in a standard reaction diagram each node appears precisely once.

The standard reaction diagram in Fig. 1A is made of two disconnected pieces, one containing the mutually linked nodes 2A, B, and C and the other containing the mutually linked nodes B + C, D, 2B, A + E, and F (Fig. 1B). Such sets of mutually linked nodes are called the linkage classes of the network. The number of linkage classes is identical to the number of pieces of which the standard reaction diagram is composed.

We say that two nodes are strongly linked if there is a directed arrow path from one to the other and also a directed arrow path from the second back to the first. Thus, the nodes A + E and F in Fig. 1A are strongly linked because there is a directed arrow path from A + E to F, namely A + E → F, and also a directed arrow path from F back to A + E, namely F → 2B → A + E. We adopt the convention that each node is strongly linked to itself.

A strong-linkage class of a reaction network is a maximal subset of its nodes that are strongly linked to each other. The parts of Fig. 1B that are surrounded by dashed outlines correspond to the strong-linkage classes in our example network. A terminal strong-linkage class is a strong-linkage class in which no node reacts to a node in another strong-linkage class. (We say that one node reacts to another node whenever the first sits at the tail and the second sits at the head of the same reaction arrow.) Nodes belonging to terminal strong-linkage classes are called terminal (pink in Fig. 1B). Nodes that are not terminal are called nonterminal (blue in Fig. 1B).

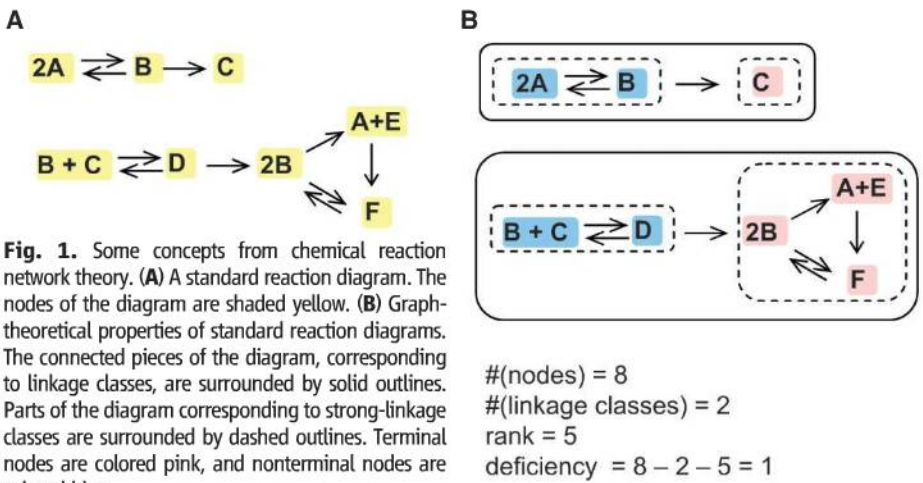

Fig. 1. Some concepts from chemical reaction network theory. (**A**) A standard reaction diagram. The nodes of the diagram are shaded yellow. (**B**) Graph-theoretical properties of standard reaction diagrams. The connected pieces of the diagram, corresponding to linkage classes, are surrounded by solid outlines. Parts of the diagram corresponding to strong-linkage classes are surrounded by dashed outlines. Terminal nodes are colored pink, and nonterminal nodes are colored blue.

By the rank of a reaction network we mean the maximum number of linearly independent reactions that the network contains. We can make this precise in the following way: With each reaction, we associate a reaction vector (*18*) obtained by subtracting the reactant node from the product node. Thus, we associate with reaction 2A → B the reaction vector B – 2A; with B → 2A we associate the reaction vector 2A – B; and so on. The five reaction vectors, B – 2A, D – B – C, 2B – D, A + E – 2B, and F – A – E, constitute a linearly independent set, and every other reaction vector for the network of Fig. 1A can be written as a linear combination of these. Thus, the rank of the network is five.

In formulating the reaction vector for a given reaction, we have subtracted the reactant node from the product node. In fact, we shall be interested in the difference of any two nodes, even those that belong to different reactions. For example, the difference of the nodes B + C and B is B + C – B = C. If, as in this example, the difference of two nodes is a nonzero multiple of a single species S, we say that the nodes "differ only in species S."

Next, we introduce the important concept of deficiency. The deficiency of a network is an integer index obtained by subtracting both the number of linkage classes and the rank from the number of nodes. For the network of Fig. 1 the deficiency is one, because there are eight nodes, two linkage classes, and its rank is five. The deficiency of a network will invariably be a nonnegative integer (*13*). The relationship between the size and the deficiency of a network is at best weak; very large networks often have very low deficiency.

Lastly, a mass-action system is said to have "absolute concentration robustness in species S" if the system admits a positive steady state and if in all positive steady states the concentration of S is the same.

We now have the vocabulary required for stating our main result, which is proved (section S3) in the supporting online material (SOM). Motivation for the proof (section S2) and generalizations (section S4) of the theorem are discussed there as well. A software implementation of the theorem is available for download (*19*).

Theorem: Consider a mass-action system that admits a positive steady state and suppose that the deficiency of the underlying reaction network is one. If, in the network, there are two

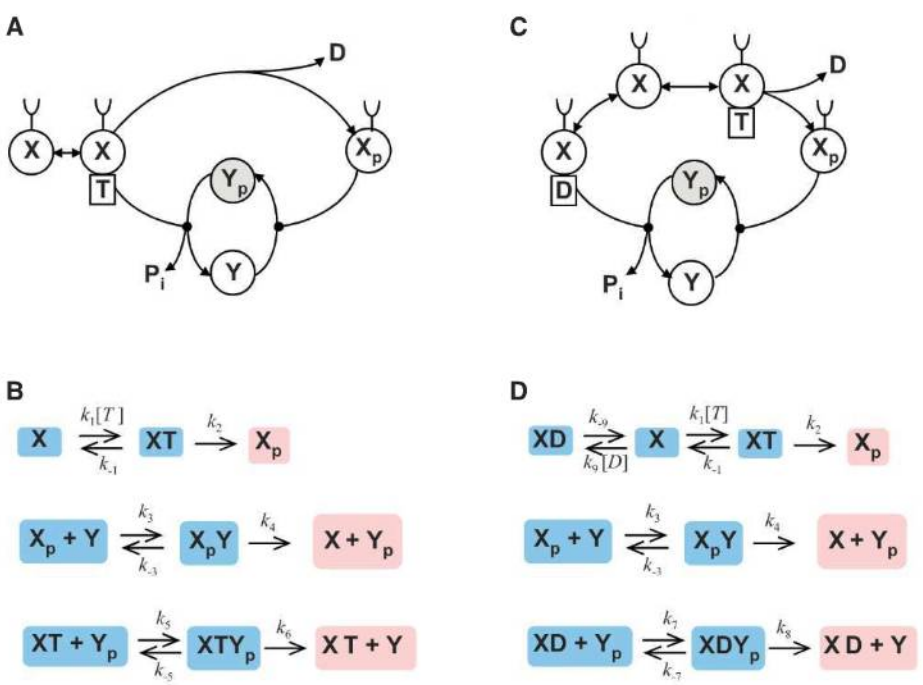

Fig. 2. The EnvZ-OmpR system. (**A**) A schematic diagram of an EnvZ-OmpR model in which ATP is the cofactor in phospho-OmpR dephosphorylation. P_i denotes phosphate ion. (**B**) The mass-action model underlying (A). [*T*] denotes the ATP concentration, assumed fixed. Terminal nodes are colored pink, and nonterminal nodes are colored blue. (**C**) A schematic diagram of an EnvZ-OmpR model in which ADP is the cofactor in phospho-OmpR dephosphorylation. (**D**) The mass-action model underlying (C). [*D*] denotes the ADP concentration, assumed fixed.

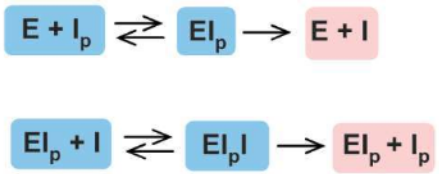

Fig. 3. A core ACR module in a model of the IDHKP-IDH system. Terminal nodes are colored pink, and nonterminal nodes are colored blue.

nonterminal nodes that differ only in species S, then the system has absolute concentration robustness in S.

The theorem becomes false if the requirement that the deficiency be one is dropped. In fact, there are networks with a deficiency of two that otherwise satisfy all the conditions of the theorem for which ACR obtains and still others for which ACR does not obtain. Moreover, no mass-action system with a deficiency of zero that is consistent with mass conservation can exhibit ACR relative to any species (*20*).

We now turn to applications of the theorem, beginning with a model of a prototypical two-component signaling system (*21*, *22*), for which approximate concentration robustness has been observed experimentally (*7*). The *Escherichia coli* EnvZ-OmpR system consists of the sensor kinase EnvZ, denoted X in Fig. 2A, and the response-regulator OmpR, denoted Y. Both the sensor and the response-regulator have phosphorylated forms, denoted X_p and Y_p. X phosphorylates itself by binding and breaking down adenosine triphosphate (ATP) (T in Fig. 2) (*21*, *22*), X_p catalyzes the transfer of a phosphoryl group to free Y (*21*, *22*), and X, together with ATP (*23*, *24*) or adenosine diphosphate (ADP) (D in Fig. 2) (*25*) as a cofactor, dephosphorylates Y_p. The crucial chemical species in the system is Y_p, a transcription factor that regulates the expression of various protein pores.

The EnvZ-OmpR module has been modeled (*9*) by using the differential equations derived from the mass-action kinetic system of Fig. 2B, where the effects of ADP as a dephosphorylation cofactor have been neglected. Note that the underlying network and its corresponding differential equations conserve the total concentrations Θ_X and Θ_Y of X-containing and Y-containing species. Analysis (*9*) of the mass-action equations indicates that, in all positive steady states (corresponding to various combinations of the parameters Θ_X and Θ_Y), the concentration of Y_p depends solely on rate constants (*9*). Thus, the mass-action model of Fig. 2B exhibits ACR in Y_p.

To apply the theorem to Fig. 2B, we note that the network has nine nodes and three linkage classes. It is not difficult to verify that the rank of the network is five. Therefore, the deficiency of the network is $9 - 3 - 5 = 1$. Moreover, the nodes $XT + Y_p$ and XT are nonterminal, and they differ only in the species Y_p. Thus, the theorem asserts that, if the mass-action model shown in Fig. 2B admits a positive steady state (as it does), then the model has ACR in Y_p. This is consistent with the earlier ad hoc analysis (*9*). The theorem also ensures ACR for a network model, displayed in Fig. 2D (*25*, *26*), in which ADP, rather then ATP, is the dominant cofactor (*27*, *28*) for Y_p dephosphorylation. This and other model variants are treated in the SOM (Section S5).

ACR also obtains in the mass-action model of Fig. 3 (*11*), which lies at the core of more elaborate models for the *E. coli* IDHKP-IDH glyoxylate bypass regulation system. [Approximate concentration robustness has been observed experimentally (*1*) in this system.] Here, I denotes the active, unphosphorylated TCA cycle enzyme isocitrate dehydrogenase (IDH). The inactive, phosphorylated form is denoted I_p. E denotes the bifunctional enzyme IDH kinase-phosphatase (IDHKP). The deficiency is again one: The network has six nodes, two linkage classes, and a rank of three, and there are two nonterminal nodes, $EI_p + I$ and EI_p, that differ only in the species I. Thus, the theorem asserts that, if a positive steady state exists (as it does), then the model has ACR in I.

The EnvZ-OmpR and IDHKP-IDH systems both use bifunctional enzymes that act simultaneously as a kinase and a phosphatase. This observation highlights the connection between the biological implementation of ACR-possessing modules and the theorem's requirement for two nonterminal nodes that differ only in a species. If the dephosphorylation reaction in Fig. 2B were catalyzed by some phosphatase Z and not by XT, we would replace the third piece in the network of Fig. 2B with $Z + Y_p \rightleftarrows ZY_p \rightarrow Z + Y$. The resulting network would cease to have two nonterminal nodes that differ only in a species, and the theorem would not apply. In fact, ACR would be lost.

The mass-action models discussed here freely invoke irreversible reactions. The omitted reverse reactions generally have rate constants so small that, for practical purposes, the reactions themselves can be safely ignored. In such instances, the reduced model is deemed to be an approximate but reliable guide to the behavior of a fuller mass-action system with some or all of the reverse reactions included. In particular, it is reasonable to expect that the fuller model would exhibit strong but imperfect robustness. These considerations are discussed more fully in the SOM (section S6).

Lastly, we emphasize that the ideal of absolute concentration robustness is unlikely to be attained exactly for in vivo experimental systems, where biochemical modules do not exist by themselves and often interact with the intracellular environment. Therefore, complete reaction network models for experimental systems should not be expected to exhibit ACR exactly. Nevertheless, the theorem presented here describes a general class of core subnetworks, which, taken by themselves, do give rise to ACR and which, to the extent that they approximate their more completely articulated parent networks, may confer on the fuller systems imperfect yet strong robustness.

References and Notes

1. D. C. LaPorte, P. E. Thorsness, D. E. Koshland Jr., *J. Biol. Chem.* **260**, 10563 (1985).
2. N. Barkai, S. Leibler, *Nature* **387**, 913 (1997).
3. U. Alon, M. G. Surette, N. Barkai, S. Leibler, *Nature* **397**, 168 (1999).
4. T. M. Yi, Y. Huang, M. I. Simon, J. Doyle, *Proc. Natl. Acad. Sci. U.S.A.* **97**, 4649 (2000).
5. A. Levchenko, P. A. Iglesias, *Biophys. J.* **82**, 50 (2002).
6. A. Eldar *et al.*, *Nature* **419**, 304 (2002).
7. E. Batchelor, M. Goulian, *Proc. Natl. Acad. Sci. U.S.A.* **100**, 691 (2003).
8. M. Kollmann, L. Løvdok, K. Bartholomé, J. Timmer, V. Sourjik, *Nature* **438**, 504 (2005).
9. G. Shinar, R. Milo, M. R. Martínez, U. Alon, *Proc. Natl. Acad. Sci. U.S.A.* **104**, 19931 (2007).
10. A. Csikász-Nagy, O. S. Soyer, *J. R. Soc. Interface* **5** (suppl. 1), S41 (2008).
11. G. Shinar, J. D. Rabinowitz, U. Alon, *PLOS Comput. Biol.* **5**, e1000297 (2009).
12. J. A. de Visser *et al.*, *Evolution* **57**, 1959 (2003).
13. M. Feinberg, *Lectures on Chemical Reaction Networks—Written Version of Lectures Delivered at the Mathematics Research Center, University of Wisconsin, Madison*, www.che.eng.ohio-state.edu/~FEINBERG/LecturesOnReactionNetworks/ (1979).
14. M. Feinberg, *Chem. Eng. Sci.* **42**, 2229 (1987).
15. M. Feinberg, *Arch. Ration. Mech. Anal.* **132**, 311 (1995).
16. G. Craciun, Y. Tang, M. Feinberg, *Proc. Natl. Acad. Sci. U.S.A.* **103**, 8697 (2006).
17. What we call "nodes" in the present paper are termed "complexes" in the chemical reaction network theory literature.
18. The reaction vectors reside in the vector space of all formal linear combinations of species.
19. E. Eden, G. Shinar, Reaction Network Analyzer V1.0, www.weizmann.ac.il/mcb/UriAlon/people/GuyShinar/index.html (2009).
20. G. Shinar, U. Alon, M. Feinberg, *SIAM J. Appl. Math.* **69**, 977 (2009).
21. L. Pratt, T. J. Silhavy, in *Two-Component Signal Transduction*, J. A. Hoch, T. J. Silhavy, Eds. (American Society for Microbiology, Washington, DC, 1995), pp. 105–127.
22. A. M. Stock, V. L. Robinson, P. N. Goudreau, *Annu. Rev. Biochem.* **69**, 183 (2000).
23. M. M. Igo, A. J. Ninfa, J. B. Stock, T. J. Silhavy, *Genes Dev.* **3**, 1725 (1989).
24. W. Hsing, T. J. Silhavy, *J. Bacteriol.* **179**, 3729 (1997).
25. Y. Zhu, L. Qin, T. Yoshida, M. Inouye, *Proc. Natl. Acad. Sci. U.S.A.* **97**, 7808 (2000).
26. According to (*25*), ADP participates in phospho-OmpR dephosphorylation by stimulating phosphoryl hydrolysis, not by serving as a substrate in ATP reconstitution.
27. S. Sanowar, H. Le Moual, *Biochem. J.* **390**, 769 (2005).
28. Experiments on the PhoP-PhoQ two-component system suggest that phospho-PhoQ dephosphorylation by PhoP is stimulated by ADP, not by the ATP analog p[NH]ppA (*27*).

29. We are grateful to U. Alon for comments, insight, and support; E. Eden for writing the software implementation of the theorem; and A. Cohen, G. Enciso, R. Kishony, D. Koster, M. Laub, A. Mayo, R. Milo, and J. Rabinowitz for their help. Supported by NSF grant BES-0425459, NIH grant 1R01GM086881-01, and the Kahn Family Foundation.

Supporting Online Material

www.sciencemag.org/cgi/content/full/327/5971/1389/DC1
SOM Text
Figs. S1 and S2
References

15 October 2009; accepted 12 February 2010
10.1126/science.1183372

In Crystallo Posttranslational Modification Within a MauG/Pre–Methylamine Dehydrogenase Complex

Lyndal M. R. Jensen,[1] Ruslan Sanishvili,[2] Victor L. Davidson,[3] Carrie M. Wilmot[1]*

MauG is a diheme enzyme responsible for the posttranslational modification of two tryptophan residues to form the tryptophan tryptophylquinone (TTQ) cofactor of methylamine dehydrogenase (MADH). MauG converts preMADH, containing monohydroxylated βTrp^{57}, to fully functional MADH by catalyzing the insertion of a second oxygen atom into the indole ring and covalently linking βTrp^{57} to βTrp^{108}. We have solved the x-ray crystal structure of MauG complexed with preMADH to 2.1 angstroms. The c-type heme irons and the nascent TTQ site are separated by long distances over which electron transfer must occur to achieve catalysis. In addition, one of the hemes has an atypical His-Tyr axial ligation. The crystalline protein complex is catalytically competent; upon addition of hydrogen peroxide, MauG-dependent TTQ synthesis occurs.

Diversity of the cellular proteome is created by genetically encoded polypeptides and their subsequent chemical modification. Most posttranslational modifications (such as phosphorylation, glycosylation, and ubiquitination) occur at the protein surface, enabling direct contact between the processing enzyme and the site of modification. In contrast, protein cofactors essential for function often require in situ modification of amino acids buried within a protein. The formation of some of these is autocatalytic, such as the fluorophore in green fluorescent protein, but others require external enzymes (*1*). MauG is a diheme enzyme (*2*) that completes synthesis of the catalytic cofactor tryptophan tryptophylquinone (TTQ) (*3*) from two Trp residues in the β-polypeptide chain of methylamine dehydrogenase (MADH), a metabolic enzyme of methylotrophic and autotrophic bacteria (*4*). In MADH from *Paracoccus denitrificans*, two oxygen atoms are incorporated into the indole ring of βTrp^{57} and a covalent bond is formed between the indole rings of βTrp^{57} and βTrp^{108} (Scheme 1) (*5*).

The natural substrate for MauG is a 119-kD protein precursor of MADH (preMADH) with monohydroxylated βTrp^{57} and no cross-link (*6*, *7*). PreMADH can be generated by expression of recombinant MADH in the background of a *mauG* deletion (*6*). MauG catalyzes a six-electron oxidation to complete TTQ biosynthesis (*8*). Oxidizing equivalents may be provided by three moles of either O_2 (plus an electron donor) or H_2O_2 (*8*, *9*). As such, the overall reaction can be viewed as three two-electron oxidations (of unknown order) to catalyze (i) insertion of an OH group at C6 of βTrp^{57}, (ii) formation of the cross-link between βTrp^{57} and βTrp^{108}, and (iii) oxidation of the quinol to the quinone. MauG contains two c-type hemes, the diferric form being the resting state. The hemes are covalently bound to the protein and have a His ligand to the iron. Typically, c-type hemes function as electron transfer mediators or catalytically in certain peroxidases, and indeed there is a sequence relationship between MauG and bacterial diheme cytochrome c peroxidases (diheme CCPs) (*10*). However, unlike diheme CCPs or other c-type hemes, MauG can activate molecular oxygen and forms an unprecedented diheme *bis*-Fe(IV) intermediate that is catalytically competent (*11*). This intermediate is composed of an Fe(IV)=O (ferryl) heme with the second oxidizing equivalent stored as Fe(IV) at the second heme. It is an intriguing alternative to Compound I, an Fe(IV)=O heme/porphyrin cation radical, which is the activated oxygen species required for cytochrome P450 and heme-dependent peroxidase–catalyzed chemistry (*12*, *13*).

The x-ray crystal structure of the MauG-preMADH complex of *P. denitrificans* has been determined to 2.1 Å resolution (fig. S1 and table S1) (*14*). The asymmetric unit consists of two molecules of MauG and one of preMADH (Fig. 1A) forming a 203.6-kD complex. MADH is an $\alpha_2\beta_2$

Scheme 1. Overall reaction catalyzed by MauG.

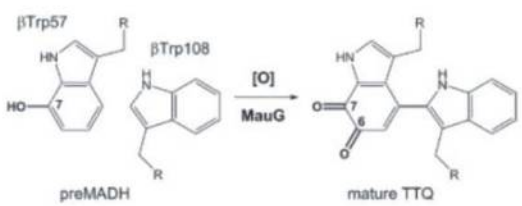

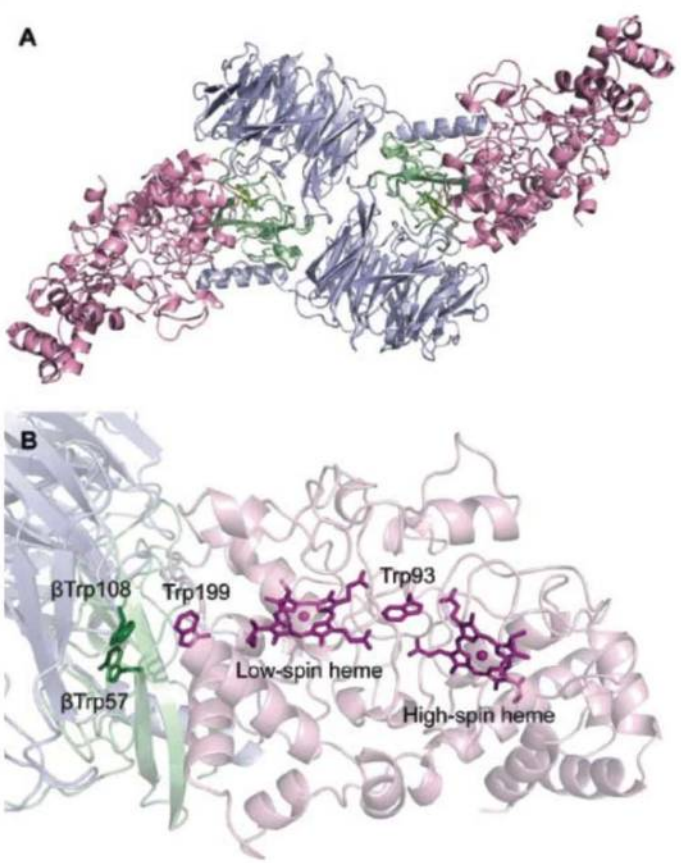

Fig. 1. (**A**) Overall ribbon representation of the MauG-preMADH complex. (**B**) Spatial layout of potential redox groups. Color code: pink, MauG; blue, preMADH α; green, preMADH β. The hemes, Trp^{93}, and Trp^{199} of MauG, as well as βTrp^{108} and monohydroxylated βTrp^{57} of preMADH, are drawn explicitly in stick representation. Figures were produced with PyMOL (www.pymol.org/).

[1]Department of Biochemistry, Molecular Biology and Biophysics, University of Minnesota, Minneapolis, MN 55455, USA. [2]General Medicine and Cancer Institutes Collaborative Access Team (GM/CA-CAT), Biosciences Division, Argonne National Laboratory, Argonne, IL 60439, USA. [3]Department of Biochemistry, University of Mississippi Medical Center, Jackson, MS 39216, USA.

*To whom correspondence should be addressed. E-mail: wilmo004@umn.edu

heterotetramer that contains two active sites and consequently two sites of posttranslational modification. MauG is monomeric and binds in an identical orientation to each αβ half of preMADH, with 2870 Å^2 of surface area buried at each interface. The preMADH structure is essentially identical to mature MADH (*5*) except at βTrp^{57} and βTrp^{108}, the residues that are modified by MauG. As predicted by ^{18}O isotope labeling and mass spectrometry studies, βTrp^{57} of preMADH is monohydroxylated at the C7 carbon of the indole ring with no cross-link between the Trp residues (Fig. 2A) (*7*). The two Trps are in buried positions comparable to their positions in the mature enzyme. They have no direct contact to any part of MauG, the edge of the βTrp^{108} indole ring being closest to the interface (Fig. 1B). There is remarkable separation between the MauG hemes and the nascent TTQ site, with a distance of 40.1 Å between the most distant heme iron and βTrp^{108} (table S2).

The electron paramagnetic resonance (EPR) spectrum of diferric MauG identified two distinct c-type hemes: one high-spin and one low-spin (*2*). Addition of H_2O_2 to diferric MauG resulted in formation of the unusual diheme Fe(IV)=O/Fe(IV) reactive intermediate, as evidenced by Mössbauer and EPR spectroscopies (*11*). The Mössbauer spectrum of the intermediate was modeled as an Fe(IV)=O heme and a six-coordinate Fe(IV) heme. The crystal structure reveals that the MauG heme closest to preMADH is six-coordinate and exhibits a rare His-Tyr axial ligation (Fig. 3A). The axial Tyr^{294} ligand is likely responsible for the ability of this heme to stabilize Fe(IV) without requiring an exogenous ligand. Sequence alignments of known MauGs show that the Tyr is strictly conserved (fig. S2) (*2*). In contrast, the diheme CCPs, which do not stabilize the *bis*-Fe(IV) state, have either a Met or His in this position (fig. S2) (*2*, *10*).

Spectroscopic data indicate that O_2 binding and activation, or direct reaction with H_2O_2, occurs at the high-spin five-coordinate heme observed in the crystal structure (*11*). This is the heme farthest from preMADH in the complex, and thus demands a catalytic mechanism involving long-range interprotein electron and radical transfer (Fig. 1B). There is no evidence of solvent ligation at the coordination site trans to the proximal His^{35} at this heme (Fig. 3, B and C). It was previously shown that the initial two-electron oxidation of preMADH by MauG exhibits a random-binding kinetic mechanism in which the presence of preMADH neither stimulates nor impedes the reaction of MauG with H_2O_2, O_2, or CO (*15*). The structure of the MauG-preMADH complex is consistent with that finding because it shows that the sites of H_2O_2/O_2 and preMADH binding are well separated. This kinetic mechanism is in contrast to that of other enzymes that generate high-valent iron species as intermediates, such as the cytochrome P450 variants, which have ordered mechanisms (*16*). In the distal pocket of the five-coordinate high-spin heme, the ring of Pro^{107} is 4.3 Å from the heme iron (Fig. 3C). This is similar to the distance between the organic substrate and iron in ordered-mechanism oxygenases, such as cytochrome P450$_{cam}$ in complex with camphane (4.3 Å) (*17*). The rigidity of Pro^{107} may afford it the structural role of the substrate in an ordered mechanism by creating a stable O_2 binding site and helping to keep the reactive oxygen species localized at the iron (*16*). As such, the distal pocket of the five-coordinate high-spin heme of MauG may be regarded as constitutively "on" with respect to its ability to activate O_2.

The other characterized *bis*-Fe(IV) enzyme intermediate is the nonheme Fe(IV)$_2O_2$ (Intermediate Q) of methane monooxygenase (*18*). It has a diamond core structure with an Fe···Fe interatomic distance of 2.46 Å. In contrast, the separation of the two heme irons in MauG is 21.1 Å. Despite this distance, the Fe(IV)=O/Fe(IV) intermediate forms very rapidly (>300 s^{-1}) and has remarkable stability, decaying at a rate of 2×10^{-4} s^{-1} in the absence of preMADH (*15*). Trp^{93} of MauG is positioned between the two hemes such that the propionates of the high-spin and low-spin hemes are 3.3 Å and 3.8 Å, respectively, from the Trp indole ring (Fig. 1B). This Trp is conserved in both MauGs and diheme CCPs (*2*). It has been suggested to play a role in electron transfer between the hemes in the latter. Its position in MauG also suggests a role in mediating electron transfer between the hemes after H_2O_2/O_2 binding and the subsequent generation of the *bis*-Fe(IV) species. MauG exhibits negative redox cooperativity between the c-type hemes in cycling between the diferric and diferrous forms upon successive one-electron redox events. The hemes have similar intrinsic oxidation-reduction midpoint potential (E_m) values with facile electron transfer between them. Thus, although the determined E_m values are distinct (−159 mV and −244 mV), MauG acts as a single diheme two-electron cofactor going through a valence-delocalized Fe(III)/Fe(II) state (*19*). In contrast, the E_m values of the hemes of diheme CCPs are separated by more than 600 mV (*20*), and their reactive state is a mixed-valance Fe(III)/Fe(II) species (*10*). In comparing the structures of MauG and diheme CCP, the two hemes and intervening Trp overlay well (fig. S3).

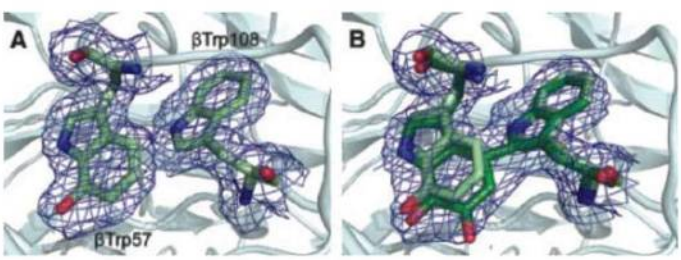

Fig. 2. Site of TTQ formation in MADH. **(A)** $2F_{obs} - F_{calc}$ electron density for the MauG-preMADH complex (resolution 2.1 Å). **(B)** The first $2F_{obs} - F_{calc}$ electron density calculated with MauG-preMADH + H_2O_2 structure factors (resolution 2.1 Å) and MauG-preMADH model phases with the preMADH βTrp^{57} and βTrp^{108} side chains omitted. Electron densities were contoured at 1σ. Carbon coloring: light green, preMADH; dark green, preMADH + H_2O_2.

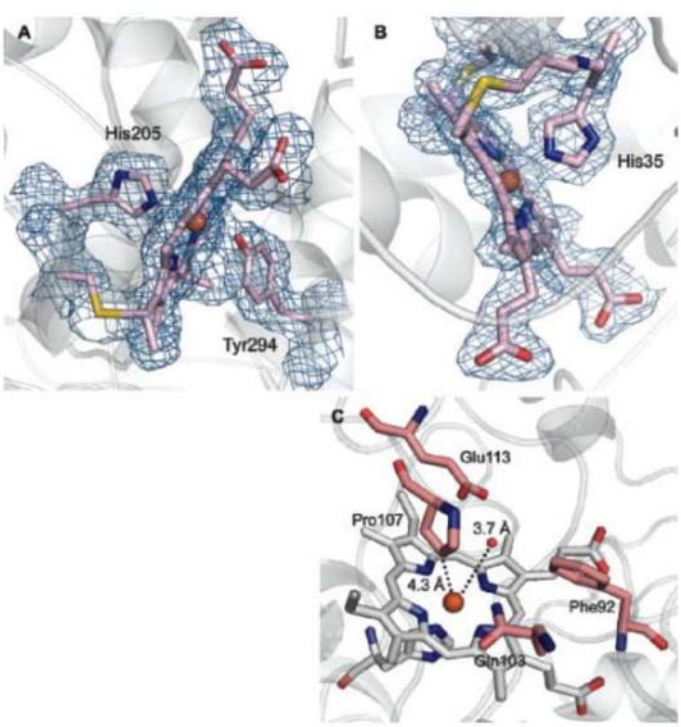

Fig. 3. MauG hemes. **(A)** Six-coordinate low-spin heme (HEC600). **(B)** Five-coordinate high-spin heme (HEC500). **(C)** Residues that line the distal pocket. $2F_{obs} - F_{calc}$ electron density was contoured at 1σ.

A Ca^{2+} ion is bound in an identical position in both enzymes (fig. S3B). Hence, a structural change altering the spatial relationship between the hemes is not responsible for the different redox and catalytic activities of the two enzymes. The key difference in the diheme unit of MauG is the distal Tyr^{294} ligand to the low-spin heme, which is a Met or His in diheme CCPs. Therefore, Tyr^{294} appears to be the major determinant in the redox properties and ability of MauG to stabilize the *bis*-Fe(IV) state.

The catalytic competence of the MauG-preMADH complex was examined in crystallo by solving the crystal structure after treatment with excess H_2O_2 (table S1) (*14*). The initial electron density (to 2.1 Å resolution) clearly showed that the second oxygen atom had been incorporated at C6 of βTrp^{57} and that a cross-link had been formed between βTrp^{57} and βTrp^{108} (Fig. 2B). It has not been possible to crystallize preMADH alone, so the catalytic requirement for MauG in H_2O_2-dependent TTQ synthesis was confirmed in solution under conditions that matched those of crystallization (fig. S4) (*9*). The structures before and after H_2O_2 addition are superimposable (root mean square deviation 0.158 Å), except for the posttranslational modifications. The TTQ cofactor of mature MADH purified from source (PDB code 2BBK) overlays well with that generated in the H_2O_2-treated MauG-preMADH crystals (*5*). Thus, the complex is catalytically competent and no major conformational rearrangements of the two proteins are required. At the center of the interface, halfway between the MauG low-spin heme and preMADH βTrp^{108}, is MauG residue Trp^{199} (Fig. 1B). This residue may facilitate electron transfer across the interface through stabilization of a transient radical, although it is not conserved in other MauG sequences (fig. S2). The catalytic competence of the crystals also indicates a processive mechanism in which MauG and preMADH do not dissociate between each of the three two-electron oxidations. Furthermore, solvent must provide the second oxygen incorporated at βTrp^{57} C6, as this carbon is 43.7 Å from the Fe(IV)=O. The distal side of the high-spin heme of H_2O_2-treated crystals has residual electron density not present in the MauG-preMADH structure. The low occupancy and complexity of the electron density prevent it from being modeled, but it is consistent with a mixture of species that could include diatomics, such as hydroperoxo, and is evident in both copies in the asymmetric unit, thereby confirming that reaction with H_2O_2 occurs at this site (fig. S5).

This structure reveals that the purpose of the high-valent intermediate in MauG is to provide an oxidant with an extremely high reduction potential to extract electrons from the preMADH substrate, generating reactive radical intermediates that then acquire the oxygen atom from solvent and form the covalent cross-link between the Trp side chains. As such, the preMADH structure contributes substantially to the catalytic reaction through positioning the reacting portions of the Trps and creating the required chemical environment for TTQ synthesis. Thus, the post-translational biosynthetic reaction requires both substrate-assisted and long-range catalysis.

References and Notes

1. V. L. Davidson, *Biochemistry* **46**, 5283 (2007).
2. Y. Wang *et al.*, *Biochemistry* **42**, 7318 (2003).
3. W. S. McIntire, D. E. Wemmer, A. Chistoserdov, M. E. Lidstrom, *Science* **252**, 817 (1991).
4. V. L. Davidson, *Adv. Protein Chem.* **58**, 95 (2001).
5. L. Y. Chen *et al.*, *J. Mol. Biol.* **276**, 131 (1998).
6. A. R. Pearson *et al.*, *Biochemistry* **43**, 5494 (2004).
7. A. R. Pearson, S. Marimanikkuppam, X. Li, V. L. Davidson, C. M. Wilmot, *J. Am. Chem. Soc.* **128**, 12416 (2006).
8. Y. Wang *et al.*, *J. Am. Chem. Soc.* **127**, 8258 (2005).
9. X. Li, L. H. Jones, A. R. Pearson, C. M. Wilmot, V. L. Davidson, *Biochemistry* **45**, 13276 (2006).
10. G. W. Pettigrew, A. Echalier, S. R. Pauleta, *J. Inorg. Biochem.* **100**, 551 (2006).
11. X. Li *et al.*, *Proc. Natl. Acad. Sci. U.S.A.* **105**, 8597 (2008).
12. I. G. Denisov, T. M. Makris, S. G. Sligar, I. Schlichting, *Chem. Rev.* **105**, 2253 (2005).
13. H. P. Hersleth, U. Ryde, P. Rydberg, C. H. Görbitz, K. K. Andersson, *J. Inorg. Biochem.* **100**, 460 (2006).
14. See supporting material on *Science* Online.
15. S. Lee, S. Shin, X. Li, V. Davidson, *Biochemistry* **48**, 2442 (2009).
16. T. M. Makris, R. Davydov, I. G. Denisov, B. M. Hoffman, S. G. Sligar, *Drug Metab. Rev.* **34**, 691 (2002).
17. R. Raag, T. L. Poulos, *Biochemistry* **30**, 2674 (1991).
18. E. G. Kovaleva, M. B. Neibergall, S. Chakrabarty, J. D. Lipscomb, *Acc. Chem. Res.* **40**, 475 (2007).
19. X. Li, M. Feng, Y. Wang, H. Tachikawa, V. L. Davidson, *Biochemistry* **45**, 821 (2006).
20. V. Fulop, N. J. Watmough, S. J. Ferguson, *Adv. Inorg. Chem.* **51**, 163 (2000).

21. Supported by NIH grants GM66569 (C.M.W.) and GM41574 (V.L.D.) and Minnesota Partnership for Biotechnology and Medical Genomics grant SPAP-05-0013-P-FY06. Computer resources were provided by the Basic Sciences Computing Laboratory of the University of Minnesota Supercomputing Institute, and we thank C. Ergenekan for his support. X-ray data were collected at the Kahlert Structural Biology Laboratory (KSBL) at the University of Minnesota and GM/CA-CAT at the Advanced Photon Source (APS), Argonne National Laboratory, Argonne, IL. GM/CA-CAT is funded by National Cancer Institute grant Y1-CO-1020 and National Institute of General Medical Sciences grant Y1-GM-1104. Use of the Advanced Photon Source was supported by the U.S. Department of Energy, Basic Energy Sciences, Office of Science, under contract DE-AC02-06CH11357. We thank E. Hoeffner for KSBL support and the staff at Sector 23, APS, for their support, especially M. Becker, S. Corcoran, V. Nagarajan, and D. Yoder. We thank S. Shin for performing the experiment shown in fig. S4. Coordinates and structure factors have been deposited in the Protein Data Bank with acquisition codes 3L4M (MauG-preMADH complex) and 3L4O (MauG-preMADH complex treated with H_2O_2).

Supporting Online Material

www.sciencemag.org/cgi/content/full/327/5971/1392/DC1
Materials and Methods
Figs. S1 to S5
Tables S1 and S2
References

25 September 2009; accepted 19 January 2010
10.1126/science.1182492

NEW PRODUCTS FOCUS: PCR/RT-PCR

TAQMAN PRI-miRNA ASSAYS

The TaqMan Pri-miRNA Assays are a set of real-time polymerase chain reaction (PCR) assays that enable researchers to measure the activity of specific microRNA (miRNA) genes by detecting and quantifying levels of expressed primary miRNA transcripts. Based on the latest Sanger miRBase content, this new line consists of more than 1,200 primary miRNA assays for human, mouse, and rat that have been designed using a stringent bioinformatic pipeline and the TaqMan Assay chemistry. Each assay delivers the specificity and sensitivity necessary to accurately measure primary miRNA transcript expression levels from a single genomic locus, without the requirement for a fully defined primary transcript sequence.

Applied Biosystems and Invitrogen

For info: 800-955-6288 | www.appliedbiosystems and www.invitrogen.com

QUANTITATIVE REAL-TIME ANALYSIS

The DyNAmo ColorFlash qPCR (quantitative polymerase chain reaction) Kits for fast, real-time analysis provide detection and quantification of DNA sequences from various sources. The kits are designed to ease qPCR setup and minimize errors by producing a simple way to track pipetting of reaction components. The two kits, DyNAmo ColorFlash SYBR Green qPCR Kit and DyNAmo ColorFlash Probe qPCR Kit, feature an innovative multicolor system. The Master Mix contains a blue dye, and a separate sample buffer contains a yellow dye. The qPCR reactions mix containing both components is green. With this patent-pending multicolor system, pipetting of both the master mix and the sample can be easily monitored, decreasing the risk of errors.

Finnzymes

For info: +358-9-2472-3291 | www.finnzymes.com

MELTING ANALYSIS KITS

Epigenetics researchers can now detect changes in methylation status in real-time using high-resolution melting (HRM) analysis. The EpiTect HRM polymerase chain reaction (PCR) kit provides a master mix format for the detection of changes in the CpG (C-phosphate-G) methylation status of bisulfite-converted DNA. The kit is designed to run on all real-time PCR cyclers, including the Rotor-Gene Q, which provides a highly specific melting curve. HRM technology enables a rapid characterization of DNA samples based on their melting behavior following PCR amplification, and is suitable for screening large numbers of samples and for detecting changes in the methylation degree of specific DNA regions.

Qiagen

For info: 240-686-7660 | www.qiagen.com/epigenetics

RT-PCR KITS

The Quantifast Multiplex RT-PCR and Rotor-Gene Multiplex RT-PCR kits are new reverse transcription–polymerase chain reaction (RT-PCR) tools. The Quantifast kits perform fast real-time RT-PCR without requiring optimization on both standard and fast real-time cyclers for one-step applications. The Rotor-Gene Kit allows detection of up to four targets per tube and includes optimized protocols for precise results on the Rotor-Gene Q real-time cycler.

Qiagen

For info: 800-362-7737 | www.qiagen.com

ADJUSTABLE SPACING PIPETTOR

The six-channel Voyager electronic pipettor features a mechanism that alters tip spacing at the press of a button. The Voyager incorporates a small motor that moves the center-to-center tip spacing quickly and smoothly at any point in the protocol, and requires only one hand to operate. Users can preset up to three distinct tip spacings in a way that accommodates most labware vessels. The spacing can be adjusted from 9.0 mm to 19.5 mm. Two models are available, in volume ranges of 10–300 µl and 50–1,250 µl. Both models work with 24-well plates, 48-well plates, and many other formats.

Integra Biosciences

For info: +41-81-286-9530 | www.integra-biosciences.com

SAMPLE QUANTIFICATION SYSTEM

SlingShot is a DNA quantification system that allows researchers to sequence their libraries of rare samples and lower costs, improve data quality, and speed the time to results in DNA sequencing. It also allows the sequencing of rare samples. It can improve the productivity of next generation sequencing tools from Roche, Illumina, and Applied Biosystems by exploiting the unique microfluidic properties of integrated fluidic circuits (IFCs) to detect only amplifiable molecules within the sample mixture. IFCs use extremely small amounts of sample, so this technology opens up the ability to sequence rare libraries where suboptimal amounts of the tissue are available. The ability of IFCs to count individual molecules—using digital polymerase chain reaction—also eliminates the need for costly library titration to ready samples for sequencing.

Fluidigm Europe

For info: +33-44-259-3861 | www.fluidigm.com

Electronically submit your new product description or product literature information! Go to www.sciencemag.org/products/newproducts.dtl for more information.

Newly offered instrumentation, apparatus, and laboratory materials of interest to researchers in all disciplines in academic, industrial, and governmental organizations are featured in this space. Emphasis is given to purpose, chief characteristics, and availabilty of products and materials. Endorsement by *Science* or AAAS of any products or materials mentioned is not implied. Additional information may be obtained from the manufacturer or supplier.

POSITIONS OPEN

UtahStateUniversity

TENURE-TRACK FACULTY POSITION
Departments of Chemistry and Biochemistry and Biology
USTAR Initiative
Utah State University

The Utah Science, Technology and Research (USTAR) initiative, along with the Departments of Chemistry and Biochemistry and Biology at Utah State University, invites applications for a tenure-track position at any rank. Candidates must have a Ph.D. in biochemistry, biology, or a related field, with postdoctoral and faculty experience preferred. The successful applicant will develop a funded research program in some area of phototrophic microbes, and will be expected to teach at the graduate and undergraduate levels. Preference will be given to candidates with research programs that complement the USTAR Biofuels research program goals of developing phototrophic microbes as a feedstock for biofuels. The position is funded by a grant from the USTAR initiative, a statewide program that aims to promote commercialization of technologies at the state universities. Applicants should submit curriculum vitae, a concise description of future research projects, associated major research infrastructure needs, and the names and e-mail addresses of three references online at **website: http://jobs.usu.edu requisition 052021).** Evaluation of applications will begin March 15, 2010, and will continue until the position is filled. For further information please visit our **website: http://www.chem.usu.edu**. *Utah State University is an Equal Opportunity/Affirmative Action Employer committed to assembling a diverse faculty. Women and members of minority groups are strongly encouraged to apply.*

ASSISTANT PROFESSOR OF BIOTECHNOLOGY

The Biology Department at The Catholic University of America has an opening for a tenure-track Assistant Professor position in its new Biotechnology Program (**website: http://biotechnology.cua.edu**). The Biology Department also has a strong research emphasis in basic cell and molecular biology and offers undergraduate and graduate programs including the Ph.D. (**website: http://biology.cua.edu**). The successful candidate will teach graduate courses in biotechnology, assist in further development of the biotech program, and maintain an externally sponsored research program in an area of biotechnology. We seek candidates who have a strong publication record and experience in the biotechnology industry, research as well as product development. Please send curriculum vitae, a statement of career interests, and three letters of reference by April 30, 2010, to: **Dr. Venigalla Rao, Department of Biology, The Catholic University of America, 620 Michigan Avenue N.E., Washington, DC 20064. E-mail: rao@cua.edu.**

The Catholic University of America was founded in the name of the Catholic Church as a national university and center of research and scholarship. Regardless of their religious affiliation, all faculty are expected to respect and support the University's mission. *The Catholic University of America is an Affirmative Action/Equal Opportunity Employer, Veterans/Persons with Disabilities/Minorities/Females.*

CANCER STEM CELL FACULTY POSITION

Join an internationally respected group in regenerative medicine and stem cell research. The Wake Forest Institute for Regenerative Medicine (WFIRM) and the Comprehensive Cancer Center of Wake Forest University are soliciting applications to fill a mid-career, tenure-track, or tenured faculty position in cancer stem cell research and tumor microenvironment. Candidates should hold a Ph.D. or M.D. Primary appointment with WFIRM; joint appointment in the Department of Cancer Biology. Electronically submit curriculum vitae and concise statement of research plans to **e-mail: swilder@wfubmc.edu**. *Affirmative Action/Equal Opportunity Employer.*

POSITIONS OPEN

DIRECTOR
Pittsburgh NMR Center for Biomedical Research
Carnegie Mellon University, Pittsburgh, PA

The Pittsburgh Nuclear Magnetic Resonance Center, jointly sponsored by Carnegie Mellon University and the University of Pittsburgh, seeks a new Director. The Center is dedicated to advancing state-of-the-art in vivo magnetic resonance imaging and magnetic resonance spectroscopy processes and tools to better understand tissue and organ function, and to making these tools available to the greater biomedical research community. We seek candidates with outstanding records of accomplishment and innovation, and a vision for development of this research-driven collaborative enterprise. Applicants at the Associate or Full Professor level will be considered.

Applicants should submit a cover letter describing their qualifications and interest in this position, curriculum vitae, and contact information for three individuals who can provide letters of recommendation to: **Aaron P. Mitchell, Ph.D., Chair, Nuclear Magnetic Resonance Center Director Search Committee, Department of Biological Sciences, Carnegie Mellon University, 4400 Fifth Avenue, Pittsburgh, PA 15213.** Please electronically send these materials to **e-mail: nmr-search@andrew.cmu.edu**.

Carnegie Mellon offers outstanding health, retirement, and tuition benefits.

The University is an Equal Opportunity/Affirmative Action Employer committed to building a diverse faculty. Women and members of minority groups underrepresented in academia are especially encouraged to apply.

ASSISTANT PROFESSOR, TENURE TRACK

The Department of Zoology at Oklahoma State University (**website: http://zoology.okstate.edu**) invites applications for an Assistant Professor in organismal (including humans) evolution. Applicants should have a Ph.D., postdoctoral experience, teaching experience, and success in obtaining extramural funding. Responsibilities include establishing an extramurally funded research program, mentoring M.S. and Ph.D. students, and teaching at the undergraduate and graduate levels. Applicants should submit a letter of application, curriculum vitae, separate statements of research interests and teaching philosophy, and three publications electronically to **e-mail: kristen.baum@okstate.edu** or by surface mail to: **Dr. Kristen Baum, Chair, Search Committee, Department of Zoology, Oklahoma State University, 501 Life Sciences West, Stillwater, OK 74078.** Three letters of recommendation should be sent directly by the applicant's references by surface mail. Application review will begin 15 April 2010, with employment beginning 1 January 2011. Filling of this position is contingent upon availability of funding. *Oklahoma State University is an Affirmative Action/Equal Employment Opportunity/E-Verify Employer committed to diversity. OSU Stillwater is a tobacco-free campus.*

ASSISTANT, ASSOCIATE, or FULL PROFESSOR
Computational Biology
Microbiology and Cell Science Department
University of Florida

The Department of Microbiology and Cell Science at the University of Florida invites applications and nominations for a 12-month, tenure-track position at Assistant, Associate, or Full Professor level to develop an independent research program in computational biology. Applicants should have a Ph.D. in the biological or computer sciences with a strong publication record in computational biology. The successful candidate is expected to develop an outstanding research program, supervise Ph.D. candidates, and be an innovative instructor. To apply, electronically submit curriculum vitae, description of research interests, and names of three references in one PDF file to **website: http://jobs.ufl.edu/applicants/ requisition #0804059.** For questions concerning this position, contact **Professor Graciela Lorca, Chair of Search and Screen Committee, e-mail: glorca@ufl.edu**. Review of applications begins April 1, 2010. *The University of Florida is an Equal Opportunity Employer.*

LAB MANAGEMENT:
THE HUMAN ELEMENTS

You've reached a career milestone: managing your own lab. This recognition of your achievements attests to your hard work, attention to detail, commitment to a goal—and outstanding science. But be prepared. You're about to face challenges you may not have considered. **By Carol Milano**

Susan Morris

"People skills are teachable. Make a commitment to learn consistently, not in fits and starts."

As **Frank Slack,** a Yale University professor of molecular, cellular and developmental biology, quickly discovered, "To be successful at running the lab, being a good scientist isn't enough. It suddenly becomes all these different roles we weren't trained for, like psychiatrist and personnel manager."

Those responsibilities often require new skills. Here's how some of your peers are mastering the "human elements."

Networking and Collaborating

When you run your own lab, "networking" isn't just about finding the next job. It means cultivating productive relationships, which succeed only when they are reciprocal. Mutual trust grows through willing exchange of information or services.

Start by developing contacts inside and outside your own institution—locally, nationally, and even internationally. Find your professional association's nearest chapter. Ask your mentors and colleagues which organizations they belong to. Once you join one, get involved. Volunteering for a committee or writing for the chapter newsletter, for instance, makes you much more visible.

"You and the people you're managing will have to speak in public or mingle effectively at meetings and conferences," says **Susan Morris,** president of Morris Consulting Group, which coaches research scientists. To minimize uneasiness and build confidence if you're shy, she suggests:

- **Network in small chunks.** Set a maximum of two carefully chosen events a month, ideally at your highest-energy time of day.
- **Arrive early.** Entering an uncrowded room is less unnerving than a noisy one, where most people are already conversing.
- **Go with a "buddy."** Preferably someone who can introduce you to several people.
- **Talking to a stranger can be intimidating.** Safe "starters" include asking their current job, how they got it, why they chose this event, or other groups they belong to. Seek topics of mutual interest, such as that gathering's focus. If you can offer information about anything that's mentioned, jot a note on the person's card. Follow up promptly.

Frequently traveling to give lectures, **Jennifer Lippincott-Schwartz,** chief of cellular biology metabolism at the US National Institutes of Health (NIH), National Institute of Child Health and Human Development, values professional meetings, despite the time drain. "I make contacts, hear things that would be difficult to pull out just by reading the literature, and meet people doing things relevant to our work." Almost without trying, she says, collaborations develop.

Taking part on national panels "is a responsibility as senior members of the scientific community," believes **Kelly Frazer,** who heads the new Division of Genome Information Sciences at University of California, San Diego School of Medicine. She finds those she's on, like the expert scientific panel for the genomewide association program (a trans-NIH initiative led by the National Human Genome Research Institute), "very beneficial because of the contact with people and with what's going on." In a rapidly moving field, Frazer uses these events to stay connected through informal exchanges over coffee, lunch, and dinners. I listen to the science, give input, have discussions, hear others' ideas, and look at the work."

Lippincott-Schwartz prods every lab member to attend at least one professional meeting a year. "People don't realize how social science is! By talking science during these trips, you learn what's important to the field, what the major questions are, where your science fits the broader, bigger scheme, and how what you're doing interests other people (or not)." continued »

UPCOMING FEATURES

Careers in Bioinformatics/Systems Biology—April 9

Bio/Pharma: Mythbusting about Industry—April 23

Careers in Water Science (Online Only)—May 14

FACULTY POSITIONS

Federal Ministry of Education and Research

ZENTREN FÜR INNOVATIONSKOMPETENZ
UNTERNEHMEN REGION
Die BMBF-Innovationsinitiative Neue Länder

IN SEARCH OF EXCELLENCE!

The German Federal Ministry of Education and Research (BMBF) is supporting the further development of the six Centres for Innovation Competence (German: Zentren für Innovationskompetenz, ZIK), set up in 2004, by establishing new fast-track research groups. Scientists with excellent references and international expertise are invited to send in their applications by **30 April 2010**. Women are especially invited to apply. Preference will be given to disabled applicants with equal qualifications. For further details on the application requirements, please go to **www.unternehmen-region.de**.

OncoRay
Dresden University of Technology

The Centre for Innovation Competence (German: Zentrum für Innovationskompetenz, ZIK) OncoRay – Center for Radiation Research in Oncology – is developing innovative methods for biologically individualised, technologically optimised radiation therapy for improving cancer cures. The OncoRay was jointly established in 2004 as an interdisciplinary research centre by Dresden University of Technology, the University Hospital and the Research Center Dresden-Rossendorf. It is attached to the Medical Faculty, and offers first-class research facilities, internationally acknowledged expertise in translational cancer and radiation research and a dedicated postgraduate school offering an MSc and a PhD programme (www.OncoRay.de). Dresden offers a prime research environment, and is a culturally attractive, family-friendly city with a high quality of life.

The Carl Gustav Carus Medical Faculty of Dresden University of Technology, together with the German Federal Ministry of Education and Research (BMBF), is seeking for the OncoRay:

Associate Professor (W2)/Junior Research Group Leader
"Biomarkers for Individualised Radiotherapy"

The professor will be appointed for five years. A tenure-track option, dependent on positive evaluation, is possible. The successful candidate will establish an interdisciplinary and international team of excellent scientists that will develop novel biomarkers for the prediction of the response of cancer to radiotherapy and innovative drugs for the development of individualised treatment strategies. Eligible candidates will have a PhD or MD degree, an excellent postdoctoral scientific track record in tumour biology, genetics or molecular pathology, for example, and teaching experience. Experience in radiation biology is not a prerequisite, and can be obtained on site.

Junior Research Group Leader
"In-Vivo Dosimetry for Novel Types of Radiation"

The successful candidate will establish an international team of highly qualified scientists and technologists in technology-based physics research. The team will develop radiation detectors for image-based in-vivo dosimetry for radiation therapy with protons and ions, fast techniques of signal processing, and data acquisition and processing in real time. Eligible candidates will have a PhD degree, alongside several years of research experience in experimental nuclear, radiation or particle physics, particularly in developing and using radiation detectors as well as in technologies and methods for the recording and processing of detection signals. Experience in physics and technologies of medical imaging are not a prerequisite, and can be obtained on site.

Funding for the research groups is available over a period of five years, and includes a budget for personnel, excellent laboratories, sustainables and travel costs.

Please send your application to:

Biomarkers:
Professor H. Reichmann
Dekan der Medizinischen Fakultät
Carl Gustav Carus
Technische Universität Dresden
Fetscherstrasse 74
01307 Dresden
Germany

In-Vivo Dosimetry:
Professor Michael Baumann
Sprecher ZIK OncoRay
Fetscherstrasse 74
01307 Dresden
Germany

and, for either application, also to:

Project Management Jülich
Division Technological and Regional Innovations (TRI)
Forschungszentrum Jülich GmbH
Zimmerstrasse 26–27
10969 Berlin
Germany
Email: k.-d.husemann@fz-juelich.de

For further information, please contact:
Professor Michael Baumann (michael.baumann@oncoray.de); www.oncoray.de; and the website of the Medical Faculty (Stellenanzeigen)

ICCAS – Innovation Center Computer Assisted Surgery
University of Leipzig

ICCAS was founded in 2005 as one of six Centres for Innovation Competence (German: Zentren für Innovationskompetenz, ZIK) at the second-oldest university in Germany. Since then, the centre has successfully established itself as an international interdisciplinary research institution.

In 2010 two new research groups will be established within the centre, supported by the German Federal Ministry of Education and Research (BMBF). ICCAS, in collaboration with the BMBF, is now seeking applications from highly motivated and outstanding junior scientists for two

Junior Research Group Leader positions

The key initiative of ICCAS is to carry out research and development work on applying methods and tools for system software for the modern surgical workplace (Therapy Imaging and Model Management System – TIMMS). Specific applications of computer-assisted surgery include, but are not limited to, neurosurgery, ENT surgery and cardiovascular surgery. This work assumes the realisation of an integrated digital operating room (OR), a surgical planning unit and other aspects of the treatment path. In order to achieve these strategic aims, two research groups with specific areas of interest will be established:

Junior Research Group: Digital Patient and Process Model

- Mathematical modelling and informatics-based structuring of patient data sets
- Specification and modelling of surgical workflows including standard operating procedures
- Software-engineering-based prototyping of patient and process modelling systems as well as semantic-aware tools and services in the context of surgical assist systems

Junior Research Group: System Tools for Surgical Cockpit

- Integration of the patient and process models in a near-real set-up
- Knowledge and decision management
- Projects with strong relation to existing commercial products and prototypes
- Cooperation with projects focusing on OR architecture, medical technology, medical devices and human-machine interaction

Candidates for both positions should be familiar with the broad areas of software and systems engineering, health informatics, computer-assisted radiology and surgery, or related fields. A strong background in computer science is desirable with evidence of the ability to pursue and lead a research programme. Most important, however, is the ability to build up and manage a large cross-disciplinary collaborative team.

The two junior research group leaders have the opportunity to form their own research group with four scientists each. The groups are provided with secured funding for five years, and are endowed with an above-average budget and excellent infrastructure of state-of-the-art demonstration OR and computer facilities. They will be supported by a centre manager and the administrative and scientific staff of ICCAS, and will be immersed in an active academic and student environment.

The Medical Faculty offers the **possibility of a "Junior Professor" (W1) position** in the above-mentioned scientific field. The successful group leader may be offered a tenured position after positive evaluation.

Please send your application to:

Universität Leipzig
Medizinische Fakultät
ICCAS
Professor J. Meixensberger
Semmelweisstrasse 14
04103 Leipzig
Germany

and

Project Management Jülich
Division Technological and Regional Innovations (TRI)
Forschungszentrum Jülich GmbH
Zimmerstrasse 26–27
10969 Berlin
Germany
Email: k.-d.husemann@fz-juelich.de

For further information, please contact:
Professor Jürgen Meixensberger (meix@medizin.uni-leipzig.de); www.iccas.de

CELISCA – Center for Life Science Automation University of Rostock

The international Centre for Innovation Competence (German: Zentrum für Innovationskompetenz, ZIK) CELISCA offers an ideal environment for effective interdisciplinary research and development projects. Under our roof, engineers and natural scientists cooperate closely to find innovative solutions for current and future problems and tasks. The main research areas include automation and engineering, chemistry and biotechnology, screening and analytics, process information technologies and automation assessment.

CELISCA, together with the German Federal Ministry of Education and Research (BMBF), is now inviting applications for the position of a

Junior Research Group Leader "Life Science Automation – Systems and Process Technologies"

The technological focus of the group is a comprehensive workflow in a multi-robot/multi-operator environment, coupled with the application focus in the field of catalysis for drug development and drug testing (synthesis and process analytics).

The research activities of the group will include systems and method developments for high-throughput screening and process analytics of catalyst systems for the development of bioactive compound libraries and their integration into hierarchically organised workflow management for multi-robot environments with a flexible consideration of the system operators.

Conditions of employment include a PhD (Information Technology, Chemistry, Electrical Engineering, Physics, etc.) and experience in the fields of the interdisciplinary research profile of the research group, in project-financed research and in international cooperation.

Additionally, we expect experience in leading a research group, goal-oriented and application-oriented working, flexibility and resilience, social skills and a high degree of interdisciplinarity.

The research group is provided with secured funding for five years, and is endowed with an above-average budget and an excellent infrastructure.

Please send your application to:

CELISCA
Professor Kerstin Thurow
Friedrich-Barnewitz-Strasse 8
18119 Rostock
Germany
Email: kerstin.thurow@celisca.de

and

Project Management Jülich
Division Technological and Regional Innovations (TRI)
Forschungszentrum Jülich GmbH
Zimmerstrasse 26–27
10969 Berlin
Germany
Email: k.-d.husemann@fz-juelich.de

For further information, please contact:
Professor Kerstin Thurow (kerstin.thurow@celisca.de); www.celisca.de

FunGene – Functional Genomics Ernst Moritz Arndt University of Greifswald

With around 12,000 students, Ernst Moritz Arndt University is a small university on the coast of the Baltic Sea. Life science research constitutes one of its major research areas. The Faculty of Natural Sciences and the Medical School of the University recently joined forces and resources in a Centre for Innovation Competence (German: Zentrum für Innovationskompetenz, ZIK) for Functional Genomics (FunGene), which is supported by the German Federal Ministry of Education and Research (BMBF). Over the last five years, functional genomics has developed into one of the major research fields of the university, with state-of-the-art facilities for transcriptomics and high-throughput proteomics. Research is focused on the following areas: systems biology of model organisms, pathogenomics and infection biology (Gram-positive bacteria), and functional genomics in molecular medicine and its biotechnological application. The research groups are involved in a number of national and international research consortia.

Within the framework of FunGene, the centre is being expanded by establishing two BMBF-supported junior research groups in the fields of pathoproteomics and applied proteomics. Funding of the groups includes laboratory set-up, consumables and additional personnel (postdoctoral and technical positions) for five years. FunGene, in collaboration with the BMBF, is looking for a

Junior Research Group Leader "Pathoproteomics"

We are seeking to recruit an outstanding young scientist with a strong publication record in functional genomics and infection biology (imaging techniques). The successful candidate will have access to the outstanding proteomics technology facilities in Greifswald. High priority will be given to candidates who are able to stimulate research networks on proteomics of bacterial pathogens in Germany and Europe. Candidates should have a strong publication record either in pathogenomics (imaging techniques) or in infection biology. A successful group leader may be considered for a **tenure-track option** by the university.

Junior Research Group Leader "Applied Proteomics"

We are seeking to recruit an outstanding scientist with a strong background in proteomics and bioinformatics of microbial pathogens. High priority will be given to candidates who are able to develop gel-based and gel-free proteomics into high-throughput workflows for the analysis of infection-related questions in an epidemiological context. Expertise in the field of proteomics should be documented by a related PhD and a strong publication record. Based on the research network that is established in Greifswald, the proposed research plan should develop approaches that allow a temporal and integrated analysis of the infecting bacterial pathogen and the host side, aiming for improvements in diagnosis and an adjustment of therapeutic regimens. The group should develop the existing network with the biotechnological and pharmaceutical industry. A successful group leader may be considered for a **tenure-track option** by the university.

Please send your application to:

FunGene
Professor Michael Hecker
Ernst-Moritz-Arndt-Universität Greifswald
Institut für Mikrobiologie
Friedrich-Ludwig-Jahn-Strasse 15
17487 Greifswald, Germany
Email: hecker@uni-greifswald.de

and

Project Management Jülich
Division Technological and Regional Innovations (TRI)
Forschungszentrum Jülich GmbH
Zimmerstrasse 26–27
10969 Berlin, Germany
Email: k.-d.husemann@fz-juelich.de

For further information, please contact: Professor Michael Hecker (hecker@uni-greifswald.de); www.functional-genomics.uni-greifswald.de/

MacroNano Ilmenau University of Technology

IMN MacroNano® is an interdisciplinary institute at Ilmenau University of Technology. Its focus is on intensifying interdisciplinary research in the area of micro- and nanotechnologies, spanning the field from basic science to applications. A distinctive goal is to foster the transfer of knowledge among scientists and between scientists and commercial research partners in joint R&D projects. This leads to a continuous advancement of R&D expertise within the IMN MacroNano® and for its scientific partners. Currently, IMN MacroNano® comprises 39 research and junior research groups from the schools of Mechanical Engineering, Electrical Engineering and Information Technology, Mathematics and Natural Science, and Computer Science and Automation, inter alia, at the Centre for Innovation Competence (German: Zentrum für Innovationskompetenz, ZIK) IMN MacroNano.

Ilmenau University of Technology, with support from the German Federal Ministry of Education and Research (BMBF), will accommodate a junior research group "Three-Dimensional Nanostructuring" at ZIK IMN MacroNano, and is looking for a

Junior Research Group Leader "Three-Dimensional Nanostructuring" Associate Professor (W2, tenure track)

The successful candidate will simultaneously fill a tenure-track faculty position of an associated professorship ("W2" professorship, tenure track) at the school that fits his or her scientific profile best. The junior research group will be equipped with start-up funding for five years, including positions for four scientific staff as well as the means for investments and running expenses.

The focus will be on candidates with an exceptional research background in the field of novel methods of three-dimensional nanostructuring. Foci of research may be: the scalable, fast and parallel construction of functional nanostructures in three dimensions or nanostructuring on three-dimensionally shaped surfaces, especially in micro-systems. The results of the field of research shall enable scalable micro-nano integration.

The successful candidate will have teaching obligations including basic courses on a BSc level and advanced classes in the master programmes "Micro- and Nanotechnology" and "Miniaturised Biotechnology". Proof of teaching ability needs to be enclosed in the application. Applicants need to fulfil the requirements of §77 of the "Thüringer Hochschulgesetz". Specifically, they must have an outstanding PhD degree, additional scientific qualifications and international work experience. An active contribution to the academic self-administration is expected, and experience in securing research grants is requested.

Please send your application to:

Technische Universität Ilmenau
Dezernat für
Personalangelegenheiten
Kennziffer ZIK/2010
Postfach 10 05 65
98684 Ilmenau
Germany

and

Project Management Jülich
Division Technological and Regional Innovations (TRI)
Forschungszentrum Jülich GmbH
Zimmerstrasse 26–27
10969 Berlin, Germany
Email: k.-d.husemann@fz-juelich.de

For further information, please contact:
Professor Martin Hoffmann; phone: +49 (0)3677 69-3402; email: macronano@tu-ilmenau.de; www.macronano.de

ultra optics Friedrich Schiller University of Jena

"ultra optics", the interdisciplinary Centre for Innovation Competence (German: Zentrum für Innovationskompetenz, ZIK) at Friedrich Schiller University (FSU), is developing novel concepts for controlling light even under extreme conditions with respect to wavelength, power and time. The centre is dedicated not only to fundamental research, but also to the development of the physical and technical prerequisites for next-generation active and passive optical systems and their application. The work is carried out through cooperation with partners from science and industry.

In 2010 two new research groups will be established within the centre, supported by the German Federal Ministry of Education and Research (BMBF). Their research group leaders will each set up their own team of four scientific staff, and realise their own research concept in the field of modern optics and photonics. The groups will initially be funded for five years, and are endowed with an above-average budget and excellent laboratory equipment. They will be immersed in the scientific environment of Professor Andreas Tünnermann, director of the FSU Institute of Applied Physics and the Fraunhofer Institute for Optics and Precision Engineering, and will have access to research infrastructure within both.

Friedrich Schiller University and the Fraunhofer Institute for Optics and Precision Engineering, together with the BMBF, are now inviting applications for two junior research group leader positions:

Junior Research Group Leader Applied Physics: Manufacturing Technologies in Advanced Micro- and Nano-Optics

The candidate has a strong record in advanced manufacturing processes for micro- and nano-optics, with expert knowledge in the design of passive photonic elements as well as their linear experimental analysis. Practical experience in electron and laser lithography would be desirable.

Junior Research Group Leader Applied Physics: Diamond-/Carbon-Based Optical Systems

The candidate must have a strong scientific background in modelling, design and application of advanced opto-mechanical systems. An important part of this candidate's interest is the investigation of optic and photonic elements under extreme lighting conditions.

Applicants fulfilling the formal requirements, possessing outstanding expertise and matching the research topics of the department **can be appointed as Junior Professors.** Candidates for both positions must have a PhD in physics or a closely related area and should not be older than 35 years at time of application. Superb communication skills and a commitment to excellence in both teaching and research are required.

Please send your application to:

Friedrich-Schiller-Universität Jena
Physikalisch-Astronomische Fakultät
Dean Professor R. Kowarschik
Max-Wien-Platz 1
07743 Jena
Germany

and

Project Management Jülich
Division Technological and Regional Innovations (TRI)
Forschungszentrum Jülich GmbH
Zimmerstrasse 26–27
10969 Berlin, Germany
Email: k.-d.husemann@fz-juelich.de

For further information, please contact:
Professor Andreas Tünnermann (Andreas.Tuennermann@uni-jena.de); www.ultraoptics.de

Design a better world. Engineer young minds.

BE PART OF THE FOUNDING FACULTY OF LEADERS AND INVENTORS

The Singapore University of Technology and Design (SUTD), established in collaboration with MIT, has a mission to advance knowledge and nurture technically grounded leaders and innovators to serve societal needs. This will be accomplished, with a focus on Design, through an integrated multi-disciplinary curriculum and multi-disciplinary research.

MIT's involvement is multi-faceted and includes developing new courses and curricula, helping with early deployment of courses in Singapore, assisting with faculty and student recruiting, mentoring and career development, collaborating on major joint research projects including a major international new design centre, and student exchanges. Many of the newly hired SUTD faculty will spend up to a year at MIT in a specially tailored programme for collaboration and professional development.

SUTD plans to be a centre for learning, knowledge creation and dissemination, and like MIT be a melting pot for scholarship and practice. SUTD aspires to do what MIT has done for its locale and the US economy; be an engine of growth for Singapore, the region and the world. In collaboration with MIT, SUTD will bring together the best minds and ideas to create and sustain enormous technological, financial and social impacts for a better future.

SINGAPORE UNIVERSITY OF TECHNOLOGY AND DESIGN

Established in collaboration with MIT

SUTD will matriculate its first intake of students in 2011. The University's programmes will be based on four pillars leading to separate degree programmes in Architecture and Sustainable Design, Engineering Product Development, Engineering Systems and Design, and Information Systems Technology and Design. Design, as an academic discipline, cuts across the curriculum and will be the framework for novel research and educational programmes.

FACULTY MEMBERS

The qualifications for the faculty position include: an earned doctorate in Architecture, any field in Engineering, or Basic Sciences and Social Sciences, a strong commitment to teaching at the undergraduate and graduate levels, a demonstrated record of or potential for scholarly research, and excellent communication skills.

We invite applications for interdisciplinary faculty appointments at all levels, with many opportunities available in particular at the Assistant and Associate Professor levels. Duties include teaching of graduate and undergraduate students, research, supervision of student research, advising undergraduate student projects, and service to SUTD and the community. Faculty will be expected to develop and sustain a strong research programme. Attractive research grant opportunities are also available.

Successful candidates can look forward to internationally competitive remuneration, and assistance for relocation to Singapore.

If you share SUTD's vision on multi-disciplinary curricula and research with a focus on Design in the broadest sense, please contact us.

Enquiries for the above mentioned position can be addressed to Anthony Keh at **anthonykeh@sutd.edu.sg**

To learn more about SUTD, please visit www.sutd.edu.sg.

Friedrich-Schiller-Universität Jena

The Institute of Applied Optics at the Department of Physics and Astronomy is seeking a

W2-Professor for Applied Physics/ Applied Optics for Ophthalmology

Exceptionally well-qualified candidates must work in the field of modern applied optics for ophthalmology. A close collaboration of the candidate within the research topic Optics/Photonics of the University is expected. Moreover, the cooperation with other faculties of our university, especially with the School of Medicine, extra-university research institutes, and the optical industry should be extended. Duties of the position include a full teaching load at all levels in experimental physics and optics.

Applicants must have a PhD degree and "Habilitation" (or a similar scientific qualification) and a strong commitment to teaching.

The University of Jena aims at increasing the number of female faculty members and thus encourages applications of qualified women scientists. Disabled persons will be preferred, if equally qualified.

Applications should include curriculum vitae, list of scientific publications, a statement on teaching and research interests as well as a list of obtained research grants and should be submitted by **April 30, 2010** to the **Dean, Physikalisch-Astronomische Fakultät, Friedrich-Schiller-Universität Jena, Max-Wien-Platz 1, 07743 Jena, Germany.**

Neuropharmacology, Faculty

The Center for Substance Abuse Research (CSAR) and the Department of Pharmacology at Temple University School of Medicine invite applicants for a tenure track faculty appointment at the level of Assistant or Associate Professor. CSAR is a multidisciplinary enterprise encompassing faculty from multiple departments/colleges at the University. CSAR has a P30 Center Grant and a Training Grant funded by NIDA. Interested individuals should have a PhD and/or MD degree, postdoctoral experience, and an active, funded research program. Candidates should have the ability to enhance and interface with existing ongoing research in the Center (www.temple.edu/medicine/csar). We are especially interested in a neuropharmacologist investigating the neurobiology of addiction or pain processes. Candidates are expected to maintain a vigorous research program, in addition to educating graduate and professional students.

Please submit a curriculum vitae, a research program summary, a statement of career objectives, and the names and contact information of at least three references to:

Alan Cowan, PhD, Chair, CSAR Search Committee, Department of Pharmacology, Temple University School of Medicine, 3420 N. Broad Street, Philadelphia, PA 19140 or acowan@temple.edu.

School of Medicine
TEMPLE UNIVERSITY®

Temple University is an EEO/AA employer and strongly encourages applications from women and minorities. Further information is available at **www.medschool.temple.edu**

Weill Cornell Medical College in Qatar

DIABETES, OBESITY & METABOLIC SYNDROME (DOMS) CENTER

BIOMEDICAL RESEARCH PROGRAM **FACULTY POSITIONS**

Weill Cornell Medical College in Qatar (WCMC-Q), a branch of Weill Cornell Medical College of Cornell University, seeks Clinical Research & Translational Biomedical Science investigators to join its new Diabetes, Obesity & Metabolic Syndrome (DOMS) Center.

Program Focus

The WCMC-Q DOMS Center will address major health challenges in Qatar and the region by developing integrated clinical and translational research projects. Qatar, which has a high prevalence of diabetes, obesity and associated disorders, offers an excellent opportunity to develop innovative programs.

A key component of WCMC-Q's recently established biomedical research program, the Center will be part of a vibrant scientific community, which Qatar is developing through initiatives such as Education City, a 2500-acre campus that houses branch campuses of some of the world's leading universities. Outstanding collaborative opportunities exist within the program, with investigators at Weill Cornell Medical College and Cornell University in New York, and with partners in Qatar, including Hamad Medical Corporation, the nation's premier not-for-profit healthcare provider, and Sidra Medical and Research Center, a specialty teaching hospital that is scheduled to open in 2012.

The WCMC-Q DOMS Center's overarching vision is to create a collaborative, multidisciplinary team environment, endowed with a comprehensive support infrastructure. Investigators will be able to draw on state-of-the-art facilities, including genomics, proteomics, imaging, and computational and biostatistics cores; in addition, specialized clinical research support teams, comprising regulatory and clinical coordinators, will facilitate the timely launch of new projects. The Center will also develop educational and clinical training programs and partner with public health initiatives.

Details regarding the WCMC-Q program and facilities can be accessed at: **www.qatar-med.cornell.edu.**

Qualifications

This is an open rank search for six investigators recruited at the Assistant, Associate and Full Professor levels. Candidates must have an MD and/or PhD degree and expertise in one of two categories:

- **Clinical Research**
- **Translational Biomedical Science**

A highly competitive salary and comprehensive foreign-service benefits package with a competitive start-up package will be provided.

Process

Qualified applicants willing to relocate to Doha are invited to submit a letter of application outlining their interest in the position and a description of research interests and future research plans (3-5 pages), as well as a curriculum vitae to:

http://job.qatar-med.cornell.edu *

* Please select the appropriate position under the Academic positions, complete requested information, and upload documents.

The screening of applications will begin immediately and continue until suitable candidates are identified. Please note that due to the high volume of applications, only short-listed candidates will be contacted. Short-listed candidates will be asked to provide names of three references.

Cornell University is an equal opportunity, affirmative action educator and employer

Weill Cornell Medical College in Qatar

Qatar Foundation

ACQUIRING PEOPLE SKILLS

- Ask if your university holds workshops for new supervisors on management, delegating, interviewing, or other interpersonal responsibilities.
- Use available books, like *Academic Scientists at Work,* by Jeremy Boss and Susan Eckert (Springer-Verlag, 2002) and Kathy Barker's *At the Helm: A Laboratory Navigator* (Cold Spring Harbor Laboratory Press, 2001). Slack, impressed with how "it spells out all you need to run your own lab," gives a copy of the Boss-Eckert book to each postdoc progressing to the next position.
- Look for a special interest group on campus or nearby, such as Women in Science and Engineering. Members are often generous with support and information.
- Consider a few sessions with a private coach. Morris Consulting Group trains individual scientists seeking stronger managerial skills, and it recently published, *Leadership Essentials for Women Scientists: Tips, Tools and Techniques to Advance Your Career* (equally relevant to men.)
- "People skills are teachable," Susan Morris assures. "Make a commitment to learn consistently, not in fits and starts."

Every network needs ongoing maintenance—allocate at least one hour a week for brief steps that keep your name in front of people. "Make a follow-up call, meet for coffee, or send a handwritten note," says Morris.

You'll probably work with departments and scientists inside and outside your own institution. Lippincott-Schwartz encourages collaboration within her group. "Each person is an equal part. I try to get people talking to each other in small groups, making sure to include everyone who's interested in this topic. It's so cool to see people with different expertise working together—their energy feeds on each other."

"I know our lab isn't able to do everything," Slack acknowledges. "We seek collaboration where we think someone could be constructive in a project. Fortunately, Yale is very collaborative; its 400 bio labs have most of the expertise we've needed. It just takes a few e-mail rounds: 'do you work on X?' They may say 'No, but try Y'. "

Finding academic science increasingly interactive, Frazer sees large collaborations encompassing diverse skill sets. Her new international grant has five M.D. clinicians and five Ph.D. biologists, plus genomicists and informatics specialists, in San Diego, Vancouver, and Toronto. Beyond monthly phone meetings of all 20 researchers, Frazer has frequent contact with other genomicists. The entire group will meet in both Toronto and San Diego annually.

Joerg Schaefer directs the Cosmogenic Dating Lab at Columbia University's Lamont-Doherty Earth Observatory. His lab collaborates with scientists on related projects, all over the world, including with a New Zealand team for nearly a decade. They stay in close contact through Skype and other technologies. The complexity of establishing a partnership in a distant country calls for exceptionally resourceful networking. Through another Lamont lab, Schaefer was able to join a collaboration, the Asian Monsoon Project, with the nation of Bhutan.

Sustain previous collaborations, recommends **Michel Tremblay,** director of McGill University's Rosalind and Morris Goodman Cancer Center, with 300 students, postdocs, and technicians. "When you leave a lab and get out on your own, it may be a different kind of project. Your [previous colleagues] won't follow you. If you had a good relationship with your ex-mentor, maintain it."

Which collaborations thrive? Setting mutual goals fosters strong, honest, productive interaction. "Especially with virtual relationships, take incremental steps to build trust," Morris recommends. Spell out communication pathways at the very beginning: how often, in what form, and who gets to know what? "With a global team, have at least one face-to-face meeting to establish ground rules."

Mentoring

"There's a big difference between mentorship and directing research," explains Tremblay. "Don't micromanage—mentoring isn't telling the scientist what to do. Like a good parent, offer guidance, but let the [mentee] develop. Give freedom. Treat individuals as partners." Good mentors, he adds, know their way around the university and understand how to get to the right people.

"Learn to juggle many different things simultaneously, but keep emotionally steady because people in your lab really look to you," says Lippincott-Schwartz. "It's a huge roller coaster every time you send out a paper—everyone's going through emotional ups and downs. To be cheerleader is critical." When a project isn't working well, talk through options, brainstorm new ideas, and ask, "So if we get this result, then what?" Lippincott-Schwartz doesn't prevent anyone from trying a new idea they feel strongly about. "I might argue against it, but I won't say, 'No, don't.'"

"My door is always open," declares Slack, inviting everyone to see him whenever they want, show him data, or call him to the microscope. "I don't go to them every day, or even every week. I tend to encourage by steering, not forcing, and giving a little space to find their own way."

To Frazer, it's vital for managers "to be open, honest, and straightforward, but simultaneously kind and compassionate. The fun stuff is easy. Deflecting a potential problem is harder."

When one new postdoc was, as Frazer described it, "all over the place," she discreetly intervened. "It was important for him to stay on track and learn to get things done, or else he'll have a tough time in future jobs." In giving well-defined assignments, she would emphasize, "This is the task," then thank him warmly upon completion. After four months, things are improving. "Now when we have a conversation, he realizes, 'I have to focus, not be distracted,'" Frazer reports.

In academia, teaching is central, Tremblay observes. continued »

Faculty Positions in the Division of Chemical and Life Sciences and Engineering

The Division of Chemical and Life Sciences and Engineering at the King Abdullah University of Science and Technology (KAUST) invites applications from outstanding scientists to complement and enhance our research in the molecular life sciences. We are particularly interested to further develop the following disciplines:

- Structural Biology
- Synthetic Biology
- Protein Biochemistry and Proteomics

KAUST (http://www.kaust.edu.sa) provides state-of-the-art facilities and technical support to conduct research in these areas. The instrumentation includes NMR, electron microscopy and mass spectroscopy and both computational and bioinformatics support is ensured through close collaboration with the Computational Bioscience Research Centre.

Applicants will have a PhD in a biological science or a related discipline, post-doctoral research experience and are committed to collaborative and interdisciplinary research within KAUST and with our global research partners. Successful candidates will build their own research groups, participate in the graduate teaching program and supervise Masters and PhD students.

KAUST is dedicated to a respect for diversity and the highest standards of merit–based selection of the finest faculty without regard to ethnicity, gender, or religious belief. We do, however, particularly encourage women to apply. The level of appointment will be commensurate with experience.

Those interested in pursuing this unique opportunity should send a CV (including publication lists and contact information for at least three potential references) and a statement of research interests.

For more information, please visit www.kaust-aea.cam.ac.uk or email info@kaust-aea.cam.ac.uk

Applications will be considered until all positions have been filled.

KAUST

Université de Neuchâtel unine

FACULTE DES SCIENCES

The University of Neuchâtel, Switzerland, offers the position of an

Assistant professor in Biology of arthropod vectors of pathogens

The candidate is expected to have a strong research background which complements well with the parasitology interests of the Institute. He/she will have an experience in the biology of vectors of pathogens focused on the physiology of ectoparasites, capable to combine both field and laboratory methods and showing an international recognized research program. The successful candidate is asked to teach in the bachelor of biology and first year medical studies as well as in the Master Biology of Parasites and Ecoethology.

Starting date: August 1, 2010 or date to be discussed.

Candidates with a Ph.D. should submit their application, both electronically and on paper, **before April 12, 2010** to Prof. Bruno Betschart, head of the search committee, Institute of Biology, Faculty of Science, University of Neuchâtel, PO Box 158, 2009 Neuchâtel – Switzerland, email: **bruno.betschart@unine.ch.**

Applications should include a letter of motivation, curriculum vitae with a description of research, teaching, grants, and administrative records; a complete list of publications; a copy of academic diplomas; a statement of research interest and projects of up to 3 pages. The candidate should ask three experts to send a letter of recommendation to the head of the search committee.

The University of Neuchâtel encourages women to apply.

Further information is available from Prof. B. Betschart or on the web site **www.unine.ch/sciences** , under « emploi ».

RUHR-UNIVERSITÄT BOCHUM

RUB

The Ruhr-University Bochum is one of Germany's leading research universities. The University draws its strengths from both the diversity and the proximity of scientific and engineering disciplines on a single, coherent campus. This highly dynamic setting enables students and researchers to work across traditional boundaries of academic subjects and faculties. Host to 32,600 students and 4,700 staff, the Ruhr-University is a vital institution in the Ruhr area, which has been selected as European Capital of Culture for the year 2010.

PROFESSORSHIP (W3) IN PHYSICAL CHEMISTRY

The **Faculty of Chemistry and Biochemistry** at the Ruhr-University Bochum, Germany, invites applications for a Professorship (W3) in Physical Chemistry.

We are searching for an internationally visible researcher in the field of material science; physical chemistry of surfaces and interfaces. The research topics and experimental methods should be complementary to the research activity of the other physical chemistry groups in the department.

The successful applicant must be able to teach all courses of Physical Chemistry. Knowledge of German is not required in the beginning, but will be expected as a teaching language within the first five years. All master courses are taught in English. Candidates are expected to be able to acquire and coordinate externally funded projects.

Ruhr-University Bochum seeks to foster the careers of women and therefore explicitly encourages women to apply. Disabled persons with equivalent qualification will be favoured.

Qualified candidates are asked to submit their application including C.V., list of publications and talks, teaching record and research activities including a list of previous funding, and copies of degree certificates by **April 24, 2010** to the **Dean of the Faculty of Chemistry and Biochemistry, Ruhr-University Bochum, 44780 Bochum, Germany.**
E-mail: chemie-dekanat@rub.de

Zertifikat seit 2006 audit familiengerechte hochschule

University of Zurich

The Faculty of Science of the University of Zurich is seeking to fill the position of an

Assistant Professor in Statistical Genomics

We are searching for individuals with an excellent research record in statistical genomics, including – but not limited to – research on whole-genome association studies, population genomics, identification of somatic mutations in disease, and the analysis of ultra high-throughput sequencing (UHTS) data in human or other model systems. A proven research record in complex genome-scale data analysis, as well as in the development of statistical or computational methods to analyze such data, is essential. The successful candidate will have demonstrated a keen interest in advancing biological knowledge through his or her research, and be highly interactive and open to collaboration. He or she will be expected to establish an independent research group within the University Research Priority Program Systems Biology/ Functional Genomics (www.sysbio.uzh.ch), and will have access to state-of-the-art research facilities provided by the University, and by the Functional Genomics Center Zurich (www.fgcz.uzh.ch), a technology platform for UHTS, transcriptomics, proteomics, and metabolomics. There are excellent opportunities for interactions with other groups of the University of Zurich and the ETH Zurich, as well as with the Swiss Systems Biology Initiative (SystemsX.ch), and the Swiss Institute for Bioinformatics (SIB).

This six-year non-tenure track assistant professorship carries limited teaching responsibilities (in English or German) and includes an attractive start-up package and significant support for running operations. Applications, including detailed curriculum vitae, publications list, short statement of research and teaching interests, and the names and addresses of three academic referees should be addressed to Prof. Michael Hengartner, Dean of the Faculty of Science, Winterthurerstrasse 190, 8057 Zurich, Switzerland, and submitted as a single PDF file to jobs@mnf.uzh.ch. For further information, please contact Prof. J. Jiricny at jiricny@imcr.uzh.ch. The application deadline is June 15, 2010.

The University of Zurich is an equal opportunity employer. Applications from women candidates are particularly encouraged.

Center for Immunology and Microbial Disease
Albany Medical College

Faculty Position

The Center for Immunology and Microbial Disease at Albany Medical College invites applications for a tenure-track faculty position from individuals who have a doctoral degree, postdoctoral experience, and demonstrated research productivity. Those with an interest in microbiology and/or host-pathogen interactions are particularly encouraged to apply. The successful candidate will be expected to establish an independent, extramurally funded research program and participate in the teaching of medical and graduate students. The basic science departments at Albany Medical College are organized as interdisciplinary research centers and the Center for Immunology and Microbial Disease has a focus on microbial pathogenesis and immune defense, particularly as related to biothreat agents and emerging infections. Faculty at the Albany Medical College receive competitive salaries, attractive start-up packages, and access to the Center's ABSL-3/BSL-3, Microbiology and Immunology Core Labs. In addition, we have established a close relationship with the New York State Department of Health Wadsworth Laboratories, providing a diverse environment that is rich in infectious disease expertise. Albany Medical College is located in a mid-sized city within the upstate New York Capital Region, and has easy access to Boston, New York City, and the Adirondack Mountains.

Applicants should send their curriculum vitae, a statement of research plans, and three letters of reference to:

Faculty Search Committee
Center for Immunology & Microbial Disease
Albany Medical College
47 New Scotland Avenue, MC-151
Albany, NY 12208

For further information about the Center, visit **www.amc.edu/Academic/Research/imd.htm**.

An Equal Opportunity/Affirmative Action Employer.
Women and minorities are encouraged to apply.

SCHOOL OF MEDICINE & DENTISTRY
UNIVERSITY of ROCHESTER MEDICAL CENTER

Faculty Position in Neurotoxicology

Applications are invited for a tenure-track faculty position at the Assistant or Associate Professor level in the Department of Environmental Medicine at the University of Rochester. We seek an outstanding individual with a strong commitment to excellence in research, scholarship and teaching. The Department of Environmental Medicine hosts an NIEHS Environmental Health Sciences Center of Excellence, an EPA Particulate Matter Center and an NIEHS Toxicology Graduate Training Program (**http://www2.envmed.rochester.edu/envmed/iindex.html**). This individual is expected to maintain a vigorous, creative and independent research program.

We are especially interested in applicants that apply cutting-edge approaches to fundamental questions in neurotoxicology that examine the relationship between environmental exposures and neurodegenerative and/or neurodevelopmental diseases and disorders. The successful candidate will join a highly interactive faculty with research interests in neurotoxicology, cardiopulmonary and developmental toxicology, osteotoxicology, immunotoxicology and the molecular biology of xenobiotic receptors and transporters. Competitive salary, start-up packages and access to the many Facility Cores of the NIEHS Center and the Medical Center are provided. The University of Rochester Medical Center is undergoing a major expansion of its research facilities and infrastructure, with an emphasis on the areas of neuromedicine, cancer, cardiovascular disease, immunology & infectious disease and musculoskeletal disease.

Applicants should send a CV, a statement of research interests including future plans, and the names of 3-5 references to: **Dr. Deborah A. Slechta, Search Committee Co-Chair, Box EHSC, Department of Environmental Medicine, University of Rochester School of Medicine, Rochester, NY 14642, (deborah_cory-slechta@urmc.rochester.edu)**.

The University of Rochester is an Equal Opportunity Employer.

ITC faculty position A - Associate/Assistant Professor - ACH 48507

The Immunotherapy Center and Department of Medicine at the Medical College of Georgia seek applicants for a faculty position primarily focused on basic research related to inflammatory processes linked to disease syndromes. The successful applicant will join an established research program dedicated to studying counter-regulatory and immune tolerance mechanisms, and using this knowledge to develop novel immunotherapies to improve clinical outcomes. Current research topics include fundamental studies on immune tolerance mechanisms, and assessing the contribution of tolerance mechanisms to chronic inflammatory diseases such as cancer, infectious and autoimmune diseases and transplant survival. Applicants should have a PhD or MD/PhD and a documented record of productivity in an area of basic or clinical immunology research that supplements or complements these research topics. Preference will be given to candidates with established research programs, although applications from exceptional younger investigators will also be considered. The successful applicant will hold joint appointments in the Immunotherapy Center and the Department of Medicine, and will have access to exceptional core research facilities (listed at **http://www.mcg.edu/Core/Labs/**) and modern custom-designed laboratory space. Generous start-up packages are available to support this recruitment. The Medical College of Georgia is an EEO/AA/Equal Access Employer, and is a growing state-supported academic medical center located in a historic city with outstanding recreational and lifestyle opportunities. For further information please contact: **Andrew Mellor, PhD, Director of the Immunotherapy Center (amellor@mcg.edu) Medical College of Georgia, Augusta, GA 30912-3220**.

ITC(IDI) faculty position B - Associate Professor/Professor - ACH 51226

The Immunotherapy Discovery Institute (IDI) at the Medical College of Georgia seeks qualified candidates for a senior faculty position to promote translational research related to an aspect of chronic inflammatory disease syndromes. The successful applicant will have the opportunity to work with established research teams in the MCG Immunotherapy Center and clinical faculty in the Department of Medicine. An endowed chair is available for exceptionally qualified individuals with a proven track record of productivity in translational medicine related to immunotherapy in any of the following clinical areas, autoimmune, allergic and infectious diseases, transplantation, vaccine design and development. Investigators in the MCG Immunotherapy Center are studying immune counter-regulatory and tolerance mechanisms, and are developing novel immunotherapies to improve clinical outcomes such as the use of novel vaccine adjuvants to treat cancer patients. Current research topics include fundamental studies on immune tolerance mechanisms, and assessing the contribution of such mechanisms to chronic inflammatory diseases such as cancer, infectious and autoimmune diseases and tissue transplant survival. Applicants should have a MD or MD/PhD and a documented record of productivity in an area of clinical immunology research that complements these research strengths. Preference will be given to candidates with documented experience of promoting clinical research and managing early phase clinical trials. The successful applicant will hold joint appointments in the Immunotherapy Discovery Institute and the Department of Medicine, and will have access to exceptional core research facilities (listed at **http://www.mcg.edu/Core/Labs/**) and laboratory space. Generous start-up packages are available to support this recruitment. The Medical College of Georgia is an EEO/AA/Equal Access Employer, and is a growing state-supported academic medical center located in a historic city with outstanding recreational and lifestyle opportunities. For further information please contact: **Andrew Mellor, PhD, co-Chair Immunotherapy Discovery Institute (amellor@mcg.edu), Medical College of Georgia, Augusta, GA 30912-3220**.

THE UNIVERSITY of TENNESSEE HEALTH SCIENCE CENTER

OPEN RANK FACULTY POSITION
DEPARTMENT OF PHYSIOLOGY
UNIVERSITY OF TENNESSEE
HEALTH SCIENCE CENTER IN MEMPHIS (UTHSC)

We invite applications from outstanding scientists in the field of Cardiovascular Research for an open rank position in the Department of Physiology. The ideal candidate is an investigator with an established multi-grant-funded research program and ability to lead a group of investigators. Physician-scientists are encouraged to apply with the possibility of part-time involvement in patient care. The position comes with state-of-the-art laboratories, an attractive start up package, a competitive salary with a lucrative incentive bonus, along with access to a unique mouse genetics reference population (**http://cgb.uthsc.edu**). Senior applicants will be considered for an Endowed Professorship. Cardiovascular research at UTHSC has a long tradition of excellence and is one of the strategic areas of expansion with several new recruitments and a dedicated research building under development. Vascular biology, ion channel and cardiac physiology are our current research themes. Based on extramural funding the Department of Physiology is currently ranked fourth nationally by the American Physiological Society (**http://physio1.uthsc.edu**).

To apply, please submit curriculum vitae, summary of current and proposed research programs, teaching experience and interests, and contact information for three to five references, in a single Word or PDF document to:

Gabor Tigyi, M.D., Ph.D.
Harriett Van Vleet Professor and Chair
Department of Physiology
E-Mail: PhysiologySearch@uthsc.edu

Review will begin upon receipt of the application.

The University of Tennessee is an EEO/AA/Title VI/Title IX, Section 504/ADA/ADEA Employer.

UAB THE UNIVERSITY OF ALABAMA AT BIRMINGHAM

DEPARTMENT OF PATHOLOGY
DIRECTOR
DIVISION OF MOLECULAR AND CELLULAR PATHOLOGY

The Department of Pathology at the University of Alabama at Birmingham (UAB) is pleased to announce recruitment for Director of the Division of Molecular and Cellular Pathology. UAB ranks in the top ten for NIH funding to Departments of Pathology and was recently ranked third in the nation for faculty scholarly productivity in the discipline of Pathology. We are inviting applications from qualified candidates at the Associate or full Professor level. This is a full-time, tenure-earning or tenured position through the Department of Pathology, Schools of Medicine and Dentistry. The candidate should have a doctoral degree: (M.D. and/or Ph.D). It is anticipated that candidates will have a nationally recognized extramurally funded research program and the administrative experience necessary to lead a group of talented basic research scientists. Potential synergy with current research strengths in the department would be considered a strength. These include nationally recognized researchers in cancer pathobiology, cardiovascular, immunology, bone, extracellular matrix, diabetes and redox biology. The Director will be responsible for the leadership and career development of 15-20 faculty and will play a major role in strategic planning for research in the division.

UAB is a leading research institution consistently ranked in the top 25 institutions in the country in NIH research funding. Outstanding Centers, including a recently awarded Center for Clinical and Translational Science, and a broad range of specialized core facilities are among the attractions at the Institution. The position will remain open until filled. Individuals who wish to be considered should submit a comprehensive curriculum vitae, detailed application letter, statement of research interests, and the names of at least three individual references to: **Victor Darley-Usmar, Ph.D., Professor and Interim Division Director, Vice-Chair for Research, Division of Molecular and Cellular Pathology, Department of Pathology, University of Alabama at Birmingham, 901 19th Street South, Biomedical Research Building II, Room 312, Birmingham, AL 35294-2172** or email **PATH-MCPRecruit@mail.ad.uab.edu**.

The University of Alabama is an Affirmative Action/Equal Opportunity Employer. Women and minority applicants are encouraged to apply.

"I tend to encourage by steering, not forcing, and giving a little space to find their own way."
—Frank Slack

FEATURED PARTICIPANTS

Columbia University
www.columbia.edu

McGill University
www.mcgill.ca

Morris Consulting Group
www.morrisconsulting.biz

National Human Genome Research Institute
www.genome.gov

University of California, San Diego
www.ucsd.edu

US National Institutes of Health
www.nih.gov

Yale University
www.yale.edu

"Promote your young faculty members through lecturing responsibilities, such as teaching fourth-year undergraduates. That makes them better known to students deciding which laboratory to choose for graduate studies." Remind research students to make a career plan. Instead of directing where to do further training, you might say, "these few labs are the best in their fields. The P.I. is well known for mentorship. These are some I wouldn't choose because of track record, funding, field of research, or networking."

One touchy situation: a young researcher with consistently disappointing performance. "Some P.I.s won't get involved at all. It's very hard to say, 'academia is not for you,'" Tremblay finds. "Sometimes you must tell your mentee, 'These are your strengths. Here is where you are weak. I think you might not make it as a faculty member at a top university. You have good expertise in other aspects of research, such as administration. You would be great in translational research or clinical trials.'"

When a postdoc heads toward another job, "Leave space for them to start their own program. It takes generosity," says Tremblay, "to allow this best trainee in the last year to start a new one to bring along. Have an open discussion with each trainee about what they'd like to do next. Provide tools for them to move forward," including the time and resources to carve something from the current project.

Motivating and Managing

A corporate lab's objective is meeting the business goal. An academic lab's goal "is whatever the PI got money for," Morris notes. "Every department meeting, every printed document, every conversation should reinforce that 'the mission of this lab is to....' Constantly remind people that we're not here to do our individual experiments. This is part of something bigger."

Morris cites the "complex demographics of lab personnel. Managing and leading require respecting differences between cultures and generations. Accept that work can be done in individual or innovative ways," Morris suggests. "One person may complete projects by setting a timeline for each day's work, while another needs the adrenaline of last-minute pressure, completing the project by several all-nighters. Yet both produce a quality product."

To promote a team's trust and cooperation, Tremblay advises setting clear expectations for your lab, staying aware of what's going on there, and quickly resolving conflicts within your group.

What constitutes conflict? Hogging a piece of equipment or writing notes in a native language instead of lab language affects everyone. Ideally, Morris advises, let lab members resolve minor tensions, stepping in only when something escalates enough to disrupt the research. "Establishing and following performance guidelines that define appropriate versus inappropriate lab behavior is essential to becoming an effective lab manager. Make every employee aware of guidelines and consequences for not complying," says Morris.

Clarify academic realities, too, Tremblay stresses. A researcher may be the inventor of a discovery, and receive acknowledgment through an ensuing patent with his/her institution, but the university owns everything done in any lab on its property. "To make sure everyone is treated fairly, keep your lab well organized so you're clear about who's done what, who started what. People should get the credit they deserve. That's what justifies the hard work, especially on licenses, patents, and publications."

Some of Schaefer's lab members go on lengthy field excursions, to locations as far-flung as Patagonia or New Zealand. "Working globally, the areas we study are always beautiful, and we post wonderful photos. Then the researchers come back and share their adventures on the field trip. It makes everyone feel very involved."

Schaefer's team-building has a firm foundation: "I make it clear that I expect everyone who works here to have fun. We have lunch together once a month, off campus. Every week, one group goes out after work, for beer."

Slack's lab prefers champagne, popping open at least one bottle a month to celebrate a birthday, new grant, or accepted paper. He cooks an annual dinner for all 17 researchers at his home. The team takes one day trip each year, like canoeing.

Slack's annual State of the Lab address "honestly assesses where we are in terms of new money, new people, our papers, our goals for that year. We'll all know what our colleagues are working toward. I give information and want them to tell me what they think. They get to speak up about direction, or any area where they think we should focus or add effort."

His entire team gets involved in hiring. "Any postdoc I consider comes to the lab for a day, meets everyone to talk about science one-on-one, and has lunch and dinner. Each of my people reports on the interaction. We check motivation, interest, and personality," Slack confides. "We have few interpersonal issues because we try to encourage smart, socially adept people to join. And we demand they each be a good lab citizen."

Carol Milano is an independent journalist in New York City, covering health care and science.

DOI: 10.1126/science.opms.r1000086

WVNano

West Virginia University

Director for the WVNano Initiative

West Virginia University seeks applications and nominations for an exceptional leader with strong technical, strategic planning and team-building skills to become the Director of WVNano, the West Virginia University initiative for nanoscale science and engineering, and education (NSEE). WVNano (**http://wvnano.wvu.edu**) is an exciting University-wide initiative to accelerate both NSEE and nanotechnology research to a high level of competitiveness. WVNano is an intensely interdisciplinary effort involving over 25 researchers from the colleges representing science, engineering, health science, and education. WVNano is funded by university, state, and federal sources. The strategic plan is dynamic and has resulted in ten new faculty positions. A significant number of additional NSEE-related faculty searches are also underway by the University's Colleges.

The Director will promote the sense of community within WVNano and be responsible for the Initiative's vision, leadership, advocacy, and management. The Director will report directly to the Vice President for Research and Economic Development. Acceptable candidates must have a demonstrated commitment to and current knowledge of interdisciplinary research and education relevant to NSEE; demonstrated technical, administrative, and communication skills; an earned doctoral degree; and an established record of leading and fostering large interdisciplinary research efforts. Evidence of significant academic research and educational expertise and/or experience leading large research programs is required. The academic appointment will be commensurate with the candidate's background.

Applications should be submitted electronically to **nanoresearch@mail.wvu.edu** (list WVNano Director in the subject line). Applications should include (1) a statement describing the applicant's qualifications and vision for the future of WVNano; (2) a complete curriculum vitae, including a record of scholarly activity and leadership experience; and (3) the names and contact information for at least five references. The position will remain open until filled. Questions regarding the position should be addressed to: **Fred L. King, Chair WVNano Director Search Committee, (Fred.King@mail.wvu.edu (304) 293-4611**).

West Virginia University is an Affirmative Action, Equal Opportunity Employer, dedicated to building a culturally diverse and pluralistic faculty and staff committed to working in a multicultural environment. Applications from women, minorities, individuals with disabilities and covered veterans are encouraged. Individuals that are part of dual career couples are also encouraged to apply.

DIRECTOR, CARDIO-METABOLIC DISEASE RESEARCH PROGRAM

The Julius L. Chambers Biomedical Biotechnology Research Institute (BBRI) at North Carolina Central University invites applications for the position of Director for the Cardio-Metabolic Disease Research Program. The Program Director will have a unique opportunity to lead a multidisciplinary, inter-institutional research program located in a 40,000 sq. ft. facility. This state-of-the-art building also houses programs in cancer research and neurobiology. A range of research-related resources are available. These include genotyping and cell/tissue culture core facilities, visualization and imaging laboratory, modern animal care and use facility, and common user equipment rooms.

The ideal candidate should have experience managing interdisciplinary aspects of cardio-metabolic research programs. Current research interests in this program include renal physiology and mechanisms of end-organ damage, obesity, mechanisms of vascular disease, G-protein-coupled receptor cell signaling, and the vasoregulatory roles of physiological calcium. The Program Director will be expected to support existing research programs and forge additional translational research partnerships between the various academic units at NCCU in biomedical, behavioral, and social science areas as well as with many academic and research institutions, agencies and corporations in Research Triangle Park area and the state. The proximity of NCCU to North Carolina Research Triangle Park and other colleges and universities will afford the Director a rich opportunity to develop joint programs with a high probability for long-term success.

Applicants must hold a Ph.D. and/or M.D. and should excel as an educator and researcher. The applicant should have a strong record of sponsored research program management and meet requirements for a tenure-track faculty appointment at the Associate Professor or Professor level in one of the departments in the College of Science and Technology. Additional requirements include: demonstrated administrative and scientific leadership, a strong record of peer-reviewed research publications, research funding, prior teaching experience at the undergraduate and graduate levels, evidence of outreach activities, work with diverse populations (especially at the graduate level) and other professional accomplishments. Review of applicants will begin immediately and will continue until the position is filled. Applicants should submit *curriculum vitae*, a description of research interests, and contact information for three references to: **Yvette Thompson, Executive Assistant, Division of Graduate Education and Research, Room 309 Hubbard-Totten Building, 1801 Fayetteville Street, North Carolina Central University, Durham, NC 27707,** or via email **ythompson@nccu.edu**. For more information about the BBRI and NCCU visit **http://www.nccu.edu/BBRI**.

North Carolina Central University is a constituent institution of the University of North Carolina System and an Equal Opportunity, Affirmative Action Employer. NCCU complies with the Immigration Reform and Control Act of 1986.

EXECUTIVE DIRECTOR OF THE THOMPSON CENTER FOR AUTISM & NEURODEVELOPMENTAL DISORDERS

THOMPSON ENDOWED CHAIR IN CHILD HEALTH

The University of Missouri Thompson Center for Autism and Neurodevelopmental Disorders seeks an Executive Director and Thompson Endowed Chair in Child Health. The Executive Director and Chair will provide leadership to the Center, its faculty, staff and programs while advancing the knowledge of effective therapies for autism and neurodevelopmental disorders. The Executive Director and Chair will report to the Provost and Vice-Chancellor and will work in collaboration with the Thompson Center Foundation Board of Directors.

The Thompson Center opened in 2005 and in a very short time has become a national leader in autism through its collaborative research, training and service programs. A new and expanded facility is opening in the summer of 2010. Currently, the Center provides services to over 2000 children, youth and young adults annually.

The successful candidate must have proven experience as a leader and possess strong management skills with the ability to manage budgets within a not-for-profit setting. In addition, successful candidates must have the ability to work collaboratively with a broad range of constituents both internal and external.

Candidates may be an MD/DO, MD/PhD or DO/PhD and hold the rank of associate or professor. Board certification in the appropriate medical subspecialty required. The successful candidate will possess a national reputation built upon a distinguished record of achievement in research, teaching and clinical care of autistic and neurodevelopmental patients.

Qualified candidates should submit their CV to:

Deedra Hartung
Executive Vice President,
Managing Principal
Cejka Search/Executive Search
4 CityPlace Drive, Suite 300
St. Louis, MO 63141
Phone: 800 209-8143 ext. 63518
E-mail: dhartung@cejkasearch.com

The Search Committee is especially interested in qualified candidates who can contribute, through their research, teaching, and/or service, to the diversity and excellence of the academic community. The University of Missouri is an Equal Opportunity Employer and complies with the guidelines of the Americans with Disabilities Act of 1990.

ID#134821C74 cejkasearch.com

University of California, San Francisco…A Health Sciences Campus

MOLECULAR CELL BIOLOGIST POSITION
FULL TIME IN RESIDENCE FACULTY POSITION

The candidate is a molecular and cell biologist whose primary interest is in the development and repair of bone and cartilage. The candidate will establish or must already have established an active and independently funded research program. He/she will teach professional and graduate students, interact with the basic science as well as the clinical faculty of the School of Medicine in relevant research and teaching endeavors. The candidate must have demonstrated expertise in musculoskeletal tissue research as it relates to bone and cartilage development and repair, and the genetics of skeletal tissues.

The incumbent will provide leadership in molecular and cellular skeletal biology research, be an active member of Departmental and UCSF campus committees, advise interested faculty and residents in their research activities, and provide lectures to faculty, residents, and medical students as part of the Department of Orthopaedic Surgery core curriculum.

Applicants must have Ph.D. and postdoctoral experience, and an extensive background in computational and experimental methods. The candidate must also have a demonstrated involvement in quality research through accepted or published writings in peer-reviewed journals, comprehensive expertise in vertebrate skeletal biology, genetics, and bone and cartilage regeneration and repair.

UCSF seeks candidates whose experience, teaching, research, or community service has prepared them to contribute to our commitment to diversity and excellence.

Send curriculum vitae and three blind letters of reference to:

Dr. Thomas Parker Vail
Department of Orthopaedic Surgery
University of California, San Francisco
500 Parnassus Ave, San Francisco, 94143-0728

UCSF is an Equal Opportunity/Affirmative Action Employer. The University undertakes affirmative action to assure equal employment opportunity for underutilized minorities and women, for persons with disabilities, and for covered veterans. All qualified applicants are encouraged to apply, including minorities and women.

ASSISTANT/ASSOCIATE PROFESSOR

Applications are invited for a tenure-track position, Assistant or Associate Professor, North Carolina Central University's (NCCU's) Nutrition Research Program, the North Carolina Research Campus (NCRC), Kannapolis, North Carolina. The NCRC Research Campus is a thriving community where scientists from six universities join with those from industries in conducting research to understand nutrition and its relationship to disease. To learn more about NCRC, please visit **www.ncresearchcampus.net**. The successful candidate will be expected to establish extramurally funded research studies, collaborate with other NCRC and NCCU investigators and train students in her/his field of expertise. Nutrition research currently conducted in NCCU's laboratory focuses on the use of Zebrafish to study the mechanisms by which signaling molecules guide and pattern vascular networks during angiogenesis (formation of new blood vessels). Studies are performed to provide insight to the suppression of cardiovascular diseases and the mechanisms of anti-angiogenesis in combating cancers. A research program complementary or synergistic to this would be preferable. However, mechanism-based cancer prevention research using dietary agents and in-vivo models or nutrigenomics would be welcomed as well.

Applicants must hold a Ph.D. and/or M.D., and have a record of research productivity and support. Review of applicants will begin immediately and will continue until the position is filled. Applicants should submit by mail or email *curriculum vitae*, a description of research interests, and contact information for three references to: **Connie Key, Julius L. Chambers Biomedical/Biotechnology Research Institute, North Carolina Central University, 700 George Street, Durham, NC 27707,** or via email **chkey@nccu.edu**. For more information about the BBRI and NCCU visit **http://www.nccu.edu/BBRI**.

North Carolina Central University is a constituent institution of the University of North Carolina System and an Equal Opportunity, Affirmative Action Employer. NCCU complies with the Immigration Reform and Control Act of 1986.

Dept. of Microbiology & Molecular Genetics
Center for Biopreparedness & Infectious Disease
Faculty Position in Innate Immunity

MEDICAL COLLEGE OF WISCONSIN

We are seeking a tenure-track Assistant or Associate Professor whose research lies within the broad area of **innate immunity**.

The successful applicant will join a collegial group of interactive, well-funded and productive investigators and will be expected to establish a strong, independent research program and participate in graduate and medical student teaching. Strong programs in virology, bacteriology, and immunology will facilitate collaborations and ensure good mentoring. This recruitment is complemented by college-wide initiatives in cancer research, cardiovascular research, and stem cell biology/regenerative medicine.

Competitive salary support, start-up funds and renovated laboratory space will be provided, as well as access to state-of-the-art core facilities. A PhD and/or MD degree and postdoctoral experience are essential. Applications will be considered as they arrive but should be received by April 9, 2010; applicants should submit a curriculum vitae, statement of research interests, and the names of three references to: **Dr. Paula Traktman, Chairman, Dept. of Microbiology and Molecular Genetics, Medical College of Wisconsin, 8701 Watertown Plank Rd., Milwaukee, WI 53226; e-submissions should be sent to kthompso@mcw.edu.**

http://www.mcw.edu/microbiology
http://www.mcw.edu/BiopreparednessInfectiousDiseaseCenter.htm

EEO/AA/M/F/D/V

NIEHS
National Institute of Environmental Health Sciences
National Institutes of Health

Deputy Director

Research Triangle Park, North Carolina

The NIH is seeking exceptional candidates for the position of Deputy Director, NIEHS, to assist in leading the preeminent center for environmentally related health research in the world. The Deputy Director, NIEHS, also participates in leadership of the National Toxicology Program. This position offers a unique opportunity to become part of a team providing strong and visionary leadership toward reducing the burden of human illness and dysfunction from environmental causes. The Deputy Director will help manage a high-level complex organization and must demonstrate integrity and fairness upholding the highest standards of scientific research and business practices. NIEHS conducts and supports interdisciplinary research related to environmentally relevant exposures and diseases and translating that into improvements in both clinical and public health. The Deputy Director will have a critical role in translation of NIEHS basic research findings to human health, particularly new approaches to disease prevention.

Applicants must have senior-level research experience and knowledge of research programs in one or more scientific areas related to environmental effects on human health. Candidates should have a track record of demonstrated leadership of a successful research program which includes partnerships with outside groups as well as extensive planning, program assessment, and analysis of program objectives; the development of plans for the resolution of major operational problems and issues; and management of financial and human resources, including selecting, managing, and motivating staff using fair and equitable staffing/recruitment practices.

Applicants must possess an M.D. and/or doctoral degree and have senior-level research. Adherence to NIH ethics policies is required. Salary is commensurate with experience, and full Federal benefits, including leave, health and life insurance, retirement and savings plan (401k equivalent) will be provided.

Please send questions regarding the position to: Search Committee Chair, Yvonne Maddox at maddoxy@mail.nih.gov and questions regarding the Institute/Division to: John Pritchard at pritcha3@mail.nih.gov.

Interested persons should submit curriculum vitae, contact information for three people to provide a reference, a statement regarding reasons for interest in the position incorporating how you would implement your vision into the NIEHS strategic plan, and identify unique qualifications by **March 31, 2010** to: Ms. Stephanie Jones, NIEHS, Office of Human Resources, P.O. Box 12233, Mail-drop K1-1, Research Triangle Park, NC 27709 or e-mail: jones17@mail.nih.gov Vacancy: NIEHS-11-OD-2010.

http://dir.niehs.nih.gov

DHHS and NIH are Equal Opportunity Employers. This position is subject to a background investigation.

U.S. DEPARTMENT OF HEALTH AND HUMAN SERVICES
National Institutes of Health

FDA Food and Drug Administration
COMMISSIONER'S
Fellowship Program
Protecting Public Health Through Science and Regulation

FDA Commissioner's Fellowship Program

Touch the Lives of All Americans!

The FDA Commissioner's Fellowship Program is a two-year training program designed to attract top-notch health professionals, food scientists, epidemiologists, engineers, pharmacists, statisticians, physicians and veterinarians. The Fellows work minutes from the nation's capital at FDA's new state-of-the-art White Oak campus in Silver Spring, Maryland or at other FDA facilities. The FDA Commissioner's Fellowship offers competitive salaries with generous funds available for travel and supplies.

Coursework and Preceptorship

The FDA Commissioner's Fellowship program combines coursework designed to provide an in-depth understanding of science behind regulatory review with the development of a carefully designed, agency priority, regulatory science project.

Who Should Apply?

Applicants must have a Doctoral level degree to be eligible. Applicants with a Bachelor's degree in an Engineering discipline will also be considered. Candidates must be a U.S. citizen, a non-citizen national of the U.S., or have been admitted to the U.S. for permanent residence before the program start date. For more information, or to apply, please visit: **www.fda.gov/commissionersfellowships/default.htm**.

Applications will be accepted from January 1, 2010 – March 15, 2010

Boehringer Ingelheim

caesar
center of advanced european studies and research

MAX-PLANCK-GESELLSCHAFT

Boehringer Ingelheim, caesar and the Max-Planck-Society announce an

Independent Junior Research Group

"Cellular Degradation Mechanisms in Neurodegenerative Diseases"

The candidate should be interested in general mechanisms of cellular degradation pathways during neurodegenerative diseases in particular autophagocytosis or degradation in the endosome, lysosome or proteasome.

The Junior Research Group will be established at the center of advanced european studies and research in Bonn (caesar; www.caesar.de), an interdisciplinary research center associated with the Max-Planck-Society.

Funding of the Research Group covers a set-up package, the position of the group leader, a technician, one PhD and one post-doctoral fellowship, secretarial support, plus consumables, and is (initially) for 5 years. The successful candidate should have experience in one of the above mentioned research areas.
Applications should include a CV, a list of publications, a one-page summary of scientific achievements, a two-page research plan and two letters of recommendation. Successful candidates will be invited to a symposium in May 2010 in Bonn.

Boehringer Ingelheim is a family-owned, research-driven global pharmaceutical company, founded in 1885 and committed to the goal of serving humankind through research into diseases and the development of new drugs and therapies. Boehringer Ingelheim operates with 41,300 employees in 47 countries across the globe.
caesar (center of advanced european studies and research, located in Bonn, Germany) is conducting research in the field of neurosciences focussing on sensory systems, neurophotonics and neurodegenerative diseases. State-of-the-art techniques for imaging, molecular biology as well as chemical and material sciences open excellent opportunities in basic and applied research. caesar is associated with the Max-Planck-Society.
The **Max Planck Society for the Advancement of Science** is an independent, non-profit research organization that primarily promotes and supports basic research. The society currently operates 80 institutes and research facilities with more than 23,400 employees, including 4,400 scientists.

Boehringer Ingelheim, caesar and the Max-Planck-Society are committed to equal opportunities and to employing disabled persons.

Please send your application **no later than April 15, 2010** to:
Prof. Dr. U. B. Kaupp, Forschungszentrum caesar, Ludwig-Erhard-Allee 2, D - 53175 Bonn.
For further information please contact Prof. Dr. U. B. Kaupp, phone: +49 (0)228 9656 100 or u.b.kaupp@caesar.de

MEETINGS

TEXAS TECH UNIVERSITY
Edward E. Whitacre Jr. College of Engineering

The Maddox Chairs *in Energy* at Texas Tech University

The Edward E. Whitacre Jr. College of Engineering at Texas Tech University is committed to leveraging these **two exceptionally large endowed chairs at over $7 million each**, to become one of the nation's leaders in finding solutions to the world's energy challenges. The college is seeking world-class researchers in solar and sustainable energy as candidates for the Maddox Chairs.

Donovan Maddox Distinguished Engineering Chair *in Solar Energy*

Candidates are expected to have national and international reputation in solar energy based on research publications. In addition, a record of acquiring external resources to support research, team building, and mentoring of associates and graduate and undergraduate students is necessary. The holder of the Donovan Maddox Chair will be expected to not only bring his or her own research activities to the Whitacre College of Engineering, but also to build a collaborative community of scholars at Texas Tech dedicated to solar energy research, thereby building a world-class research program. The appointment will be as a full professor in the Whitacre College of Engineering.

Jack Maddox Distinguished Engineering Chair *in Sustainable Energy*

Candidates with exceptional and diverse backgrounds in energy sciences and engineering are sought for this endowed position. The successful candidate will demonstrate a national and international reputation for contributions to the solution or advancement of the state of the art on a variety of research issues in the sustainable energy fields including energy efficiency, biofuels, wind power, tidal power, geothermal, and energy storage. The successful candidate, along with the Donavan Maddox Chair in Solar Energy, will set the tone, vision, and the path in order to build a nationally and internationally recognized program at Texas Tech University in sustainable energy research. The appointment will be as a full professor in the Whitacre College of Engineering.

Screening will begin upon the receipt of applications and will continue until the position is filled. Candidates names will not be made public until the final stages of the search. Curriculum vitae and the names and contact information of at least four references should be submitted at www.coe.ttu.edu/maddox. To nominate a colleague for these chairs, visit www.coe.ttu.edu/maddox. Nominations can be made anonymously.

Questions about the Jack Maddox or Donovan Maddox Chairs should be directed to:
Jack Maddox and Donovan Maddox Search Committees
Texas Tech University | Whitacre College of Engineering
Box 43103 | Lubbock, Texas 79409-3013 | engineeringdean.coe@ttu.edu | 1.800.528.5583

Texas Tech University | Whitacre College of Engineering
1.800.528.5583 | www.coe.ttu.edu/maddox

An Affirmative Action/Equal Opportunity Employer Americans with Disabilities Employer

35TH FEBS CONGRESS MOLECULES OF LIFE

Welcome to FEBS 2010, jointly organised by the Swedish Society for Biochemistry and Molecular Biology and the Norwegian Biochemical Society

June 26–July 1, 2010 • Gothenburg, Sweden • at Gothenburg Convention Centre (Svenska Mässan)

Programme highlights

Nobel Laureate lectures:	Roger Tsien (UCSD; Nobel Prize 2008) Venki Ramakrishnan (MRC-LMB; Nobel Prize 2009) Elizabeth Blackburn (UCSF; Nobel Prize 2009) John Walker (MRC-MBU; Nobel Prize 1997)
Datta lecture:	Juleen Zierath (Karolinska Institute)
Krebs lecture:	Harald Stenmark (Norwegian Radium Hospital)
Bücher lecture:	Svante Pääbo (MPI Leipzig)
EMBO lecture:	Uri Alon (Weizmann Institute)
IUBMB lecture:	Susan Lindquist (Whitehead Institute)

Congress symposia

A - **Molecules in Health and Disease**
B - **Molecular Networks**
C - **Molecules at Work**
D - **Cellular Compartments**
E - **Biomolecular Design and Function**

Workshops on technology developments

- Sequencing technology
- Proteomics technologies
- Metabolomics
- Protein structures
- Life imaging
- Dynamic modelling
- Protein interactions
- Molecular imaging
- Protein expression
- Lipidomics
- Network modelling
- Bioinformatics

Activities by FEBS committees and working groups

- **Science & Society**
- **Education**
- **Women in Science**

Important dates

Early registration	February 26, 2010
Deadline for support application	February 26, 2010
Abstract deadline	March 31, 2010
Congress starts	June 26, 2010 at 17.00

YOUNG SCIENTIST FORUM
LIFE OF MOLECULES
June 23-26 2010 Gothenburg

www.febs2010.org

Bial AWARD 2010

The Bial Foundation promotes the award designated as **Bial Award 2010**. The Awards will be:

Bial Merit Award in Medical Sciences - €200.000

Designed to distinguish an intellectual written work on any freely chosen medical topic. To meet the elegibility conditions research of high quality and scientific relevance must be presented.

Bial Award in Clinical Medicine - €100.000

Designed to distinguish an intellectual written work on any freely chosen medical topic on clinical practice. At least one of the authors must be a native physician of a Portuguese speaking country.

Distinctions (up to a maximum of four) - €5.000 each

Applications deadline - until the 31st October 2010
Regulation available at *www.bial.com*, or can be sent at request.

FUNDAÇÃO Bial
Institution of public utility

À Av. da Siderurgia Nacional 4745-457 S. Mamede do Coronado - Portugal • Tel. +351 22 986 6100 • Fax +351 22 986 6190 • fundacao@bial.com • www.bial.com

FACULTY POSITIONS

FACULTY POSITION
Section of Endocrinology
Tulane School of Medicine

Tenure-track position, **ASSISTANT** or **ASSOCIATE PROFESSOR** level. Section focus is on diabetes. Funded candidates with molecular and/or clinical pathophysiology are encouraged to apply. Research and teaching responsibilities. Adjunct appointment(s) with physiology, biochemistry, pharmacology also possible. Section has a strong clinical research/clinical trials program. Clinical samples/materials available for collaborative clinical/translational research. Section also involved in epidemiology studies and a pilot program of clinical translation of stem cell therapy in diabetes. Curriculum vitae, research and teaching goals, three references to **website: http://vfonseca@tulane.edu**. Search open until qualified applicant is identified. *Affirmative Action/Equal Opportunity Employer. Women and minorities invited to apply.*

TENURE-TRACK NEURODEGENERATION RESEARCH POSITION

Pittsburgh Institute for Neurodegenerative Diseases, University of Pittsburgh, seeks an established, full-time faculty member to conduct laboratory research on neurodegenerative diseases. Applicants should have an M.D. or Ph.D. degree, a track record of extramural funding, and must be eligible to work in the U.S.A. Generous startup package is available, and there is a possibility of an endowed chair. Applicants should electronically submit curriculum vitae and a brief statement of research interest to **J. Timothy Greenamyre, Chair, Search Committee, Department of Neurology, e-mail: neurologyinfo@upmc.edu**.

The University of Pittsburgh is an Affirmative Action/Equal Opportunity Employer.

POSITIONS OPEN

TENURE-TRACK ALZHEIMER'S POSITION

Pittsburgh Institute for Neurodegenerative Diseases, University of Pittsburgh, seeks an established, full-time faculty member to conduct laboratory research on Alzheimer's and related disorders. Applicants should have an M.D. or Ph.D. degree, a track record of extramural funding, and must be eligible to work in the U.S.A. Generous startup package is available and there is a possibility of an endowed chair. Applicants should electronically submit curriculum vitae and a brief statement of research interest to **J. Timothy Greenamyre, Chair, Search Committee, Department of Neurology, e-mail: neurologyinfo@upmc.edu**.

The University of Pittsburgh is an Affirmative Action/Equal Opportunity Employer.

POSTDOCTORAL POSITIONS will be available in March 2010 in the Department of Cell Biology and Physiology at the University of Pittsburgh School of Medicine to study (1) the mechanisms of trafficking of the dopamine transporter and the regulation of the transporter function by trafficking; and (2) the mechanisms of epidermal growth factor receptor endocytosis and its role in signaling. Candidates with training and interest in cell biology and neuroscience, transgenic and xenograft mouse models, mass spectrometry, virus-mediated protein expression, quantitative live-cell fluorescence microscopy, and computational modeling are encouraged to apply. Please electronically send curriculum vitae and names of references to **Alexander Sorkin, e-mail: sorkin@pitt.edu**. *The University of Pittsburgh is an Equal Opportunity/Affirmative Action Employer.*

POSITIONS OPEN

POSTDOCTORAL POSITIONS (2) available immediately for neuroscientists who are interested to study the functional mechanisms of communication between the basal forebrain and the cerebral cortex using in vivo optogenetics and developmental fate-mapping methods. Applicant will join a dynamic and creative neuroscience center at Rutgers-Newark (**website: http://www.cmbn.rutgers.edu**), 13 miles from midtown Manhattan, New York City. Salary based on NIH postdoctoral scale, full benefits. Electronically send curriculum vitae and the names of and contact information of three references to: **Laszlo Zaborszky, M.D.-Ph.D., e-mail: zaborszky@axon.rutgers.edu; website: http://zlab.rutgers.edu**). Deadline for application: April 1, 2010. *For the fate-mapping studies, applicants must be U.S. citizens or green card holders. Affirmative Action/Equal Opportunity Employer.*

MARKETPLACE

High Efficiency Gene Transfer into Stem Cells

RetroNectin®

Recombinant Human Fibronectin Fragment

Use of RetroNectin®-based gene transduction protocols dramatically enhances the efficiency of retrovirus or lentivirus-mediated gene transfer into mammalian cells. RetroNectin® is a recombinant polypeptide consisting of three functional domains derived from the human fibronectin. RetroNectin®'s enhancement of gene transduction efficiency is hypothetically due to co-localization of retroviral particles and target cells on the RetroNectin® molecule. Recent experiments demonstrate Retronectin®'s efficacy on stem cells.

- **Highly Efficient Retroviral or Lentiviral Gene Transfer** into Stem Cells*
- **No Polybrene Required** for Transduction
- **Facilitates development of innovative protocols** for proliferation of cells carrying a transferred gene, maintaining the function of the cells, and increasing transplant efficiency

* carrying VLA-4 and/or VLA-5 cell surface receptors

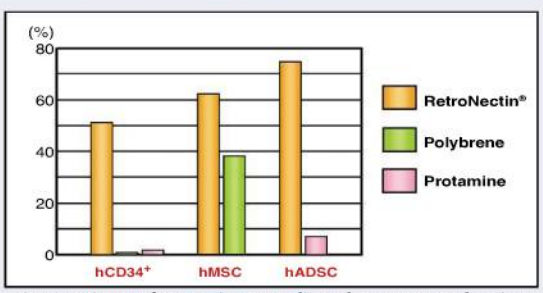

Comparison of retrovirus-mediated gene transduction efficiency in various methods into human stem cells.

RetroNectin® enables and enhances retrovirus-mediated gene transfer into stem cells which express lower levels of GALV envelope receptor, such as hCD34+ or hADSC

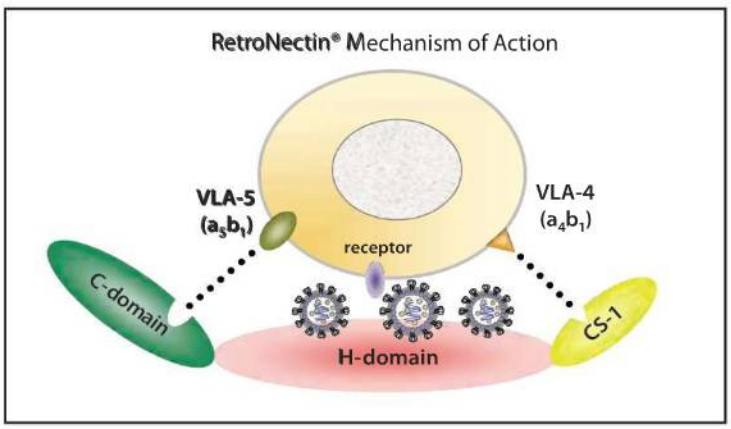

TaKaRa

For more information
www.takara-bio.com

Japan:
Takara Bio Inc.
+81 77 543 7247
www.takara-bio.com

Europe:
Takara Bio Europe S.A.S.
+33 1 3904 6880
www.takara-bio.eu

USA:
Clontech Laboratories, Inc
A Takara Bio Company
888-251-6618
www.takara-bio.us

China:
Takara Biotechnology
(Dalian) Co., Ltd.
+86 411 8764 1681
www.takara.com.cn

Korea:
Takara Korea
Biomedical Inc.
+82 2 2081 2525
www.takara.co.kr

"The fastest separations and the gold standard method.

That's **electroforward** thinking."

Next-generation precast gels. No special buffers required.

Introducing long shelf life Mini-PROTEAN™ TGX (**T**ris-**G**lycine e**X**tended) Gels from Bio-Rad. The innovative TGX formulation delivers consistent, linear separation without the need for expensive, specialized buffers.

Get results faster with:

- Run times as short as 15 minutes
- Transfer in as little as 15 minutes
- New bottom-opening cassette design for faster setup and less handling for downstream applications

Gel with us at **www.miniprotean.com**.

Research. Together.